

# DOES CARTILAGE DAMAGE DOOM THE JOINT?

*Diagnosis and impact of subtle cartilage defects  
in the (equine) joint*

*Nikae te Moller*

2019

Moller, Nikae te

Does cartilage damage doom the joint?

Diagnosis and impact of subtle cartilage defects in the (equine) joint

Dissertation Utrecht University, Faculty of Veterinary Medicine

(With a summary in Dutch)

**ISBN** 978-94-93184-18-3

**Cover design** Matthijs Nolst Trenité

**Lay-out** Nikae te Moller and Matthijs Nolst Trenité

**Printed by** Proefschrift All In One (AIO)

© N.C.R. te Moller 2019

All rights reserved. No part of this thesis may be reproduced in any form without prior written permission of the author.

# DOES CARTILAGE DAMAGE DOOM THE JOINT?

*Diagnosis and impact of subtle cartilage defects  
in the (equine) joint*

## **Leidt kraakbeenschade tot de onontkoombare ondergang van het gewricht?**

*Diagnose en impact van subtiele kraakbeendefecten in  
het (paarden) gewricht*

(met een samenvatting in het Nederlands)

### **Proefschrift**

ter verkrijging van de graad van doctor aan de Universiteit Utrecht  
op gezag van de rector magnificus, prof. dr. H.R.B.M. Kummeling,  
ingevolge het besluit van het college voor promoties  
in het openbaar te verdedigen op  
dinsdag 10 december 2019 des middags te 4.15 uur

door

Nikae Catharina Rolande te Moller

geboren op 28 september 1990  
te Winterswijk

**Promotoren** Prof. dr. P.R. van Weeren  
Prof. dr. J. Töyräs  
Prof. dr. H. Brommer

Dit proefschrift werd mede mogelijk gemaakt met financiële steun van  
IDEXX Laboratories.

# CONTENTS

Chapter 1	General introduction	7
<hr/>		
<b>Part I</b>	<b>Shining light upon articular cartilage damage</b>	19
<hr/>		
Chapter 2	Arthroscopic optical coherence tomography provides detailed information on articular cartilage lesions in horses	21
Chapter 3	Semi-automated International Cartilage Repair Society scoring of equine articular cartilage lesions in optical coherence tomography images	41
Chapter 4	Optical coherence tomography enables accurate measurement of equine cartilage thickness for determination of speed of sound	65
Chapter 5	Estimation of articular cartilage properties using multivariate analysis of optical coherence tomography signal	83
Chapter 6	Arthroscopic near infrared spectroscopy enables simultaneous quantitative evaluation of articular cartilage and subchondral bone in vivo	101
<hr/>		
<b>Part II</b>	<b>The impact of subtle cartilage defects and the role of exercise</b>	127
<hr/>		
Chapter 7	Structural, compositional and functional changes of joint tissues in a long-term equine carpal groove model featuring blunt and sharp cartilage damage	129
Chapter 8	How exercise influences equine joint homeostasis	175
<hr/>		
Chapter 9	Summarizing discussion	201
Addendum	Nederlandse samenvatting (Summary in Dutch)	216
	Dankwoord (Acknowledgements)	225
	List of publications	232
	Curriculum Vitae	235



# CHAPTER 1

## General introduction

---

## **The pivotal element of the moving body - a well-functioning synovial joint**

Synovial joints facilitate free movement of one bone in relation to another and are therefore the pivotal elements of the moving body in all vertebrates. The horse has always been kept primarily for its athletic performances, both in its historical roles in warfare, transport and agriculture, and nowadays in its role as a sport and leisure animal. This emphasis on physical exercise means that high demands are placed upon the equine musculoskeletal system, in particular the appendicular joints. To be able to cope with these high demands, well-functioning joints are of vital importance and not uncommonly even a matter of life and death.

The synovial joint is a complex organ consisting of several key components (fig. 1). The articulating bone ends are covered with articular cartilage. This thin layer of hyaline cartilage consists of water and an abundant extracellular matrix (ECM) wherein chondrocytes are sparsely distributed (1-2% of the cartilage volume). It contains no nerves or blood vessels. The ECM is predominantly composed of collagen (mainly type II but also less abundant minor collagens<sup>1</sup>) and proteoglycans (mainly aggrecan). Other non-collagen molecules in the ECM include hyaluronic acid polymers to which aggrecan monomers are attached and cartilage oligomeric matrix protein (COMP). Proteoglycans attract water through their negatively charged glycosaminoglycan side chains. This creates a swelling pressure that is resisted by the collagen network in which the proteoglycans are retained. The unique combination of compressive stiffness and tensile strength of the articular cartilage is important for its main functions: transmission of the forces placed upon the joint, and distribution of stresses over the underlying bone. Furthermore, cartilage provides almost frictionless contact between the articulating joint surfaces.<sup>1-3</sup>

The bone ends, covered with cartilage, are enclosed within a joint capsule. The inner lining of the capsule, the synovial membrane, is a thin structure of 1-3 cell layers thick with many nerve endings and small blood vessels. It allows exchange of all components but macromolecules between blood and the synovial fluid that fills up the joint cavity. This makes the synovial fluid an ultrafiltrate of blood plasma to which various components are added by articular tissues. The synovial fluid serves as a joint lubricant and helps redistributing forces during loading and unloading. Furthermore, it fulfils an important role in the nourishment of the articular cartilage layer which is avascular in nature and thus depends mainly on diffusion from and to the synovial fluid for its nutrition and removal of waste products.<sup>4</sup> Also, the synovial fluid functions as an important communication medium between the various tissues.



Some joints contain additional intra-articular structures such as ligaments and menisci. In a functional, healthy joint, a dynamic equilibrium between cellular processes within and between all these components is maintained. Internal disturbances caused by changes in the environment, affecting the system directly or indirectly, are kept within narrow limits by automatic adjustments to preserve normal tissue function and development. Walter B. Cannon was the first who named this concept 'homeostasis'.<sup>5</sup> The term applies to the body in general, but also to its constituent elements<sup>6</sup>, including the joint. Given the close interaction, the concomitant crosstalk and the reciprocal feedback mechanisms between the various joint components, joint homeostasis should be considered a variable or dynamic equilibrium rather than a static state.<sup>7</sup>

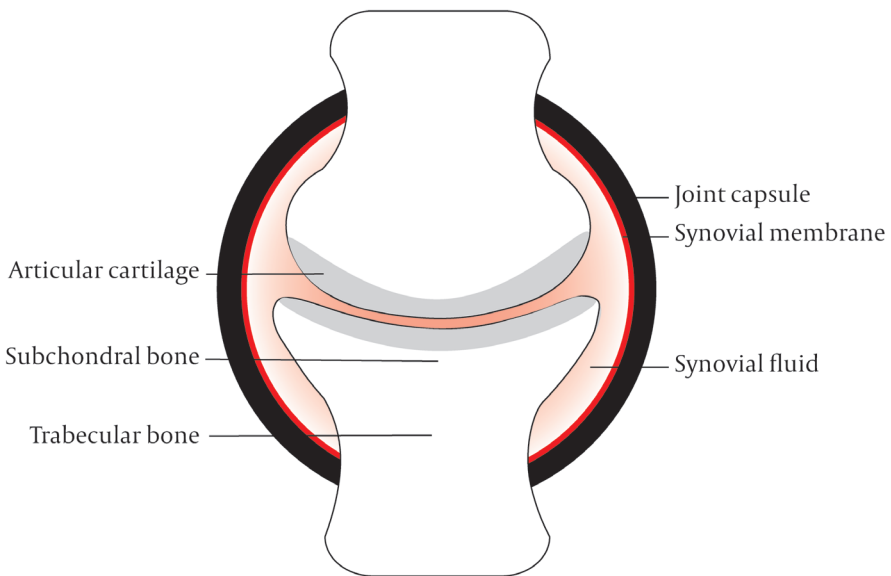


**Fig. 1** Schematic representation of a synovial joint.

Under physiologic conditions, the subchondral bone directly beneath the articular cartilage layer is not in direct contact with the synovial cavity. However, the two structures have an intimate association. Therefore, alterations of either tissue modulate the properties and function of the other, through biochemical and molecular crosstalk across their interface.<sup>8</sup> Crosstalk between bone and cartilage plays an important role in joint homeostasis.

## Why should we care about cartilage?

Disturbances in joint homeostasis that cannot be kept within physiological limits cause an imbalance between catabolic and anabolic processes and can lead to the onset and progression of joint disorders such as osteoarthritis.<sup>2,7,9</sup> Osteoarthritis (OA) is a joint disorder that not only affects millions of people worldwide<sup>10</sup>; it is also a common burden in animals. Particularly in the horse industry the high incidence of OA is an important concern.<sup>11</sup> Osteoarthritis is characterized by progressive articular cartilage degeneration, accompanied by pathologic changes in other joint tissues including bone remodelling, synovitis and changes in synovial fluid composition and volume, eventually leading to joint pain, swelling and stiffness.<sup>12</sup> Despite substantial experimental and clinical work that has been carried out on promising new avenues for cartilage repair, there is no effective therapy available to heal the joint or even halt the progression of this disease.<sup>13</sup> The well-known statement by William Hunter<sup>14</sup> “... an ulcerated cartilage is universally allowed to a very troublesome disease [...] and that, when destroyed, it is never recovered.” still holds today.

It is common to read in modern literature that OA was traditionally referred to as “wear-and-tear” of the cartilage but nowadays is considered a “whole joint disease”<sup>12</sup> with an important role for low-grade inflammation.<sup>15</sup> Although there is certainly support for this change in view, realizing that the role of inflammation, the involvement of the whole joint and even of the central nervous system were already under discussion in the late nineteenth and early twentieth century, puts our advancing insights in a somewhat humble perspective.<sup>16-19</sup> Despite these advancing insights, novel or not, and exciting developments in OA research, the underlying complexities of the disease are still unclear. Attempts to delineate different OA phenotypes to help our understanding and improve therapeutic effectiveness have resulted in a wide range of studies with different outcomes, characteristics and methodologies, raising new challenges.<sup>20</sup> In general, risk factors of OA include abnormal loading (involving both single-impact trauma and repetitive impulse loading), aging, sex, genetic predisposition, obesity, malformation and developmental joint diseases.<sup>21,22</sup> Traumatic injury, in fact a result of abnormal loading, can also lead to articular cartilage degeneration which is referred to as post-traumatic OA.<sup>23</sup> However, because of the long time it may take to develop OA, it is difficult to test the exact relationship between joint injuries and the events leading to OA on the longer term.

This is particularly true for focal cartilage defects that are commonly observed during diagnostic arthroscopies both in horses and humans and are subject of discussion on if, when and how they should be approached therapeutically.<sup>24-26</sup> Although a recent systematic review came to the conclusion that development of OA

in patients with untreated focal defects in the knee joint could not be demonstrated within 2 years, cartilage lesions were shown to be progressive at follow-up.<sup>27</sup> Given its very limited regenerative capacity related to the lack of collagen turnover<sup>28</sup>, it seems likely that injured cartilage, at a certain stage, does play a role in further degradative processes in the joint. This idea is also supported by animal models of OA based on the induction of cartilage defects.<sup>29-31</sup>

## **Tools for in vivo measurement of articular cartilage health status and joint homeostasis**

Arthroscopy is the clinical gold standard for in vivo assessment of articular cartilage condition and evaluation of cartilage defects but has certain shortcomings. These include subjective interpretation by the surgeon, its insensitivity for small lesions or pathological changes below a seemingly intact surface, and the limited accessibility to certain parts of the joint.<sup>32-33</sup> Magnetic resonance imaging (MRI) or contrast enhanced computed tomography (CT) could partly overcome these shortcomings by providing cross-sectional, quantitative information on cartilage morphology and composition. However, disadvantages of these techniques include the lack of adequate resolution to detect microstructural changes, relatively long acquisition times, radiation exposure (CT) and costs.<sup>34</sup> Besides, they cannot be used during arthroscopic repair surgery and feasibility in horses is mostly limited to the distal parts of the appendicular joints.

Cartilage defect-specific factors (e.g. size, depth and location) are criteria for treatment selection and are used as outcome measures in clinical trials.<sup>35-37</sup> However, surgeons were found to over or underestimate defect sizes during arthroscopy depending on the size of the lesion. Accuracy and reliability were highly influenced by lesion size and location, as well as by the measuring method that was used.<sup>38,39</sup> Furthermore, variability in lesion location, size and number have been identified as major flaws in the design of surgical trials on the management of cartilage defects. They contribute to bias, limiting interpretation and generalization of results between studies.<sup>40</sup> For both clinical and research purposes, the possibility to determine characteristics of cartilage defects and the condition of the surrounding cartilage (that might not show any visual changes yet but be subject to early stage degeneration) in a more accurate and objective manner with non-destructive techniques would thus be of great value.

Focusing merely on the cartilage to optimize diagnosis and treatment outcome would, however, not do justice to the concept of the joint as an organ, with joint homeostasis as the key element in (re-establishing) joint health. Therefore, a better

and more quantitative insight in the relation between lesion development, joint homeostasis and functionality is needed. This requires inclusion of other joint structures like the synovial membrane and the subchondral bone. The synovial fluid is in direct contact with all relevant structural elements of a joint except the subchondral bone and undergoes continuous turnover. Therefore, its biomarker profile can be seen as a mirror of joint homeostasis.<sup>41</sup> Synovial fluid biomarker profiling could be a valuable addition to the use of advanced imaging techniques in the quest for better understanding of changes prior to OA development and for treatment selection protocols that will serve the development of a personalized medicine approach in joint repair.

Studying the disease continuum in naturally occurring OA is very challenging. Not only due to the long time it may take for OA to develop, but also because cartilage defects often occur in the presence of other intra-articular injuries and with varying times of onset.<sup>40</sup> The availability of patient material representing early stages of cartilage defects and degeneration is limited, as these stages are almost invariably clinically silent. Pain is not always apparent; is often intermittent and can arise at various stages.<sup>42</sup> As a result, patient material usually represents more advanced stages of OA and the availability of healthy cartilage as control tissue is extremely limited. A wide range of animal models have been used to study OA development in response to known initiating factors.<sup>43</sup> However, the use of experimental animals raises ethical concerns and there is a societal ambition to reduce animal experiments. This has driven the development of advanced in vitro models that can mimic the in vivo biological interactions of the various joint components<sup>44</sup> and have the potential of replacing animal models. Furthermore, mechanobiological models can help predicting disease progression following traumatic injury based on computational algorithms.<sup>45</sup> Nevertheless, in vivo models will remain crucial for validation of such approaches. Advantages of the horse over other animals include the similarity between equine and human articular cartilage, joint size, the possibilities for a full range of analysis techniques including imaging, objective quantitative gait analysis and (serial) synovial fluid collection, the ability to have controlled exercise and, importantly, the horse being a target species in itself.<sup>46,47</sup>

## AIMS AND OUTLINE OF THIS THESIS

The aims of this thesis were 1) to investigate the potential of advanced intra-articular techniques to improve arthroscopic diagnosis of subtle changes in cartilage structure, composition and mechanical properties in the horse, and 2) to quantify the longer-term progression of artificial cartilage defects and their effect on other joint tissues in the horse by multiple modality monitoring of changes at a structural, compositional and functional level in vivo and ex vivo.

In **part I**, the feasibility of diagnostic intra-articular imaging techniques including optical coherence tomography (OCT), ultrasound (US) and near infrared spectroscopy (NIRS) are explored in ex vivo and in vivo experiments.

Chapters 2 and 3 describe how the diagnostic value of arthroscopy could be improved with intra-articular OCT. In **chapter 2** this was done by assessing cartilage thickness and various morphological characteristics of articular cartilage defects using OCT in the equine metacarpophalangeal joint in an ex vivo setting. **Chapter 3** shows how reliability of the International Cartilage Repair Society (ICRS) scoring system of these cartilage defects could be improved by using semi-automated software for scoring of lesion severity. Chapters 4 through 6 investigate methods to obtain quantitative information through processing of advanced intra-articular imaging data and hence to improve the thus far mainly subjective visual arthroscopic diagnosis of early signs of cartilage degeneration. In **chapter 4** this is done by multivariate analysis of OCT data for determining structural integrity, composition and mechanical properties of articular cartilage. In **chapter 5**, OCT-determined cartilage thickness is combined with US time-of-flight measurements to determine speed of sound in cartilage. **Chapter 6** demonstrates the potential of arthroscopic NIRS to simultaneously monitor progressive degeneration of cartilage and subchondral bone in the equine stifle joint in an in vivo cartilage repair model.

In **part II**, the longer-term progression of artificial cartilage lesions and their impact on joint homeostasis and functionality are monitored in an equine carpal groove model. Since joint loading is related to both progressive degeneration of articular cartilage and, on the other hand, to maintenance of joint health, special attention is given to the relationship between exercise and joint homeostasis.

**Chapter 7** investigates the structural changes that develop in various joint tissues sequentially to the creation of two morphologically different types of cartilage lesions. Lesion progress is monitored in vivo with arthroscopic OCT and NIRS as

well as with radiographs over a period of 9 months. Structural changes in cartilage, synovium and subchondral bone are evaluated macroscopically and microscopically and by micro-CT analysis. Also, the question if structural changes are reflected in joint homeostasis (measured as synovium gene expression and synovial fluid biomarker profiles) and/or at a functional level (cartilage biomechanical properties and joint function based on gait quality) is addressed. **Chapter 8** provides a review of what is known about the relationship between exercise and joint homeostasis and cartilage health, an issue that is inextricably linked to chapter 7. It is assumed that continuation of (excessive) loading is an important factor in the progressive degeneration of articular cartilage. On the other hand, exercise is considered to be of crucial importance for homeostatic balance, joint development and durable joint function. Chapter 8 deals with this paradox of the influence of exercise on joints.

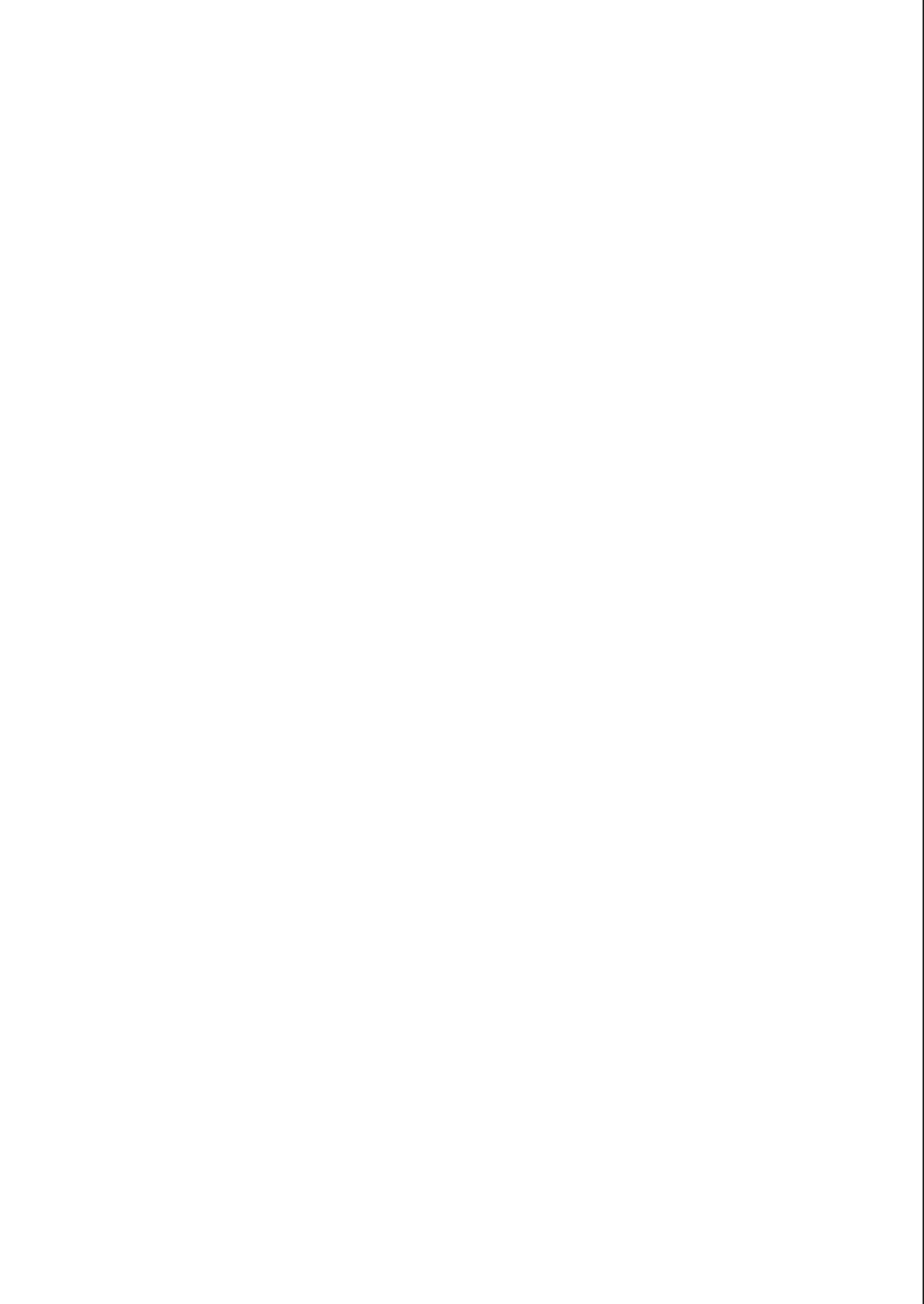
## REFERENCES

1. Luo Y, Sinkeviciute D, He Y, et al. The minor collagens in articular cartilage. *Protein Cell*. 2017;8(8):560-572.
2. Goldring MB, Marcu KB. Cartilage homeostasis in health and rheumatic diseases. *Arthritis Res Ther*. 2009;11(3):224.
3. Kawcak CE. Biomechanics in Joints. In: McIlwraith CWE, D.D. F, Kawcak CE, van Weeren PR, eds. *Joint Disease in the Horse*. 2nd ed. St. Louis: Elsevier; 2016:25-32.
4. Levick JR. Microvascular architecture and exchange in synovial joints. *Microcirculation*. 1995;2(3):217-233.
5. Cannon WB. Physiological regulation of normal states: Some tentative postulates concerning biological homeostatics. *Jubil Vol Charles Richet*. 1926:91-93.
6. Cannon WB. Organization for physiological homeostasis. *Physiol Rev*. 1929;9(3).
7. de Grauw JC. Molecular monitoring of equine joint homeostasis. *Vet Q*. 2011;31(2):77-86.
8. Findlay DM, Kuliwaba JS. Bone-cartilage crosstalk: a conversation for understanding osteoarthritis. *Bone Res*. 2016;4:16028.
9. Chu CR, Andriacchi TP. Dance between biology, mechanics, and structure: A systems-based approach to developing osteoarthritis prevention strategies. *J Orthop Res*. 2015;33(7):939-947.
10. Martel-Pelletier J, Barr AJ, Cicuttini FM, et al. Osteoarthritis. *Nat Rev Dis Prim*. 2016;2(1):16072.
11. Penell JC, Egenvall A, Bonnett BN, Olson P, Pringle J. Specific causes of morbidity among Swedish horses insured for veterinary care between 1997 and 2000. *Vet Rec*. 2005;157(16):470-477.
12. Loeser RF, Goldring SR, Scanzello CR, Goldring MB. Osteoarthritis: A disease of the joint as an organ. *Arthritis Rheum*. 2012;64(6):1697-1707.
13. Malda J, Groll J, van Weeren PR. Rethinking articular cartilage regeneration based on a 250-year-old statement. *Nat Rev Rheumatol*. July 2019. [Epub ahead of print]
14. Hunter W. On the structure and diseases of articulation cartilage. *Philos Trans R Soc L*. 1743;9(267):514-521.
15. Robinson WH, Lepus CM, Wang Q, et al. Low-grade inflammation as a key mediator of the pathogenesis of osteoarthritis. *Nat Rev Rheumatol*. 2016;12(10):580-592.
16. Dobson GP, Letson HL, Grant A, et al. Defining the osteoarthritis patient: back to the future. *Osteoarthr Cartil*. 2018;26(8):1003-1007.
17. Forsbrook WHR. *A Dissertation on Osteo-Arthritis*. London: H.K. Lewis; 1893.
18. Garrod AE. *A Contribution to the Theory of the Nervous Origin of Rheumatoid Arthritis*. *J R Soc Med*. 1888;71(1):89-105.
19. Garrod AE. Discussion on "The etiology and treatment of osteo-arthritis and rheumatoid arthritis." In: *Proceedings of the Royal Society of Medicine*. 1924;17:1-4.
20. Bierma-Zeinstra SM, Van Middelkoop M. Osteoarthritis: In search of phenotypes. *Nat Rev Rheumatol*. 2017;13(12):705-706.
21. Felson DT, Lawrence RC, Dieppe PA, et al. Osteoarthritis: New Insights. Part 1: The Disease and Its Risk Factors. *Ann Intern Med*. 2000;133(8):635-645.
22. Blagojevic M, Jinks C, Jeffery A, Jordan KP. Risk factors for onset of osteoarthritis of the knee in older adults: a systematic review and meta-analysis. *Osteoarthr Cartil*. 2010;18(1):24-33.
23. Buckwalter JA, Felson DT. Post-traumatic arthritis: Definitions and burden of disease. In: Olson SA, Guilak F, eds. *Post-Traumatic Arthritis: Pathogenesis, Diagnosis and Management*. Springer, New York, USA; 2015:7-15.

24. Widuchowski W, Widuchowski J, Trzaska T. Articular cartilage defects: Study of 25,124 knee arthroscopies. *Knee*. 2007;14(3):177-182.
25. Cohen JM, Richardson DW, McKnight AL, Ross MW, Boston RC. Long-Term Outcome in 44 Horses with Stifle Lameness After Arthroscopic Exploration and Debridement. *Vet Surg*. 2009;38(4):543-551.
26. de Windt TS, Concaro S, Lindahl A, Saris DBF, Brittberg M. Strategies for patient profiling in articular cartilage repair of the knee: a prospective cohort of patients treated by one experienced cartilage surgeon. *Knee Surgery, Sport Traumatol Arthrosc*. 2012;20(11):2225-2232.
27. Houck DA, Kraeutler MJ, Belk JW, Frank RM, McCarty EC, Bravman JT. Do Focal Chondral Defects of the Knee Increase the Risk for Progression to Osteoarthritis? A Review of the Literature. *Orthop J Sport Med*. 2018;6(10): eCollection.
28. Heinemeier KM, Schjerling P, Heinemeier J, et al. Radiocarbon dating reveals minimal collagen turnover in both healthy and osteoarthritic human cartilage. *Sci Transl Med*. 2016;8(346):346ra90.
29. Bolam CJ, Hurtig MB, Cruz A, McEwen BJE. Characterization of experimentally induced post-traumatic osteoarthritis in the medial femorotibial joint of horses. *Am J Vet Res*. 2006;67(3):433-447.
30. Marijnissen ACA, van Roermund PM, Verzijl N, Tekoppele JM, Bijlsma JWJ, Lafeber FPJG. Steady progression of osteoarthritic features in the canine groove model. *Osteoarthr Cartil*. 2002;10(4):282-289.
31. Maninchedda U, Lepage OM, Gangl M, et al. Development of an Equine Groove Model to Induce Metacarpophalangeal Osteoarthritis: A Pilot Study on 6 Horses. *PLoS One*. 2015;10(2):e0115089.
32. Vanderperren K, Martens A, Haers H, Duchateau L, Saunders JH. Arthroscopic visualisation of the third metacarpal and metatarsal condyles in the horse. *Equine Vet J*. 2009;41(6):526-533.
33. Spahn G, Klinger HM, Baums M, Pinkepank U, Hofmann GO. Reliability in arthroscopic grading of cartilage lesions: results of a prospective blinded study for evaluation of inter-observer reliability. *Arch Orthop Trauma Surg*. 2011;131(3):377-381.
34. Nelson BB, Kawcak CE, Barrett MF, McIlwraith CW, Grinstaff MW, Goodrich LR. Recent advances in articular cartilage evaluation using computed tomography and magnetic resonance imaging. *Equine Vet J*. 2018:1-16.
35. Behery O, Siston RA, Harris JD, Flanigan DC. Treatment of cartilage defects of the knee: expanding on the existing algorithm. *Clin J Sport Med*. 2014;24(1):21-30.
36. Bekkers JEJ, Inklaar M, Saris DBF. Treatment Selection in Articular Cartilage Lesions of the Knee: A Systematic Review. *Am J Sports Med*. 2009;37(1\_suppl):148S-155S.
37. de Windt TS, Bekkers JEJ, Creemers LB, Dhert WJA, Saris DBF. Patient profiling in cartilage regeneration: prognostic factors determining success of treatment for cartilage defects. *Am J Sports Med*. 2009;37 Suppl 1(1\_suppl):58S-62S.
38. Siston RA, Geier D, Bishop JY, et al. The high variability in sizing knee cartilage defects. *J Bone Jt Surg - Ser A*. 2013;95(1):70-75.
39. Flanigan DC, Carey JL, Brophy RH, et al. Interrater and Intrarater Reliability of Arthroscopic Measurements of Articular Cartilage Defects in the Knee. *J Bone Jt Surg*. 2017;99(12):979-988.
40. Worthen J, Waterman BR, Davidson PA, Lubowitz JH. Limitations and sources of bias in clinical knee cartilage research. *Arthroscopy*. 2012;28(9):1315-1325.
41. van den Boom R. Synovial fluid as a mirror of equine joint (patho) physiology. 2004.
42. van Weeren PR, de Grauw JC. Pain in osteoarthritis. *Vet Clin North Am Equine Pract*. 2010;26(3):619-642.
43. Cope PJ, Ourradi K, Li Y, Sharif M. Models of osteoarthritis: the good, the bad and the promising. *Osteoarthr Cartil*. 2018; 27(2):230-239.



44. Piluso S, Li Y, Abinzano F, et al. Mimicking the Articular Joint with In Vitro Models. *Trends Biotechnol.* April 2019.[Epub ahead of print]
45. Orozco GA, Tanska P, Florea C, Grodzinsky AJ, Korhonen RK. A novel mechanobiological model can predict how physiologically relevant dynamic loading causes proteoglycan loss in mechanically injured articular cartilage. *Sci Rep.* 2018;8(1):15599.
46. Malda J, Benders KE, Klein TJ, et al. Comparative study of depth-dependent characteristics of equine and human osteochondral tissue from the medial and lateral femoral condyles. *Osteoarthritis Cartilage.* 2012;20:1147-1151.
47. McIlwraith CW, Fortier L a., Frisbie DD, Nixon a. J. Equine Models of Articular Cartilage Repair. *Cartilage.* 2011;2(4):317-326.



# PART I

Shining light upon articular  
cartilage damage

---



# CHAPTER 2

## Arthroscopic optical coherence tomography provides detailed information on articular cartilage lesions in horses

*The Veterinary Journal* 197, 589-595 (2013)

---

N.C.R. te Moller<sup>1</sup>

H. Brommer<sup>1</sup>

J. Liukkonen<sup>2</sup>

T. Virén<sup>3</sup>

M. Timonen<sup>2</sup>

P.H. Puhakka<sup>2,4</sup>

J.S. Jurvelin<sup>2</sup>

P.R. van Weeren<sup>1</sup>

J. Töyräs<sup>2,4</sup>

---

<sup>1</sup>Department of Equine Sciences, Faculty of Veterinary Medicine, Utrecht University, Yalelaan 114, Utrecht 3508 TD, The Netherlands, <sup>2</sup>Department of Applied Physics, Faculty of Science and Forestry, University of Eastern Finland, Kuopio FI-70211, Finland, <sup>3</sup>Cancer Centre, Kuopio University Hospital, Kuopio FI-70211, Finland, <sup>4</sup>Department of Clinical Neurophysiology, Kuopio University Hospital, Kuopio FI-70211, Finland

## **ABSTRACT**

Arthroscopy enables direct inspection of the articular surface, but provides no information on deeper cartilage layers. Optical coherence tomography (OCT), based on measurement of reflection and backscattering of light, is a diagnostic technique used in cardiovascular surgery and ophthalmology. It provides cross-sectional images at resolutions comparable to that of low-power microscopy. The aim of this study was to determine if OCT is feasible for advanced clinical assessment of lesions in equine articular cartilage during diagnostic arthroscopy.

Diagnostic arthroscopy of 36 metacarpophalangeal joints was carried out *ex vivo*. Of these, 18 joints with varying degrees of cartilage damage were selected, wherein OCT arthroscopy was conducted using an OCT catheter (diameter = 0.9 mm) inserted through standard instrument portals. Five sites of interest, occasionally supplemented with other locations where defects were encountered, were arthroscopically graded according to the International Cartilage Repair Society (ICRS) classification system. The same sites were evaluated qualitatively (ICRS classification and morphological description of the lesions) and quantitatively (measurement of cartilage thickness) on OCT images.

OCT provided high resolution images of cartilage enabling determination of cartilage thickness. Comparing ICRS grades determined by both arthroscopy and OCT revealed poor agreement. Furthermore, OCT visualised a spectrum of lesions, including cavitation, fibrillation, superficial and deep clefts, erosion, ulceration and fragmentation. In addition, with OCT the arthroscopically inaccessible area between the dorsal MC<sub>3</sub> and P<sub>1</sub> was reachable in some cases. Arthroscopically-guided OCT provided more detailed and quantitative information on the morphology of articular cartilage lesions than conventional arthroscopy. OCT could therefore improve the diagnostic value of arthroscopy in equine orthopaedic surgery.

## INTRODUCTION

Arthroscopy is widely used for the detection of articular cartilage lesions in human as well as in equine healthcare and is considered the clinical gold standard for *in vivo* assessment of the status of articular cartilage. It enables direct visual inspection and mechanical probing of the cartilage surface and adjacent structures. Arthroscopic evaluation of articular cartilage has been reported to correlate well with histopathological scoring systems<sup>1,2</sup> and to be consistent with most clinical characteristics in human knee osteoarthritis.<sup>3</sup>

Arthroscopic scoring of the status of articular cartilage, however, does have certain shortcomings. Grading of cartilage lesions depends on the surgeon's subjective interpretation of what is seen. This limits the quantitiveness of the evaluation and makes the inter-observer reliability poor.<sup>4,5</sup> In particular, the differentiation between intact and softened cartilage, as well as the differentiation between superficial and deep cartilage lesions are major obstacles.<sup>5</sup>

A second limitation is the insensitivity of arthroscopic assessment for pathological changes below a seemingly intact cartilage surface. Consequently, small lesions that do not yet reach the surface may be overlooked. A third limitation is the restricted area of the joint surface that can be visualised mainly due to joint geometry and limited lighting conditions at certain areas.<sup>6</sup> This limits access to the articular surface of the proximal phalanx (P<sub>1</sub>). In the forelimb, only the dorsal margin of P<sub>1</sub> can be visualised but this area is often not representative of the status of the entire articular surface. In an earlier study using equine joints, arthroscopic grading of lesions located at the visible area of the proximal phalanx (P<sub>1</sub>) in the metacarpophalangeal (MCP) joint resulted in an underestimation of the total damage in joints with mild cartilage damage and an overestimation in joints with severe lesions.<sup>7</sup>

To overcome the subjective aspect of visual assessment, different arthroscope-guided mechanical probing techniques have been introduced in recent years. Measuring cartilage stiffness with arthroscopic indentation devices provides quantitative information on alterations in mechanical properties of the articular cartilage, which may be indicative for early degeneration.<sup>8-11</sup> The integration of a miniature ultrasound transducer at the tip of the indentation instrument enables simultaneous determination of the cartilage thickness at the tested location that is necessary for accurate determination of the mechanical characteristics.<sup>12-14</sup>

Additionally, quantitative ultrasound imaging may provide information on intrinsic structural properties of the cartilage.<sup>15,16</sup> Quantitative ultrasound arthroscopy has already been successfully applied for characterization of cartilage injuries and degeneration in human joints *in vivo*.<sup>17</sup> However, with this technique the speed of sound is usually assumed to be constant, which is not the case in pathologically altered cartilage. This may affect the reliability of the measurements.<sup>18</sup> Moreover, the visual information on cartilage structure is restricted by the limited resolution of ultrasound images.

A quantitative diagnostic technique that could potentially overcome the limitations of conventional arthroscopy and provide a better resolution than ultrasound arthroscopy is optical coherence tomography (OCT). This imaging technique is based on the measurement of reflection and backscattering of near infra-red light from tissues probed with a beam of near infra-red light. From a series of laterally adjacent depth-scans cross-sectional digital images are produced at resolutions comparable to that of low-power microscopy, thereby providing non-destructive near real-time 'optical biopsies' of the investigated tissue.<sup>19-21</sup> OCT has been widely investigated for its application in different medical fields, including dermatology and gastroenterology and it is already being clinically used in cardiovascular surgery and ophthalmology.<sup>22</sup> Its feasibility for articular cartilage diagnostics has been evaluated with good results in an *in vitro* setting using bovine cartilage<sup>23</sup> and *in situ* and *ex vivo* using human knee cartilage.<sup>24</sup> In an *ex vivo* setting the sensitivities of OCT and ultrasound were compared using equine cartilage.<sup>25</sup> Furthermore, OCT has been applied in porcine and human joints during arthroscopy *in vivo*.<sup>26-28</sup> The latter studies showed the potential value of OCT for clinical use in human joints as an adjunct to arthroscopy for (early) detection of cartilage lesions and degeneration. The OCT-generated high-resolution cross-sectional images, in combination with the small size of the optical catheter that allows access to joint areas that cannot be reached by other arthroscopic techniques, make OCT a potential solution to overcome the limitations of conventional arthroscopy.

The aim of the present study was to test whether OCT would be helpful in the advanced clinical assessment of lesions in equine articular cartilage in the MCP joint during arthroscopy. This was done by assessing cartilage thickness and various morphological characteristics of articular cartilage defects using OCT in an *ex vivo* setting representative to clinical diagnostic arthroscopy and comparing the outcome with conventional visual assessment by means of arthroscopy.



## MATERIALS AND METHODS

### Sample collection

Thirty-six fresh distal forelimbs of adult horses (age >2 years) were obtained from a slaughterhouse and stored at 7°C until arthroscopy was performed 2-3 days later. To select a range of joints representing different stages of cartilage degeneration, standard diagnostic arthroscopy of the dorsal aspect of the MCP joint was performed (McIlwraith, 2005a) using a 4 mm, 30° arthroscope (Storz). Occurrence and severity of cartilage lesions at the dorsal eminences of the proximal phalanx (P<sub>1</sub>) and at the dorsoproximal area of the condyles and sagittal ridge of the third metacarpal bone (MC<sub>3</sub>) were scored using the SFA (Société Française d'Arthroscopie) scoring system.<sup>29,30</sup> Briefly, the depth of the cartilage lesions was classified on a 0-4 scale and the size of the lesion was estimated as a percentage of the visible cartilage surface. An SFA score was then calculated using a specific formula resulting in a continuous variable ranging from 0% to 100% indicating the stage of cartilage degeneration.<sup>30</sup> Eighteen joints were selected for OCT arthroscopy. This selection represented a range of degeneration with increasing severity (SFA scoring ranging from 0.70% to 33.25%). After completing conventional arthroscopy, the selected joints were stored at -20°C until performing OCT arthroscopy.

### OCT arthroscopy

The standard portal at the dorsal aspect of the joint<sup>31</sup> was used for the arthroscope and dorsomedial or dorsolateral portals were used for the OCT catheter (C7 Dragonfly Intravascular Imaging Catheter). The OCT catheter (d = 0.9 mm) was guided into the joint through a custom made hollow instrument under arthroscopic control (fig. 1). The OCT imaging and measurements of cartilage lesions were performed using the Ilumien PCI Optimization System (St. Jude Medical; wavelength 1305 ± 55 nm, in plane pixel size of 10 x 10 µm<sup>2</sup>, slice thickness 100 µm, frame rate 100 frames/s).

Five sites of interest (SOIs) for each joint were defined: the medial and lateral dorsal eminences of P<sub>1</sub> (P<sub>1</sub>M and P<sub>1</sub>L), known to be often involved in early OA,<sup>32</sup> the opposing sites at the medial and lateral condyles of MC<sub>3</sub> (MC<sub>3</sub>M and MC<sub>3</sub>L) at a joint angle position of 180°, and the central aspect of the sagittal ridge of MC<sub>3</sub>, in between the locations on the medial and lateral condyles (fig. 2). Apart from the SOIs, lesions on other locations of the visible cartilage surface, found by arthroscopy or accidentally found by randomly scanning the surface with the OCT catheter were also imaged. Lastly, it was tried to increase the visible area of P<sub>1</sub> by manoeuvring the OCT catheter in between the surfaces of P<sub>1</sub> and MC<sub>3</sub> (P<sub>1</sub>-MC<sub>3</sub>), abaxial (lateral or medial) to the sagittal ridge. Whenever this was successful, this area was also scanned with OCT.

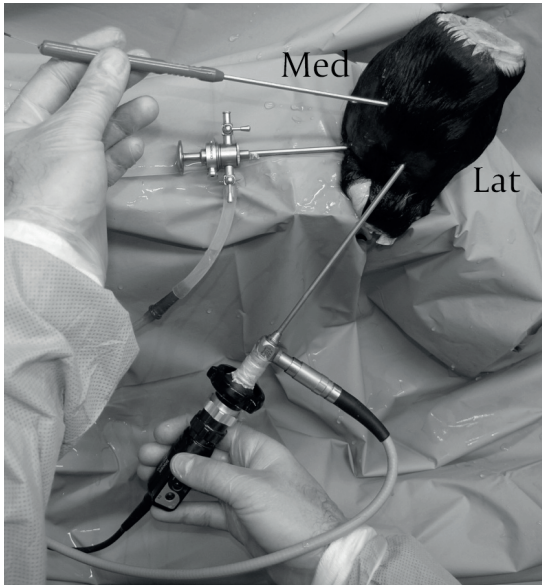


**Fig. 1** OCT arthroscopy imaging of an equine MCP joint. A standard portal is used for the arthroscope and a dorsomedial portal is used for the OCT catheter.

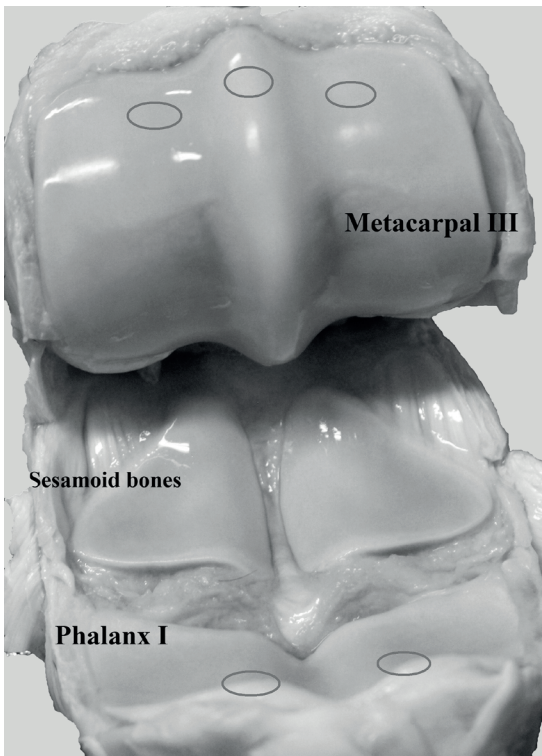


**Fig. 2** The five sites of interest are indicated by red ovals: the tips of the medial and lateral eminences of the first phalanx (P1M and P1L), the opposing sites on the medial and lateral condyles (MC3M and MC3L) and the central part of the sagittal ridge (SR) of the third metacarpal bone in between the former sites.

## Data analysis

### *Thickness measurements of articular cartilage*

The cartilage thickness at the SOIs was measured using the integrated software of the OCT device. For each site, the mean and standard deviation for intact and damaged cartilage, as well as the overall thickness was calculated.

### *Qualitative comparison between arthroscopy and OCT imaging*

The cartilage was graded according to the International Cartilage Repair Society (ICRS) classification system for focal cartilage injuries: ICRS 0, normal; ICRS 1, softening, superficial fibrillation, superficial laceration and fissures; ICRS 2, defect involves <50% of cartilage thickness; ICRS3, defect involves >50% of cartilage thickness; ICRS4, defects extending into the subchondral bone (Brittberg and Winalski, 2003), by using videos recorded during the arthroscopies. Subsequently, the OCT images were blind coded and graded along the ICRS classification system. The agreement of the ICRS grades obtained with these two techniques was assessed using a strict parallel inter-item correlation analysis (SPSS 19, IBM).

Since ICRS grading cannot discriminate between different subsurface lesions as visualised by OCT, the acquired OCT images were qualitatively assessed by describing the morphological characteristics of the detected lesions (terminology based on Pritzker and Aigner, 2010). After assessment, the OCT morphological characteristics (OMCs) detected at the visible cartilage surface, were divided to seven categories: OMC 0, intact cartilage; OMC 1, cavitation; OMC 2, fibrillation of the cartilage surface; OMC 3A, superficial horizontal cleft (<50% of the cartilage thickness); OMC 3B, deep horizontal cleft (>50% of the cartilage thickness); OMC 4, erosion; OMC 5, anomaly beneath the surface. Each site could be assigned to more than one OMC. Images representing the detected OMCs were tabulated with their corresponding arthroscopic images. In addition, the spectrum of OMCs per arthroscopic ICRS lesion grade was evaluated. Lesions that were found at the cartilage surface in between MC3 and P1, were described based on the OCT images but could not be connected to ICRS grades as these sites were inaccessible with an arthroscope.

## RESULTS

Ninety-four sites in 18 joints imaged with arthroscope-guided OCT were evaluated. These included 82 SOIs (16 P1M, 18 P1L, 14 MC3M, 17 MC3L, 17 SR) and 12 other sites. Fig. 3 shows a typical example of the acquired high resolution OCT images. The articular cartilage is shown in a transverse section where the interface between cartilage and

subchondral bone (SC bone) can be discerned as a dark line. This allowed accurate measurements of the thickness of the cartilage layer (table 1). In 3/94 measurement sites the thickness could not be measured due to excessive absorption of light.

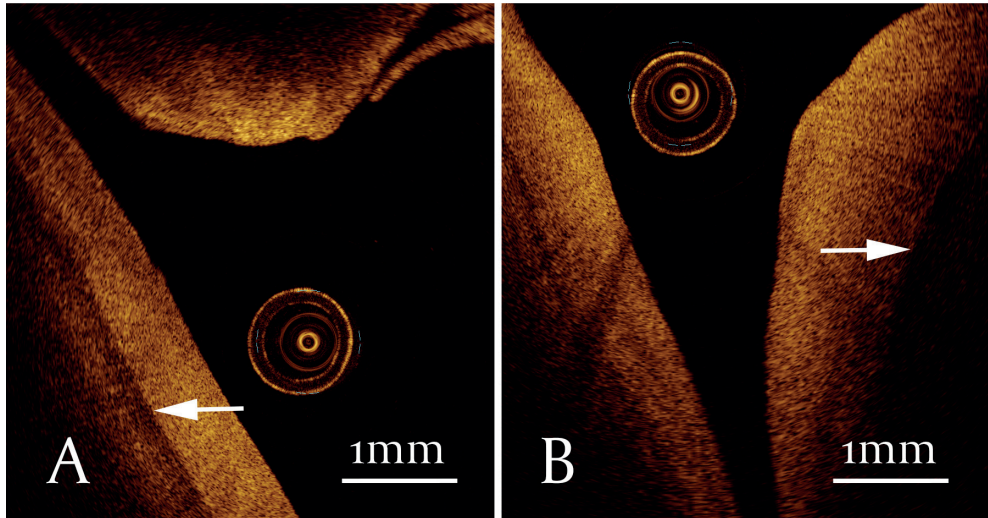


**Fig. 3** Normal cartilage of the sagittal ridge of MC<sub>3</sub> (A) and the dorsal eminence of P<sub>1</sub> (B). The interface between cartilage and subchondral bone is clearly visible (white arrow).

**Table 1** Mean cartilage thickness per site of interest. Thickness ( $\mu\text{m}$ ) of intact and damaged cartilage (defined as OMC<sub>0</sub> and OMC<sub>>0</sub>, respectively) as well as the overall thickness is shown for each SOI (mean  $\pm$  SD)<sup>a</sup>.

	P <sub>1</sub> M	P <sub>1</sub> L	MC <sub>3</sub> M	MC <sub>3</sub> L	SR
Intact	n = 2 1335 $\pm$ 92	n = 1 880	n = 4 723 $\pm$ 48	n = 6 753 $\pm$ 91	n = 12 815 $\pm$ 196
Damaged	n = 12 1122 $\pm$ 188	n = 16 1016 $\pm$ 294	n = 10 781 $\pm$ 145	n = 11 776 $\pm$ 106	n = 5 898 $\pm$ 253
Total	n = 14 1152 $\pm$ 191	n = 17 1008 $\pm$ 286	n = 14 764 $\pm$ 126	n = 17 768 $\pm$ 99	n = 17 839 $\pm$ 209

<sup>a</sup>P<sub>1</sub>M/P<sub>1</sub>L, medial/lateral dorsal eminence of proximal phalanx; MC<sub>3</sub>M/MC<sub>3</sub>L, medial/lateral third metacarpal condyle; SR, sagittal ridge of third metacarpal bone.

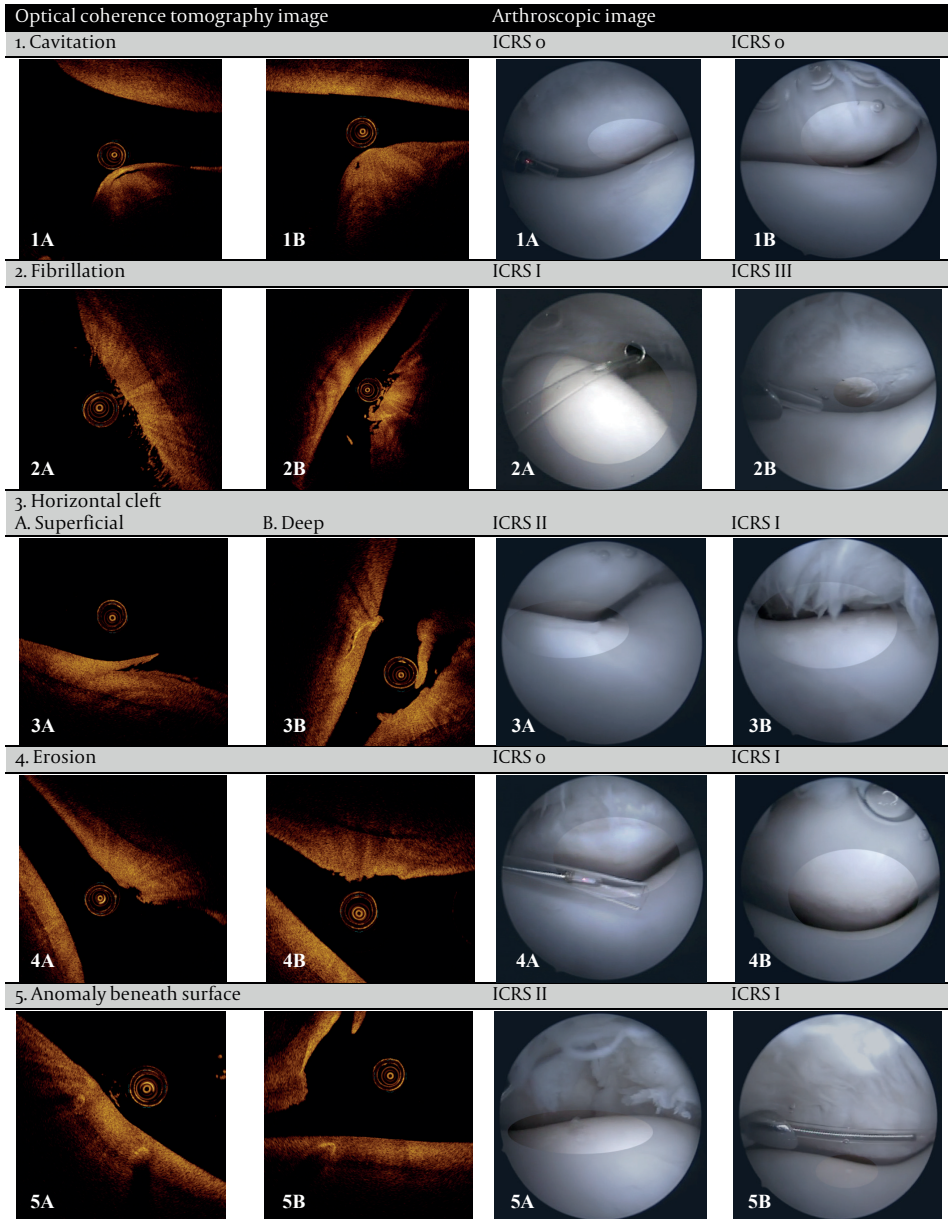


**Fig. 4** Representative images of the OCT morphological characteristics (OMCs) that were found at arthroscopically visible sites within the MCP joint and their corresponding arthroscopic images with ICRS lesion grade. The OCT catheter is visible in some arthroscopic images (2A, 2B, 4A, 5B) and in all OCT images as a circle (diameter = 0.9 mm).

### Comparison between arthroscopic scoring and OCT data

By means of conventional arthroscopic evaluation, 36 sites were graded as ICRS 0, 37 sites as grade I, 12 sites as grade II and 7 sites as grade III. There were no ICRS grade IV lesions. One site was classified as OCD grade II according to the ICRS OCD lesion classification (Brittberg and Winalski, 2003). The OCT ICRS grades differed from the arthroscopic ICRS grades in 46/94 cases, with higher OCT ICRS grades in 29 cases. Based on the inter-item correlation analysis, the agreement at ICRS grades determined by both arthroscopy and OCT was poor ( $r = 0.503$ ).

A spectrum of OMCs could be distinguished: cavitation, fibrillation of the cartilage surface, superficial and deep horizontal cleft formation and erosion. Besides these cartilage lesions, anomalies under the cartilage surface appeared as bright spots on the OCT image. Representative images for each OMC and the corresponding arthroscopic images are provided in fig. 4. For each ICRS grade a varying spectrum of OMCs was found and on the other hand, specific OMCs could be found in several ICRS grades (fig. 5). The OCD lesion appeared to be attached to the subchondral bone and had a fragment diameter of 2.2 mm (fig. 6).

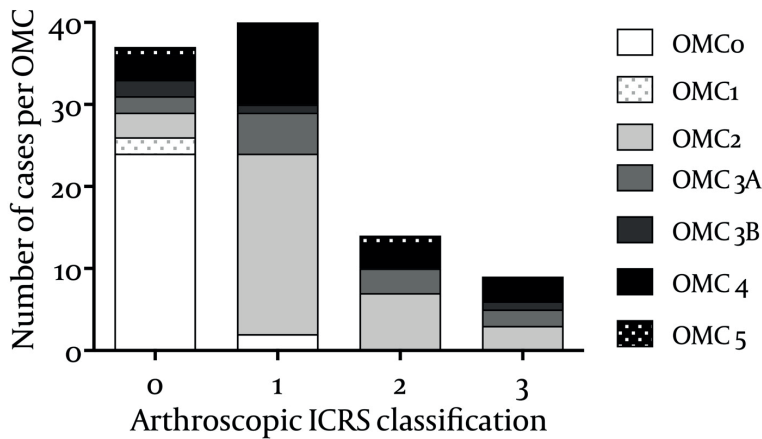


**Fig. 5** For each ICRS grade a varying spectrum of OMCs was found, including OMCs that indicate more severe lesion types than based on ICRS grading: OMC 1, cavitation; OMC 2, fibrillation; OMC 3A, superficial horizontal cleft; OMC 3B, deep horizontal cleft; OMC 4, erosion; OMC 5, anomaly beneath the surface.

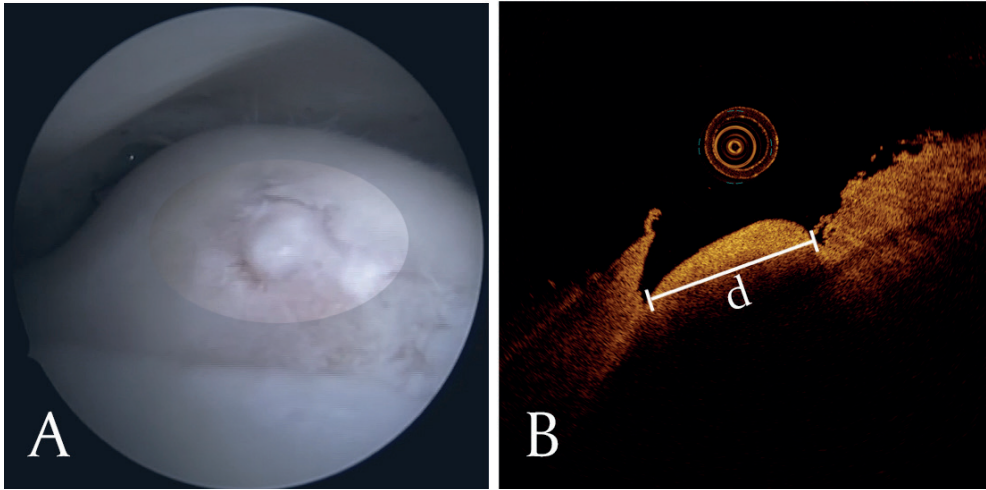


**Fig. 6** The OCD lesion on arthroscopy (A) and the corresponding OCT image (B). Based on the OCT image the fragment is still attached to the subchondral bone and the diameter (d) of the lesion is 2.2 mm.

In eight cases, the OCT catheter could reach the central area of the MCP joint in between MC3 and P1. The additional OMCs that were found at this location were: ulceration (full depth erosion) with and without fragmentation and vertical cleft formation (fig. 7).

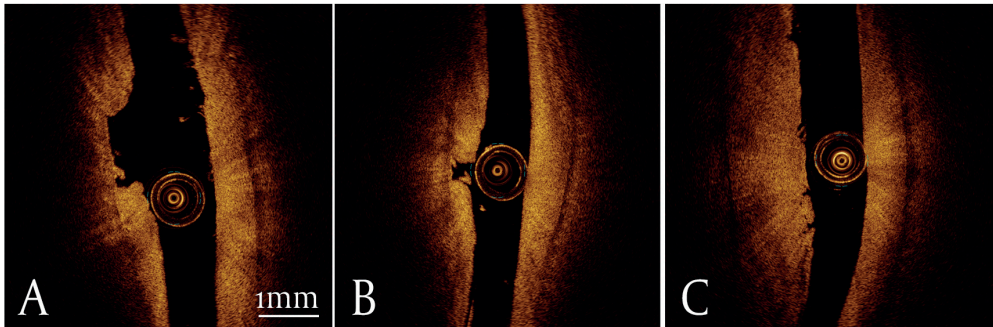


**Fig. 7** OCT Morphological Characteristics (OMCs) of articular cartilage lesions found in between P1 and MC3, showing ulceration (A), ulceration and cartilage fragmentation (B) and superficial vertical clefts (C).

## DISCUSSION

In this study the potential value of OCT for advanced clinical assessment of articular cartilage lesions in the equine MCP joint was investigated. By providing high-resolution cross-sectional images, OCT arthroscopy supplied detailed information on both the surface layer as well as the underlying tissue structure, visualising a full spectrum of articular cartilage characteristics. The full thickness images enabled determination of the cartilage thickness as well as the extension of cartilage lesions. Furthermore, the thin OCT catheter could be directed successfully into the arthroscopically inaccessible region between the central areas of the proximal articular surface of P1 and the distal articular surface of MC3, but only in 8/18 cases. Therefore, information on the cartilage status of a larger surface area, in particular of P1, is obtained with OCT.

The OCT ICRS grades differed from the arthroscopic ICRS grades in 46/94 cases, indicating that OCT evaluation would change the diagnosis on the cartilage status in those cases. Based on the inter-item correlation analysis, the agreement at ICRS grades determined by both arthroscopy and OCT was poor ( $r = 0.503$ ). The discrepancy in the ICRS grades may be due to the possibility of accurate measurements of lesion depth using OCT images. As this is not possible in conventional arthroscopy, differentiating between ICRS scores 2 and 3 is challenging and this may explain the poor reproducibility of arthroscopic grading of cartilage injuries as reported by Spahn et al.<sup>33</sup> Surgeons using the ICRS scoring should therefore be aware of the fact that OCT arthroscopy could provide more reliable ICRS scoring than conventional arthroscopy. This study was limited to the ICRS grading system only, so it is not clear if and to what extent this applies for other scoring systems as well.

Obtaining detailed cross-sectional OCT images allows more precise description of lesion types compared to conventional arthroscopy. Detailed information on lesion characteristics is of importance to assess the possibility for natural repair to take place.<sup>34</sup> Especially in the early phases of degeneration, accurate establishment of the lesion type and severity can help in determining if any intervention (pharmacological and/or surgical) is needed and, if so, what treatment would carry the best prognosis. In addition, the cross-sectional information on the cartilage status given by OCT is appropriate for the follow-up of regeneration processes of the cartilage layer and for monitoring effectiveness of therapeutic interventions.<sup>25,35,36</sup> Another non-destructive imaging technique with the potential to detect early phases of degeneration and subsurface changes in articular cartilage is magnetic resonance imaging (MRI).<sup>37</sup> However, although MRI can provide quantitative information on



cartilage morphology and composition, it currently lacks adequate resolution to detect microstructural changes.<sup>37,38</sup> The high-resolution near real-time visualisation of the cartilage in combination with the possibility to incorporate the OCT catheter in an arthroscope, makes OCT a valuable additional tool during arthroscopic surgery. A potential guiding role in surgical interventions, like articular cartilage debridement, has been proposed.<sup>24</sup>

Extension of the visible area of the articular surface of P<sub>1</sub> would be of diagnostic and prognostic value since initial cartilage degeneration often arises at the dorsal articular margin and progresses to the central parts when the disease becomes more advanced.<sup>32</sup> Using the current OCT catheter, the area between P<sub>1</sub> and MC<sub>3</sub> could be reached in several, but not all joints. This is due to the fact that the catheter has a limited flexibility and for reaching the central area of the joint some space between the articulating bones; i.e. laxity of the collateral ligaments is needed. Hence, lack of compliance of the collateral ligaments may prevent the catheter entering the central joint area. Development of a more flexible and even thinner instrument could increase the visible area even more.

Despite the improved accuracy with respect to lesion characterization by OCT arthroscopy, as compared to plain arthroscopy, the visual assessment still remains subjective. To overcome this, recent studies have focused on quantitative characterization using morphological<sup>24,35</sup> and optical parameters.<sup>23,39,40</sup> The optical surface reflection coefficient (ORC), variation of surface reflection (VSR), OCT roughness index (ORI) and optical backscattering (OBS) are optical parameters that have been investigated using bovine and equine cartilage *in vitro* and *ex vivo*. They appeared to have potential for the quantification of the integrity of the cartilage surface, as well as of changes beneath the surface, although further development is required for implementation in clinical practice.<sup>23,25</sup> The cross-sectional OCT images have been shown to be highly consistent with histological sections<sup>36,41</sup> and also to have a good correlation with a modified Mankin score.<sup>24,42</sup> Comparison with biochemical or biomechanical parameters of articular cartilage could further validate OCT as a valuable, quantitative diagnostic technique for this tissue.

In this study we focused on MCP joints of adult horses. The articular cartilage layer of this joint typically had a thickness of around 1 mm in P<sub>1</sub> and 0.8 mm in MC<sub>3</sub>. In most human joints and also in some other equine joints such as the femoropatellar and femorotibial joints, the thickness of the articular cartilage layer exceeds the penetration depth of the OCT system which is 1.5-2 mm. This limits visualisation to the more superficial layers, making proper classification of cartilage lesions more

challenging. Further development of the OCT system might increase the penetration depth, although this is challenging due to the light absorption in cartilage. Another possibility might be the simultaneous arthroscopic use of OCT and ultrasound.<sup>43</sup> Since arthroscopic ultrasound imaging can provide information on the deeper tissue layers, a combined OCT-ultrasound system could possibly overcome the penetration limitation of OCT.<sup>25</sup>

Apart from the additional value of OCT for optimising the choice of treatment and guiding surgical interventions, as well as its potential role as a follow-up method for cartilage lesions in general, there is a more specific role for its use in equine osteochondrosis (a disorder that is much more common in horses than in humans). The presence of osteochondral (OC) fragments is the most common indication for performing arthroscopy in the equine MCP (and also metatarsophalangeal) joint,<sup>31</sup> and the relatively thin cartilage layer in this joint allows highly accurate quantitative measurements of OC lesion characteristics (i.e. determination of fragment diameter and visualisation of the remaining attachment to the subchondral bone) that are of critical importance for intervention and prognosis. This makes OCT a particularly interesting imaging modality for use in equine orthopaedic surgery. However, before routine clinical application is possible, further developmental and validation work needs to be done. At this stage, high costs involved are prohibitive for clinical use in the horse. However, once the experimental technique becomes more common in human medicine, developments may go fast and costs can be expected to diminish rapidly. Then, clinical use in the horse may become feasible.

## **CONCLUSIONS**

OCT arthroscopy provides detailed information on the characteristics of articular cartilage lesions in the equine MCP joint. Although further developmental and validation work is needed, OCT seems to be a very promising tool for both human and equine use. OCT overcomes the most important limitations related to articular cartilage imaging and classification using conventional arthroscopy.

## **CONFLICT OF INTEREST STATEMENT**

None of the authors of this paper has a financial or personal relationship with other people or organizations that could inappropriately influence or bias the content of the paper.

## **ACKNOWLEDGEMENTS**

Financial support from Kuopio University Hospital (EVO Grant 5227), Strategic funding of the University of Eastern Finland, Paivikki and Sakari Sohlberg Foundation, Academy of Finland (132367), Sigrid Juselius Foundation, Jenny and Antti Wihuri Foundation, TBDB graduate school, Instrumentarium foundation.

## REFERENCES

1. Oakley SP, Portek I, Szomor Z, et al. Arthroscopy - a potential "gold standard" for the diagnosis of the chondropathy of early osteoarthritis. *Osteoarthritis Cartilage*. 2005;13(5):368-378.
2. Acebes C, Roman-Blas JA, Delgado-Baeza E, Palacios I, Herrero-Beaumont G. Correlation between arthroscopic and histopathological grading systems of articular cartilage lesions in knee osteoarthritis. *Osteoarthritis Cartilage*. 2009;17(2):205-212.
3. Kuzmanova SI, Solakov PT, Atanassov AN, Andreev SA. Relevance between arthroscopic pathology and clinical characteristics in knee osteoarthritis. *Folia Med (Plovdiv)*. 2000;42(4):19-22.
4. Oakley SP, Lassere MN. A critical appraisal of quantitative arthroscopy as an outcome measure in osteoarthritis of the knee. *Semin Arthritis Rheum*. 2003;33(2):83-105.
5. Spahn G, Klinger HM, Baums M, Pinkepank U, Hofmann GO. Reliability in arthroscopic grading of cartilage lesions: results of a prospective blinded study for evaluation of inter-observer reliability. *Arch Orthop Trauma Surg*. 2011;131(3):377-381.
6. Vanderperren K, Martens A, Haers H, Duchateau L, Saunders JH. Arthroscopic visualisation of the third metacarpal and metatarsal condyles in the horse. *Equine Vet J*. 2009;41(6):526-533.
7. Brommer H, Rijkenhuizen AB, Brama PA, Barneveld A, van Weeren PR. Accuracy of diagnostic arthroscopy for the assessment of cartilage damage in the equine metacarpophalangeal joint. *Equine Vet J*. 2004;36(4):331-335.
8. Lane JM, Chisena E, Black J. Experimental knee instability: early mechanical property changes in articular cartilage in a rabbit model. *Clin Orthop Relat Res*. 1979;(140):262-265.
9. Lyyra T, Jurvelin J, Pitkanen P, Vaatainen U, Kiviranta I. Indentation instrument for the measurement of cartilage stiffness under arthroscopic control. *Med Eng Phys*. 1995;17(5):395-399.
10. Brama PA, Barneveld A, Karssenberg D, Van Kampen GP, van Weeren PR. The application of an indenter system to measure structural properties of articular cartilage in the horse. Suitability of the instrument and correlation with biochemical data. *J Vet Med Physiol Pathol Clin Med*. 2001;48(4):213-221.
11. Bae WC, Temple MM, Amiel D, Coutts RD, Niederauer GG, Sah RL. Indentation testing of human cartilage: sensitivity to articular surface degeneration. *Arthritis Rheum*. 2003;48(12):3382-3394.
12. Laasanen MS, Toyras J, Hirvonen J, et al. Novel mechano-acoustic technique and instrument for diagnosis of cartilage degeneration. *Physiol Meas*. 2002;23(3):491-503.
13. Saarakkala S, Laasanen MS, Jurvelin JS, et al. Ultrasound indentation of normal and spontaneously degenerated bovine articular cartilage. *Osteoarthritis Cartilage*. 2003;11(9):697-705.
14. Kiviranta P, Lammentausta E, Toyras J, Kiviranta I, Jurvelin JS. Indentation diagnostics of cartilage degeneration. *Osteoarthritis Cartilage*. 2008;16(7):796-804.
15. Saarakkala S, Laasanen MS, Jurvelin JS, Töyräs J. Quantitative ultrasound imaging detects degenerative changes in articular cartilage surface and subchondral bone. *Phys Med Biol*. 2006;51(20):5333-5346.
16. Virén T, Saarakkala S, Kaleva E, Nieminen HJ, Jurvelin JS, Töyräs J. Minimally Invasive Ultrasound Method for Intra-Articular Diagnostics of Cartilage Degeneration. *Ultrasound Med Biol*. 2009;35(9):1546-1554.
17. Kaleva E, Virén T, Saarakkala S, et al. Arthroscopic Ultrasound Assessment of Articular Cartilage in the Human Knee Joint. *Cartilage*. 2011;2(3):246-253.
18. Toyras J, Laasanen MS, Saarakkala S, et al. Speed of sound in normal and degenerated bovine articular cartilage. *Ultrasound Med Biol*. 2003;29(3):447-454.
19. Brezinski ME, Tearney GJ, Bouma B, et al. Optical biopsy with optical coherence tomography. *Ann NY Acad Sci*. 1998;838:68-74.

20. Fercher A, Drexler W, Hitzenberger C, Lasser T. Optical coherence tomography - principles and applications. *Reports Prog Phys*. 2003;66(2):239.
21. Marschall S, Sander B, Mogensen M, Jørgensen TM, Andersen PE. Optical coherence tomography—current technology and applications in clinical and biomedical research. *Anal Bioanal Chem*. 2011;400(9):2699-2720.
22. Fercher AF. Optical coherence tomography – development, principles, applications. *Z Med Phys*. 2010;20(4):251-276.
23. Huang YP, Saarakkala S, Toyras J, Wang LK, Jurvelin JS, Zheng YP. Effects of optical beam angle on quantitative optical coherence tomography (OCT) in normal and surface degenerated bovine articular cartilage. *Phys Med Biol*. 2011;56(2):491-509.
24. Chu CR, Lin D, Geisler JL, Chu CT, Fu FH, Pan Y. Arthroscopic microscopy of articular cartilage using optical coherence tomography. *Am J Sports Med*. 2004;32(3):699-709.
25. Virén T, Huang YP, Saarakkala S, et al. Comparison of ultrasound and optical coherence tomography techniques for evaluation of integrity of spontaneously repaired horse cartilage. *J Med Eng Technol*. 2012;36(3):185-192.
26. Pan Y, Li Z, Xie T, Chu CR. Hand-held arthroscopic optical coherence tomography for in vivo high-resolution imaging of articular cartilage. *J Biomed Opt*. 2003;8(4):648-654.
27. Chu CR, Izzo NJ, Irrgang JJ, Ferretti M, Studer RK. Clinical diagnosis of potentially treatable early articular cartilage degeneration using optical coherence tomography. *J Biomed Opt*. 2007;12(5):051703.
28. Chu CR, Williams A, Tolliver D, Kwok CK, Bruno 3rd S, Irrgang JJ. Clinical optical coherence tomography of early articular cartilage degeneration in patients with degenerative meniscal tears. *Arthritis Rheum*. 2010;62(5):1412-1420.
29. Dougados M, Ayrat X, Listrat V, et al. The SFA system for assessing articular cartilage lesions at arthroscopy of the knee. *J Arthrosc Relat Surg*. 1994;10(1):69-77.
30. Ayrat X. Diagnostic and quantitative arthroscopy: quantitative arthroscopy. *Baillieres Clin Rheumatol*. 1996;10(3):477-494.
31. McIlwraith CW, Nixon AJ, Wright IM, Boening KJ. Diagnostic and surgical arthroscopy of the metacarpophalangeal and metatarsophalangeal joints. In: *Diagnostic and Surgical Arthroscopy in the Horse*. Third Ed. Edinburgh, New York: Mosby Elsevier; 2005:129-196.
32. Brommer H, van Weeren PR, Brama PA, Barneveld A. Quantification and age-related distribution of articular cartilage degeneration in the equine fetlock joint. *Equine Vet J*. 2003;35(7):697-701.
33. Spahn G, Klinger HM, Baums M, Pinkepank U, Hofmann GO. Reliability in arthroscopic grading of cartilage lesions: results of a prospective blinded study for evaluation of inter-observer reliability. *Arch Orthop Trauma Surg*. 2011;131(3):377-381.
34. McIlwraith CW, Nixon AJ, Wright IM, Boening KJ. Arthroscopic methods for cartilage repair. In: *Diagnostic and Surgical Arthroscopy in the Horse*. Third Ed. Edinburgh, New York: Mosby Elsevier; 2005:455-472.
35. Han CW, Chu CR, Adachi N, et al. Analysis of rabbit articular cartilage repair after chondrocyte implantation using optical coherence tomography. *Osteoarthritis Cartilage*. 2003;11(2):111-121.
36. Adams Jr SB, Herz PR, Stamper DL, et al. High-resolution imaging of progressive articular cartilage degeneration. *J Orthop Res*. 2006;24(4):708-715.
37. Bear DM, Williams A, Chu CT, Coyle CH, Chu CR. Optical coherence tomography grading correlates with MRI T2 mapping and extracellular matrix content. *J Orthop Res*. 2010;28(4):546-552.
38. Eckstein F, Burstein D, Link TM. Quantitative MRI of cartilage and bone: degenerative changes in osteoarthritis. *NMR Biomed*. 2006;19(7):822-854.

39. Saarakkala S, Wang SZ, Huang YP, Zheng YP. Quantification of the optical surface reflection and surface roughness of articular cartilage using optical coherence tomography. *Phys Med Biol.* 2009;54(22):6837-6852.
40. Wang SZ, Huang YP, Wang Q, Zheng YP, He YH. Assessment of depth and degeneration dependences of articular cartilage refractive index using optical coherence tomography in vitro. *Connect Tissue Res.* 2010;51(1):36-47. doi:10.3109/03008200902890161
41. Li X, Martin S, Pitris C, et al. High-resolution optical coherence tomographic imaging of osteoarthritic cartilage during open knee surgery. *Arthritis Res Ther.* 2005;7(2):R318-23.
42. Xie T, Guo S, Zhang J, Chen Z, Peavy GM. Determination of characteristics of degenerative joint disease using optical coherence tomography and polarization sensitive optical coherence tomography. *Lasers Surg Med.* 2006;38(9):852-865.
43. Yin J, Yang HC, Li X, et al. Integrated intravascular optical coherence tomography ultrasound imaging system. *J Biomed Opt.* 2010;15(1):10512.







# CHAPTER 3

## Semi-automated International Cartilage Repair Society scoring of equine articular cartilage lesions in optical coherence tomography images

*Equine Veterinary Journal* 49, 552-555 (2017)

---

N.C.R. te Moller<sup>1</sup>

M. Pitkänen<sup>2</sup>

J. K. Sarin<sup>2,3</sup>

S. Väänänen<sup>2,3</sup>

J. Liukkonen<sup>2</sup>

I.O. Afara<sup>4</sup>

P.H. Puhakka<sup>2,3</sup>

H. Brommer<sup>1</sup>

T. Niemelä<sup>5</sup>

R.-M. Tulamo<sup>5</sup>

D. Argüelles Capilla<sup>5</sup>

J. Töyräs<sup>2,3</sup>

---

<sup>1</sup>Department of Equine Sciences, Utrecht University, Utrecht, the Netherlands, <sup>2</sup>Department of Applied Physics, University of Eastern Finland, Kuopio, Finland, <sup>3</sup>Diagnostic Imaging Centre, Kuopio University Hospital, Kuopio, Finland, <sup>4</sup>Department of Electrical and Computer Engineering, Elizade University, Ondo, Nigeria, <sup>5</sup>Department of Equine and Small Animal Medicine, University of Helsinki, Helsinki, Finland

## ABSTRACT

**Background** Arthroscopic optical coherence tomography (OCT) is a promising tool for the detailed evaluation of articular cartilage injuries. However, OCT-based articular cartilage scoring still relies on the operator's visual estimation.

**Objectives** To test the hypothesis that semi-automated International Cartilage Repair Society (ICRS) scoring of chondral lesions seen in OCT images could enhance intra- and interobserver agreement of scoring and its accuracy.

**Study design** Validation study using equine cadaver tissue.

**Methods** Osteochondral samples (n = 99) were prepared from 18 equine metacarpophalangeal joints and imaged using OCT. Custom-made software was developed for semi-automated ICRS scoring of cartilage lesions on OCT images. Scoring was performed visually and semi-automatically by five observers, and levels of inter- and intraobserver agreement were calculated. Subsequently, OCT-based scores were compared with ICRS scores based on light microscopy images of the histological sections of matching locations (n = 82).

**Results** When semi-automated scoring of the OCT images was performed by multiple observers, mean levels of intraobserver and interobserver agreement were higher than those achieved with visual OCT scoring (83% vs. 77% and 74% vs. 33%, respectively). Histology-based scores from matching regions of interest agreed better with visual OCT-based scoring than with semi-automated OCT scoring; however, the accuracy of the software was improved by optimising the threshold combinations used to determine the ICRS score.

**Main limitations** Images were obtained from cadavers.

**Conclusions** Semi-automated scoring software improved the reproducibility of ICRS scoring of chondral lesions in OCT images and made scoring less observer-dependent. The image analysis and segmentation techniques adopted in this study warrant further optimisation to achieve better accuracy with semi-automated ICRS scoring. In addition, studies on in vivo applications are required.

## INTRODUCTION

Articular cartilage lesions are highly prevalent in horses (and in man) and potentially lead to post-traumatic osteoarthritis.<sup>1-3</sup> Options for cartilage repair procedures include a variety of established as well as emerging surgical techniques.<sup>4</sup> However, lesion size and depth must be taken into consideration in selecting the best possible procedure.<sup>5,6</sup> Arthroscopy directly visualises the cartilage layer and adjacent structures and is therefore considered to be the clinical reference standard for joint evaluation. Many different arthroscopic scoring systems have been used to report and compare clinical assessments of the severity of chondral injuries.<sup>7-9</sup> These scoring systems are often based on the classification of lesions according to the depth to which they extend into the cartilage layer. Although this allows for a certain consistency in the evaluation of the articular surface, it does not provide detailed information. Moreover, scoring of the depth of a cartilage lesion is based on the surgeon's estimation and it is difficult to differentiate between superficial and deep lesions.<sup>10</sup>

Earlier studies reported the additional value of optical coherence tomography (OCT) during conventional arthroscopy, which results in the more accurate determination of morphological characteristics of cartilage lesions and better quantification of parameters such as cartilage thickness, surface roughness and repair tissue area.<sup>11,12</sup> Levels of intra- and interobserver agreement in International Cartilage Repair Society (ICRS) scoring of focal lesions based on OCT images were shown to be significantly better than in arthroscopic images.<sup>13</sup> However, scoring of lesions using OCT images remains dependent on the operator's estimation.

The objective of this study was to achieve greater reliability in the scoring of articular cartilage lesions based on OCT images. Therefore, computer software that automatically segments and quantitatively evaluates the articular cartilage layer and assigns ICRS scores was introduced. The reproducibility of visual ICRS scoring by multiple observers was investigated and compared with that of semi-automated scoring of OCT images. In addition, levels of agreement between both methods and ICRS scoring of matching histology sections were determined. The study was based on the hypothesis that semi-automated lesion scoring would increase reproducibility and accuracy, and would provide more quantitative information than visual scoring.

## **MATERIALS AND METHODS**

### **Sample preparation**

Metacarpophalangeal joints of 18 equine cadaver forelimbs (Warmblood horses, aged >2 years) were opened and osteochondral blocks with sites of interest (SoIs; n = 94) as identified by ex vivo OCT arthroscopy imaging in an earlier study<sup>11</sup> were prepared using a bandsaw. Phosphate-buffered saline (PBS), containing protease inhibitors (5 mmol/L disodium ethylenediaminetetraacetic acid [EDTA] and 5 mmol/L benzamidine hydrochloric acid) was used to cool and flush the cartilage and to keep the surface moist during the whole process. Samples were frozen in cups filled with PBS at -20°C until execution of the experiment.

### **Optical coherence tomography assessment**

Osteochondral samples were thawed in their cups in a warm water bath ( $\leq 37^{\circ}\text{C}$ ) and placed in fresh PBS with protease inhibitors. OCT imaging was then performed using the ILUMIEN PCI Optimization System<sup>a</sup> (wavelength:  $1305 \pm 55$  nm) equipped with a C7 Dragonfly Intravascular Imaging Catheter<sup>a</sup> (diameter = 0.9 mm). The positions of previously defined SoIs were established using video-recorded screening and OCT images created during ex vivo OCT arthroscopy.<sup>11</sup> All locations were carefully marked with a felt-tip pen on the cartilage surface in order to find the frame best representing the SoI and to enable subsequent histological analysis of the same site. For OCT imaging, the catheter was positioned just above the SoI and parallel to the cartilage surface. Cross-sectional images (slice thickness: 100  $\mu\text{m}$  per image) were acquired from the predetermined SoIs, supplemented with new sites encountered during OCT scanning of the osteochondral blocks (total number of sites: 99). After OCT analysis, samples were frozen in PBS at -20°C until histological processing was performed.

### **Histological processing**

Immediately after the samples had thawed in a warm water bath, rectangular osteochondral samples (10 x 2 mm) were prepared from each SoI for histological analysis. The marked location was centred and the long side of the sample was set at a right angle to the axial direction of the OCT catheter to ensure similar image directions. The osteochondral samples were fixed in formalin, decalcified in EDTA and embedded in paraffin blocks. Consecutive sections of 3  $\mu\text{m}$  in thickness were cut from the centre of the sample, and stained with Safranin-O. Slices were digitally imaged using an optical microscope (Axio Imager M2)<sup>b</sup>.

## Visual International Cartilage Repair Society scoring of optical coherence tomography and histological images

Visual scoring of both OCT images and digitised histological images was performed according to the ICRS classification system for focal cartilage injuries (ICRS 0, normal; ICRS 1, softening, superficial fibrillation, superficial laceration and fissures; ICRS 2, defect involves <50% of cartilage thickness; ICRS 3, defect involves >50% of cartilage thickness; ICRS 4, defect extends into the subchondral bone<sup>9</sup>). As only chondral lesions were included in this study, scores of 0, 1, 2 or 3 were assigned. The region of interest (RoI) within the image was manually selected beforehand to ensure that each observer scored the same location (fig. 1). Scoring was performed by five veterinary surgeons and repeated three times by each observer at 1-week intervals. The images were blind-coded and randomised during the scoring sessions. The average histology-based score was used as the reference standard against which the accuracy of the scores of matching OCT images was assessed.

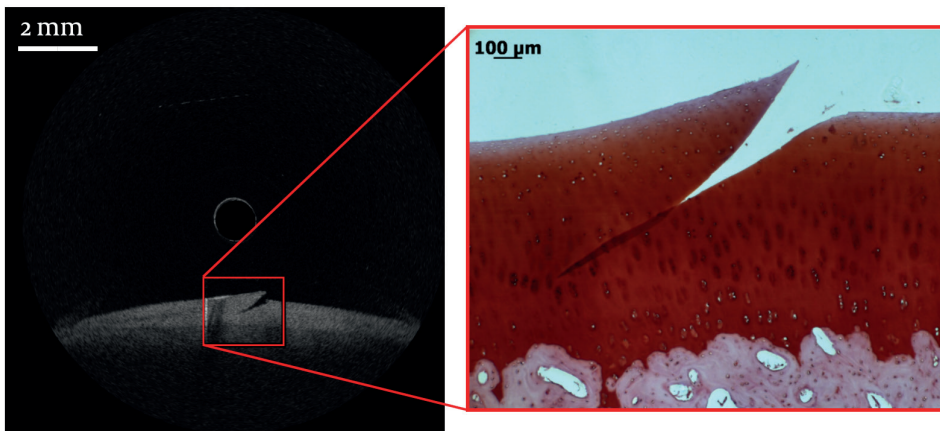


**Fig. 1** Optical coherence tomography of an equine chondral lesion resulting from articular cartilage damage with preselected region of interest and its corresponding histological presentation.

## Semi-automated International Cartilage Repair Society scoring of optical coherence tomography images

Semi-automated scoring software was created using Matlab software (Version R2014a)<sup>6</sup>. Scoring of articular cartilage lesions from OCT images involved six consecutive steps. In the first step, OCT images were preprocessed. During automatic preprocessing, the diameter of the OCT catheter (0.9 mm), was obtained in pixels and used to calibrate the image dimensions. Thereafter, the catheter was erased from the OCT image and the image was rotated so that the cartilage surface was aligned horizontally (fig. 2A). The second and third steps included the detection of the

superficial layer of the cartilage and the bone-cartilage (B-C) interface, respectively, within a ROI identified by the manual placement of a window (fig. 2B). In the fourth step, the relative lesion depth (as a percentage of the average thickness of the cartilage layer) was calculated. The surface and B-C interface were presented in a binary image (fig. 2C). A 20-pixel wide analysis window (indicated with red, dashed lines) that D) is moved horizontally in 1-pixel intervals and subsequently taking the largest value. In step 5, the optical roughness index (ORI) is calculated<sup>14</sup>. In step 6, the lesion is classified by an International Cartilage Repair Society score based on the RLD and ORI values.

$$d_{ld\_w} = \frac{\bar{d} - \min(d)}{\bar{d}}, \quad (1)$$

where  $d$  is a vector including the cartilage thickness for each column of the analysis window,  $\bar{d}$  is its average and  $\min(d)$  is the minimal thickness within the window. The calculation of  $d_{ld\_w}$  was repeated for all window locations (fig 2D), and lesion depth ( $d_{ld}$ ) was defined as the largest value of  $d_{ld\_w}$ . In step 5, the roughness of the articular surface, quantified as the optical roughness index (ORI)<sup>14</sup> was determined. Finally, the lesion was classified according to the ICRS scoring system in step 6.

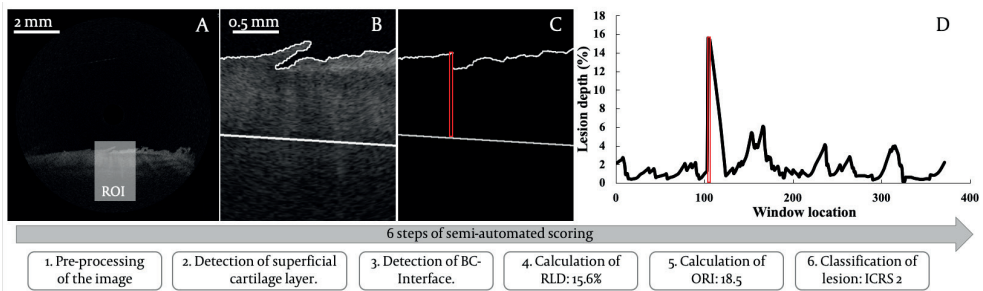


**Fig. 2** Procedure for semi-automated scoring of optical coherence tomography (OCT) images. A) In step 1, during preprocessing, image dimensions are calibrated, the OCT catheter is erased, and the articular surface is oriented horizontally. Subsequently, the region of interest (ROI) is manually determined. B) In steps 2 and 3, the ROI is analysed to detect the superficial cartilage layer and the bone-cartilage (B-C) interface. C) In step 4, the relative lesion depth (RLD) is calculated from a binary image by calculating the lesion depth in a 20-pixel wide analysis window (indicated with red, dashed lines) that D) is moved horizontally in 1-pixel intervals and subsequently taking the largest value. In step 5, the optical roughness index (ORI) is calculated<sup>14</sup>. In step 6, the lesion is classified by an International Cartilage Repair Society score based on the RLD and ORI values.

## Determination of thresholds for International Cartilage Repair Society scoring

According to the ICRS scoring system, ICRS 3 is assigned when a chondral lesion exceeds 50% of the cartilage thickness. Thresholds for ICRS 0, 1 and 2, however, have not been numerically quantified. An independent group of OCT images of a variety of articular cartilage lesions was used to calibrate these thresholds in the

semi-automated scoring software. These images had already been ICRS-scored by multiple observers in three repetitions<sup>13</sup>. The ORI and relative lesion depth for each image were determined with the software and compared with the average visually determined ICRS scores to set the thresholds for ICRS scores 1 and 2. A lesion with an ORI of  $>8.0 \mu\text{m}$  and depth of  $<8\%$  of cartilage thickness was classified as ICRS 1, and a lesion extending to a depth of 8-50% of the cartilage thickness was classified as ICRS 2. When neither of these criteria were applicable (i.e. ORI  $<8 \mu\text{m}$  and relative lesion depth  $<8\%$ ), and ICRS score of 0 was assigned. This combination of thresholds was called 'threshold combination 1' (TC1) and results obtained using TC1 were used for agreement calculations. Additionally, a second threshold combination (TC2) was defined based on visual scores of the current set of OCT images. With TC2, ICRS 1 was assigned when the ORI was  $>5.6 \mu\text{m}$  and lesion depth was  $<8\%$  of the cartilage thickness. The semi-automated scoring process is summarised in Fig 2. A more detailed explanation of the method is provided in Supplementary Item 1.

To enable comparisons between visual (OCT- and histology-based) and semi-automated scoring, the adjustable analysis window was placed precisely on the preselected RoI for visual scoring. Additionally, the same five veterinary surgeons were requested to manually select the RoI prior to semi-automated scoring such that it included the most severe part of the lesion, in order to investigate variation caused solely by RoI selection. For this, an analysis window covering the entire cartilage layer and the B-C interface, and with a fixed width (1.9 mm), was used. Three scoring rounds were executed with similar time intervals, randomisation and blind-coding as in visual scoring.

## Data analysis

For repeated visual and semi-automated ICRS scoring, levels of intra- and interobserver agreement were determined by calculating the percentages of total agreement within and between different observers. For interobserver agreement, the kappa index ( $\kappa$ ) for multiple observers and the intraclass correlation coefficient (ICC; two-way random model for single measurements) were calculated to correct for chance and the relative importance of disagreement.<sup>15-17</sup> The distribution of ICRS scores assigned to the images was evaluated and differences between methods were analysed using Kruskal-Wallis and Dunn's multiple comparison tests. The weighted  $\kappa$ <sup>15,18</sup> was calculated to evaluate intermethod agreement between OCT- and histology-based scores. For statistical analysis, Excel (Version 2010)<sup>d</sup>, IBM SPSS Statistics for Windows (Version 22.0)<sup>e</sup> and GraphPad Prism (Version 5.2)<sup>f</sup> were used. The level of significance was set at  $P \leq 0.05$ .

## RESULTS

Out of 99 images, 82 were included for analysis: three were excluded as a result of artefacts during histological processing, six as a result of insufficient quality of the OCT image (either poor resolution caused by incorrect exportation or no visible B-C interface) and eight as a result of no or poor matching between OCT images and histological sections.

### Reproducibility of visual and semi-automated scoring

As expected, repeated scoring of the preselected RoIs using the software resulted in 100% reproducibility. When the RoIs were selected manually by five different observers prior to scoring by the software, reproducibility decreased to 74% according to interobserver agreement. However, repeated scoring of these manually selected RoIs by the software resulted in higher agreement values than repeated visual scoring (33% inter-observer agreement) of the preselected RoIs by five different observers (table 1).

**Table 1** Reproducibility of visual International Cartilage Repair Society scoring and selection of the region of interest during semi-automated scoring of optical coherence tomography (OCT) images

	Visual OCT scoring of preselected RoI	Semi-automated scoring with manual RoI selection
Mean ( $\pm$ s.d.) intraobserver agreement (%)	77 $\pm$ 10.8	83 $\pm$ 2.9
Observer 1	85	83
Observer 2	87	84
Observer 3	79	81
Observer 4	60	87
Observer 5	76	79
Interobserver agreement (%)	33	74
$\kappa$	0.51	0.80
ICC (95% CI)	0.80 (0.74-0.86)	0.90 (0.87-0.93)

Total interobserver agreement percentage,  $\kappa$  and ICC were calculated using the first scoring round of each observer. 95% CI, 95% confidence interval; ICC, intraclass correlation coefficient;  $\kappa$  = kappa value for multiple observers; RoI, region of interest.

### Accuracy of optical coherence tomography-based scoring and effects of different thresholds

The distribution of ICRS scores assigned by histology differed significantly compared with those assigned by semi-automated OCT scoring (for ICRS 0, 1 and 3) and by visual OCT scoring (for ICRS 2). Visual and semi-automated OCT scoring was significantly different for images assigned to ICRS 3 with histology (fig. 3). The



highest degree of variation between the different observers for visual OCT scoring was found with ICRS scores of 0 and 1. Overall accuracy (expressed as the percentage of correct OCT evaluation relative to matching histological images; fig. 4 and table 2) and intermethod agreement between histology and semi-automated OCT scoring were better with TC<sub>2</sub> than with TC<sub>1</sub> (table 3). Visual OCT scoring achieved better intermethod agreement with histology-based scoring than semi-automated OCT scoring (table 3).

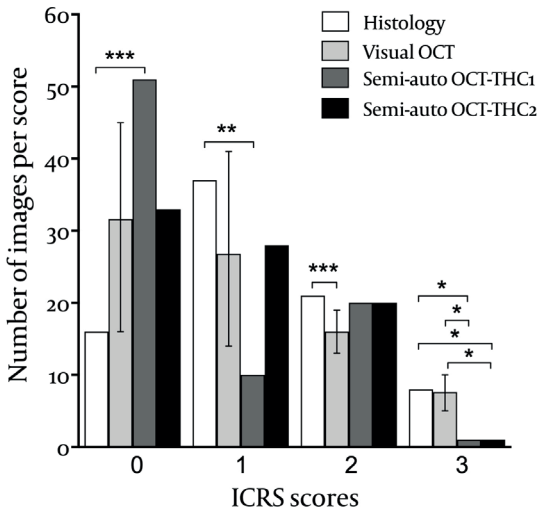


**Fig. 3** Distributions of International Cartilage Repair Society (ICRS) scores assigned to the preselected regions of interest by means of histology, visual optical coherence tomography (OCT) scoring by multiple observers and semi-automated OCT scoring with threshold combinations 1 and 2 (TC<sub>1</sub>, TC<sub>2</sub>). Data for visual OCT show the mean and range of scores by five observers. \* $P < 0.05$ ; \*\* $P < 0.01$ ; \*\*\* $P < 0.001$ .

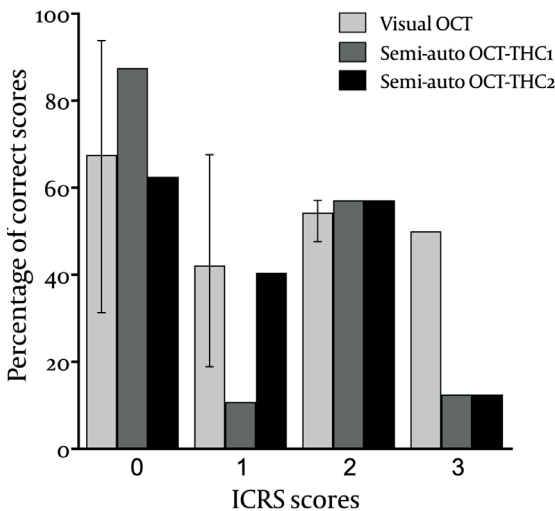


**Fig. 4** Optical coherence tomography (OCT)-based scoring as compared with histological scoring of cartilage lesions using the International Cartilage Repair Society (ICRS) scoring system. Percentages of correct scoring were calculated as the number of histologically scored images for each grade that was correctly recognized by visual OCT-based scoring and semi-automated OCT scoring with threshold combination 1 and 2 (TC<sub>1</sub>, TC<sub>2</sub>). Data for visual OCT show the mean and range of scores by five observers.

**Table 2** Optical coherence tomography (OCT)-based scoring compared with histological scoring of cartilage lesions using the International Cartilage Repair Society (ICRS) scoring system

	Histology	ICRS 0 (n = 16)	ICRS 1 (n = 37)	ICRS 2 (n = 21)	ICRS 3 (n = 8)	Percentage correct*
OCT visual observer 1	0	<b>10</b>	15	2	0	63
	1	6	<b>22</b>	7	2	60
	2	0	0	<b>11</b>	2	52
	3	0	0	1	<b>4</b>	50
OCT visual observer 2	0	<b>11</b>	23	1	0	69
	1	5	<b>12</b>	7	0	32
	2	0	1	<b>12</b>	4	57
	3	0	1	1	<b>4</b>	50
OCT visual observer 3	0	<b>13</b>	21	1	0	81
	1	3	12	2	1	32
	2	0	4	<b>12</b>	3	57
	3	0	0	6	<b>4</b>	50
OCT visual observer 4	0	<b>5</b>	10	1	0	31
	1	11	<b>25</b>	5	0	68
	2	0	2	<b>10</b>	4	48
	3	0	0	5	<b>4</b>	50
OCT visual observer 5	0	<b>15</b>	29	1	0	94
	1	1	7	4	2	19
	2	0	1	<b>12</b>	2	57
	3	0	0	4	<b>4</b>	50
OCT semi-automated TC1†	0	<b>14</b>	30	5	2	88
	1	2	<b>4</b>	4	0	11
	2	0	3	<b>12</b>	5	57
	3	0	0	0	<b>1</b>	12
OCT semi-automated TC2†	0	<b>10</b>	19	3	1	63
	1	6	<b>15</b>	6	1	41
	2	0	3	<b>12</b>	5	57
	3	0	0	0	<b>1</b>	13

TC1, threshold combination 1; TC2, threshold combination 2. Values showing the number of images that were correctly recognized by OCT-based scoring are bold. \*The percentage of correct scoring was calculated as the percentage of histologically scored images for each grade that were correctly recognized by OCT-based scoring. † Scores based on software analysis of the region of interest matching that used for visual scoring.

**Table 3** Intermethod agreement between histology-based scoring and visual or semi-automated optical coherence tomography (OCT) scoring using the International Cartilage Repair Society (ICRS) scoring system

	$\kappa$ (95% CI)
Histology-OCT visual observer 1	0.64 (0.44-0.85)
Histology-OCT visual observer 2	0.67 (0.47-0.87)
Histology-OCT visual observer 3	0.71 (0.50-0.92)
Histology-OCT visual observer 4	0.68 (0.46-0.90)
Histology-OCT visual observer 5	0.66 (0.49-0.88)
Histology-OCT semi-automated TC1	0.48 (0.31-0.66)
Histology-OCT semi-automated TC2	0.51 (0.32-0.71)

For visual OCT scoring, the first of three scoring rounds was used for each observer. 95% CI, 95% confidence interval;  $\kappa$ , weighted kappa; TC1, threshold combination 1; TC2, threshold combination 2.

## DISCUSSION

In this study, a semi-automated software package for ICRS scoring of articular cartilage lesions in OCT images was introduced in order to achieve more reliable results than those obtained with visual scoring methods in current use. Semi-automated scoring of OCT images by multiple observers resulted in higher levels of mean intraobserver and interobserver agreement compared with visual OCT scoring. Additionally, a lower standard deviation of intraobserver agreement was obtained with semi-automated scoring. However, intermethod agreement between histology- and visual-OCT-based scoring was better than that between histology-based and semi-automated OCT scoring of matching RoIs.

Two different sources of variation in the reproducibility of OCT-based scoring were investigated. For visual scoring, the RoI was selected beforehand and thus the disagreement within and between observers could be attributed mainly to the interpretation of lesion grade by each observer. Using semi-automated scoring, differences in the assessment of lesion grades based on observer interpretation were eliminated and the observers were responsible only for the selection of the RoI. The software was 100% reproducible in repeated scoring of the same RoI; however, when the RoI was selected manually prior to scoring, 74% agreement between observers was achieved. Even within each individual, small disagreements in RoI selection were found. This suggests that, in addition to the variation that arises from differences in the interpretation of lesion severity, selection of the RoI also contributes significantly to disagreement within and between observers in scoring of articular cartilage lesions. Nevertheless, the lower standard deviation shows that

the contribution of RoI selection to variations within observers is less than that of the interpretation of lesion grade. In addition to the higher levels of interobserver and mean intraobserver agreement achieved with semi-automated scoring, this implies that the software made the ICRS scoring of chondral lesions less observer-dependent.

Levels of intra- and interobserver agreement of OCT-based ICRS scoring were better than those reported for ICRS scoring by means of conventional arthroscopy.<sup>10</sup> Levels of agreement within and between observers were in the same order of magnitude as those reported previously for visual ICRS scoring of OCT images.<sup>13</sup> Intermethod agreement between histological and visual OCT scoring was higher than that between histological and semi-automated OCT scoring, indicating that visual scoring is more accurate when histology is used as the reference standard. However, it is important to note that visual scoring of both OCT and histological images was performed by the same five observers, who presumably made similar assessments for each corresponding pair of images. Scores manually assigned to the OCT images are naturally more consistent with scores manually assigned to their corresponding histological images than with scores assigned by the software. For the software, TC1 was based on an independent set of OCT images and ICRS 1 was assigned if the ORI was  $>8 \mu\text{m}$ . However, the 'real' limit may also be higher or lower. The second threshold defined for ICRS 1 based on the OCT images used in this study (TC2) resulted in better overall accuracy and intermethod agreement than TC1. This shows that the accuracy of the software can be improved by optimising the threshold combinations used to determine the ICRS score. Another factor contributing to the lower intermethod agreement between histology-based and semi-automated scoring may refer to the fact that the scoring software was unable to detect thin, closed cracks extending into the cartilage layer. As the software differentiates between ICRS scores of 2 and 3 based on calculations of relative lesion depth, this resulted in a significantly lower number of images assigned to ICRS 3. This problem warrants further optimisation of the image analysis and segmentation techniques adopted in this study.

A significantly higher number of images was classified as ICRS 0 by both visual and semi-automated OCT scoring compared with histology-based scoring. A similar observation was reported earlier.<sup>19</sup> This may be attributable to lower resolutions of the OCT images, effectively limiting the minimal discernible roughness of the cartilage surface, and the possible expansion of lesions during the preparation of histological samples. Additionally, the difficulty of matching the planes of histology and OCT images exactly should be acknowledged because only a small discrepancy in

the orientation of a slide may result in different scoring outcomes.<sup>12,19</sup> Furthermore, in the present study, the osteochondral samples were subjected to one freeze-thaw cycle prior to OCT analysis and one prior to histological processing. Repetitive freezing and thawing may lead to minor alterations in tissue structure<sup>20</sup>, although it is highly unlikely that these changes would result in alterations sufficiently visually apparent to influence lesion scoring.<sup>21-23</sup>

Magnetic resonance imaging (MRI) can be used to diagnose and assess chondral damage pre-operatively. However, defect sizes were underestimated in 74-85% of cases compared with arthroscopic visualisation after debridement.<sup>24,25</sup> The advantages of OCT imaging include its high-resolution and real-time visualisation of small morphological changes within the cartilage that can be obtained during conventional arthroscopic procedures. This is of interest not only in surgical planning and treatment selection, but also in monitoring and evaluation after cartilage repair procedures. For example, the semi-automated evaluation of cartilage defects based on OCT images may improve ICRS macroscopic evaluation of cartilage repair.<sup>26</sup> The classification of lesions in only four grades may lead to inaccuracy arising from 'intra-grade differences' (i.e. differences in lesion depth may be less between two successive grades than within the same grade), which may lead to situations in which absolute lesion changes are not apparent or are over- or under-estimated in the course of an evaluation period. Therefore, the calculation of quantitative parameters such as the ORI and relative lesion depth as a percentage of cartilage thickness is essential. Other quantitative OCT parameters of articular cartilage determined by (semi-)automated software analysis that have been reported recently include cartilage thickness, repair tissue area, various surface roughness parameters, and homogeneity, attenuation and backscattering indices.<sup>12,14,27-30</sup> A combination of these quantitative parameters is of particular relevance in the detection of early degenerative changes in areas surrounding articular cartilage lesions. Furthermore, combining 2D and 3D OCT imaging may improve the detection of structural cartilage degeneration and allow for better appreciation of lesions of the cartilage and adjacent tissue.<sup>19</sup>

In future research, we aim to explore the feasibility of semi-automated scoring of articular cartilage lesions *in vivo*. The software introduced in this study has the potential to provide surgeons with objectively determined ICRS scores of apparent defects intraoperatively. No human input other than in the manual selection of the RoI is required as the algorithm is fully automated, which will facilitate clinical implementation. Current challenges mainly relate to the positioning of the catheter to achieve perpendicular placement to the cartilage layer, which may be difficult in

narrow joint cavities in vivo, and the limited penetration depth of OCT that prevents the software from determining the B-C interface and thus further analysis in cartilage layers thicker than 1.5-2 mm. However, advancements in tissue optical clearing may enable the characterisation of thicker cartilage layers in the future.<sup>31,32</sup>

## CONCLUSIONS

The use of semi-automated scoring software improved the reproducibility of ICRS scoring of articular cartilage in OCT images and made scoring less dependent on the observer compared with visual scoring. This may offer a more reliable technique for the determination of cartilage lesion size and severity than do current (subjective) methods. The image analysis and segmentation techniques adopted in this study warrant further optimisation to achieve better accuracy with semi-automated ICRS scoring. Studies on in vivo application are required.

## SOURCES OF FUNDING

This project was supported by funding from the Academy of Finland (project 267551, University of Eastern Finland), Kuopio University Hospital (VTR projects 5041750 and 5041744) and the Department of Equine Sciences of Utrecht University.

## ACKNOWLEDGEMENTS

Dr. Chris van de Lest and dr. Hans Vernooij, Department of Equine Sciences, Utrecht University, are acknowledged for the provision of statistics advice. Professor René van Weeren, Department of Equine Sciences, is acknowledged for writing assistance and general support.

Manufacturers' addresses:

<sup>a</sup>St. Jude Medical, St. Paul, MN, USA.

<sup>b</sup>Axio Imager M2, Carl Zeiss MicroImaging, Jena, Germany.

<sup>c</sup>MathWorks Inc., Natick, MA, USA.

<sup>d</sup>Microsoft Corp, Redmond, WA, USA.

<sup>e</sup>IBM Corp, Armonk, New York, USA.

<sup>f</sup>GraphPad Software, Inc., La Jolla, CA, USA.

## REFERENCES

1. McIlwraith CW. Principles and Practices of Joint Disease Treatment. In: *Diagnosis and Management of Lameness in the Horse*. 2nd ed. St. Louis: Elsevier Saunders; 2011:840-852.
2. Widuchowski W, Widuchowski J, Trzaska T. Articular cartilage defects: Study of 25,124 knee arthroscopies. *Knee*. 2007;14(3):177-182.
3. Kramer WC, Hendricks KJ, Wang J. Pathogenetic mechanisms of posttraumatic osteoarthritis: opportunities for early intervention. *Int J Clin Exp Med*. 2011;4(4):285-298.
4. Cokelaere S, Malda J, van Weeren R. Cartilage defect repair in horses: Current strategies and recent developments in regenerative medicine of the equine joint with emphasis on the surgical approach. *Vet J*. 2016;214:61-71.
5. Bekkers JEJ, Inklaar M, Saris DBF. Treatment Selection in Articular Cartilage Lesions of the Knee: A Systematic Review. *Am J Sports Med*. 2009;37(1\_suppl):148S-155S.
6. Farr J, Cole B, Dhawan A, Kercher J, Sherman S. Clinical cartilage restoration: evolution and overview. *Clin Orthop Relat Res*. 2011;469(10):2696-2705.
7. Outerbridge RE. The etiology of chondromalacia patellae. *J bone Jt surgery British Vol*. 1961;43-B:752-757.
8. Dougados M, Ayrat X, Listrat V, et al. The SFA system for assessing articular cartilage lesions at arthroscopy of the knee. *J Arthrosc Relat Surg*. 1994;10(1):69-77.
9. Brittberg M. Evaluation of cartilage injuries and cartilage repair. *J Bone Jt Surgery-American Vol*. 2003;85-A(Supplement 2):58-69.
10. Spahn G, Klinger HM, Baums M, Pinkepank U, Hofmann GO. Reliability in arthroscopic grading of cartilage lesions: results of a prospective blinded study for evaluation of inter-observer reliability. *Arch Orthop Trauma Surg*. 2011;131(3):377-381.
11. te Moller NCR, Brommer H, Liukkonen J, et al. Arthroscopic optical coherence tomography provides detailed information on articular cartilage lesions in horses. *Vet J*. 2013;197(3):589-595.
12. Cernohorsky P, Kok AC, Bruin DM De, et al. Comparison of optical coherence tomography and histopathology in quantitative assessment of goat talus articular cartilage. *Acta Orthop*. 2015;86(2):257-263.
13. Niemelä T, Virén T, Liukkonen J, et al. Application of optical coherence tomography enhances reproducibility of arthroscopic evaluation of equine joints. *Acta Vet Scand*. 2014;56(3):1-8.
14. Saarakkala S, Wang SZ, Huang YP, Zheng YP. Quantification of the optical surface reflection and surface roughness of articular cartilage using optical coherence tomography. *Phys Med Biol*. 2009;54(22):6837-6852.
15. Fleiss JL, Cohen J. The equivalence of weighted kappa and the intraclass correlation coefficient as measures of reliability. *Educ Psychological Meas*. 1973;33:613-619.
16. Shrout PE, Fleiss JL. Intraclass correlations: Uses in assessing rater reliability. *Psychol Bull*. 1979;86(2):420-428.
17. Sertdemir Y, Burgut HR, Alparslan ZN, Unal I, Gunasti S. Comparing the methods of measuring multi-rater agreement on an ordinal rating scale: a simulation study with an application to real data. *J Appl Stat*. 2013;40(7):1506-1519.
18. Cohen J. Weighted kappa: nominal scale agreement with provision for scaled disagreement or partial credit. *Psychol Bull*. 1968;70(4):213-220.
19. Nebelung S, Brill N, Marx U, et al. Three-dimensional imaging and analysis of human cartilage degeneration using Optical Coherence Tomography. *J Orthop Res*. 2015;33(5):651-659.

20. Zheng S, Xia Y, Bidthanapally A, Badar F, Ilisar I, Duvoisin N. Damages to the extracellular matrix in articular cartilage due to cryopreservation by microscopic magnetic resonance imaging and biochemistry. *Magn Reson Imaging*. 2009;27(5):648-655.
21. Qu C, Hirviniemi M, Tiitu V, Jurvelin JS, Töyräs J, Lammi MJ. Effects of Freeze-Thaw Cycle with and without Proteolysis Inhibitors and Cryopreservant on the Biochemical and Biomechanical Properties of Articular Cartilage. *Cartilage*. 2014;5(2):97-106.
22. Szarko M, Muldrew K, Bertram JE. Freeze-thaw treatment effects on the dynamic mechanical properties of articular cartilage. *BMC Musculoskelet Disord*. 2010;11:231.
23. Changoor A, Fereydoonzad L, Yaroshinsky A, Buschmann MD. Effects of refrigeration and freezing on the electromechanical and biomechanical properties of articular cartilage. *J Biomech Eng*. 2010;132(6):064502-1-6.
24. Gomoll AH, Yoshioka H, Watanabe A, Dunn JC, Minas T. Preoperative Measurement of Cartilage Defects by MRI Underestimates Lesion Size. *Cartilage*. 2011;2(4):389-393.
25. Campbell AB, Knopp M V, Kolovich GP, et al. Preoperative MRI Underestimates Articular Cartilage Defect Size Compared With Findings at Arthroscopic Knee Surgery. *Am J Sports Med*. 2013;41(3):590-595.
26. van den Borne MPJ, Raijmakers NJH, Vanlauwe J, et al. International Cartilage Repair Society (ICRS) and Oswestry macroscopic cartilage evaluation scores validated for use in Autologous Chondrocyte Implantation (ACI) and microfracture. *Osteoarthr Cartil*. 2007;15(12):1397-1402.
27. Nebelung S, Marx U, Brill N, et al. Morphometric grading of osteoarthritis by optical coherence tomography - An ex vivo study. *J Orthop Res*. 2014;32(10):1381-1388.
28. Puhakka PH, te Moller NCR, Afara IO, et al. Estimation of articular cartilage properties using multivariate analysis of optical coherence tomography signal. *Osteoarthr Cartil*. 2015;23(12):2206-2213.
29. Brill N, Riedel J, Schmitt R, et al. 3D Human cartilage surface characterization by optical coherence tomography. *Phys Med Biol*. 2015;60(19):7747-7762.
30. Virén T, Huang YP, Saarakkala S, et al. Comparison of ultrasound and optical coherence tomography techniques for evaluation of integrity of spontaneously repaired horse cartilage. *J Med Eng Technol*. 2012;36(3):185-192.
31. Bykov A, Hautala T, Kinnunen M, et al. Imaging of subchondral bone by optical coherence tomography upon optical clearing of articular cartilage. *J Biophotonics*. 2016;9(3):270-275.
32. Zhu D, Larin K V, Luo Q, Tuchin V V. Recent progress in tissue optical clearing. *Laser Photon Rev*. 2013;7(5):732-757.



## SUPPLEMENTARY INFORMATION

### Supplementary item 1 Detailed description of the semi-automatic scoring method of optical coherence tomography images.

Scoring of articular cartilage lesions from optical coherence tomography (OCT) images includes the following steps: 1) preprocessing of the OCT images, 2) detection of the superficial layer of the cartilage, 3) detection of the bone-cartilage interface, 4) calculation of the relative lesion depth, 5) calculation of the optical roughness index (ORI), and 6) classification of the lesion according to the ICRS scoring system.

#### 1. Preprocessing of the optical coherence tomography images

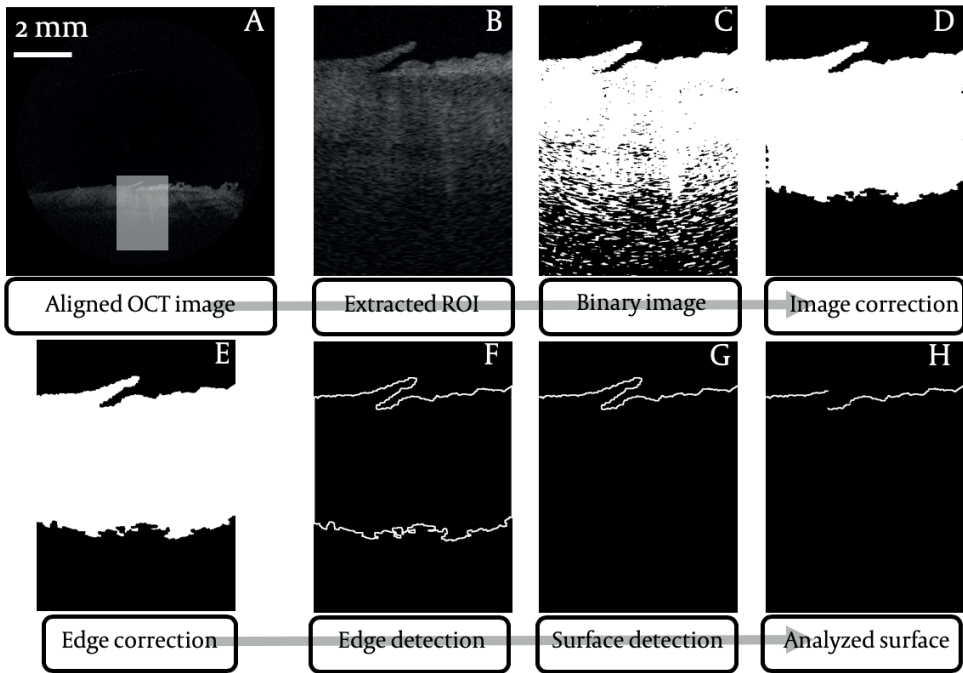
During preprocessing, the catheter is detected, its size in pixels is measured to acquire the sampling rate of the image and the catheter is erased from the OCT image according to the following steps:

1. The grayscale OCT image is transformed into a binary image using a threshold of 21% of the maximum grayscale value of the image. Subsequently, morphological closing with a 5x5 mask is performed and the holes are filled.
2. The object that covers the central pixel of the image is chosen (catheter is at the center).
3. The object is closed with a disk mask with a diameter of 7 pixels and holes in the object are filled again.
4. Other objects may touch the catheter in the image and this is corrected as follows: the roundness of the catheter object is calculated as  $R_c = d_{\text{minor}} / d_{\text{major}}$  where the lengths of the major and minor axes are the longest diameter of the object and the diameter of the object in the direction perpendicular to the major axis. Thereafter,
  - a) If  $R_c < 0.9$ , object is eroded with 3x3 filter
  - b)  $R_c$  is recalculated
  - c) Steps a and b are iterated until  $R_c \geq 0.9$
  - d) Object is dilated with a 3x3 filter to the original size, i.e., dilation is repeated with the same number of iterations as during eroding.
5. The final radius of the catheter is calculated from the equivalent diameter of the catheter and the catheter is erased from the OCT image.

Image rotation is performed to align the cartilage surface horizontally in the OCT image:

1. The original OCT image is transformed into a binary image using a threshold of 14% of the maximum grayscale value. Objects smaller than 0.25% of the total area of the image are removed and holes in the image are filled.
2. Objects, except the two largest assumed to be the cartilage layers, are removed from the image.
3. If the image includes more than one cartilage surface, the user is asked to point the cartilage surface that needs to be analyzed.
4. An ellipse is fitted to this object and the image is rotated such that the major axis of the ellipse is aligned horizontally.

**2. Detection of the superficial layer of the cartilage**



**Supplementary Fig. 1** The subsequent steps in cartilage surface detection.

The user sets a region of interest (RoI) on the horizontally-aligned cartilage in the OCT image (fig 1A). The RoI (fig. 1B) is then analyzed to detect the cartilage surface. The binary image (fig. 1C) is created by using a threshold of  $t = t_{\text{Otsu}} - (1 - t_{\text{Otsu}}) / 15$ , where the threshold  $t_{\text{Otsu}}$  has been calculated using Otsu's method.<sup>1</sup> Using  $t_{\text{Otsu}}$  directly would slightly overestimate the threshold.

Objects <5% of the total area of the RoI are removed and holes <0.1% of the total area of the RoI are filled. This is followed by removal of 1-pixel-wide bridges connecting two objects, dilation of the image with a 3-pixels-long vertical line-mask and repeated removal of areas <5% and filling of holes <1% of the total area of RoI (fig. 1D).

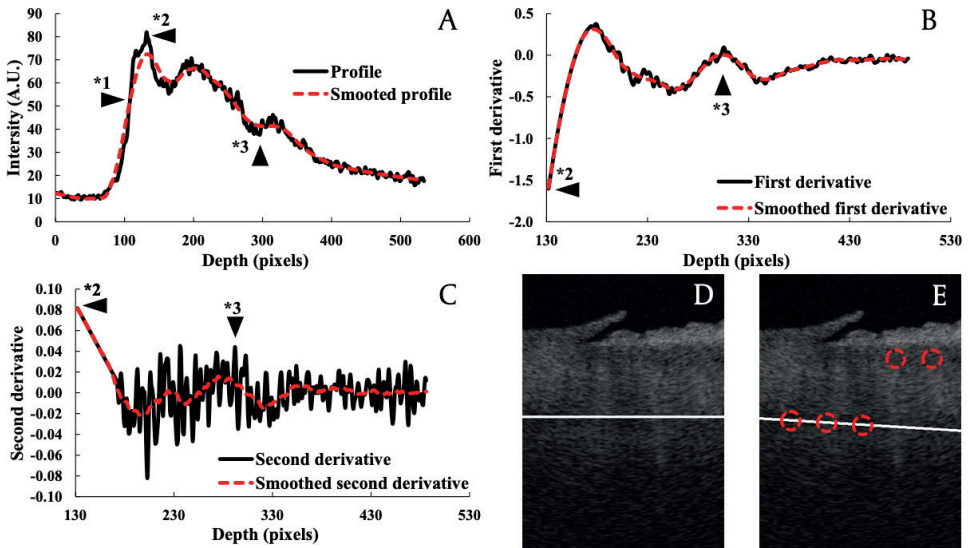
Vertical dark lines are searched from the binary image which are resulting mostly from lower intensities near the borders of the RoI. If low intensities are not present, the surface can be determined. If dark lines are found, the thresholding and image correction starting from the detection of the superficial layer are repeated for the region of the dark lines, and the corrected region is merged to the binary image. If thresholding still fails, the region with the dark line is cropped away from the binary image.

Holes <0.1% of the total area of the cartilage mask (fig. 1E) are filled.

The perimeter of the cartilage is determined from the binary image (fig. 1F). Endpoints of the cartilage surface are determined from the cartilage perimeter.

The shortest path between the two endpoints along the cartilage perimeter is determined as the cartilage surface (fig. 1G). The path is calculated with the shortest path function by using a Geodesic distance transform function with a quasi-Euclidean method. Additionally, the surface (fig. 1H) subjected to further analysis is created by choosing the lowest surface point from each column.

### 3. Detection of the bone-cartilage interface



**Supplementary Fig. 2** A) The vertical intensity profile of the ROI after the ROI is averaged in horizontal direction; B) its first derivative and C) its second derivative. D) The calculated master bone-cartilage (B-C) interface, and E) the B-C interfaces of the five sub-regions and the final determined B-C interface.

The ROI (fig. 1B) is averaged in horizontal direction (fig. 2A). The mean surface location (\*1) and the bottom of the lesion (\*2) are determined from the surface information (fig. 1H). The bone-cartilage (B-C) interface (\*3) is found deeper than the bottom of the lesion except in ICRS 4 lesions. These are detected by starting the B-C interface search from the mean surface location (\*1). The cartilage would be defined as ICRS 4 if the B-C interface is found closer to the surface than the bottom of the lesion (\*2), but since only chondral lesions were included in this study, ICRS 4 was not assigned. The profile is smoothed with Savitzky-Golay filter.

The B-C interface is detected from the first or second derivative of the intensity profile (fig. 2A). The first derivative of the smoothed profile is calculated and smoothed again (fig. 2B). If the value of the second maximum peak is greater than the threshold (0.09), the B-C interface is found. Otherwise, the derivative is calculated from the smoothed first derivative and smoothed again (fig. 2C). The minimum value of the smoothed second derivative is searched, the maximum after this point is the B-C interface. The detected B-C interface is defined as the master B-C interface (fig. 2D).

Subsequently, the ROI is horizontally divided into five half-overlapping sub-regions, and the B-C interface is calculated for each sub-region (fig. 2E). These five B-C interfaces are set to the horizontal center point of each sub-region (fig. 2E) and are compared to the master B-C interface. A sub-region is defined as an outlier if its value differs over 60 pixels ( $\sim 0.30$  mm) from the master B-C interface. The final B-C interface is determined by fitting a second or first order polynomial on the detected B-C interfaces of the non-outlier sub-regions. If three or more outliers are detected, the master B-C interface is used.

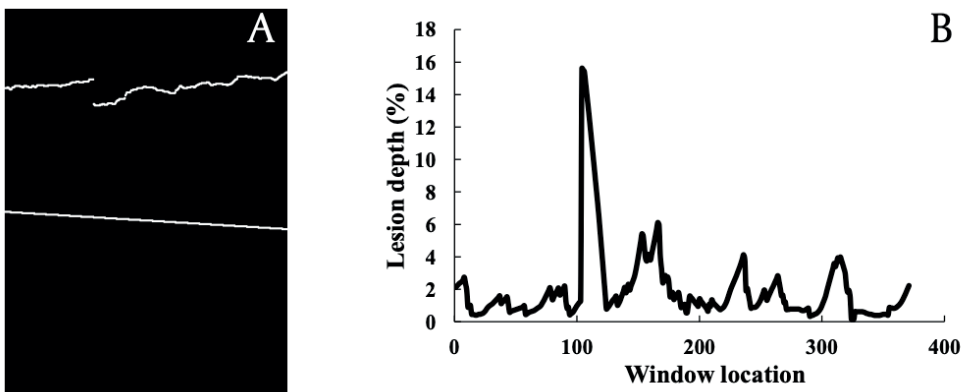
$$B-C_{\text{interface}} = \begin{cases} \text{Fitted 2}^{\text{nd}} \text{ order polynomial} & \text{Outliers} = 0 \vee 1 \text{ (among subregions 2 - 4)} \\ \text{Fitted 1}^{\text{st}} \text{ order polynomial} & \text{Outliers} = 1 \text{ (among subregions 1,5) } \vee 2 \\ \text{Master interface} & \text{Outliers} \geq 3 \end{cases}$$

#### 4. Calculation of the relative lesion depth

The surface and B-C interface are presented in a binary image (fig. 3A). A 20-pixels wide analysis window is moved horizontally in 1-pixel intervals. For each window the relative lesion depth ( $d_{\text{id}_w}$ ) was defined as

$$d_{\text{id}_w} = \frac{\bar{d} - \min(d)}{\bar{d}},$$

where  $d$  is a vector including the difference between the cartilage surface and the B-C interface for each column of the analyze window,  $\bar{d}$  is its average and  $\min(d)$  is the minimum of  $d$ . The calculation of  $d_{\text{id}_w}$  is repeated for all window locations (fig. 3B), and the lesion depth ( $d_{\text{id}}$ ) is defined as the largest value of  $d_{\text{id}_w}$ .



**Supplementary Fig. 3** A) The binary image of the surface and B-C interface and B) the relative lesion depth as function of the location of the analyze window.

### 5. Calculation of the optical roughness index

The optical roughness index (ORI) describes the roughness of the cartilage surface. The superficial layer of the cartilage is handled as one-dimensional signal. The surface signal is high-pass filtered with a 3<sup>rd</sup> order Butterworth filter in order to remove the trend from the surface using normalized cutoff frequency

$$\omega_c = \frac{0.05\text{mm}}{N_r},$$

where  $N_r$  is the number of samples per millimeter, i.e., the sampling rate, in the OCT image. Thereafter, the mean value  $\bar{y}_{\text{hp}}$  of the high-pass filtered signal  $y_{\text{hp}}$  is calculated and the ORI is determined as

$$\text{ORI} = \sqrt{\frac{(y_{\text{hp}} - \bar{y}_{\text{hp}})^2}{N}},$$

where  $N$  is the number of samples in the signal.<sup>2</sup>

### 6. Classification of the lesion according to the International Cartilage Repair Society scoring system

The International Cartilage Repair Society (ICRS) scoring system<sup>3</sup> was used to quantify the severity of the cartilage lesion (Table 1). For the threshold combinations (TC1/TC2), the ORI threshold for differentiation between ICRS 0 and ICRS 1 was determined based on the independent image set (8.0  $\mu\text{m}$ ) and the current set of images (5.6  $\mu\text{m}$ ), respectively. ICRS 2 was defined as >8% loss of cartilage based on the independent image set. For ICRS 3, the threshold was set according the ICRS 3 guidelines (>50%). For ICRS 4, negative values (>100%) were considered as the depletion of the subchondral bone.

**Supplementary table 1** International Cartilage Repair Society (ICRS) scoring system with determined thresholds

ICRS score	Relative lesion depth ( $d_{\text{id}}$ )	Optical roughness index (ORI)
0	$d_{\text{id}} < 8\%$	ORI < 8 $\mu\text{m}$ ORI/ 5.6 $\mu\text{m}$
1	$d_{\text{id}} < 8\%$	ORI $\geq$ 8 $\mu\text{m}$ / 5.6 $\mu\text{m}$
2	$8\% \geq d_{\text{id}} < 50\%$	-
3	$50\% \geq d_{\text{id}} < 100\%$	-
4	$d_{\text{id}} \geq 100\%$	-

## Supplementary references

1. Otsu N. A threshold selection method from gray-level histograms. *IEEE Trans Sys Man Cyber.* 1979;9(1):62-66.
2. Saarakkala S, Wang SZ, Huang YP, Zheng YP. Quantification of the optical surface reflection and surface roughness of articular cartilage using optical coherence tomography. *Phys Med Biol.* 2009;54(22):6837-6852.
3. Brittberg M, Winalski CS. Evaluation of cartilage injuries and repair. *J bone Jt surgeryAmerican Vol.* 2003;85-A Suppl:58-69.





# CHAPTER 4

## Optical coherence tomography enables accurate measurement of equine cartilage thickness for determination of speed of sound

*Acta Orthopaedica 87, 418-424 (2016)*

---

P.H. Puhakka<sup>1,2</sup>  
N.C.R. te Moller<sup>3</sup>  
P. Tanska<sup>1</sup>  
S. Saarakkala<sup>1,4,5</sup>  
V. Tiitu<sup>6</sup>

R.K. Korhonen<sup>1</sup>  
H. Brommer<sup>3</sup>  
T.Virén<sup>7</sup>  
J.S. Jurvelin<sup>1</sup>  
J. Töyräs<sup>1,2</sup>

---

<sup>1</sup>Department of Applied Physics, University of Eastern Finland, Kuopio, Finland, <sup>2</sup>Department of Clinical Neurophysiology, Kuopio University Hospital, Kuopio, Finland, <sup>3</sup>Department of Equine Sciences, Utrecht University, Utrecht, The Netherlands, <sup>4</sup>Department of Medical Technology, Institute of Biomedicine, University of Oulu, Oulu, Finland, <sup>5</sup>Department of Diagnostic Radiology, Oulu University Hospital, Oulu, Finland, <sup>6</sup>School of Medicine, Institute of Biomedicine, Anatomy, University of Eastern Finland, Kuopio, Finland, <sup>7</sup>Cancer Center, Kuopio University Hospital, Kuopio, Finland

## ABSTRACT

**Background** and purpose Arthroscopic estimation of articular cartilage thickness is important for scoring of lesion severity, and measurement of cartilage speed of sound (SOS) - a sensitive index of changes in cartilage composition. We investigated the accuracy of optical coherence tomography (OCT) in measurements of cartilage thickness and determined SOS by combining OCT thickness and ultrasound (US) time-of-flight (TOF) measurements.

**Material and methods** Cartilage thickness measurements from OCT and microscopy images of 94 equine osteochondral samples were compared. Then, SOS in cartilage was determined using simultaneous OCT thickness and US TOF measurements. SOS was then compared with the compositional, structural, and mechanical properties of cartilage.

**Results** Measurements of non-calcified cartilage thickness using OCT and microscopy were significantly correlated ( $\rho = 0.92$ ;  $p < 0.001$ ). With calcified cartilage included, the correlation was  $\rho = 0.85$  ( $p < 0.001$ ). The mean cartilage SOS (1,636 m/s) was in agreement with the literature. However, SOS and the other properties of cartilage lacked any statistically significant correlation.

**Interpretation** OCT can give an accurate measurement of articular cartilage thickness. Although SOS measurements lacked accuracy in thin equine cartilage, the concept of SOS measurement using OCT appears promising.

## INTRODUCTION

Optical coherence tomography (OCT) is a high-resolution, non-destructive imaging method. The resolution can be less than 5  $\mu\text{m}$ .<sup>1</sup> OCT helps, for example, in measurement of the thickness of structures in the eyes<sup>2</sup>, blood vessels<sup>3</sup>, and teeth<sup>4</sup> (Wilder-Smith et al. 2009). The potential of OCT in osteoarthritis research and clinical diagnostics is also noteworthy.<sup>5-7</sup>

Arthroscopy is a common diagnostic technique in both human and equine medicine. Arthroscopic measurement of articular cartilage thickness using OCT could help in detecting cartilage thinning<sup>8</sup> or scoring of cartilage lesion severity.<sup>9,10</sup> Studies in rabbits and goats showed high correlations between OCT and microscopy measurements of articular cartilage thickness.<sup>11-13</sup> However, no similar study has been conducted with thicker cartilage, such as in humans or horses.

The speed of ultrasound (US) is lower in osteoarthritic cartilage than in healthy cartilage.<sup>14</sup> This may be due to changes in water and proteoglycan content in the tissue and to collagen degeneration.<sup>15-17</sup> Consequently, reduced speed of sound (SOS) in articular cartilage could serve as an indicator of early and local cartilage degeneration. A technique that enables accurate arthroscopic measurement of local variations in SOS could have high diagnostic value.

We investigated the accuracy of OCT in the measurement of equine cartilage thickness, and used a novel arthroscopic technique utilizing OCT thickness measurement and US time-of-flight (TOF) measurement to determine the SOS in cartilage. We hypothesized that combining OCT and US would help to give accurate SOS determination. We assessed the applicability and accuracy of the technique with experimental measurements using phantoms and equine cartilage, and by numerically estimating the measurement uncertainty. We further compared SOS in equine cartilage with the structural, compositional, and biomechanical properties of the tissue.

## MATERIAL AND METHODS

### Sample preparation

18 metacarpophalangeal joints of 13 horses (age >2 years) were obtained from a slaughterhouse and frozen until sample preparation. 4-7 osteochondral blocks including healthy cartilage and a variety of lesions were prepared from each joint

(94 blocks in total; 34 from the proximal phalanx (P1), 34 from the dorsoproximal area of the condyles of the third metacarpal bone (MC3), 21 from the sagittal ridge of MC3 (SR), and 5 from other locations (fig. 1)). Each block included 1 measurement site, marked with ink to ensure location matching between histological evaluation, spectroscopic analysis, thickness measurements, SOS measurements, and mechanical measurements.

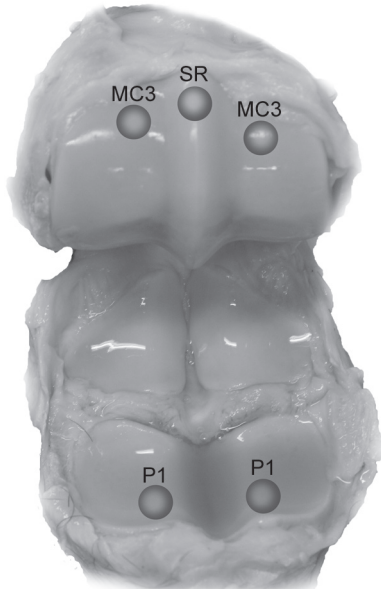


**Fig. 1** Osteochondral samples were prepared from equine metacarpophalangeal joints at 5 anatomical locations: medial and lateral proximal phalanx (P1), medial and lateral dorsoproximal areas of the condyles of third metacarpal bone (MC3), and the sagittal ridge of the third metacarpal bone (SR).

5 phantoms (2% and 4% agarose hydrogels, glass, silicone rubber, and acrylonitrile butadiene styrene) were first used for evaluation of SOS measurement based on simultaneous OCT and US recordings (described later). The thicknesses of the phantoms varied from 0.5 mm to 2.2 mm. The refractive indices of the phantom materials were determined with OCT using the modified optical length shifting method.<sup>18</sup>

### **Cartilage thickness measurement using OCT**

We used an OCT device (wavelength  $1,305 \pm 55$  nm; Ilumien PCI Optimization System; St. Jude Medical, St. Paul, MN) with a thin catheter (diameter = 0.9 mm; C7 Dragonfly; St. Jude Medical), providing cross-sectional images (axial resolution  $<20$   $\mu\text{m}$ ). The sample and the catheter were placed in phosphate-buffered saline (PBS) during the imaging process, with the catheter held manually above the ink marking or lesion, which were both visible in the OCT image. The thin low-scattering layer observed in OCT images just above the subchondral bone is assumed to correspond

to calcified cartilage.<sup>8</sup> The thickness of the non-calcified cartilage used in mechanical measurements was measured from the site of interest using the OCT system software. After matching the measurement points in the OCT and microscopy images, the thickness of non-calcified cartilage, calcified cartilage and full cartilage were measured again from the raw images, taking into account the refractive index of cartilage (1.358).<sup>18</sup> Pixel size was determined based on the known diameter of the OCT catheter and considering the refractive index of the water inside the catheter (1.322).

## Speed of sound measurements

First, the SOS in each phantom material was determined using a reference method; a custom-made acoustic microscope ( $F_c = 50$  MHz, -6 dB bandwidth = 30-73 MHz, focal length = 25 mm,  $F_s = 550$  MHz) was used to measure the TOF in the phantom and a caliper (resolution = 10  $\mu\text{m}$ ; DIGI-MET 1226 417; Helios-Preisser GmbH, Gammertingen, Germany) to measure the thickness.

The SOS in each phantom was subsequently measured using the new technique based on simultaneous OCT and US imaging. We used the OCT system and a clinically applicable US system (Clear View Ultra; Boston Scientific Corporation, Marlborough, MA) providing cross-sectional images. Both the thin US catheter (diameter = 1.0 mm,  $F_c = 40$  MHz,  $F_s = 250$  MHz; Atlantis SR Pro; Boston Scientific Corporation) and the OCT catheter were inserted through an oval-shaped, custom-made instrument channel to enable imaging of the same location simultaneously with both modalities (fig. 2). Considering the largest diameter of the instrument channel (3.33 mm), it is possible to insert the instrument into a joint through normal arthroscopy portals. The phantoms on the metal plate and the instrument were immersed in degassed distilled water during the measurements. The instrument was aligned to direct the US beam perpendicular to the phantom surface. Each phantom SOS measurement set consisted of 10 consecutive US scans at the same location recorded simultaneously with 10 adjacent OCT cross sections. 5 of these sets of measurements were subsequently performed without repositioning the catheters. The reproducibility of the technique was evaluated by performing the set of 5 measurements 3 times and repositioning the catheters between each set.

Our technique was tested further by measuring SOS in equine cartilage in the laboratory. In these measurements, degassed PBS containing disodium EDTA and benzamidine HCl was used instead of water. To mimic arthroscopic conditions, the instrument was manually held over the cartilage surface and - to ensure perpendicular US incidence angle - aligned so that the US reflection from the tidemark was maximal. The measurement was performed 5 times for each osteochondral sample. After the

measurements, the samples were stored at 20°C until they were prepared for histology.

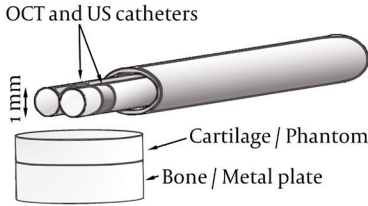


**Fig. 2** The measurement setup. Adjacent optical coherence tomography (OCT) and ultrasound (US) catheters were inserted through an instrument channel. The phantom measurements were performed in distilled water and the cartilage measurements in a bath of phosphate-buffered saline.

### Determination of time of flight (TOF) and sample thickness

TOF and sample thickness were measured from the exact raw US and OCT data, respectively. In osteochondral samples, US reflects from the cartilage surface and tidemark.<sup>19</sup> The surface of the phantom or cartilage was defined automatically, and the bottom of the phantom or cartilage tidemark was defined manually for each of the 10 OCT cross sections. A 1–mm-wide analysis window was placed under the US catheter to match the thickness and TOF measurement sites in the lateral direction (fig. 3). The average thickness within the window was calculated.

Hilbert envelopes of bandpass filtered (tenth-order Butterworth filter with upper and lower cut-off frequencies of 80 MHz and 15 MHz, respectively) ultrasound A-scan lines were determined. Phantom or cartilage surface and phantom bottom or cartilage tidemark were manually determined from as wide an area of the cross-sectional image reconstructed from the envelope signals as was feasible (fig. 3). TOF in cartilage was measured from the average time distance between the interfaces. An average TOF was determined from 10 consecutively recorded cross sections and was used with the OCT-measured thickness for SOS determination:

$$\text{SOS} = \frac{\text{Thickness}}{\text{TOF}} \quad (1)$$

### Mechanical measurements

The mechanical properties of the osteochondral samples were determined using a custom-made material testing system (resolution for deformation and force: 0.1  $\mu\text{m}$  and 5 mN, respectively)<sup>20</sup> equipped with a cylindrical plane-ended indenter (diameter = 530  $\mu\text{m}$ ). The indenter was driven into contact with the sample surface; this was seen from the reading of the load cell. Thereafter, the stress-relaxation test consisting of two 5% strain steps with a strain rate of 100% per second relative to the pre-strain thickness was performed. A relaxation slope of less than 10 Pa/min was used as the equilibrium criterion.

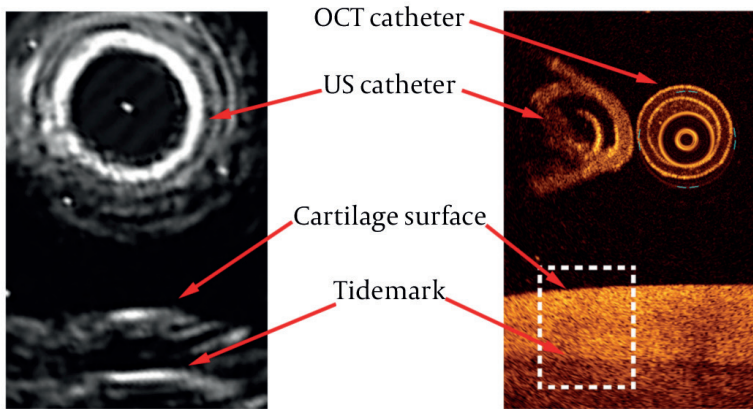


**Fig. 3** Ultrasound (US) time-of-flight was determined from the US image as the time distance between the phantom or cartilage surface and the phantom-metal interface or the tidemark. Thickness of phantom and non-calcified cartilage was determined from the OCT image as the mean thickness inside a 1-mm-wide window (dashed line) under the US catheter.

Using Abaqus (v6.10-1; Dassault Systèmes Simulia Corp., Waltham, MA) and Matlab (2012a, The MathWorks Inc., Natick, MA), an axisymmetric fibril-reinforced poroelastic finite element model was fitted to the experimental stress-relaxation data.<sup>21,22</sup> Cartilage was modeled using axisymmetric 4-node continuum pore pressure elements (CAX4P). Elastic fibrillar and biphasic porohyperelastic non-fibrillar matrices represented the collagen network and the PGs with a porous structure filled with fluid, respectively. The behavior of the collagen network was expressed with the fibril network modulus ( $E_f$ ) and that of the non-fibrillar matrix with the non-fibrillar matrix modulus ( $E_m$ ), permeability ( $k$ ), and Poisson's ratio. The Poisson's ratio (0.42) and fluid fraction (80%) were fixed<sup>23,24</sup>, while the other aforementioned material parameters were obtained through optimization, minimizing the mean square error between the experimental and simulated reaction forces. The first 5% achieved a perfect contact between the indenter and cartilage, and the optimization was conducted in the second step (5-10% strain). A more detailed description of the model is available in earlier studies.<sup>21,23-26</sup>

## Histological and spectroscopic analysis

Osteochondral blocks with the marked site of interest exactly in the middle were immersed in formalin for at least 48 hours and then processed for histological evaluation.<sup>26</sup> Three safranin-O-stained, 3- $\mu\text{m}$ -thick sections from each sample were prepared and imaged with a light microscope. Cartilage thickness was measured manually after careful comparison of measurement location with OCT image. Three investigators graded the 3 stained sections of each sample using the Mankin score.<sup>27</sup> Final grades were obtained by averaging the scores and rounding up the average to the nearest integer. Optical density (OD) measurement of safranin-O distribution was conducted by means of digital densitometry (computer-controlled CCD camera; SenSys; Photometrics Inc., Tucson, AZ) to evaluate the fixed charge distribution in tissue.<sup>28</sup> Collagen and PG contents were determined by measuring the areas under the absorption spectra at 1,585-1,720  $\text{cm}^{-1}$  and 984-1,140  $\text{cm}^{-1}$  measured from 3 unstained 5- $\mu\text{m}$ -thick sections using a Fourier transform infrared spectroscope (FTIR; Spotlight 300 FTIRI; Perkin Elmer, Waltham, MA).<sup>29</sup> Polarized light microscopic analysis of 3 unstained 5- $\mu\text{m}$ -thick sections was conducted (PLM; Leitz Orholux II POL, Leitz Wetzlar, Germany) to provide information on the orientation of the collagen fibrils.<sup>30</sup> We determined the average collagen fibril orientation in relation to the cartilage surface, and the parallelism index (PI) describing the anisotropy of the collagen matrix.

## Numerical assessment of SOS measurement error

The theoretical performance of the SOS measurement technique was numerically assessed by calculating the propagation of uncertainty. First, the effect of varying sample thickness and resolution of TOF measurement on SOS determination was studied. Perfect accuracy in thickness measurement was assumed while the thickness was varied from 0.3 mm to 3 mm, and TOF resolution corresponding to the measurement error was varied between 0  $\mu\text{s}$  and 0.05  $\mu\text{s}$ . Then we examined the effects of varying sample thickness and the resolution of thickness measurement on SOS determination. Perfect accuracy in TOF was assumed while the sample thickness and resolution of thickness measurement were varied from 0.3 mm to 3 mm and from 0  $\mu\text{m}$  to 50  $\mu\text{m}$ , respectively. In the analyses, true SOS was assumed to be 1,600 m/s.

## Statistics

All 94 osteochondral samples were included in the analysis of OCT thickness measurement. 36 samples were excluded from the analysis of SOS measurement because the US reflection from either the cartilage surface or the tidemark was too weak for TOF measurement; 9 other samples were excluded because the cartilage was too damaged for mechanical measurement.



Spearman's rank correlation coefficient was calculated to investigate the correlation between cartilage thickness measured from OCT and microscopic images of the samples. The same method was used to study the correlation between the SOS values in phantoms, measured using the reference and the novel techniques. Possible bias in the measurements was investigated using Bland-Altman analysis. The reproducibility of the SOS measurements was verified by calculating the root mean square coefficient of variation ( $CV_{rms}$  (%)) for the phantom and cartilage measurements. The statistical significance of differences in cartilage thickness and SOS values between the anatomical locations was tested using the Kruskal-Wallis test. Linear dependencies between the SOS and the cartilage properties determined were evaluated using linear mixed-model analysis, which accounts for the correlations or clusters in the data set. The present study used the joint from which the sample was prepared as a random variable. The models assume that the residuals and the random effect are normally distributed and that the residuals are homoscedastic. The normality was assessed from quantile-quantile plots and homoscedasticity by investigating the variation of residuals as a function of predicted values. The results of these analyses supported the initial assumptions. The significance level in all the analyses was set to  $p < 0.05$ . The analyses were performed using SPSS and Matlab.

## RESULTS

The SOS values in the phantoms measured using the combination of US and OCT were consistent with the values measured using the reference technique ( $\rho > 0.99$ ,  $p < 0.001$ ) and no systematic error was found based on Bland-Altman analysis (fig. 4).  $CV_{rms}$  (%) in SOS measured for the phantoms was 3.4%.

In OCT images, calcified cartilage was discernible from non-calcified cartilage and bone in all but 3 samples (fig. 5). The mean full cartilage thickness and the mean non-calcified cartilage thicknesses measured using OCT were 1.00 mm (SD 0.26) and 0.83 mm (SD 0.25), respectively. Samples from P<sub>1</sub> (mean 1.03 mm (SD 0.27)) had significantly thicker non-calcified cartilage than samples from SR (0.74 mm (SD 0.16),  $p = 0.001$ ) or MC<sub>3</sub> (0.71 mm (SD 0.13),  $p < 0.001$ ). The maximum full cartilage thickness and the maximum non-calcified cartilage thicknesses measurable with OCT were 1.80 mm and 1.44 mm, respectively. For the thinnest cartilage, the thicknesses were 0.53 mm and 0.37 mm, respectively.

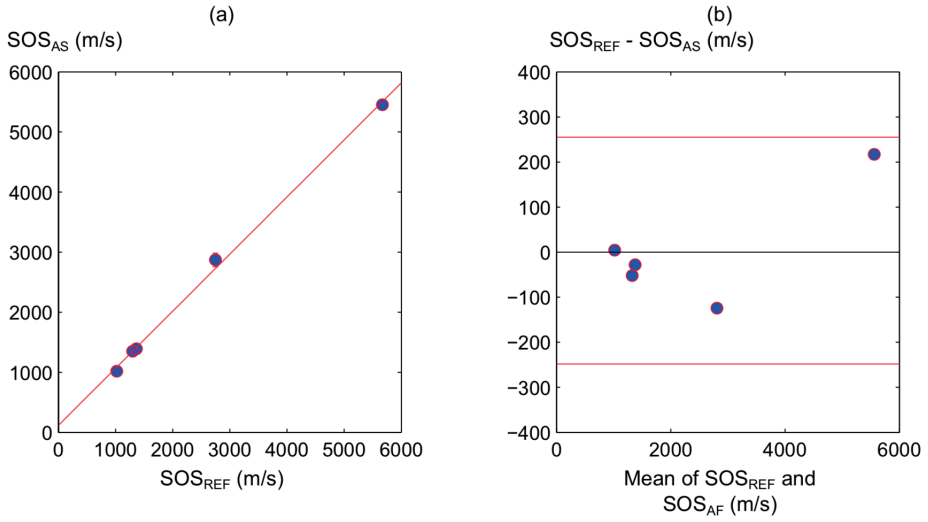


**Fig. 4** A) There was a high correlation between speed of sound in phantoms measured with the novel arthroscopic technique (SOSAS) and the reference technique (SOSREF) ( $\rho > 0.99$ ,  $p < 0.001$ ). B) Bland-Altman plot of SOSAS and SOSREF. 95% limits of agreement are shown with red lines.

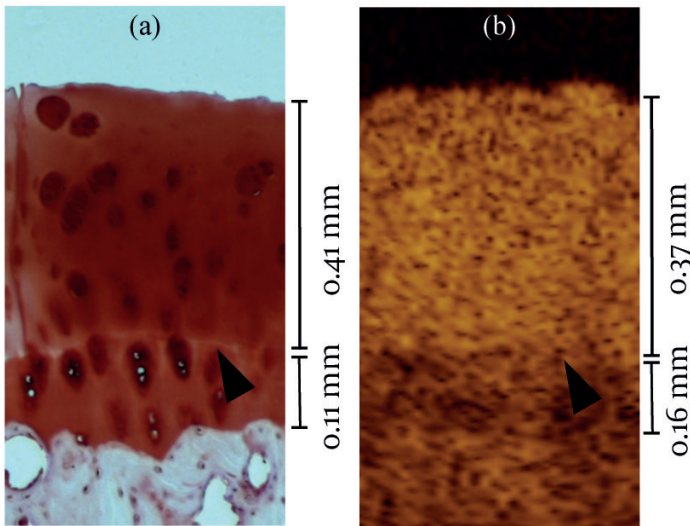


**Fig. 5** Non-calcified articular cartilage thickness was measured as the distance between the cartilage surface and the tidemark (arrowhead), seen here by light microscopy (A) and OCT (B). The full cartilage thickness also included the thickness of calcified cartilage. Calcified cartilage can be seen in OCT images as a low-scattering layer.

There was a significant correlation between full cartilage thickness measured from OCT images and that measured from microscopy images  $\rho = 0.85$  ( $p < 0.001$ ), while the corresponding correlations for non-calcified and calcified cartilage thicknesses were  $\rho = 0.92$  ( $p < 0.001$ ) and  $\rho = 0.22$  ( $p = 0.04$ ), respectively (fig. 6).

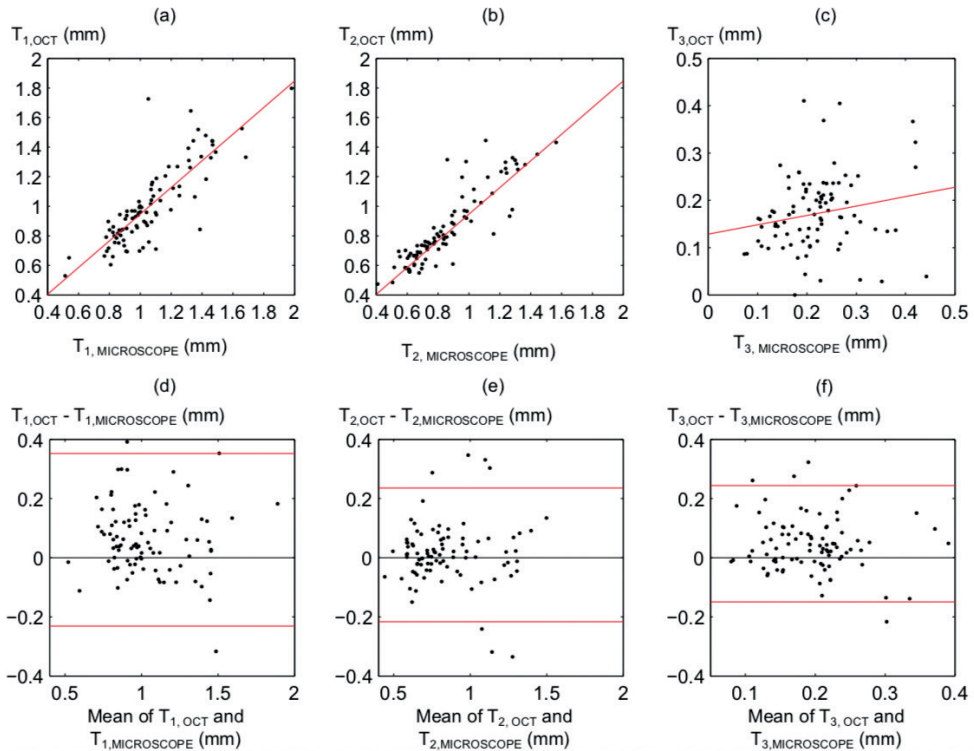


**Fig. 6** A) Correlation between full cartilage thickness measured from optical coherence tomography (OCT) image ( $T_{1,OCT}$ ) and light microscope image ( $T_{1,MICROSCOPE}$ ) ( $\rho = 0.85$ ,  $p < 0.001$ ). B) Correlation between non-calcified cartilage thickness measured from OCT image ( $T_{2,OCT}$ ) and light microscope image ( $T_{2,MICROSCOPE}$ ) ( $\rho = 0.92$ ,  $p < 0.001$ ). C) Correlation between calcified cartilage thickness measured from OCT image ( $T_{3,OCT}$ ) and light microscopy image ( $T_{3,MICROSCOPE}$ ) ( $\rho = 0.22$ ,  $p = 0.04$ ). D-F) Bland-Altman plots representing the differences between OCT measurements and microscopic measurements. The 95% limits of agreement are shown with red lines.

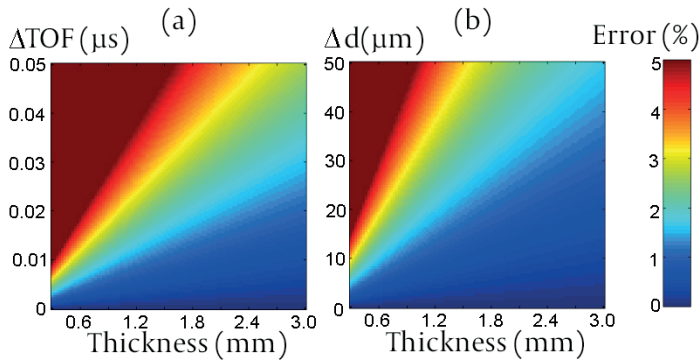
The CVrms (%) for the repeated measurements of thickness, TOF, and SOS, of the equine cartilage was 7.3%, 7.6% and 7.8%, respectively. The mean SOS in the cartilage samples was 1,636 m/s. The median Mankin scores of all the samples and of those included in the SOS measurement were 4 and 3, respectively (table 1). SOS was not significantly dependent on anatomical location ( $p = 0.3$ ). No statistically significant linear dependence was detected between SOS and the cartilage properties determined (table 2).

**Table 1** Mean speed of sound, mean non-calcified cartilage thickness, and median Mankin score of the samples included in the speed of sound measurements grouped by anatomical location.

Anatomical location	n	SOS (m/s) Mean (SD)	Thickness (mm) Mean (SD)	Mankin score Median (IQR)
MC3	26	1604 (195)	0.66 (0.16)	2 (1)
P1	7	1720 (169)	0.74 (0.26)	7 (3)
SR	16	1651 (210)	0.68 (0.14)	3 (2)
All	49	1636 (197)	0.68 (0.17)	3 (3)

MC3, dorsoproximal areas of the condyles of the third metacarpal bone; P1, proximal phalanx; SR, sagittal ridge of the third metacarpal bone; SD, standard deviation; IQR, inter quartal range

The numerical assessment of error in SOS measurements revealed that especially in thin equine cartilage, the resolutions of US and OCT systems have a prominent effect on the accuracy of SOS measurement (fig. 7).

**Fig. 7** Numerically evaluated effect of resolutions of ultrasound ( $\Delta$ TOF) measurements (A) and optical coherence tomography ( $\Delta$ d) measurements (B) on error in speed of sound values for cartilage with varying thickness.**Table 2** p-values for linear association between speed of sound and the fixed effects (structural, compositional, and biomechanical properties) using the linear mixed model.

Mankin score	OD	Collagen orientation	PI	PG content	Collagen content	$E_f$	$E_m$	k
0.521	0.771	0.421	0.924	0.844	0.355	0.381	0.528	0.449

OD, optical density; PI, parallelism index; PG, proteoglycan;  $E_f$ , fibril network modulus;  $E_m$ , non-fibrillar matrix modulus, k = permeability

## DISCUSSION

In most OCT images of the osteochondral samples, the calcified cartilage could be well discriminated from both non-calcified cartilage and subchondral bone. OCT measurements of non-calcified cartilage thickness agreed well with the microscopic measurements. Rough cartilage-bone interface and secondly light attenuation reduce the accuracy of the measurement of calcified cartilage thickness, and consequently that of the measurement of full cartilage thickness. According to our Bland-Altman analysis, the absolute difference between the 2 modalities increased with thicker cartilage. The relative difference between OCT and microscopic measurements was similar to that in previous studies that investigated rabbit and goat cartilage with thicknesses less than 1 mm.<sup>11-13</sup> A cartilage thickness of 1.1 mm in the first carpometacarpal joint in humans has been measured with OCT.<sup>8</sup> In our study, the highest measurable thickness was 1.8 mm, which agrees with the OCT light penetration limit of about 1.0-2.0 mm common for soft tissues.<sup>31</sup>

We compared light microscopic images and OCT images before selecting the thickness measurement points. Although the mismatch between the measurement locations was small in all samples, it could still be the main reason for the difference in thickness values between OCT and microscopy. Additionally, fixation and processing of the samples for microscopy may have a small shrinking effect on sample dimensions. Some inaccuracy in OCT measurements may be due to the use of the same value in the literature for the refractive index of both the non-calcified and calcified cartilage.

We hypothesized that by using OCT thickness measurement with simultaneous US TOF measurement, arthroscopic determination of cartilage SOS would be possible. The technique that we introduced enabled simultaneous measurement of US TOF in articular cartilage and cartilage thickness at the same location. Our technique may be used in conventional arthroscopy, as the instrument fits through normal arthroscopic portals.

Based on the phantom measurements, the combination of OCT and US would enable SOS measurement in layered materials. The mean SOS in the equine cartilage samples agreed with the values given in the literature (1,696 m/s).<sup>32</sup> The structure and composition of articular cartilage control its mechanical and acoustic properties.<sup>15-17,33</sup> However, no statistically significant dependence was found between SOS and the structural or mechanical properties determined.

Repeatability in SOS measurement is reduced if the surface is fibrillated, as fibrillation impairs the accuracy of locating the cartilage surface, particularly from US images. However, SOS measurements may be unnecessary when there is visible fibrillation, as osteoarthritis that has advanced as far as this can be diagnosed with conventional techniques.

We estimated the error in SOS measurement caused by inaccuracy in the thickness and TOF measurements with different cartilage thicknesses. Theoretically, the resolutions of the current OCT and US systems are sufficient for SOS measurement. However, the accuracy of the present measurement is partially limited by the less than optimal optical and acoustic contrasts between non-calcified and calcified layers. Attenuation of light and US in cartilage further limits the contrast in the tidemark, and therefore the highest cartilage thickness and TOF measurable with this technique. Thus, the technique requires further development before it would be suitable for clinical use in equine or human medicine. Advanced signal and image processing could enhance the contrast, and the use of point measurement or linear scanning instead of rotational scanning could improve measurement accuracy. Furthermore, the US frequency and intensity could be optimized to increase the penetration of US into the tissue. The accuracy of the US and light incidence angle, which should be perpendicular to the cartilage surface, could also be improved through improved probe design.

In conclusion, articular cartilage thicknesses below 1.8 mm were successfully measured with OCT. OCT-based thickness measurements were more accurate when calcified cartilage was excluded. The measurement could be used for arthroscopic detection of cartilage thinning during arthroscopy and estimation of lesion depth. Before becoming suitable for clinical use, the measurement accuracy of the SOS measurement technique presented must be improved. However, the concept of simultaneous OCT and US imaging for SOS measurement appears to be both feasible and promising.

## **ACKNOWLEDGEMENTS**

This work was supported in part by the Jenny and Antti Wihuri Foundation, Academy of Finland (132367, 140730, 267551 and 268378), Kuopio University Hospital (EVO 5041723 and 5041738, and VTR 15654156), strategic funding of the University of Eastern Finland (931053), the University of Oulu (24001200), the Department of Equine Sciences of Utrecht University, and CSC—IT Center for Science, Finland. We also thank Simo Ojanen and Eija Rahunen for technical assistance and Tuomas Selander for assistance with statistics.

## REFERENCES

1. Drexler W, Morgner U, Kärtner FX, et al. In vivo ultrahigh-resolution optical coherence tomography. *Opt Lett*. 1999;24(17):1221-1223.
2. van Velthoven MEJ, Faber DJ, Verbraak FD, van Leeuwen TG, de Smet MD. Recent developments in optical coherence tomography for imaging the retina. *Prog Retin Eye Res*. 2007;26(1):57-77.
3. Jang I-K, Tearney GJ, MacNeill B, et al. In Vivo Characterization of Coronary Atherosclerotic Plaque by Use of Optical Coherence Tomography. *Circulation*. 2005;111(12):1551-1555.
4. Wilder-Smith CH, Wilder-Smith P, Kawakami-Wong H, Voronets J, Osann K, Lussi A. Quantification of dental erosions in patients with GERD using optical coherence tomography before and after double-blind, randomized treatment with esomeprazole or placebo. *Am J Gastroenterol*. 2009;104(11):2788-2795.
5. Drexler W, Stamper D, Jesser C, et al. Correlation of collagen organization with polarization sensitive imaging of in vitro cartilage: implications for osteoarthritis. *J Rheumatol*. 2001;28(6):1311-1318.
6. Li X, Martin S, Pitris C, et al. High-resolution optical coherence tomographic imaging of osteoarthritic cartilage during open knee surgery. *Arthritis Res Ther*. 2005;7(2):R318-23.
7. Virén T, Huang YP, Saarakkala S, et al. Comparison of ultrasound and optical coherence tomography techniques for evaluation of integrity of spontaneously repaired horse cartilage. *J Med Eng Technol*. 2012;36(3):185-192.
8. Cernohorsky P, de Bruin DM, van Herk M, et al. In-situ imaging of articular cartilage of the first carpometacarpal joint using co-registered optical coherence tomography and computed tomography. *J Biomed Opt*. 2012;17(6):060501.
9. Niemelä T, Virén T, Liukkonen J, et al. Application of optical coherence tomography enhances reproducibility of arthroscopic evaluation of equine joints. *Acta Vet Scand*. 2014;56(3):1-8.
10. Te Moller NCR, Brommer H, Liukkonen J, et al. Arthroscopic optical coherence tomography provides detailed information on articular cartilage lesions in horses. *Vet J*. 2013;197(3):589-595.
11. Cernohorsky P, Kok AC, Bruin DM De, et al. Comparison of optical coherence tomography and histopathology in quantitative assessment of goat talus articular cartilage. *Acta Orthop*. 2015;86(2):257-263.
12. Han CW, Chu CR, Adachi N, et al. Analysis of rabbit articular cartilage repair after chondrocyte implantation using optical coherence tomography. *Osteoarthritis Cartilage*. 2003;11(2):111-121.
13. Rogowska J, Bryant CM, Brezinski ME. Cartilage thickness measurements from optical coherence tomography. *J Opt Soc Am Opt image Sci Vis*. 2003;20(2):357-367.
14. Myers SL, Dines K, Brandt DA, Brandt KD, Albrecht ME. Experimental assessment by high frequency ultrasound of articular cartilage thickness and osteoarthritic changes. *J Rheumatol*. 1995;22(1):109-116.
15. Joiner GA, Bogoch ER, Pritzker KP, Buschmann MD, Chevrier A, Foster FS. High frequency acoustic parameters of human and bovine articular cartilage following experimentally-induced matrix degradation. *Ultrason Imaging*. 2001;23(2):106-116.
16. Suh JK, Youn I, Fu FH. An in situ calibration of an ultrasound transducer: a potential application for an ultrasonic indentation test of articular cartilage. *J Biomech*. 2001;34(10):1347-1353.
17. Toyras J, Laasanen MS, Saarakkala S, et al. Speed of sound in normal and degenerated bovine articular cartilage. *Ultrasound Med Biol*. 2003;29(3):447-454.
18. Wang SZ, Huang YP, Wang Q, Zheng YP, He YH. Assessment of depth and degeneration dependences of articular cartilage refractive index using optical coherence tomography in vitro. *Connect Tissue Res*. 2010;51(1):36-47.

19. Modest VE, Murphy MC, Mann RW. Optical verification of a technique for in situ ultrasonic measurement of articular cartilage thickness. *J Biomech.* 1989;22(2):171-176.
20. Toyras J, Rieppo J, Nieminen MT, Helminen HJ, Jurvelin JS. Characterization of enzymatically induced degradation of articular cartilage using high frequency ultrasound. *Phys Med Biol.* 1999;44(11):2723-2733.
21. Julkunen P, Kiviranta P, Wilson W, Jurvelin JS, Korhonen RK. Characterization of articular cartilage by combining microscopic analysis with a fibril-reinforced finite-element model. *J Biomech.* 2007;40(8):1862-1870.
22. Mäkelä JTA, Huttu MRJ, Korhonen RK. Structure-function relationships in osteoarthritic human hip joint articular cartilage. *Osteoarthr Cartil.* 2012;20(11):1268-1277.
23. Korhonen RK, Laasanen MS, Toyras J, Lappalainen R, Helminen HJ, Jurvelin JS. Fibril reinforced poroelastic model predicts specifically mechanical behavior of normal, proteoglycan depleted and collagen degraded articular cartilage. *J Biomech.* 2003;36(9):1373-1379.
24. Li LP, Soulhat J, Buschmann MD, Shirazi-Adl A. Nonlinear analysis of cartilage in unconfined ramp compression using a fibril reinforced poroelastic model. *Clin Biomech (Bristol, Avon).* 1999;14(9):673-682.
25. Wilson W, van Donkelaar CC, van Rietbergen B, Ito K, Huiskes R. Stresses in the local collagen network of articular cartilage: a poroviscoelastic fibril-reinforced finite element study. *J Biomech.* 2004;37(3):357-366.
26. Kulmala K a. M, Pulkkinen HJ, Rieppo L, et al. Contrast-Enhanced Micro-Computed Tomography in Evaluation of Spontaneous Repair of Equine Cartilage. *Cartilage.* 2012;3(3):235-244.
27. Mankin HJ, Dorfman H, Lippiello L, Zarins A. Biochemical and metabolic abnormalities in articular cartilage from osteo-arthritic human hips. II. Correlation of morphology with biochemical and metabolic data. *J bone Jt surgery American Vol.* 1971;53(3):523-537.
28. Panula HE, Hyttinen MM, Arokoski JP, et al. Articular cartilage superficial zone collagen birefringence reduced and cartilage thickness increased before surface fibrillation in experimental osteoarthritis. *Ann Rheum Dis.* 1998;57(4):237-245.
29. Boskey A, Pleshko Camacho N. FT-IR imaging of native and tissue-engineered bone and cartilage. *Biomaterials.* 2007;28(15):2465-2478.
30. Rieppo J, Hallikainen J, Jurvelin JS, Kiviranta I, Helminen HJ, Hyttinen MM. Practical considerations in the use of polarized light microscopy in the analysis of the collagen network in articular cartilage. *Microsc Res Tech.* 2008;71(4):279-287.
31. Fujimoto JG, Brezinski ME, Tearney GJ, et al. Optical biopsy and imaging using optical coherence tomography. *Nat Med.* 1995;1(9):970-972.
32. Brommer H, Laasanen MS, Brama PAJ, et al. Influence of age, site, and degenerative state on the speed of sound in equine articular cartilage. *Am J Vet Res.* 2005;66(7):1175-1180.
33. Buckwalter JA, Mankin HJ. Articular cartilage. Part I: Tissue design and chondrocyte-matrix interactions. In: *Journal of Bone and Joint Surgery - Series A*; 1997:600-611.







# CHAPTER 5

## Estimation of articular cartilage properties using multivariate analysis of optical coherence tomography signal

*Osteoarthritis and Cartilage* 23, 2206-2213 (2015)

---

P.H. Puhakka<sup>1,2</sup>,  
N.C.R. te Moller<sup>3</sup>,  
I.O. Afara<sup>1</sup>,  
J.T.A. Mäkelä<sup>1</sup>,  
V. Tiitu<sup>4</sup>,

R.K. Korhonen<sup>1</sup>,  
H. Brommer<sup>3</sup>,  
T. Virén<sup>5</sup>,  
J.S. Jurvelin<sup>1</sup>,  
J. Töyräs<sup>1,2</sup>

---

<sup>1</sup>Department of Applied Physics, University of Eastern Finland, Kuopio, Finland, <sup>2</sup>Department of Clinical Neurophysiology, Kuopio University Hospital, Kuopio, Finland, <sup>3</sup>Department of Equine Sciences, Utrecht University, Utrecht, Netherlands, <sup>4</sup>School of Medicine, Institute of Biomedicine, Anatomy, University of Eastern Finland, Kuopio, Finland, <sup>5</sup>Cancer Center, Kuopio University Hospital, Kuopio, Finland

## ABSTRACT

**Objective** The aim was to investigate the applicability of multivariate analysis of optical coherence tomography (OCT) information for determining structural integrity, composition and mechanical properties of articular cartilage.

**Design** Equine osteochondral samples ( $N = 65$ ) were imaged with OCT, and their total attenuation and backscattering coefficients ( $\mu_t$  and  $\mu_b$ ) were measured. Subsequently, the Mankin score, optical density (OD) describing the fixed charge density, light absorbance in amide I region ( $A_{\text{amide}}$ ), collagen orientation, permeability, fibril network modulus ( $E_f$ ) and non-fibrillar matrix modulus ( $E_m$ ) of the samples were determined. Partial least squares (PLS) regression model was calculated to predict tissue properties from the OCT signals of the samples.

**Results** Significant correlations between the measured and predicted mean collagen orientation ( $R^2 = 0.75$ ,  $P < 0.0001$ ), permeability ( $R^2 = 0.74$ ,  $P < 0.0001$ ), mean OD ( $R^2 = 0.73$ ,  $P < 0.0001$ ), Mankin scores ( $R^2 = 0.70$ ,  $P < 0.0001$ ),  $E_m$  ( $R^2 = 0.50$ ,  $P < 0.0001$ ),  $E_f$  ( $R^2 = 0.42$ ,  $P < 0.0001$ ), and  $A_{\text{amide}}$  ( $R^2 = 0.43$ ,  $P < 0.0001$ ) were obtained. Significant correlation was also found between  $\mu_b$  and  $E_f$  ( $\rho = 0.280$ ,  $P = 0.03$ ), but not between  $\mu_t$  and any of the determined properties of articular cartilage ( $P > 0.05$ ).

**Conclusion** Multivariate analysis of OCT signal provided good estimates for tissue structure, composition and mechanical properties. This technique may significantly enhance OCT evaluation of articular cartilage integrity, and could be applied, for example, in delineation of degenerated areas around cartilage injuries during arthroscopic repair surgery.

## INTRODUCTION

Articular cartilage injury can initiate development of osteoarthritis (OA) in both human and animal joints.<sup>1,2</sup> As a consequence to injury, chondrocytes of articular cartilage may die or get damaged, cartilage matrix disruption occurs, and proteoglycan (PG) content decreases, initiating the development of post-traumatic OA.<sup>1</sup> The superficial zone of cartilage is the initial zone in which degenerative changes are typically encountered. In the early stage of cartilage degeneration tissue water content increases and the collagen fibrils are disorganized.<sup>3</sup> These changes further lead to increased permeability and decreased stiffness of articular cartilage.

Several surgical techniques, (e.g., microfracturing and tissue and cell transplantation) are used to repair cartilage injuries and prevent the development of post-traumatic OA.<sup>4</sup> The choice for the optimal repair technique is based on the location and size of the lesion<sup>5</sup>, which are usually visually assessed during arthroscopy. However, the detection of early-stage degenerative changes in tissue surrounding the lesion, by means of arthroscopic examination, is difficult.<sup>6,7</sup> To improve treatment planning, it would be beneficial to have a more accurate, high-resolution arthroscopic technique for diagnosing early-stage degeneration around injuries and to delineate the optimal cartilage region for repair. Identification of early, potentially reversible changes in articular cartilage would also be essential for development of disease-modifying treatment methods.<sup>8</sup>

Optical coherence tomography (OCT), an arthroscopically applicable technique, provides adequate resolution ( $\sim 10\text{-}20\ \mu\text{m}$ ) for detection and assessment of articular cartilage lesions.<sup>9,10</sup> Morphological features of cartilage surface observed in OCT images agree with the ones found in histological investigation.<sup>11</sup> Furthermore, abnormal organization of collagen fibrils can be detected as a lack of birefringence using polarization sensitive OCT.<sup>12</sup> OCT imaging is based on the measurement of intensity of the light backscattered from different depths of the tissue. The measured intensity depends on light attenuation in the tissue and, at each depth of the tissue, on the amount of light scattering directed to the detector. Microscopic changes in composition and structure of tissues lead to changes in attenuation and scattering properties.<sup>13</sup> Early stage degenerative changes in articular cartilage, like depletion of PGs, could possibly be detected by measuring total attenuation ( $\mu_t$ ) and backscattering ( $\mu_b$ ) coefficients with OCT. To the authors' knowledge, the differences in  $\mu_t$  or  $\mu_b$  between normal and degenerated articular cartilage have not been reported. It is known, though, that attenuation is weaker in repair tissue than in native cartilage.<sup>14</sup> Further, the decrease in collagen and chondrocyte contents has been found to decrease light attenuation in agarose scaffolds.<sup>15</sup>

Due to its layered nature, articular cartilage exhibits depth-dependent light backscattering and attenuation properties. Therefore, the  $\mu_t$  and  $\mu_b$  of the total cartilage thickness layer may not optimally represent this tissue and may not be sensitive enough to detect early stage degeneration. Thus, an alternative analysis approach for OCT data is required. In the present study, the applicability of multivariate partial least squares (PLS) regression to analyse OCT signal and predict cartilage degeneration is studied. This analytical technique has been applied for the analysis of cartilage spectroscopic data.<sup>16,17</sup> The method is used to obtain those features of the multivariate input data (predictor variable) that explain most of the variation in the reference data (response variable) of the sample.<sup>18</sup> We hypothesize that with PLS regression modelling we could obtain a more accurate approximation of articular cartilage properties as compared to measurement of bulk  $\mu_t$  and  $\mu_b$ .

## METHODS

### Sample preparation

Osteochondral samples were prepared from metacarpophalangeal joints of healthy, skeletally mature horses (N = 13) obtained from a slaughterhouse. Either left or right joint was obtained from eight horses and both from five horses. The horses had variety of chondral lesions. Osteochondral samples (N = 65) were obtained from 1 to 6 anatomical locations within each joint, namely; the tips of the medial and lateral eminences of the first phalanx (N = 34), the opposing sites on the medial and lateral condyles (N = 15), and the sagittal ridge of the metacarpal bone (N = 14). The samples were cut into osteochondral blocks with a minimum surface area of 10 × 10 mm<sup>2</sup> and the area of interest (e.g., lesion) located in the center.

### Optical coherence tomography imaging

The osteochondral samples were imaged using OCT (wavelength 1305±55 nm, axial resolution <20 µm, lateral resolution 25-60 µm; Illumien PCI Optimization System, St. Jude Medical, St. Paul, MN, USA). During the OCT imaging the samples were immersed in phosphate buffered saline (PBS). The OCT system has a rotating scanning geometry providing cross-sectional images (thickness = 0.1 mm). Each cross-sectional image consists of 504 radial scan lines obtained during one revolution (fig. 1). The system measures the intensity of the light backscattered at different depths in each scanning direction. Five adjacent cross-sectional images were recorded from each sample. The cartilage surface was automatically detected from the cross-sections, while the cartilage-bone interface was manually determined (by PP). Cartilage thickness in the samples varied between 0.40 mm and 1.39 mm. An average depthwise intensity

curve was calculated for an analysis window with a width of 21 scan lines and a height matching the cartilage thickness. Subsequently, average intensity curves of the five cross-sections in each sample were averaged. The first 5% of the curves were excluded during the analyses to avoid specular reflection at the articular surface.

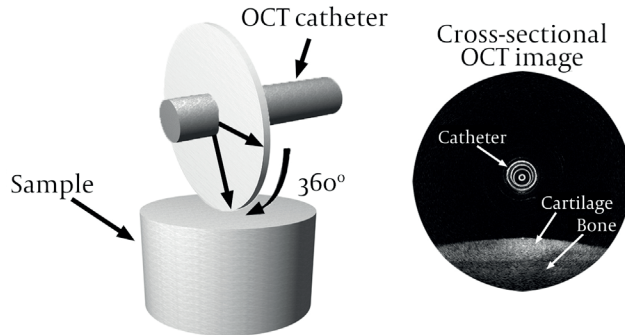


**Fig. 1** In the rotational scanning geometry, the OCT system obtains 504 radial scan lines during one 360° revolution to create a cross-sectional image of the sample. The imaging speed is 100 cross-sectional images per second.

## Biomechanical properties

Biomechanical properties of the samples were determined by means of indentation testing. The test was conducted using a custom-made material testing system (resolution for force and deformation, 5 mN and 0.1  $\mu\text{m}$ , respectively).<sup>19</sup> Cartilage thickness was measured from the OCT image of the sample. The sample was submerged in PBS and a cylindrical plane-ended indenter with a diameter of 530  $\mu\text{m}$  was driven into contact with the sample on the same location where the OCT imaging was conducted. The contact and full recovery of deformation were ensured by indenting the sample 5% of its thickness five times. Then, a stress-relaxation indentation test consisting of two 5% strain steps was performed. Strain rate was 100%/s relative to the thickness of the cartilage. Equilibrium was assumed to be achieved when the slope of relaxation rate was less than 10 Pa/min.

Abaqus (V6.10-1, Dassault Systèmes, Providence, RI, USA) and Matlab (2012a, The MathWorks Inc., Natick, MA, USA) were employed to calculate cartilage biomechanical parameters by fitting an axisymmetric fibril-reinforced poroelastic finite element model to the experimental stress-relaxation data.<sup>20–22</sup> Cartilage was modelled using axisymmetric 4-node continuum pore pressure elements (CAX4P). An elastic fibrillar matrix represented the collagen network and non-fibrillar matrix represented

primarily PGs and fluid. The fibrillar matrix was described with organized primary fibrils and randomly organized secondary fibrils.<sup>20</sup> The indenter was modelled as rigid and the cartilage-indenter contact was assumed to be frictionless and impermeable. The cartilage-bone interface was fixed in all directions. The cartilage edge and the surface not in contact with the indenter were assumed to be fully permeable (zero pore pressure). Mechanical behaviour of the collagen network was expressed with the fibril network modulus ( $E_f$ ), while non-fibrillar matrix modulus ( $E_m$ ) and permeability ( $k$ ) represented the PG/fluid complex. Fluid fraction (80%) and the Poisson's ratio of the non-fibrillar matrix (0.42) were fixed in the model<sup>22,23</sup>, whereas  $E_p$ ,  $E_m$  and permeability were obtained by minimizing the mean square error between the reaction forces in the experiment and finite element model. Since the first step was considered as a pre-strain, the optimization was performed only for the second step.

## Histology

After indentation testing, the samples were stored in a freezer (-20°C). For histological and spectroscopical analyses, the osteochondral samples were thawed, immersed in formalin for at least 48 h, and then decalcified in ethylenediaminetetraacetic acid. After further processing, three Safranin-O stained sections (thickness = 3  $\mu\text{m}$ ) for histological evaluation and three unstained sections (thickness = 5  $\mu\text{m}$ ) for spectroscopical analyses were prepared from the measurement site of each sample.

The stained sections were examined with a light microscope (Axio Imager M2, Carl Zeiss MicroImaging, Jena, Germany). Histological integrity of the samples was evaluated from their images by assigning Mankin scores.<sup>24</sup> The images of the three sections from each sample were blindly coded and scored by three investigators (NtM, JT, and VT). The final score was calculated as an average of the scores rounded to the nearest integer. Based on Mankin scores, the samples were further divided into two groups by the severity of the degeneration; from no to mild degeneration (Mankin scores 0-6) and from moderate to severe degeneration (Mankin scores 7-14).<sup>25</sup>

Depthwise PG distribution (fixed charge density) was estimated from optical density (OD) of the grayscale images of Safranin-O stained sections captured with a light microscope and a CCD camera (SenSys, Photometrics Inc., USA).<sup>26</sup> The final OD distribution was obtained as the average OD distribution of the three sections.



## Fourier transform infrared spectroscopy and polarized light microscopy

Light absorbance in amide I region ( $A_{\text{amide}}$ ; 1594-1720  $\text{cm}^{-1}$ ), representative of the collagen content, was assessed as a mean absorbance distribution in the three unstained sections using Fourier transform infrared spectroscopy (FTIR; Spotlight 300 FTIRI, Perkin Elmer, Shelton, CT, USA) analysis.<sup>27</sup> Collagen orientation with respect to cartilage surface direction was determined by means of polarized light microscopy (Ortholux II POL; Leitz Wetzlar, Wetzlar, Germany) based on Stokes parameters.<sup>28,29</sup>

## OCT analysis: total attenuation and backscattering coefficient

$\mu_t$  and  $\mu_b$  were determined by fitting the mean depthwise OCT intensity curve,  $I(d)$ , into the following equation:<sup>30</sup>

$$I(d) \propto \sqrt{\mu_b} \frac{1}{\sqrt{\left(\frac{d-d_0}{z_0}\right)^2 + 1}} \exp(-\mu_t d), \quad (1)$$

$d_0$  beam focus position and  $z_0$  the apparent Rayleigh length. Prior to fitting, the OCT system was calibrated using suspension series of water and polystyrene spheres (diameter = 5  $\mu\text{m}$ ; Phosphores Inc., Hopkinton, MA, USA).<sup>15</sup>

## OCT analysis: Partial least squares regression multivariate analysis

PLS regression models were developed to estimate cartilage properties based on depth-dependent OCT signal. Multivariate PLS regression is an analytical technique for relating potentially correlated and noisy predictor variables to one or several response variables by finding a linear regression between them in a new space.<sup>18</sup> Briefly, developed and validated PLS regression models that optimize the relationship between the predictor and response variables are used to predict the response variables of new samples from predictor variables. In the present study, the OCT intensity curves were smoothed using a fourth degree Savitzky-Golay filter and the second derivatives of the smoothed intensity curves were used as predictor variables in the PLS analyses. Mankin score, severity of degeneration,  $E_p$ ,  $E_m$ , permeability and averages of OD,  $A_{\text{amide}}$  and collagen orientation within the whole cartilage layer, the superficial zone (10% of cartilage thickness), the middle zone (15%) and the deep zone (75%) of the cartilage served as response variables.

Leave-one-out cross-validation was computed in order to determine the optimal number of PLS components of the models.<sup>31</sup> Too few components may result in under-fitting, while too many may yield over-fitted models. In leave-one-out cross-validation each sample is left out one by one and the other samples are used to predict the response property of the sample left out. The criteria for optimal model selection were based on the model with the highest coefficient of determination ( $R^2$ ) and the lowest root mean square error of cross-validation (RMSECV). Model performance was evaluated by predicting the cartilage properties of the samples from their OCT signals using the created model.<sup>32,33</sup> The root mean square error of prediction (RMSEP) was calculated from the deviation between the predicted and true response parameter values  $\hat{y}$  and  $y$ , respectively):

$$RMSEP = \sqrt{\frac{\sum_{i=1}^n (\hat{y}_i - y_i)^2}{n}}, \quad (2)$$

where  $n$  is the number of samples. For data pre-processing and multivariate analyses, custom-written software utilizing the SIMPLS algorithm in Matlab (2014a; MathWorks, Inc., Natic, MA, USA) was used.

## Statistical analyses

Relationships of  $\mu_t$  and  $\mu_b$  with other determined properties of articular cartilage were evaluated by calculating Spearman's rank correlation coefficients (IBM SPSS Statistics 19, SPSS Inc., Chicago, USA). A monotonic relationship of  $\mu_t$  and  $\mu_b$  with the cartilage properties was assumed.

## RESULTS

Mean (standard deviation) for  $\mu_t$  and  $\mu_b$  of the samples were  $2.2 \text{ mm}^{-1}$  ( $1.1 \text{ mm}^{-1}$ ) and  $13.4 \text{ mm}^{-1}$  ( $7.9 \text{ mm}^{-1}$ ) respectively. Mean and standard deviation of Mankin score, permeability,  $E_m$ ,  $E_p$ , OD,  $A_{\text{amide}}$  and collagen orientation are presented in table 1. A significant linear correlation was found between  $\mu_b$  and  $E_p$  but not between  $\mu_b$  and the Mankin score,  $k$ ,  $E_m$ , OD,  $A_{\text{amide}}$  or collagen orientation (table 2).

In the PLS analyses, three to seven PLS components were found to be optimal in the regression models created between OCT intensity curve and the different properties of articular cartilage. Correlations between the measured properties of articular cartilage and those predicted using PLS models were high for Mankin score ( $R^2 = 0.70$ ,  $RMSEP = 1.4$ ), permeability ( $R^2 = 0.74$ ,  $RMSEP = 4.4 \times 10^{-15} \text{ m}^4 \text{N}^{-1} \text{ s}^{-1}$ ), bulk OD ( $R^2 = 0.73$ ,  $RMSEP = 0.16 \text{ arb. unit}$ ) and OD in different zones of the articular cartilage ( $R^2 \geq 0.79$ ,

RMSEP  $\leq 0.25$  arb. unit) (table 1). Correlation between the predicted and measured bulk collagen orientation was good ( $R^2 \geq 0.75$ , RMSEP =  $7.1^\circ$ ), but even if the number of PLS coefficients was further reduced, the error in cross-validation remained high compared to the standard deviation of the measured orientation values. Moderate and significant correlations ( $R^2 < 0.70$ ,  $p < 0.0001$ ) were found between the measured and predicted  $E_m$ ,  $E_f$  and  $A_{amide}$  of the articular cartilage samples (table 1). The relations between the predicted and measured bulk properties of the samples are presented in figure 2. Bland-Altman plots show the agreement between the measured and predicted properties of the samples (fig. 3). Nine of all samples were initially grouped into the category of moderate to severe degeneration based on their Mankin scores. Six of those samples were similarly diagnosed when the severity of degeneration was predicted using the PLS model.

**Table 1** Mean and standard deviation for various properties of articular cartilage (response variables) and the PLS regression statistics for prediction of the variables based on depthwise OCT intensity curves.

Response variable	zone	Mean of response variable	Std of response variable	Number of Components	RMSEP	$R^2$
Mankin score	all	3.5	2.6	5	1.4	0.70
Permeability ( $\times 10^{-15} \text{ m}^4 \text{ N}^{-1} \text{ s}^{-1}$ )	all	5.5	8.7	5	4.4	0.74
$E_m$ (MPa)	all	0.25	0.24	3	0.17	0.50
$E_f$ (MPa)	all	1.74	1.18	3	0.89	0.42
OD (arb. unit)	all	1.42	0.37	5	0.16	0.73
	superficial	0.67	0.40	6	0.18	0.79
	middle	1.20	0.55	6	0.25	0.79
	deep	1.57	0.35	6	0.16	0.80
$A_{amide}$ (arb. unit)	all	42.0	4.9	4	3.7	0.43
	superficial	23.6	4.6	5	2.7	0.64
	middle	30.7	5.0	5	3.2	0.57
	deep	46.7	5.3	5	8.8	0.56
Collagen orientation (deg)	all	66.2	14.4	7	7.1	0.75
	superficial	35.9	17.0	4	11.3	0.55
	middle	58.7	16.1	4	10.6	0.56
	deep	71.7	16.8	4	11.8	0.50

Std = standard deviation, RMSEP = root mean square error in prediction,  $R^2$  = coefficient of determination,  $E_m$  = non-fibrillar matrix modulus,  $E_f$  = fibril network modulus, OD = optical density,  $A_{amide}$  = FTIR absorbance in amide I region.

**Table 2** Linear correlations between the measured compositional, structural and biomechanical properties of articular cartilage and its light attenuation and backscattering coefficient ( $\mu_t$  and  $\mu_b$ , respectively) indicated by Spearman's rank correlation coefficients ( $\rho$ ) and the corresponding P-values.

	Mankin score	Permeability ( $\times 10^{-15} \text{ m}^4 \text{ N}^{-1} \text{ s}^{-1}$ )	$E_m$ (MPa)	$E_f$ (MPa)	OD (arb. unit)	$A_{\text{amide}}$ (arb. unit)	Collagen orientation (deg)
$\mu_t$	$\rho = 0.019$	$\rho = -0.043$	$\rho = 0.107$	$\rho = 0.093$	$\rho = -0.021$	$\rho = 0.071$	$\rho = 0.129$
	$p = 0.88$	$p = 0.74$	$p = 0.41$	$p = 0.47$	$p = 0.87$	$p = 0.58$	$p = 0.31$
$\mu_b$	$\rho = -0.026$	$\rho = -0.128$	$\rho = 0.166$	$\rho = 0.280$	$\rho = 0.086$	$\rho = 0.241$	$\rho = 0.138$
	$p = 0.84$	$p = 0.33$	$p = 0.20$	$p = 0.03$	$p = 0.50$	$p = 0.06$	$p = 0.28$

$E_m$  = non-fibrillar matrix modulus,  $E_f$  = fibril network modulus, OD = optical density,  $A_{\text{amide}}$  = FTIR absorbance in amide I region,  $\mu_t$  = total attenuation coefficient,  $\mu_b$  = backscattering coefficient.

## DISCUSSION

The diagnostic value of conventional arthroscopic evaluation is limited when assessing early stage cartilage degeneration due to subjectivity.<sup>6</sup> The application of OCT under arthroscopic guidance provides more detailed images of the cartilage lesions and enhances the reproducibility of cartilage lesion scoring.<sup>34</sup> In addition, OCT could also be used to investigate microstructural tissue changes. The present study demonstrates the diagnostic potential of OCT via multivariate analysis, in assessment of degenerative changes in the composition, structure, and mechanical properties of articular cartilage.

Based on the results, the bulk attenuation and backscattering parameters, determined from OCT signal, were not sensitive enough to detect small compositional changes in articular cartilage. Both collagen and chondrocytes scatter light and affect the OCT signal.<sup>15</sup> However, possible changes in their content during degeneration were not revealed by measuring  $\mu_t$  or  $\mu_b$ . The sensitivity of the bulk attenuation coefficient for early osteoarthritic changes in articular cartilage was also questioned by Nebelung et al.<sup>35</sup> This supports the choice of multivariate analysis of the OCT signal for detailed diagnostic purposes.

The PLS models constructed based on the measured OCT signals provided high correlation especially between the measured and the predicted values of Mankin score, permeability, OD, and bulk collagen orientation. All the samples having no or mild degeneration were correctly classified by predicting their Mankin scores, whereas three out of nine samples were misclassified to have no to mild degeneration as opposed to moderate to severe degeneration. Permeability does not have effect on the optical properties of articular cartilage, but it is a good measure of many simultaneous changes in composition and structure of the tissue during

degeneration. The permeability of articular cartilage relates to the PG content of the tissue.<sup>36</sup> Therefore, the contribution of PGs to OCT signal may be the reason for the correlation between the measured and predicted permeability. In the present study, OD was used as the measure of PG content. Earlier, PGs have not been shown to affect the birefringence<sup>37</sup> or surface reflection<sup>38</sup> when measured by OCT. However, the present high correlation between measured OD and OD predicted by the PLS model might indicate a contribution of PGs to OCT light backscattering. The influence of PGs on OCT signal is of great interest as PG depletion, in addition to disorganization of collagen matrix, is one of the first signs of cartilage degeneration.<sup>39,40</sup>

It is worth noting that the OCT system used in this study was not designed for measurement of birefringence. Hence, the significant relation between the OCT signal and collagen orientation may result, in part, from varying scattering properties of fibrils oriented at different angles as well as from other compositional and structural properties that change simultaneously with disorganization of the collagen network. However, the measurement of birefringence would be a valuable addition for identification of early cartilage degeneration.<sup>7</sup> Additionally, the use of an ultra-high-resolution OCT system could improve the detection of the depthwise changes in the amount of small scattering components. The use of higher resolution would also increase the number of predictor variables in the model, and could possibly improve the accuracy of the PLS predictive model.

The relationship between the measured and predicted FTIR absorbance in amide I region (i.e., collagen content) was not strong ( $R^2 = 0.43$ ). Mechanical properties of articular cartilage are related to collagen matrix properties.<sup>20,41</sup> Therefore, the relation of OCT signal to fibril network modulus may reflect its relation to collagen content and organization. In early stage of degeneration, the collagen content abides although the fibril organization changes.<sup>3</sup> Therefore, the assessment of collagen content may be of minor importance when differentiating healthy cartilage from areas with signs of the earliest stage of degeneration.

Due to the limited light penetration, OCT imaging cannot be conducted non-invasively, but is a useful tool in arthroscopies.<sup>9,10</sup> Presently, with thin equine cartilage, the prediction ability of the PLS models was similar for each of the three cartilage zones. In OCT analysis, the structural and compositional properties in the superficial zone of articular cartilage may have the highest diagnostic value. The limited penetration depth (1-2 mm<sup>42</sup>) of the light might hinder the ability to analyse middle and deep zones of thick human articular cartilage. By choosing adequate central wavelength for the OCT light, the light penetration could be marginally

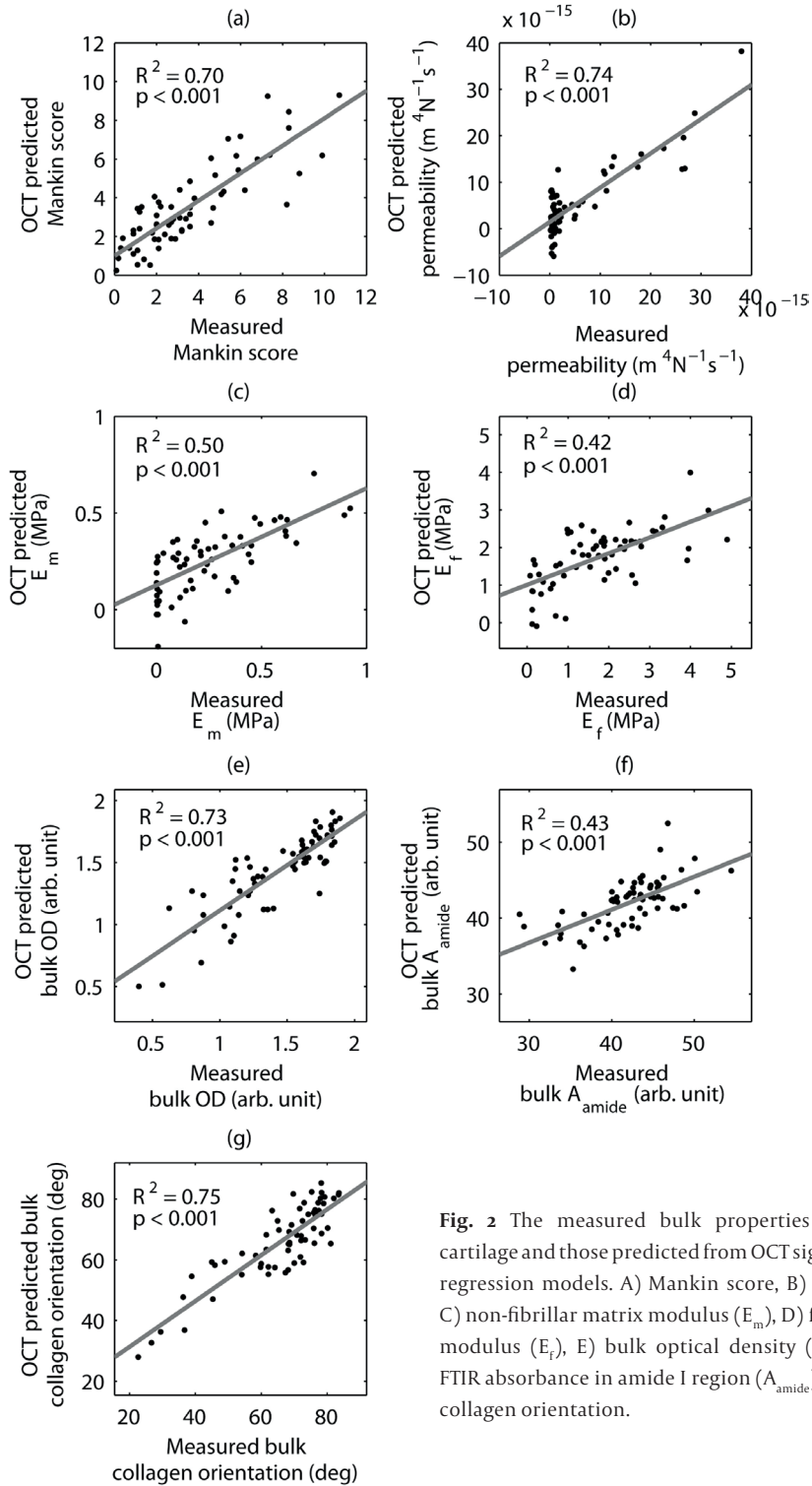


**Fig. 2** The measured bulk properties of articular cartilage and those predicted from OCT signal using PLS regression models. A) Mankin score, B) permeability, C) non-fibrillar matrix modulus ( $E_m$ ), D) fibril network modulus ( $E_f$ ), E) bulk optical density (OD), F) bulk FTIR absorbance in amide I region ( $A_{\text{amide}}$ ), and G) bulk collagen orientation.

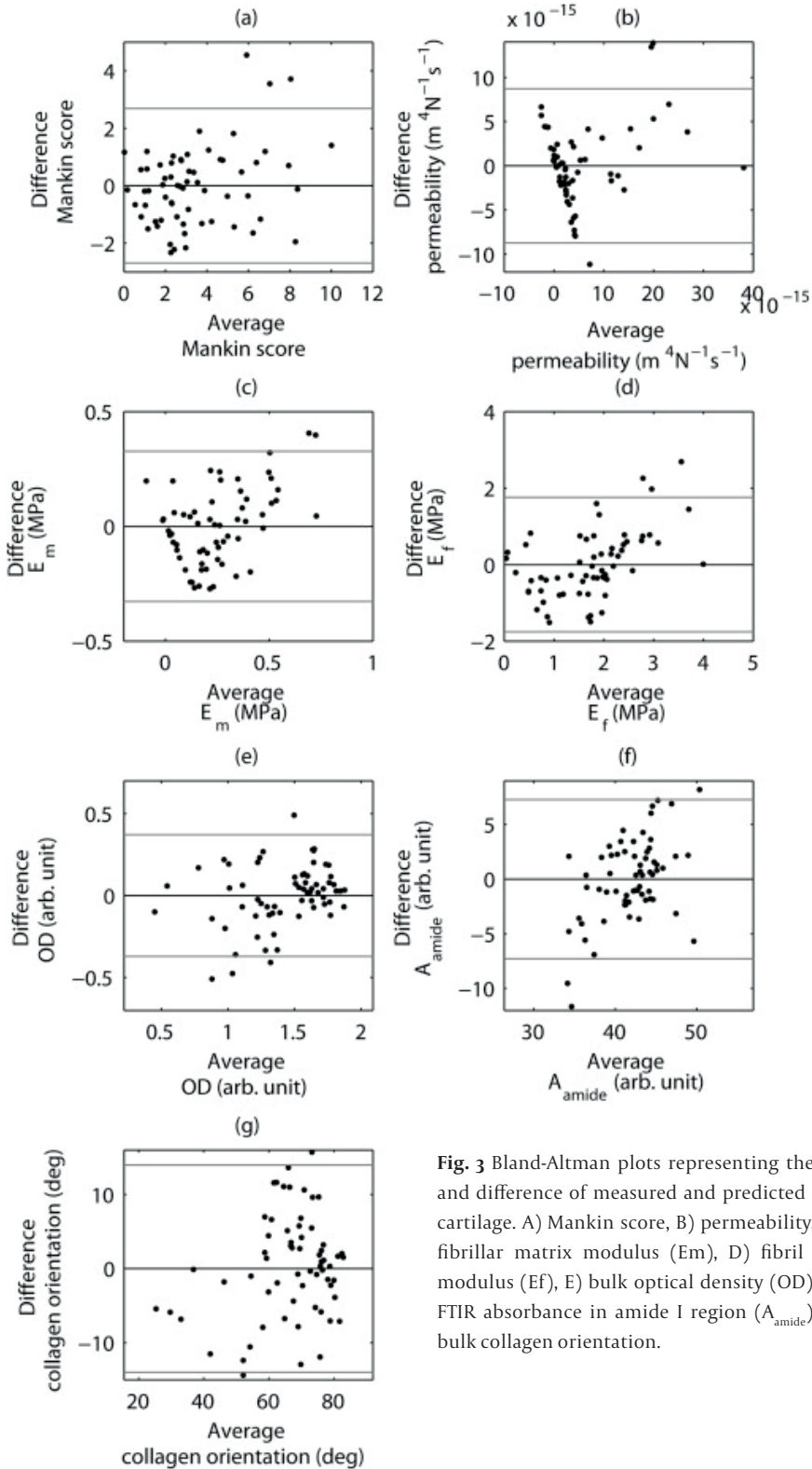


**Fig. 3** Bland-Altman plots representing the average and difference of measured and predicted articular cartilage. A) Mankin score, B) permeability, C) non-fibrillar matrix modulus ( $E_m$ ), D) fibril network modulus ( $E_f$ ), E) bulk optical density (OD), F) bulk FTIR absorbance in amide I region ( $A_{\text{amide}}$ ), and G) bulk collagen orientation.

improved.<sup>43</sup> However, the optimal choice of wavelength is a sensitive balance between increase in water absorption and decrease of scattering.<sup>44</sup> Further studies with human cartilage are needed to investigate if the evaluation of cartilage only to depth of 1-2 mm is sufficient for the diagnostics.

Following our hypothesis, multivariate analyses of depthwise optical intensity signal from OCT images of articular cartilage has potential to provide information on tissue compositional, structural and mechanical properties that are otherwise non-accessible from bulk attenuation and backscattering properties. However, Bland-Altman analysis showed a higher accuracy of the models for cartilage with no or mild degenerative changes. This arises from the under-representation of cartilage with advanced degeneration in the sample set. The errors obtained in the present study should be reduced for research purposes, but could be satisfactory for diagnostics as small errors may not affect clinical decisions. Nevertheless, the approach needs to be further validated and optimized before it can be applied clinically. For example, test set validation, which uses a set of test samples independent of the training set, could be used to further validate the performance of the multivariate models developed in this study. Further, doubling the amount of samples in training of the PLS model may improve the accuracy of the assessment and would enable use of the test set validation.<sup>18</sup> Adequate diagnostic accuracy and good intra- and inter-observer agreements in both model creation and prediction of cartilage properties are required, and they need to be thoroughly evaluated.

Quantitative OCT analysis could improve the evaluation of articular cartilage integrity. After careful calibration and validation of the PLS model, the use of the model for prediction of cartilage properties could be fast and feasible in clinical use. The present technique might be used in arthroscopic surgery in order to delineate degenerated areas around articular cartilage lesions and to aid the selection of the optimal treatment method.

## **ACKNOWLEDGEMENTS**

Funding was received from Academy of Finland (132367, 267551), University of Eastern Finland (Spearhead 931053) and Kuopio University Hospital (5041723, 5041738). The funding sources did not play any role in the study design, data collection or analysis, writing the manuscript, or decision to submit the manuscript for publication. Eija Rahunen and Simo Ojanen are acknowledged for technical assistance.



## REFERENCES

1. Buckwalter JA, Brown TD. Joint Injury, Repair, and Remodeling. *Clin Orthop Relat Res.* 2004;423:7-16.
2. Caron JP. Osteoarthritis. In: Ross MW, Dyson SJ, eds. *Diagnosis and Management of Lameness in the Horse.* 2nd ed. Saint Louis: Elsevier Saunders; 2011:655-668.
3. Buckwalter JA, Mankin HJ. Articular cartilage. Part II: degeneration and osteoarthritis, repair, regeneration, and transplantation. In: *Journal of Bone and Joint Surgery - Series A;* 1997:612-632.
4. Hunziker EB. Articular cartilage repair: basic science and clinical progress. A review of the current status and prospects. *Osteoarthr Cartil.* 2002;10(6):432-463.
5. Gomoll AH, Filardo G, de Girolamo L, et al. Surgical treatment for early osteoarthritis. Part I: cartilage repair procedures. *Knee Surgery, Sport Traumatol Arthrosc.* 2012;20(3):450-466.
6. Brismar BH, Wredmark T, Movin T, Leandersson J, Svensson O. Observer reliability in the arthroscopic classification of osteoarthritis of the knee. *J bone Jt surgery British Vol.* 2002;84(1):42-47.
7. Chu CR, Williams A, Tolliver D, Kwoh CK, Bruno 3rd S, Irrgang JJ. Clinical optical coherence tomography of early articular cartilage degeneration in patients with degenerative meniscal tears. *Arthritis Rheum.* 2010;62(5):1412-1420.
8. Chu CR, Williams AA, Coyle CH, Bowers ME. Early diagnosis to enable early treatment of pre-osteoarthritis. *Arthritis Res Ther.* 2012;14(3):212.
9. Pan Y, Li Z, Xie T, Chu CR. Hand-held arthroscopic optical coherence tomography for in vivo high-resolution imaging of articular cartilage. *J Biomed Opt.* 2003;8(4):648-654.
10. te Moller NCR, Brommer H, Liukkonen J, et al. Arthroscopic optical coherence tomography provides detailed information on articular cartilage lesions in horses. *Vet J.* 2013;197(3):589-595.
11. Chu CR, Lin D, Geisler JL, Chu CT, Fu FH, Pan Y. Arthroscopic microscopy of articular cartilage using optical coherence tomography. *Am J Sports Med.* 2004;32(3):699-709.
12. Drexler W, Stamper D, Jesser C, et al. Correlation of collagen organization with polarization sensitive imaging of in vitro cartilage: implications for osteoarthritis. *J Rheumatol.* 2001;28(6):1311-1318.
13. Xu C, Schmitt JM, Carlier SG, Virmani R. Characterization of atherosclerosis plaques by measuring both backscattering and attenuation coefficients in optical coherence tomography. *J Biomed Opt.* 2008;13(3):034003.
14. Cernohorsky P, Kok AC, Bruin DM De, et al. Comparison of optical coherence tomography and histopathology in quantitative assessment of goat talus articular cartilage. *Acta Orthop.* 2015;86(2):257-263.
15. Puhakka PH, Ylärinne JH, Lammi MJ, et al. Dependence of light attenuation and backscattering on collagen concentration and chondrocyte density in agarose scaffolds. *Phys Med Biol.* 2014;59(21):6537-6548.
16. Li G, Thomson M, Dicarolo E, et al. A chemometric analysis for evaluation of early-stage cartilage degradation by infrared fiber-optic probe spectroscopy. *Appl Spectrosc.* 2005;59(12):1527-1533.
17. Afara I, Prasadam I, Crawford R, Xiao Y, Oloyede A. Non-destructive evaluation of articular cartilage defects using near-infrared (NIR) spectroscopy in osteoarthritic rat models and its direct relation to Mankin score. *Osteoarthritis Cartilage.* 2012;20(11):1367-1373.
18. Wold S, Sjöström M, Eriksson L. PLS-regression: a basic tool of chemometrics. *Chemom Intell Lab Syst.* 2001;58(2):109-130. doi:10.1016/S0169-7439(01)00155-1
19. Toyras J, Rieppo J, Nieminen MT, Helminen HJ, Jurvelin JS. Characterization of enzymatically induced degradation of articular cartilage using high frequency ultrasound. *Phys Med Biol.* 1999;44(11):2723-2733.

20. Julkunen P, Kiviranta P, Wilson W, Jurvelin JS, Korhonen RK. Characterization of articular cartilage by combining microscopic analysis with a fibril-reinforced finite-element model. *J Biomech.* 2007;40(8):1862-1870.
21. Mäkelä JTA, Huttu MRJ, Korhonen RK. Structure-function relationships in osteoarthritic human hip joint articular cartilage. *Osteoarthr Cartil.* 2012;20(11):1268-1277.
22. Korhonen RK, Laasanen MS, Toyras J, Lappalainen R, Helminen HJ, Jurvelin JS. Fibril reinforced poroelastic model predicts specifically mechanical behavior of normal, proteoglycan depleted and collagen degraded articular cartilage. *J Biomech.* 2003;36(9):1373-1379.
23. Li LP, Soulhat J, Buschmann MD, Shirazi-Adl A. Nonlinear analysis of cartilage in unconfined ramp compression using a fibril reinforced poroelastic model. *Clin Biomech (Bristol, Avon).* 1999;14(9):673-682.
24. Mankin HJ, Dorfman H, Lippiello L, Zarins A. Biochemical and metabolic abnormalities in articular cartilage from osteo-arthritic human hips. II. Correlation of morphology with biochemical and metabolic data. *J bone Jt surgeryAmerican Vol.* 1971;53(3):523-537.
25. Ehrlich MG, Houle PA, Vigliani G, Mankin HJ. Correlation between articular cartilage collagenase activity and osteoarthritis. *Arthritis Rheum.* 1978;21(7):761-766.
26. Király K, Lapveteläinen T, Arokoski J, et al. Application of selected cationic dyes for the semiquantitative estimation of glycosaminoglycans in histological sections of articular cartilage by microspectrophotometry. *Histochem J.* 1996;28(8):577-590.
27. Boskey A, Pleshko Camacho N. FT-IR imaging of native and tissue-engineered bone and cartilage. *Biomaterials.* 2007;28(15):2465-2478.
28. Massoumian F, Juskaitis R, Neil MA, Wilson T. Quantitative polarized light microscopy. *J Microsc.* 2003;209(Pt 1):13-22.
29. Rieppo J, Hallikainen J, Jurvelin JS, Kiviranta I, Helminen HJ, Hyttinen MM. Practical considerations in the use of polarized light microscopy in the analysis of the collagen network in articular cartilage. *Microsc Res Tech.* 2008;71(4):279-287.
30. Faber DJ, van der Meer FJ, Aalders MCG, van Leeuwen TG. Quantitative measurement of attenuation coefficients of weakly scattering media using optical coherence tomography. *Opt Express.* 2004;12(19):4353.
31. Lorber A, Kowalski BR. Alternatives to Cross-Validatory Estimation of the Number of Factors in Multivariate Calibration. *Appl Spectrosc.* 1990;44(9):1464-1470.
32. Wang L, Chapman J, Palmer RA, et al. Classification of atherosclerotic rabbit aorta samples with an infrared attenuated total reflection catheter and multivariate data analysis. *Appl Spectrosc.* 2006;60(10):1121-1126.
33. Afara IO, Prasadam I, Moody H, Crawford R, Xiao Y, Oloyede A. Near infrared spectroscopy for rapid determination of Mankin score components: a potential tool for quantitative characterization of articular cartilage at surgery. *Arthroscopy.* 2014;30(9):1146-1155.
34. Niemelä T, Virén T, Liuukkonen J, et al. Application of optical coherence tomography enhances reproducibility of arthroscopic evaluation of equine joints. *Acta Vet Scand.* 2014;56(3):1-8.
35. Nebelung S, Marx U, Brill N, et al. Morphometric grading of osteoarthritis by optical coherence tomography - An ex vivo study. *J Orthop Res.* 2014;32(10):1381-1388.
36. Maroudas A. Physicochemical properties of articular cartilage. In: Freeman MAR, ed. *Adult Articular Cartilage.* Kent: Pitman Medical Publishing; 1979:215-290.
37. Xie T, Guo S, Zhang J, Chen Z, Peavy GM. Determination of characteristics of degenerative joint disease using optical coherence tomography and polarization sensitive optical coherence tomography. *Lasers Surg Med.* 2006;38(9):852-865.

38. Saarakkala S, Wang SZ, Huang YP, Zheng YP. Quantification of the optical surface reflection and surface roughness of articular cartilage using optical coherence tomography. *Phys Med Biol*. 2009;54(22):6837-6852.
39. Martel-Pelletier J, Boileau C, Pelletier J-P, Roughley PJ. Cartilage in normal and osteoarthritis conditions. *Best Pract Res Clin Rheumatol*. 2008;22(2):351-384.
40. Mäkelä JTA, Rezaeian ZS, Mikkonen S, et al. Site-dependent changes in structure and function of lapine articular cartilage 4 weeks after anterior cruciate ligament transection. *Osteoarthr Cartil*. 2014;22(6):869-878.
41. Mow VC, Ratcliffe A, Poole AR. Cartilage and diarthrodial joints as paradigms for hierarchical materials and structures. *Biomaterials*. 1992;13(2):67-97.
42. Drexler W. Ultrahigh-resolution optical coherence tomography. *J Biomed Opt*. 2004;9(1):47.
43. Sharma U, Chang EW, Yun SH. Long-wavelength optical coherence tomography at 17  $\mu\text{m}$  for enhanced imaging depth. *Opt Express*. 2008;16(24):19712.
44. Bouma BE, Nelson LE, Tearney GJ, Jones DJ, Brezinski ME, Fujimoto JG. Optical Coherence Tomographic Imaging of Human Tissue at 1.55  $\mu\text{m}$  and 1.81  $\mu\text{m}$  Using Er- and Tm-Doped Fiber Sources. *J Biomed Opt*. 1998;3(1):76.



# CHAPTER 6

## Arthroscopic near infrared spectroscopy enables simultaneous quantitative evaluation of articular cartilage and subchondral bone in vivo

*Scientific Reports 8, 13409 (2018)*

---

J.K. Sarin<sup>1,2</sup>

N.C.R. te Moller<sup>3</sup>

I.A.D. Mancini<sup>3</sup>

H. Brommer<sup>3</sup>

J. Visser<sup>4</sup>

J. Malda<sup>3,4</sup>

P.R. van Weeren<sup>3</sup>

I.O. Afara<sup>1</sup>

J. Töyräs<sup>1,2</sup>

---

<sup>1</sup>Department of Applied Physics, University of Eastern Finland, Kuopio, Finland, <sup>2</sup>Diagnostic Imaging Center, Kuopio University Hospital, Kuopio, Finland, <sup>3</sup>Department of Equine Sciences, Faculty of Veterinary Medicine, Utrecht University, Utrecht, The Netherlands, <sup>4</sup>Department of Orthopaedics, University Medical Center Utrecht, Utrecht, The Netherlands

## ABSTRACT

Arthroscopic assessment of articular tissues is highly subjective and poorly reproducible. To ensure optimal patient care, quantitative techniques (e.g., near infrared spectroscopy (NIRS)) could substantially enhance arthroscopic diagnosis of initial signs of post-traumatic osteoarthritis (PTOA). Here, we demonstrate, for the first time, the potential of arthroscopic NIRS to simultaneously monitor progressive degeneration of cartilage and subchondral bone *in vivo* in Shetland ponies undergoing different experimental cartilage repair procedures. Osteochondral tissues adjacent to the repair sites were evaluated using an arthroscopic NIRS probe and significant ( $p < 0.05$ ) degenerative changes were observed in the tissue properties when compared with tissues from healthy joints. Artificial neural networks (ANN) enabled reliable ( $\rho = 0.63$ – $0.87$ , NMRSE = 8.5–17.2%, RPIQ = 1.93–3.03) estimation of articular cartilage biomechanical properties, subchondral bone plate thickness and bone mineral density (BMD), and subchondral trabecular bone thickness, bone volume fraction (BV), BMD, and structure model index (SMI) from *in vitro* spectral data. The trained ANNs also reliably predicted the properties of an independent *in vitro* test group ( $\rho = 0.54$ – $0.91$ , NMRSE = 5.9%–17.6%, RPIQ = 1.68–3.36). However, predictions based on arthroscopic NIR spectra were less reliable ( $\rho = 0.27$ – $0.74$ , NMRSE = 14.5–24.0%, RPIQ = 1.35–1.70), possibly due to errors introduced during arthroscopic spectral acquisition. Adaptation of NIRS could address the limitations of conventional arthroscopy through quantitative assessment of lesion severity and extent, thereby enhancing detection of initial signs of PTOA. This would be of high clinical significance, for example, when conducting orthopaedic repair surgeries.

## INTRODUCTION

Osteoarthritis (OA) is a disabling disease associated with joint pain and restricted mobility, especially in the elderly.<sup>1,2</sup> Post-traumatic OA (PTOA), however, affects people of all ages and is initiated by joint trauma<sup>3</sup>, e.g., cartilage, meniscus, and ligament tears. These traumas conventionally require arthroscopic intervention, which is a common technique in both human and equine medicine. Mechanisms involved in the degeneration of articular cartilage have been extensively researched, and several studies<sup>3,4</sup> have suggested changes in the subchondral bone properties to contribute to the initiation and progression of OA. In addition, subchondral bone is susceptible to morphological and compositional changes due to alterations in the stress distribution<sup>5,6</sup>; these changes can substantially influence joint functionality. Conventional arthroscopy is, however, based on qualitative visual and tactile assessment, rendering the technique subjective with suboptimal reliability<sup>7,8</sup>. Reliable evaluation of defects and the surrounding tissues is essential in choosing the optimal repair procedure and, thus, for halting the progression of PTOA.<sup>9,10</sup> This highlights the need for novel quantitative arthroscopic techniques, such as ultrasound<sup>11</sup>, optical coherence tomography (OCT<sup>12</sup>), and near infrared spectroscopy (NIRS<sup>13</sup>).

NIRS is a non-destructive optical technique in which the sample is irradiated with light, and the scattered and reflected light is collected. The technique enables rapid evaluation of tissues *in vivo* and eliminates the need for invasive, destructive, and slow chemical analysis.<sup>14</sup> NIRS enables swift assessment of cartilage biomechanical properties<sup>13,15-18</sup> and composition<sup>13</sup>, as well as subchondral bone structure<sup>19</sup>. The spectral range between 0.4 and 2.5  $\mu\text{m}$  enables assessment of the tissue at various depths due to the wavelength-dependent penetration depth.<sup>20</sup> The shorter wavelengths penetrate through the cartilage matrix into the subchondral and trabecular bone<sup>21</sup>, whereas longer wavelengths (closer to the mid infrared region) are restricted to the superficial layer of cartilage<sup>20</sup>. While there are several *in vitro* studies on the application of NIRS for cartilage assessment<sup>13,15-18,21,22</sup>, only a few have investigated the potential of this optical technique *in vivo*<sup>23-27</sup>. Furthermore, in these *in vivo* studies, cartilage condition was only evaluated using simple and poorly effective analytical approaches, such as determining the ratio of spectral peaks. Robust and effective analytical techniques, such as neural networks, could enable more accurate and reliable estimation of cartilage properties from the near infrared (NIR) spectral data. Advances in multivariate analysis techniques and the increase in available computational resources have enabled accurate modelling of the relationships between complex NIR spectral data and reference parameters, such as cartilage biomechanical properties. Partial least squares regression (PLSR) is currently

the most common technique in chemometrics for analysis of NIR spectral data.<sup>28</sup> However, artificial neural networks (ANN) combined with variable selection methods have recently been introduced for analysis of cartilage spectral data<sup>22,29,30</sup> and have shown potential for evaluation of tissue properties.

We hypothesize that arthroscopic NIRS enables reliable simultaneous evaluation of articular cartilage and subchondral bone *in vivo* via adaptation of ANN. To test this hypothesis, arthroscopic and *in vitro* NIRS measurements were conducted on tissue surrounding experimental cartilage repair sites in equine joints at the 12-month end-point and compared with unaffected tissue harvested from matching sites in healthy control ponies. As references, articular cartilage biomechanical properties and subchondral bone microstructure and density were determined via indentation testing and computed tomography, respectively. To investigate the relationship between the spectral data and reference parameters, ANN with forward variable selection technique was adapted.

## METHODS

Two cylindrical ( $d = 9$  mm) chondral lesions were surgically created on the medial femoral ridges of both femoropatellar joints of Shetland ponies ( $N = 7$ , 6 females and 1 male, Age =  $8.8 \pm 3.5$  years, total of 28 lesions). Each lesion was treated by filling it with Gelatin Methacryl (GelMA) hydrogel (3 varieties) or fibrin glue<sup>31</sup>. The repair procedure (fibrin glue, GelMA cap, GelMA, or reinforced GelMA) was randomized (proximal or distal lesion site and left or right knee) for each defect. A mixture of allogeneic mesenchymal stem cells (MSCs) and chondrons (80/20% ratio) at different concentrations was implanted in each defect. In the fibrin glue group, a low cell concentration (2 million cells/ml) was used, whereas the GelMA cap group had 1 million cells in a small volume of GelMA on the bottom of the defect, covered by a layer of cell free GelMA. In the last two groups, a high concentration (20 million cells/ml) was implanted in GelMA gel, and in the reinforced GelMA group, GelMA was reinforced with a 3D printed scaffold (melt electrospun polycaprolactone mesh)<sup>32</sup>.

After 12 months, the ponies were sacrificed and the osteochondral defects, together with the surrounding tissues, were examined via conventional and NIRS arthroscopes. Subsequently, osteochondral blocks were extracted for further analysis. As control, a similar osteochondral block was extracted from both femoropatellar joints of healthy ponies ( $N_{\text{control}} = 3$ , Age =  $10.3 \pm 4.7$  years), ensuring an overall representative sample population. The animal studies were approved by the Ethics Committee of



Utrecht University for Animal Experiments in compliance with the Institutional Guidelines on the Use of Laboratory Animals and carried out in a surgical theatre at the Department of Equine Sciences, Utrecht University, The Netherlands (Permission DEC 2014.III.11.098). The control ponies were acquired from a slaughterhouse in Utrecht, The Netherlands.

### Arthroscopic near infrared spectroscopy

Near infrared (NIR) spectral measurements ( $N_{\text{ponies}} = 7$ ,  $N_{\text{per joint}} = 12$ ,  $N_{\text{total}} = 164$ , 4 locations arthroscopically unreachable) were acquired arthroscopically in vivo by an experienced board-certified equine surgeon (>500 arthroscopies, Diplomate European College of Veterinary Surgeons) at the 12-month time-point immediately upon sacrifice. The arthroscopies were performed by utilizing a traditional arthroscope (4 mm, 30° inclination, Synergy HD3, Arthrex, Naples, FL, USA) as a monitoring tool and a novel, robust, and reusable arthroscopic NIRS fibre probe as a measurement tool (fig. 1a). Twelve locations surrounding cartilage repair sites were measured (fig. 1b) by orientating the fibre probe in perpendicular contact with cartilage surface. At each measurement point, 15 spectra were recorded, each being the average of ten successive spectra; the total duration of data acquisition was 2.4 seconds per measurement location. Arthroscopic images were recorded with a conventional arthroscope during the operation to enable reliable location tracking. Ringer's solution (Fresenius, Bad Homburg v.d.H., Germany) containing sodium chloride (8.6 g/L), potassium chloride (0.3 g/L), and calcium chloride (0.33 g/L) was used for joint distension. Following the measurements, osteochondral samples were extracted after removing the skin and overlying tissues of the joint (fig. 1b). The samples were frozen (-20 °C) until required for laboratory NIRS, biomechanical, and computed tomography (CT) measurements.

### In vitro near infrared spectroscopy

The in vitro NIRS measurements ( $N_{\text{ponies}} = 10$ ,  $N_{\text{per joint}} = 12$ ,  $N_{\text{total}} = 236$ ; same 4 locations excluded as during arthroscopy) were acquired in similar conditions as in arthroscopy, i.e., hardware, immersion solution, and temperature, apart from using the conventional arthroscope for navigation. At each measurement point, three successive spectra were acquired, each consisting of 10 co-added scans.

The NIRS system consisted of spectrometers (AvaSpec-ULS2048L,  $\lambda = 0.35 - 1.1 \mu\text{m}$ , resolution = 0.6 nm and AvaSpec-NIR256-2.5-HSC,  $\lambda = 1.0 - 2.5 \mu\text{m}$ , resolution = 6.4 nm, Avantes BV, Apeldoorn, The Netherlands), a light source (AvaLight-HAL-(S)-Mini,  $\lambda = 0.36 - 2.5 \mu\text{m}$ , Avantes BV), and a custom arthroscopic fibre probe (Avantes BV). The reusable stainless-steel fibre probe ( $d = 3.25 \text{ mm}$ ) is sterilisable in an autoclave at

121°C and its tip resembles the shape of a traditional arthroscopic hook. The probe tip window ( $d = 2 \text{ mm}$ ) contains 114 optical fibres ( $d = 100 \mu\text{m}$ ), with 100 fibres emitting and 14 fibres (7+7) collecting light to the spectrometers. Avasoft software (version 8.7.0, Avantes BV) was used for spectral acquisition.

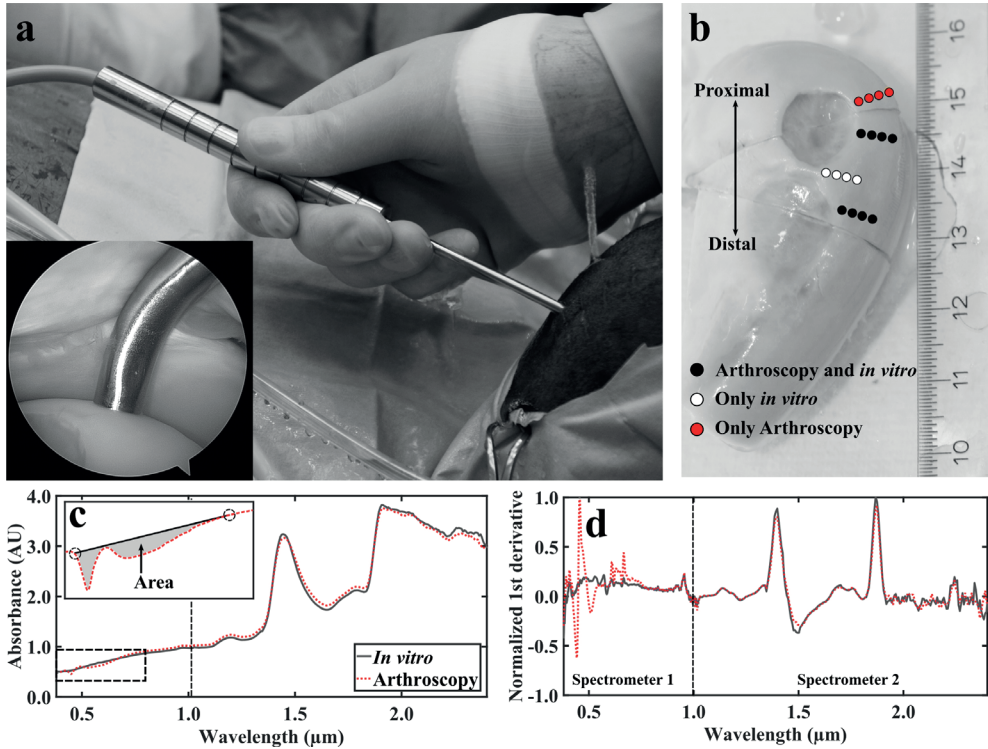


**Fig. 1** The novel fibre optic probe in an equine knee joint *in vivo* (a) with the probe tip in contact with cartilage surface (inset). Locations of NIRS measurements conducted *in vivo* during arthroscopy and *in vitro* in the laboratory (b). Comparison of average smoothed (c) and first derivative pre-processed (d, not used for modelling) spectra collected *in vivo* and *in vitro* with two separate spectrometers to cover the wide spectral region. NIRS measurement locations indicated with white and black dots were subjected to biomechanical and  $\mu\text{CT}$  reference measurements (b). For the red dots, values of reference parameters were only predicted based on ANN models. In subfigure c, calculation of area between a two-point linear fit and measured spectrum was applied to detect outlier spectra. In subfigure d, the 1<sup>st</sup> derivative spectra (not used for analysis) highlight the contribution of light from the conventional arthroscope at the spectral region of  $0.42 - 0.75 \mu\text{m}$ .

## Spectral preprocessing

A 3<sup>rd</sup> order Savitzky-Golay filter was applied for smoothing of spectral data separately for the two spectrometers due to differences in their wavelength resolution. For cartilage and subchondral bone properties, the smoothing points were 25 and 13, and 45 and 13 points, respectively. The spectral region 1.9 – 2.5  $\mu\text{m}$  was discarded from the analyses due to spectral saturation caused by high absorption of water.

In the arthroscopic NIRS measurements, interference from the light source of the conventional arthroscope was observed in the visible spectral region ( $\lambda \approx 0.42 - 0.75 \mu\text{m}$ , fig. 1d). Therefore, this region was applied only as an indicator for probe orientation and not used in the modelling. For arthroscopic NIRS, sufficient contact of the probe with cartilage surface is essential, as the irrigation fluid (i.e., saline) is an effective absorber of NIR light. To evaluate contact between the probe and cartilage surface, the area between a two-point linear fit and the measured spectrum (in a spectral region 0.42 – 0.75  $\mu\text{m}$ ) was calculated (fig. 1c). Four measurement locations were excluded due to high contribution from the arthroscope light source. Additionally, seven spectra (with the largest area between a linear fit and measured spectrum) out of the fifteen measured spectra from all measurement locations were excluded. Coefficient of variation was determined between the arthroscopic and in vitro spectra in spectral region 0.75 – 1.9  $\mu\text{m}$  ( $3.7 \pm 1.9\%$ ).<sup>17</sup>

## Optical coherence tomography

After in vitro NIRS measurements, the measurement locations were marked with a felt tip pen. These points were imaged with OCT ( $\lambda = 1305 \pm 55 \text{ nm}$ , axial resolution  $<20 \mu\text{m}$ , lateral resolution 25 – 60  $\mu\text{m}$ ; Ilumien PCI Optimization System, St. Jude Medical, St. Paul, MN, USA) by aligning a catheter (C7 Dragonfly, St. Jude Medical) over the measurement points (fig. 1b) and performing a pullback imaging, thus imaging the NIRS measurement locations and the surrounding tissue (fig. 2A-C). The samples were submerged in phosphate-buffered saline (PBS) during the imaging. Cartilage thickness was then determined from the OCT images of each location for biomechanical measurements.

## Biomechanical measurements

Biomechanical properties of cartilage surrounding the repairs ( $N_{\text{ponies}} = 10$ ,  $N_{\text{per joint}} = 12$ ,  $N_{\text{total}} = 236$ ) were determined via indentation testing. The samples were glued on a custom-made sample holder, which was mounted on a goniometer (Model #55-841, Edmund Optics Inc., Barrington, NJ, USA) to align the cartilage surface perpendicular with the face of a plane-ended non-porous cylindrical indenter ( $d = 0.53 \text{ mm}$ ). Measurements were performed with the samples submerged in PBS. The indentation

system consisted of a 250 g load cell (accuracy  $\pm 0.25\%$ , Model 31, Honeywell Sensotec Sensors, Columbus, OH, USA) and an actuator (displacement resolution  $0.1 \mu\text{m}$ , PM500-1 A, Newport, Irvine, CA, USA).

First, the indenter was driven into initial contact with the sample. The contact was then ensured by indenting the sample five times using 2% strain. The measurement protocol consisted of four stress-relaxation steps (each of 5% strain) with a ramp velocity of 100%/s and a relaxation time of 600 seconds between the steps, followed by dynamic sinusoidal loading ( $f = 1.0 \text{ Hz}$ ) with a strain amplitude of 1%. The equilibrium modulus ( $E_{\text{eq}}$ ) was determined from the linear region of the stress-relaxation curve by assuming Poisson's ratio of  $\nu = 0.1$ , whereas the dynamic modulus ( $E_{\text{dyn}}$ ) was calculated as a ratio of the stress and strain amplitudes of the sinusoidal loading assuming a Poisson's ratio of  $\nu = 0.5$ <sup>33,34</sup>.

Computed tomography and segmentation

Samples were imaged while submerged in PBS with a micro-CT scanner (Skyscan 1172, Skyscan, Kontich, Belgium) to determine subchondral bone plate and trabecular bone bone volume fraction (BV), bone mineral density (BMD), bone thickness, and trabecular bone structure model index (SMI). The samples were imaged using an isotropic voxel size of  $12.15 \times 12.15 \times 12.15 \mu\text{m}^3$  and 100 kV tube voltage, along with hydroxyapatite phantoms (500, 1000, and 1250  $\text{mg}/\text{cm}^3$ ). To ensure reliable location tracking for the segmentation, plastic cubes of approximately 8  $\text{mm}^3$  were set on the NIRS measurement locations (Fig. 1b). From each measurement location, a cylindrical (diameter = 4.0 mm, height = 5.0 mm) region of interest (ROI) was virtually extracted, and the subchondral plate and trabecular bone were segmented (fig. 2 D-F). The extraction, segmentation, and analysis of bone properties were performed with DataViewer (Skyscan) and CTAn (Skyscan) programs. A global segmentation threshold (BMD = 0.46  $\text{g}/\text{cm}^3$ ) was determined by comparing the binarized and original grayscale images.

## Artificial neural network

The relationship between NIR spectra and reference parameters was investigated using ANN. The ponies were divided into calibration (60%,  $N = 4$  and  $N_{\text{control}} = 2$ , 142 spectra), validation (30%,  $N = 2$  and  $N_{\text{control}} = 1$ , 70 spectra), and test (10%,  $N = 1$ , 24 spectra) groups. For each reference parameter, in vitro models with spectral regions  $0.75 - 1.90 \mu\text{m}$  (Model 2) and  $0.40 - 1.90 \mu\text{m}$  (Model 3) were developed based on in vitro NIR spectra and optimized by determining the most reliable wavelengths via the forward variable selection technique<sup>22,29</sup>. The optimal model was chosen based on the smallest root mean square error (RMSE) of the test group. Additionally, a model

(0.75 – 1.90  $\mu\text{m}$ , Model 1) was developed in which the most reliable wavelengths were determined by evaluating RMSE values of two sets: the test group and the arthroscopic measurements. For each location of the arthroscopic measurements, the final predicted value was resolved as an average of non-negative predicted values. During ANN modelling, the Levenberg-Marquardt backpropagation algorithm was used, while hyperbolic tangent and linear activation functions were employed in the hidden and output layers, respectively. To avoid overfitting, model training was halted after the validation error did not decrease in six successive iterations. The neural network architecture was limited to a maximum of eight neurons in the hidden layer and the analysis was performed in MATLAB (Matlab R2017b, MathWorks Inc., Natick, MA, USA) using the neural network toolbox (Version 11.0). To further evaluate model performance and reliability, the normalized RMSE (NRMSE) and ratio of performance to inter-quartile range (RPIQ)<sup>35</sup> were calculated for in vitro training set (calibration and validation), independent test group, and arthroscopic predictions separately. The NRMSE is determined as RMSE relative to the reference parameter range, whereas RPIQ<sub>i</sub> is determined as

$$\text{RPIQ} = \frac{\text{IQR}}{\text{RMSE}}, \quad (1)$$

where IQR is the inter-quartile range of the measured data. The RPIQ<sub>i</sub> was chosen due its suitability for non-normally distributed data<sup>35</sup> and the threshold for reliable models was set to  $\text{RPIQ}_i \geq 2$ , based on previous studies<sup>36,37</sup>.

### Statistical analyses

Reference properties had a non-normal distribution (Shapiro-Wilk normality test,  $p < 0.0003$ ) and, thus, non-parametric tests were employed in statistical analysis. Statistical significance of differences in tissue properties between cartilage repair and control ponies was investigated by using the Mann-Whitney U test in SPSS (Version 23, SPSS Inc., IBM Company, Armonk, NY, USA);  $p < 0.05$  was set as the limit for statistical significance. Two-tailed Spearman ( $\rho$ ) correlation coefficients were determined between the measured and NIRS predicted reference parameter values.

Data of the current study is available from the corresponding author on reasonable request.

## RESULTS

Significant differences ( $p < 0.05$ ) between the cartilage repair and control groups were observed in values of measured cartilage biomechanical properties (adjacent to the repair site), subchondral bone plate BV, and BMD (figs. 2, 3, and supplementary figs. S1-5). Nevertheless, no significant differences ( $p = 0.16 - 0.93$ ) were observed in cartilage thickness between the groups (supplementary fig. S1). The optimal predictive models (Model 1,  $\rho_{\text{Calibration\&Validation}} = 0.63-0.87$ ,  $\text{RPIQ}_{\text{Calibration\&Validation}} = 1.93-3.03$ ) reliably predicted the tissue properties ( $\rho_{\text{Test}} = 0.54 - 0.91$ ,  $\text{RPIQ}_{\text{Test}} = 1.68 - 3.36$ ) of the independent test group apart from subchondral bone BV ( $\rho_{\text{Calibration\&Validation}} = 0.69$ ,  $\text{RPIQ}_{\text{Calibration\&Validation}} = 1.34$ ,  $\rho_{\text{Test}} = 0.58$ ,  $\text{RPIQ}_{\text{Test}} = 1.30$ ) from in vitro spectral data (table 1) for the four locations at different distances from the repaired lesion (fig. 3), thus accurately differentiating between healthy and post-traumatic tissue. Furthermore, cartilage models (average  $\text{RPIQ}_{\text{Calibration\&Validation}} = 2.76$ ,  $\text{RPIQ}_{\text{Test}} = 3.26$ ) were superior to subchondral bone plate (average  $\text{RPIQ}_{\text{Calibration\&Validation}} = 1.99$ ,  $\text{RPIQ}_{\text{Test}} = 1.95$ ) and trabecular bone models (average  $\text{RPIQ}_{\text{Calibration\&Validation}} = 2.09$ ,  $\text{RPIQ}_{\text{Test}} = 2.27$ ). In addition, arthroscopic predictions with optimal predictive models (Model 1) also enabled differentiation between healthy and post-traumatic tissue (fig. 3). Although, the prediction performance ( $\rho = 0.27 - 0.74$ ,  $\text{RPIQ} = 0.81 - 1.70$ ) was inferior when compared to in vitro predictions, possibly due to errors (e.g., non-perfect contact of the probe and cartilage surface) introduced during arthroscopic spectral acquisition. For the locations with only arthroscopic measurements (Methods: fig. 1B, red dots), the trends of predicted values (Model 1) were consistent with those of measured values at other locations (supplementary figs. S1-5). Additionally, predictive models based on in vitro spectral data from the 0.75 to 1.9  $\mu\text{m}$  region (Model 2) were optimal for estimating cartilage and subchondral bone plate properties, whereas models with a wider spectral region (0.4 - 1.9  $\mu\text{m}$ , Model 3) incorporating the visible region were optimal for predicting subchondral trabecular bone properties (table 1).

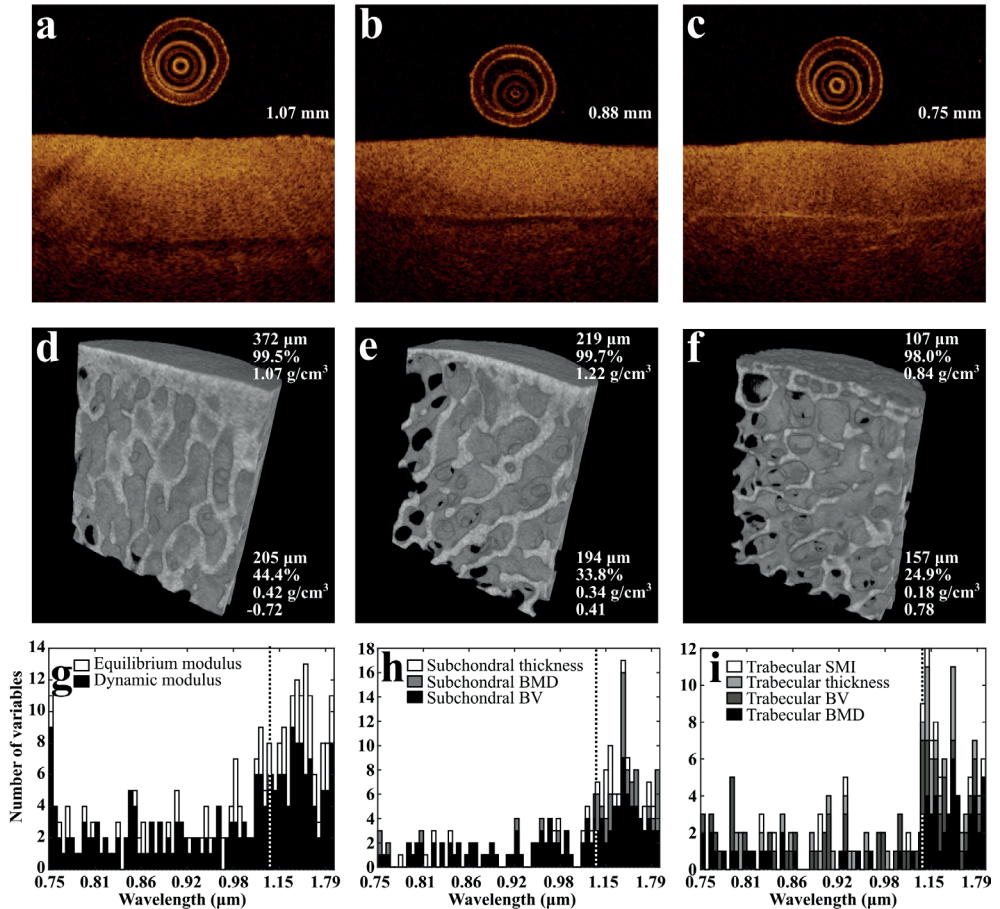


**Fig. 2** Optical coherence tomography (OCT) images from 3 locations, including cartilage thickness (a-c) along with corresponding micro-CT images of the underlying subchondral bone plate and subchondral trabecular bone (d-f). Subchondral plate thickness, bone volume fraction (BV), and bone mineral density (BMD) (d-f, top-right corner), and trabecular bone thickness, BV, BMD, and structural model index (SMI) (d-f, bottom-right corner) are presented. In addition, the optimal wavelengths for ANN models (Model 1) are presented (g-i). The width of each bar is 10 wavelengths (i.e., maximum number of variables in subfigure g is 20, as two variables are displayed). The dashed line indicates a separation of the spectral measurement regions of the two spectrometers.

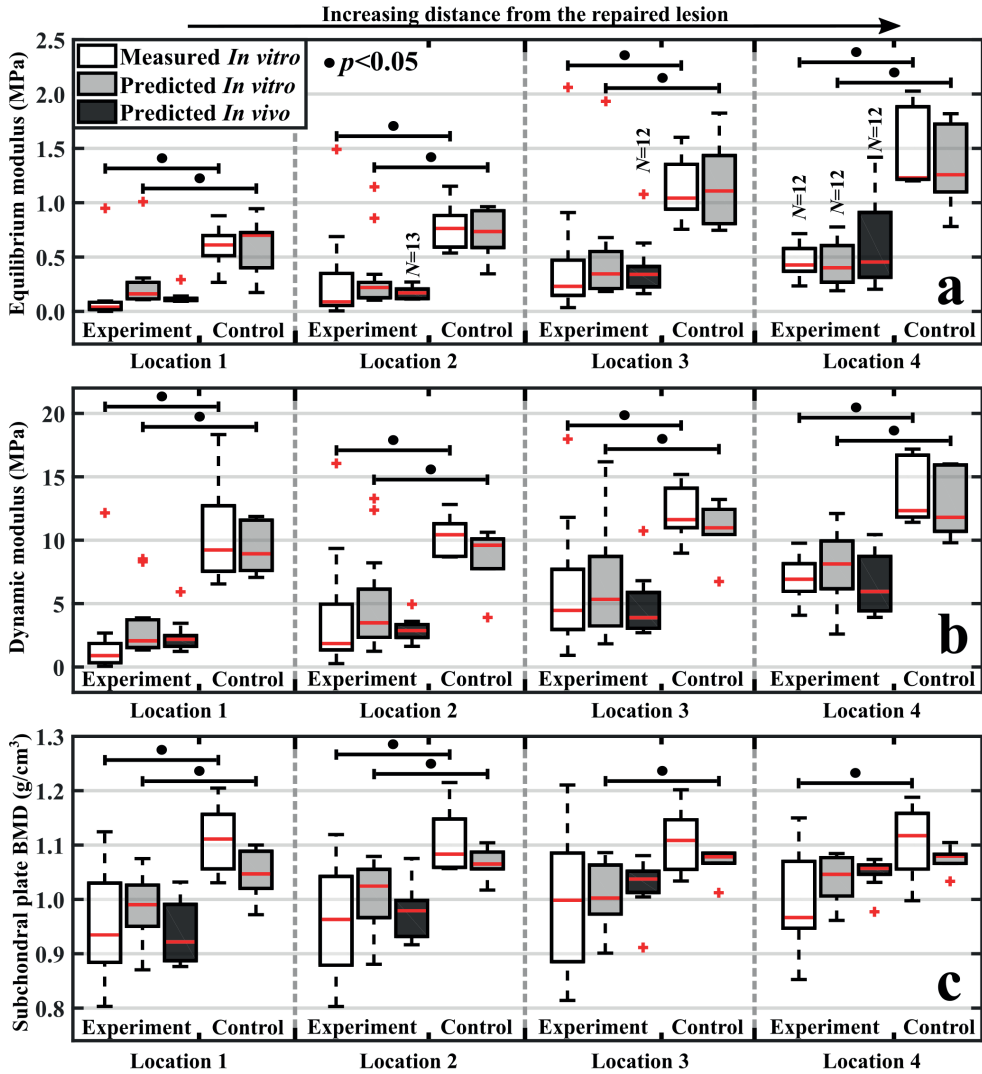


Fig. 3 Boxplots for experiment (post-traumatic) and control (healthy) groups with median (red line), quartiles (25% and 75%) and outliers (red cross) of *in vitro* measured (white bars) cartilage equilibrium modulus (a), dynamic modulus (b), and subchondral bone plate BMD (c) for the four locations at increasing distances from the lesion. Additionally, predictions based on the optimal model (Model 1) for *in vitro* and arthroscopic NIRS measurements are presented (grey and black bars, respectively). For each location, experiment and control groups had 12 – 14 and 6 measurements, respectively.



Mean (95% Confidence interval)	Spectral region (µm)	Number of variables	Calibration & Validation			In vitro			Arthroscopic			
			p	NRMSE	RPIQ <sub>cal</sub>	p	NRMSE	RPIQ <sub>in vitro</sub>	p	NRMSE	RPIQ <sub>arthro</sub>	
579 (506, 652)	0.75-1.90*	74	0.873	8.5%	3.14	0.890	5.9%	3.36	0.736	<0.0001	14.5%	1.46
	0.75-1.90	85	0.874	9.0%	2.96	0.835	7.0%	2.85	0.466	<0.0001	23.5%	0.90
	0.40-1.90	52	0.699	17.6%	1.51	0.876	7.2%	2.76	-	-	-	-
7.25 (6.61, 7.89)	0.75-1.90*	214	0.775	16.5%	2.38	0.910	14.0%	3.16	0.692	<0.0001	19.7%	1.70
	0.75-1.90	61	0.793	15.8%	2.50	0.943	12.2%	3.63	0.544	<0.0001	21.8%	1.53
	0.40-1.90	133	0.853	12.4%	3.19	0.963	7.3%	6.07	-	-	-	-
98.4 (98.1, 98.7)	0.75-1.90*	133	0.689	7.1%	1.34	0.582	23.2%	1.30	0.384	<0.0001	10.4%	0.81
	0.75-1.90	171	0.790	4.7%	2.03	0.867	9.5%	3.17	0.358	0.0002	18.5%	0.46
	0.40-1.90	110	0.737	3.8%	2.45	0.697	10.3%	2.93	-	-	-	-
1.00 (0.99, 1.02)	0.75-1.90*	39	0.632	17.2%	2.18	0.539	17.6%	1.68	0.268	0.0063	24.0%	1.61
	0.75-1.90	88	0.725	15.0%	2.49	0.732	16.0%	1.85	-0.179	0.07	31.3%	1.23
	0.40-1.90	18	0.544	18.3%	2.04	0.757	15.6%	1.90	-	-	-	-
174 (166, 182)	0.75-1.90*	27	0.729	14.0%	2.45	0.896	9.9%	2.86	0.507	<0.0001	22.0%	1.45
	0.75-1.90	182	0.750	18.9%	1.81	0.950	12.0%	2.36	0.364	0.0002	32.8%	0.97
	0.40-1.90	143	0.794	18.5%	1.85	0.896	12.9%	2.19	-	-	-	-
30.5 (29.8, 31.3)	0.75-1.90*	56	0.781	11.2%	2.26	0.871	12.7%	2.15	0.547	<0.0001	20.8%	1.46
	0.75-1.90	28	0.703	12.4%	2.04	0.911	10.5%	2.60	0.325	0.0008	32.3%	0.94
	0.40-1.90	39	0.742	12.3%	2.06	0.949	10.6%	2.57	-	-	-	-
0.247 (0.237, 0.258)	0.75-1.90*	69	0.735	13.2%	2.08	0.856	14.7%	1.89	0.346	0.0003	22.9%	1.35
	0.75-1.90	103	0.739	13.3%	2.06	0.795	16.0%	1.73	0.266	0.0066	25.4%	1.22
	0.40-1.90	36	0.763	11.8%	2.30	0.929	11.6%	2.40	-	-	-	-
169 (167, 172)	0.75-1.90*	34	0.679	14.4%	1.86	0.816	16.9%	2.46	0.442	<0.0001	17.6%	1.50
	0.75-1.90	69	0.776	12.4%	2.16	0.850	13.3%	3.12	-0.065	0.51	25.7%	1.03
	0.40-1.90	63	0.628	14.8%	1.81	0.821	14.0%	2.98	-	-	-	-
0.367 (0.316, 0.417)	0.75-1.90*	13	0.728	11.8%	2.15	0.889	12.9%	2.59	0.465	<0.0001	19.8%	1.64
	0.75-1.90	104	0.844	10.6%	2.38	0.906	11.1%	3.02	0.217	0.028	37.0%	0.88
	0.40-1.90	52	0.825	10.9%	2.33	0.886	9.9%	3.40	-	-	-	-

**Table 1** Two-tailed Spearman (ρ) correlation coefficients between the measured and predicted values of cartilage; equilibrium (E<sub>cal</sub>) and dynamic moduli (E<sub>dyn</sub>), subchondral bone plate; bone volume fraction (BV), bone mineral density (BMD), and thickness, and trabecular bone; BV, BMD, thickness, and structure model index (SMI). Calibration & Validation indicates the correlation coefficient for both calibration and validation groups (nine ponies, N = 212), whereas the Test indicates the correlation coefficient for the independent test group (one pony, N = 24). In addition, the normalized root mean square error (NRMSE) and ratio of performance to inter-quartile range (RPIQ) are presented for these groups as well as for the arthroscopic data. The upmost row (\*) of each parameter, indicates the model with optimized wavelength selection for arthroscopic predictions (Model1). For all in vitro correlations, p-values were <0.01.

## DISCUSSION

Currently, no quantitative arthroscopic tools are available for evaluation of cartilage and subchondral bone and thus orthopaedic surgeons have to manage with subjective visual scoring of injury severity and tissue probing with a metallic hook.<sup>7</sup> Although several arthroscopic instruments for biomechanical assessment of cartilage (e.g., Artscan<sup>38</sup>) have been introduced, several practical issues (e.g., poor inter-observer reliability) have limited their usage during routine arthroscopies<sup>38</sup>. In addition, ultrasound and OCT imaging have been suggested, but these have not yet gained wide acceptance for arthroscopic evaluation of cartilage<sup>11,12</sup>. For arthroscopic evaluation of subchondral bone, there are currently no clinical tools available; nevertheless, arthroscopic ultrasound imaging has been shown to provide information on the subchondral bone<sup>39</sup>. CT and MRI are widely used for diagnostics of joint injuries, but these techniques cannot be utilized during arthroscopic repair surgery. As a result, the presently introduced NIRS probe could be used to accurately localize cartilage and bone defects, as well as the spread of tissue degeneration from an injury during arthroscopy, therefore potentially leading to better outcome of the tissue repair. Predictive models based on ANN provided accurate estimates of reference parameters for an independent *in vitro* test group. Although predictions based on spectra collected during *in vivo* arthroscopies had slightly higher errors (i.e., weaker performance), they were able to discriminate between healthy and post-traumatic tissue. These findings suggest that NIRS is a promising technique for *in vivo* assessment of articular cartilage and subchondral bone properties.

Near infrared spectroscopy has been applied previously in human arthroscopies by Spahn et al. and Hofmann et al. to evaluate the condition of cartilage<sup>23-27</sup>. However, no study has applied NIRS for evaluation of subchondral bone properties *in vivo*, or for simultaneous assessment of cartilage and subchondral bone integrity, or for prediction of tissue properties based on *in vivo* NIRS arthroscopy. In the aforementioned studies, a spectral region of 0.9 – 1.7  $\mu\text{m}$  was utilized, whereas a wider region of 0.4 – 1.9  $\mu\text{m}$  was utilized in the present study. Furthermore, the previous studies applied a simple univariate approach based on the ratio of spectral peaks for assessments of cartilage condition<sup>25,27</sup>, while a more advanced analytical approach based on ANN was adopted in this study.

The spectral region 0.75 – 1.9  $\mu\text{m}$  was optimal for prediction of cartilage biomechanical and subchondral bone plate properties (i.e., subchondral plate thickness, BV, and BMD), while models that also incorporated the visible region (0.4 – 0.75  $\mu\text{m}$ ) enhanced the reliability of predicting subchondral trabecular bone properties (i.e.,

trabecular thickness, BV, BMD, and SMI). This is due to better penetration of visible light through cartilage and into subchondral bone<sup>20</sup>. Nevertheless, the errors of arthroscopic predictions were higher for subchondral bone plate and trabecular bone properties compared to cartilage biomechanical properties, possibly due to contributions from the overlying cartilage matrix. Furthermore, since probe contact with the cartilage surface affects the transmission of light into the tissue, this is possibly the reason for the weaker prediction of bone properties based on arthroscopic spectral measurements. Detailed understanding of wavelength-dependent light penetration would provide insight that enables quantification of the effect of the overlying cartilage in future studies.

The overall errors of prediction based on spectral data collected during arthroscopies were higher compared to those based on *in vitro* measurements. This is probably due to the difficulty in ensuring perfect probe contact with cartilage surface during arthroscopic spectral acquisition due to the geometrical constraints in the live situation. In the analysis, predictions based on the best 8 arthroscopic spectra (out of 15 recorded for each measurement location) resulted in the most reliable predictions; however, these spectra were not necessarily obtained through perfect probe contact. To enhance the identification of optimal spectra for each measurement location, additional indicators or classification algorithms, e.g., support vector machines and decision trees, could be utilized. However, this was beyond the scope of the current investigation. Additionally, for future studies the pressure between the arthroscopic NIR probe and cartilage surface should be quantitatively measured in order to minimize its effect on the resulting NIR spectra and consequently the prediction accuracy<sup>40,41</sup>.

The gold standard multivariate technique used in multiple applications (e.g., determining soil properties) is PLSR; however, ANN has in many occasions outperformed PLSR<sup>42,43</sup>. Furthermore, ANN modelling does not require extensive preprocessing<sup>22</sup>, whereas PLSR often requires scatter correction and derivative preprocessing for optimal performance. Generally, ANNs, in particular deep neural networks ( $\geq 2$  hidden layers), are considered to require more data. However, only shallow neural networks (with single hidden layer) were utilized in this study. Therefore, similar estimates of minimum number of observations can be applied for shallow ANN models as multivariate models, such as PLSR and multiple linear regression (MLR). Consequently, we deem over hundred observations to be sufficient with more being always better. In addition, roughly 200 observations were recommended by Bujang et al. when applying MLR<sup>44</sup>. Although the number of spectra ( $N = 24$ ) in the independent test set was low, this test provides an unbiased evaluation

of model performance. Furthermore, the relatively small prediction errors ensured that the models were well-generalized for new samples. As expected, the forward variable selection technique improved the performance and robustness of the models by reducing the number of wavelengths; this is consistent with our previous study<sup>22</sup>. The prediction errors in cartilage biomechanical properties based on arthroscopic spectra were substantially lower with the variable selection technique employed in the present study compared to the genetic algorithm approach applied in our previous study<sup>30</sup>.

The correlations demonstrated by the models arise from overtone vibrations of chemical bonds in the main constituents of articular cartilage and subchondral bone, i.e., water, proteoglycans, collagen (types I and II), and hydroxyapatite. The most common bonds in these tissue constituents are OH, SH, NH, CH, and  $\text{PO}_4$ <sup>45,46</sup>. Water is the most abundant constituent (up to 80%) in cartilage<sup>45</sup> and thus the OH bond has a substantial influence on the spectral response of cartilage. The main peaks associated with the tissue water content appear between 0.95–1.10  $\mu\text{m}$ , 1.40–1.55  $\mu\text{m}$ , and 1.80–2.00  $\mu\text{m}$  due to second overtone OH stretching, first overtone OH stretching, and second overtone OH bending vibrations, respectively<sup>47</sup>. The spectral regions 0.95–1.10  $\mu\text{m}$  and 1.40–1.55  $\mu\text{m}$  also include contributions from the second and first overtones of NH stretching vibrations<sup>47</sup>, respectively. In addition, overtones of CH stretching vibrations can be observed at spectral regions 0.85–0.95  $\mu\text{m}$ , 1.10–1.25  $\mu\text{m}$ , and 1.65–1.80  $\mu\text{m}$ <sup>47</sup>. Spectral data from regions of stronger vibrations (first overtones) contribute more to model performance as observed from the histograms of selected wavelengths (figs. 2 G-I). The spectral region associated with the first overtone OH stretching vibration (1.40–1.55  $\mu\text{m}$ ) contributes substantially to the models, particularly for articular cartilage and subchondral bone plate parameters. For subchondral trabecular bone, the emphasis shifts towards the lower wavelengths (1.05–1.2  $\mu\text{m}$ ) due to better penetration depth of the light<sup>20</sup>.

The relationship between NIR spectra and cartilage biomechanical properties has been previously investigated *in vitro* with univariate<sup>15,18</sup> and multivariate<sup>13,16,17</sup> analysis (i.e., PLSR). These studies utilized relatively narrow spectral regions with moderate and good correlations, whereas in this study a wider region was utilized along with ANN combined with a variable selection technique. Afara et al. investigated subchondral bone properties with a similar spectral region in a rat model with promising results<sup>19</sup>. However, cartilage in a rat knee joint is substantially thinner than in human and equine knee joints<sup>48,49</sup>. Thus, the findings in the present study indicate that NIRS is a feasible technique for assessment of subchondral bone properties, even through thicker human and equine cartilage. Nevertheless, additional studies are required to confirm the validity of the NIRS technique in human patients.

No statistically significant difference was observed in cartilage thickness between control ponies and ponies with repaired cartilage defects. However, significant variation in cartilage biomechanical properties was observed between the groups. In PTOA, cartilage surrounding the site of a defect experiences higher strains<sup>6</sup>, therefore altering the tissue's biomechanical competence and possibly leading to remodelling of the subchondral bone<sup>50</sup>. For subchondral plate properties, statistically significant differences were observed in values of BV and BMD between the groups, which is consistent with current knowledge on early-stage subchondral bone changes in OA<sup>50,51</sup>.

A possible limitation of this study is the potential effect of dependency as arthroscopic and in vitro measurements were conducted on the same ponies (the experimental group); however, this enabled comparison between the in vitro and in vivo environments, and provided valuable information for further development of in vivo NIRS applications. An additional limitation is that the arthroscopic spectra were found to include contributions from the conventional arthroscope light source, thereby limiting the useful spectral range to the NIR region (0.75 – 1.90  $\mu\text{m}$ ) because of interference in the visible spectral region.

## Outlook

Near infrared spectroscopy is a promising quantitative technique for simultaneous arthroscopic assessment of cartilage biomechanical properties and subchondral bone structure and density. This technique could substantially enhance assessment of the clinical status of joints by enabling quantitative detection of initial signs of PTOA around chondral lesions. This would be of high clinical significance, e.g., when conducting articular repair surgery.

## ACKNOWLEDGEMENTS

Doctoral Programme in Science, Technology and Computing (SCITECO) of University of Eastern Finland, Kuopio University Hospital (VTR projects 5041750 and 5041744, PY210 Clinical Neurophysiology), the Academy of Finland (project 267551), Orion Research Foundation sr, and Finnish foundation of technology promotion financially supported this study. The research leading to these results has received funding from the European Community's Seventh Framework Programme (FP7/2007-2013) under grant agreement 309962 (HydroZONES), the European Research Council under grant agreement 647426 (3D-JOINT), and the Dutch Arthritis Foundation (LLP-12 and LLP-22). Finnilä, M. and Malo, M. are acknowledged for the guidance in the CT acquisition and segmentation.

## REFERENCES

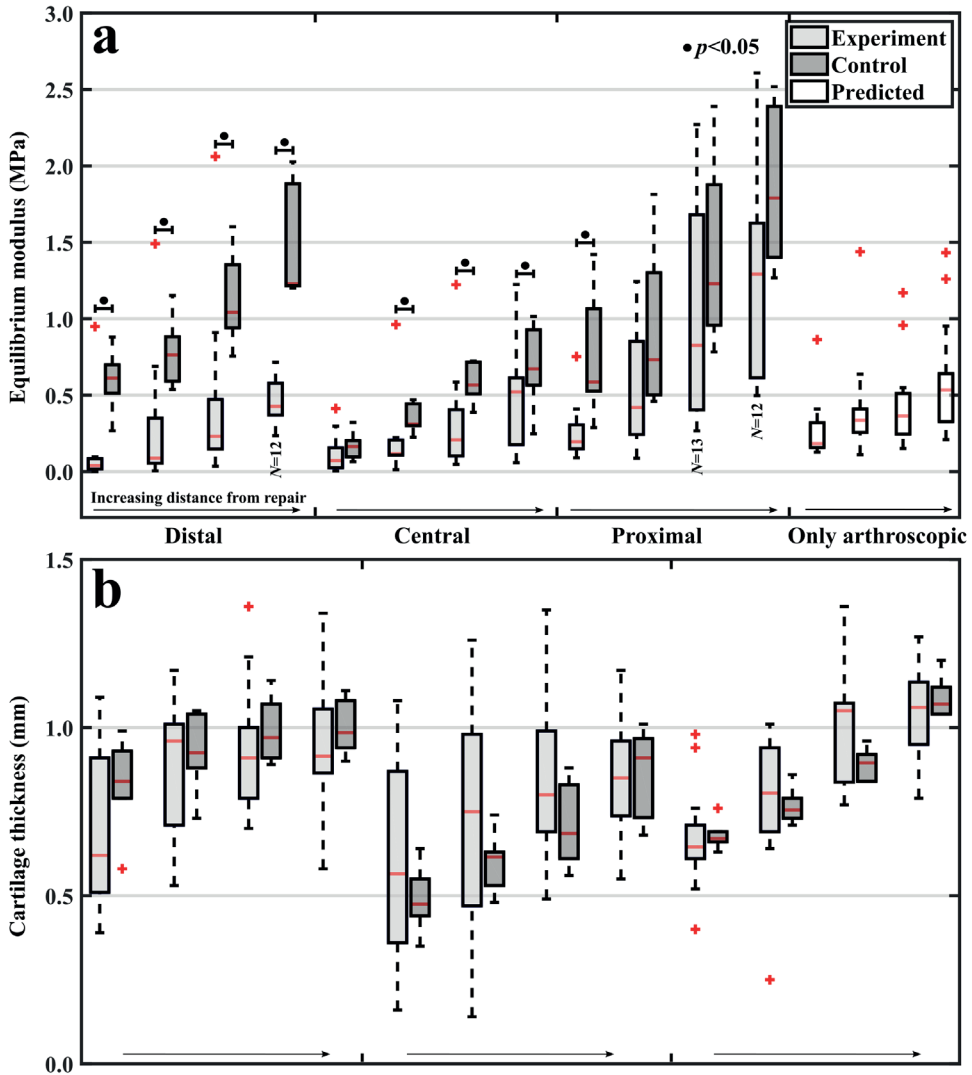
1. Buckwalter JA, Martin JA. Osteoarthritis. *Adv Drug Deliv Rev.* 2006;58(2):150-167.
2. Buckwalter JA, Brown TD. Joint Injury, Repair, and Remodeling: roles in post-traumatic osteoarthritis. *Clin Orthop Relat Res.* 2004;423:7-16.
3. Radin EL, Paul IL, Tolkoff MJ. Subchondral bone changes in patients with early degenerative joint disease. *Arthritis Rheum.* 1970;13(4):400-405.
4. Radin EL, Rose RM. Role of subchondral bone in the initiation and progression of cartilage damage. *Clin Orthop Relat Res.* 1986;(213):34-40.
5. Madry H, van Dijk CN, Mueller-Gerbl M. The basic science of the subchondral bone. *Knee Surgery, Sport Traumatol Arthrosc.* 2010;18(4):419-433.
6. Venäläinen MS, Mononen ME, Salo J, et al. Quantitative Evaluation of the Mechanical Risks Caused by Focal Cartilage Defects in the Knee. *Sci Rep.* 2016;6:37538.
7. Spahn G, Klinger HM, Hofmann GO. How valid is the arthroscopic diagnosis of cartilage lesions? Results of an opinion survey among highly experienced arthroscopic surgeons. *Arch Orthop Trauma Surg.* 2009;129(8):1117-1121.
8. Brismar BH, Wredmark T, Movin T, Leandersson J, Svensson O. Observer reliability in the arthroscopic classification of osteoarthritis of the knee. *J Bone Jt Surg.* 2002;84(1):42-47.
9. Favero M, Ramonda R, Goldring MB, Goldring SR, Punzi L. Early knee osteoarthritis. *RMD Open.* 2015;1(Suppl 1):e000062.
10. Chu CR, Williams AA, Coyle CH, Bowers ME. Early diagnosis to enable early treatment of pre-osteoarthritis. *Arthritis Res Ther.* 2012;14(3):212.
11. Virén T, Saarakkala S, Kaleva E, Nieminen HJ, Jurvelin JS, Töyräs J. Minimally Invasive Ultrasound Method for Intra-Articular Diagnostics of Cartilage Degeneration. *Ultrasound Med Biol.* 2009;35(9):1546-1554.
12. Li X, Martin S, Pitris C, et al. High-resolution optical coherence tomographic imaging of osteoarthritic cartilage during open knee surgery. *Arthritis Res Ther.* 2005;7(2):R318-23.
13. Afara IO, Hauta-Kasari M, Jurvelin JS, Oloyede A, Töyräs J. Optical absorption spectra of human articular cartilage correlate with biomechanical properties, histological score and biochemical composition. *Physiol Meas.* 2015;36(9):1913-1928.
14. Rolfe P. In Vivo Near-Infrared Spectroscopy. *Annu Rev Biomed Eng.* 2000;2(1):715-754.
15. Marticke JK, Hösselbarth A, Hoffmeier KL, et al. How do visual, spectroscopic and biomechanical changes of cartilage correlate in osteoarthritic knee joints? *Clin Biomech (Bristol, Avon).* 2010;25(4):332-340.
16. Stumpfe ST, Pester JK, Steinert S, et al. Is there a correlation between biophotonical, biochemical, histological, and visual changes in the cartilage of osteoarthritic knee-joints? *Muscles Ligaments Tendons J.* 2013;3(3):157-165.
17. Sarin JK, Amis M, Brommer H, Argüelles D, Töyräs J, Afara IO. Near Infrared Spectroscopic Mapping of Functional Properties of Equine Articular Cartilage. *Ann Biomed Eng.* 2016;44(11):3335-3345.
18. Hanifi A, Palukuru U, McGoverin C, et al. Near infrared spectroscopic assessment of developing engineered tissues: correlations with compositional and mechanical properties. *Analyst.* 2017;142(8):1320-1332.
19. Afara IO, Prasadam I, Crawford R, Xiao Y, Oloyede A. Near infrared (NIR) absorption spectra correlates with subchondral bone micro-CT parameters in osteoarthritic rat models. *Bone.* 2013;53(2):350-357.

20. Padalkar M V., Pleshko N. Wavelength-dependent penetration depth of near infrared radiation into cartilage. *Analyst*. 2015;140(7):2093-2100.
21. McGoverin CM, Lewis K, Yang X, Bostrom MPG, Pleshko N. The contribution of bone and cartilage to the near-infrared spectrum of osteochondral tissue. *Appl Spectrosc*. 2014;68(10):1168-1175.
22. Sarin JK, Rieppo L, Brommer H, Afara IO, Saarakkala S, Töyräs J. Combination of optical coherence tomography and near infrared spectroscopy enhances determination of articular cartilage composition and structure. *Sci Rep*. 2017;7(1):10586.
23. Spahn G, Plettenberg H, Nagel H, et al. Evaluation of cartilage defects with near-infrared spectroscopy (NIR): an ex vivo study. *Med Eng Phys*. 2008;30(3):285-292.
24. Spahn G, Klinger HM, Baums M, et al. Near-infrared spectroscopy for arthroscopic evaluation of cartilage lesions: results of a blinded, prospective, interobserver study. *Am J Sports Med*. 2010;38(12):2516-2521.
25. Spahn G, Felmet G, Hofmann GO. Traumatic and degenerative cartilage lesions: arthroscopic differentiation using near-infrared spectroscopy (NIRS). *Arch Orthop Trauma Surg*. 2013;133(7):997-1002.
26. Spahn G, Plettenberg H, Hoffmann M, Klemm H-T, Brochhausen-Delius C, Hofmann GO. The frequency of cartilage lesions in non-injured knees with symptomatic meniscus tears: results from an arthroscopic and NIR- (near-infrared) spectroscopic investigation. *Arch Orthop Trauma Surg*. 2017;137(6):837-844.
27. Hofmann GO, Marticke J, Grossstück R, et al. Detection and evaluation of initial cartilage pathology in man: A comparison between MRT, arthroscopy and near-infrared spectroscopy (NIR) in their relation to initial knee pain. *Pathophysiology*. 2010;17(1):1-8.
28. Wold S, Sjöström M, Eriksson L. PLS-regression: a basic tool of chemometrics. *Chemom Intell Lab Syst*. 2001;58(2):109-130.
29. May R, Dandy G, Maier H. Review of Input Variable Selection Methods for Artificial Neural Networks. In: *Artificial Neural Networks-Methodological Advances and Biomedical Applications*. InTech; 2011.
30. Sarin JK, te Moller N, Brommer H, et al. Spectroscopic evaluation of post-traumatic osteoarthritis in Shetland ponies. In: *Optics InfoBase Conference Papers. Vol Part F9o-O. Biophotonics Congress: Biomedical Optics Congress 2018*; 2018.
31. Mancini IA. Objective gait analysis as a tool to improve longitudinal monitoring of long-term large animal studies into cartilage repair. In: *Sorrento, Italy: 13th World Congress of ICRS*; 2016.
32. Visser J, Melchels FPW, Jeon JE, et al. Reinforcement of hydrogels using three-dimensionally printed microfibrils. *Nat Commun*. 2015;6:6933.
33. Hayes WC, Keer LM, Herrmann G, Mockros LF. A mathematical analysis for indentation tests of articular cartilage. *J Biomech*. 1972;5(5):541-551.
34. Danso EK, Mäkelä JTA, Tanska P, et al. Characterization of site-specific biomechanical properties of human meniscus—Importance of collagen and fluid on mechanical nonlinearities. *J Biomech*. 2015;48(8):1499-1507.
35. Bellon-Maurel V, Fernandez-Ahumada E, Palagos B, Roger J-M, McBratney A. Critical review of chemometric indicators commonly used for assessing the quality of the prediction of soil attributes by NIR spectroscopy. *TrAC - Trends Anal Chem*. 2010;29(9):1073-1081.
36. Peng Y, Xiong X, Adhikari K, Knadel M, Grunwald S, Greve MH. Modeling Soil Organic Carbon at Regional Scale by Combining Multi-Spectral Images with Laboratory Spectra. *Bond-Lamberty B, ed. PLoS One*. 2015;10(11):e0142295.
37. Jia X, Chen S, Yang Y, Zhou L, Yu W, Shi Z. Organic carbon prediction in soil cores using VNIR and MIR techniques in an alpine landscape. *Sci Rep*. 2017;7(1).

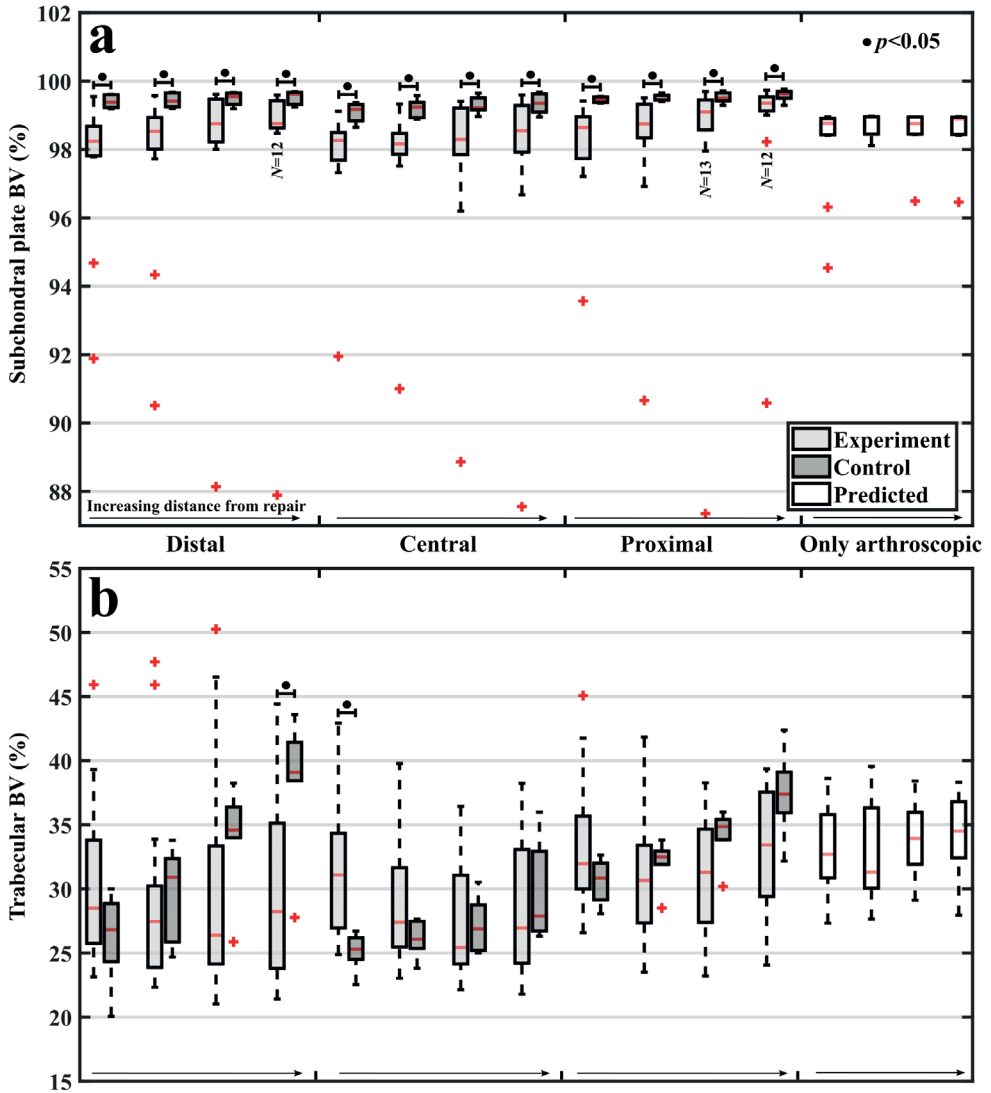
38. Timonen MA, Töyräs J, Aula AS, Karjalainen JP, Riekkinen O, Jurvelin JS. Technical and practical improvements in arthroscopic indentation technique for diagnostics of articular cartilage softening. *J Med Eng Technol.* 2011;35(1):40-46.
39. Liukkonen J, Hirvasniemi J, Joukainen A, et al. Arthroscopic ultrasound technique for simultaneous assessment of articular cartilage and subchondral bone: an in vitro and in vivo feasibility study. *Ultrasound Med Biol.* 2013;39(8):1460-1468.
40. Cugmas B, Bregar M, Bürmen M, Pernuš F, Likar B. Impact of contact pressure-induced spectral changes on soft-tissue classification in diffuse reflectance spectroscopy: problems and solutions. *J Biomed Opt.* 2014;19(3):37002.
41. Horbert V, Lange M, Reuter T, et al. Comparison of Near-Infrared Spectroscopy with Needle Indentation and Histology for the Determination of Cartilage Thickness in the Large Animal Model Sheep. *Cartilage.* 2019;10(2):173-185.
42. Goldshleger N, Chudnovsky A, Ben-Dor E. Using reflectance spectroscopy and artificial neural network to assess water infiltration rate into the soil profile. *Appl Environ Soil Sci.* 2012;2012.
43. Ni Y, Zhang G, Kokot S. Simultaneous spectrophotometric determination of maltol, ethyl maltol, vanillin and ethyl vanillin in foods by multivariate calibration and artificial neural networks. *Food Chem.* 2005;89(3):465-473.
44. Bujang MA, Sa'at N, Sidik TMITAB. Determination of minimum sample size requirement for multiple linear regression and analysis of covariance based on experimental and non-experimental studies. *Epidemiol Biostat Public Heal.* 2017;14(3):e12117-1-e12117-9.
45. Buckwalter JA, Mankin HJ. Articular cartilage: tissue design and chondrocyte-matrix interactions. *Instr Course Lect.* 1998;47:477-486.
46. Buckwalter JA, Glimcher MJ, Cooper RR, Recker R. Bone biology. I: Structure, blood supply, cells, matrix, and mineralization. *Instr Course Lect.* 1996;45:371-386.
47. Heise HM, Donald A. Burns, Emil W. Ciurczak (Eds.): *Handbook of near-infrared analysis*, 3rd ed. *Anal Bioanal Chem.* 2009;393(5):1387-1389.
48. Malda J, Benders KE, Klein TJ, et al. Comparative study of depth-dependent characteristics of equine and human osteochondral tissue from the medial and lateral femoral condyles. *Osteoarthr Cartil.* 2012;20:1147-1151.
49. Malda J, de Grauw JC, Benders KEM, et al. Of Mice, Men and Elephants: The Relation between Articular Cartilage Thickness and Body Mass. *Orgel JPRO, ed. PLoS One.* 2013;8(2):e57683.
50. Heijink A, Gomoll AH, Madry H, et al. Biomechanical considerations in the pathogenesis of osteoarthritis of the knee. *Knee Surgery, Sport Traumatol Arthrosc.* 2012;20(3):423-435.
51. Intema F, Hazewinkel HAW, Gouwens D, et al. In early OA, thinning of the subchondral plate is directly related to cartilage damage: results from a canine ACLT-menisectomy model. *Osteoarthr Cartil.* 2010;18(5):691-698.



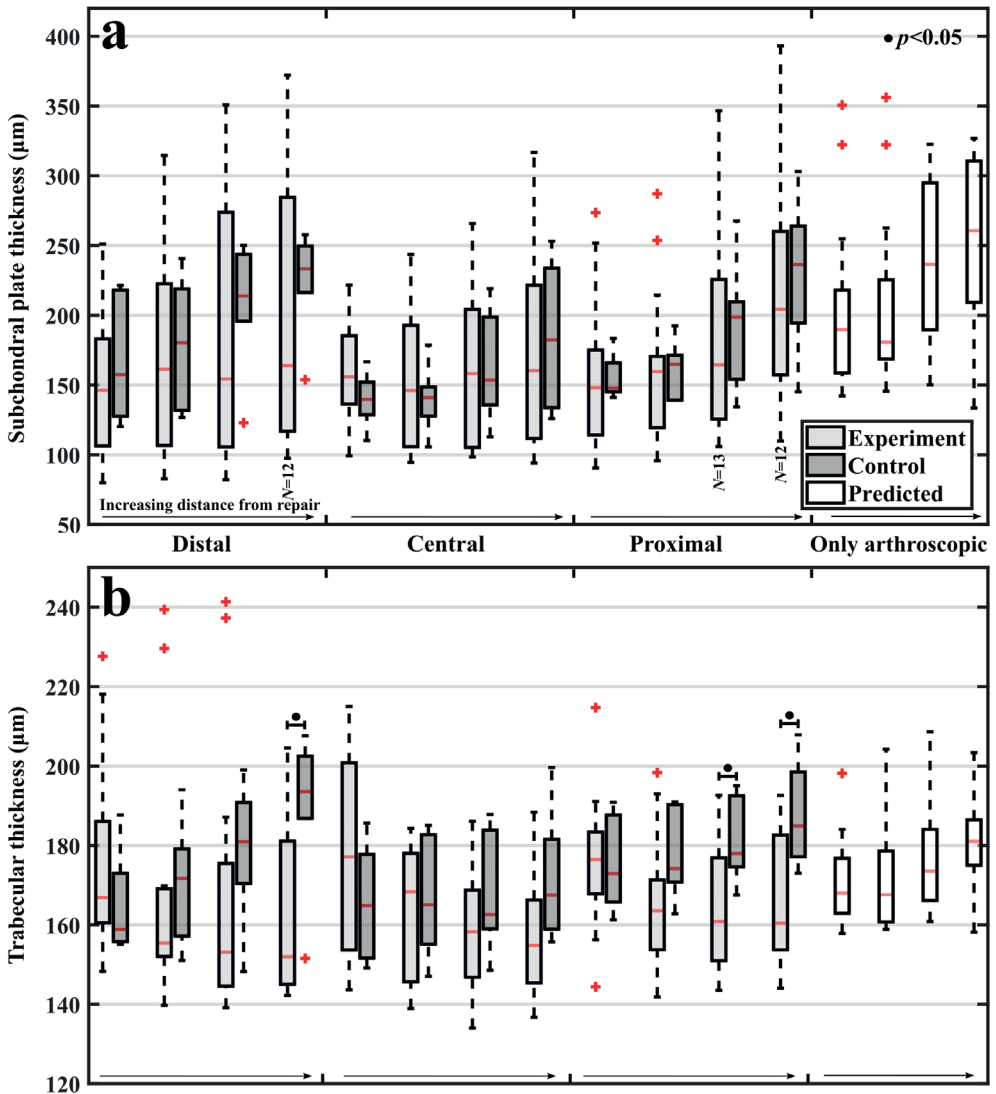
## SUPPLEMENTARY INFORMATION



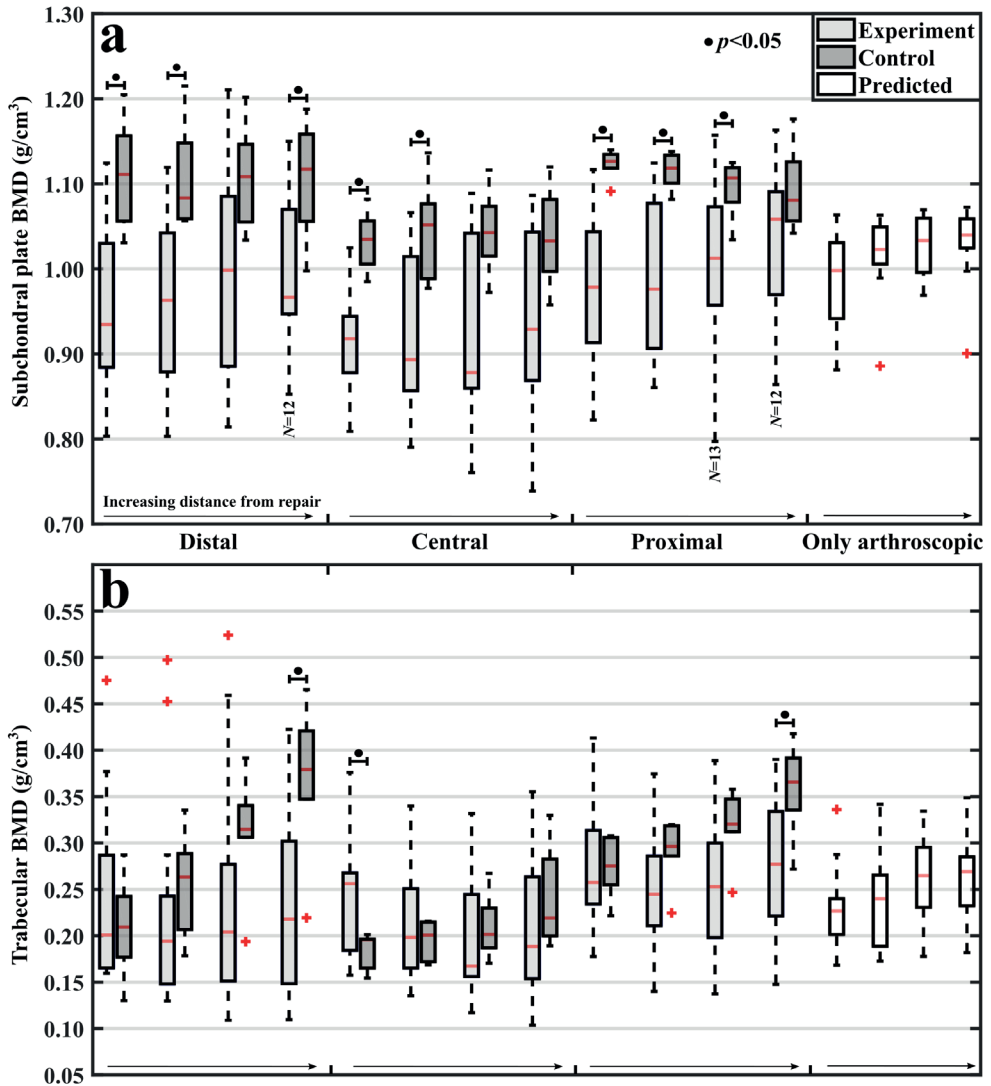
**Supplementary Fig. S1** Boxplots with median, quartiles (25% and 75%) and outliers of equilibrium modulus (a), and cartilage thickness (b) between the experimental and control groups. For each presented bar of experiment and control groups, the number of measurements were 14 and 6, respectively. Few locations had varying number of measurements (marked in subfigure a) due to limited accessibility during arthroscopy. Additionally, predictions from the locations with only arthroscopic NIRS measurements (Figure 2b, red dots) are presented (white bars). For each anatomical location (distal, central, and proximal), the leftmost bar presents the location closest to the repair.



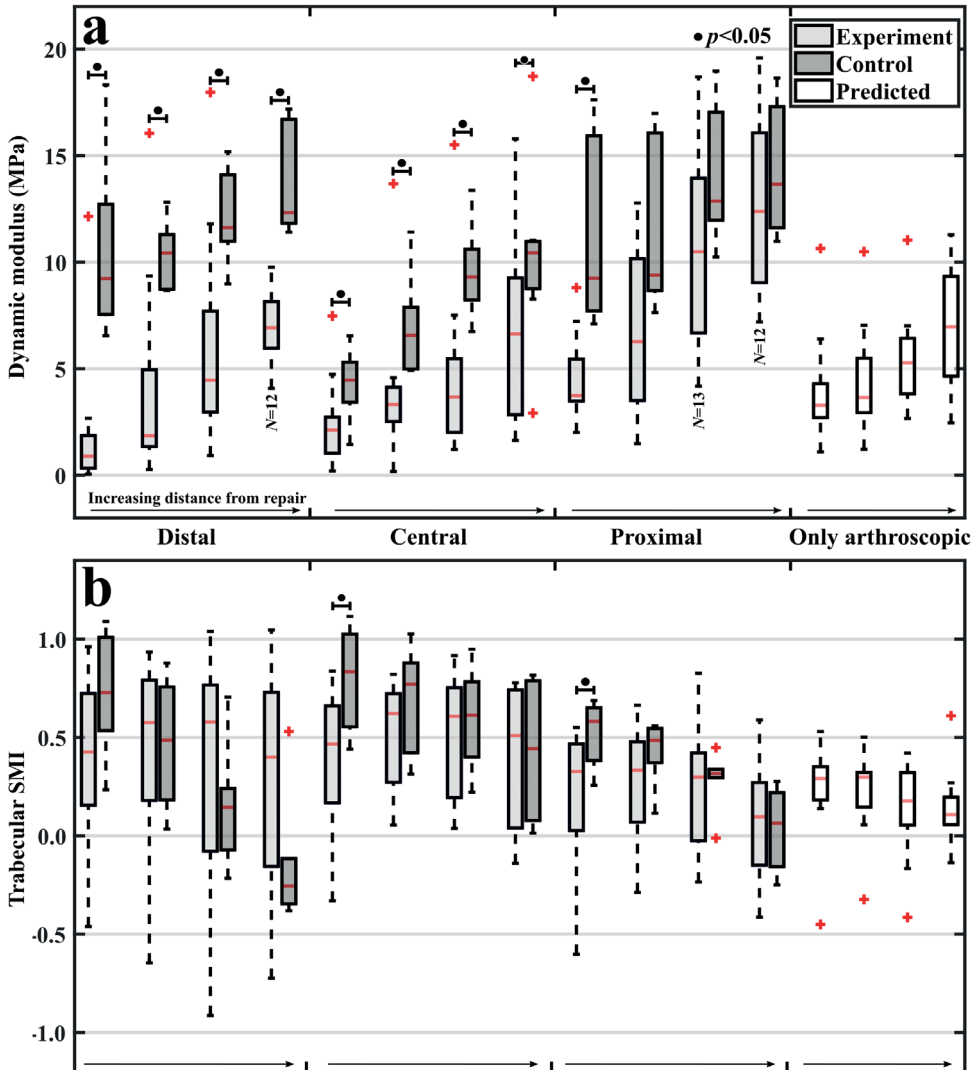
**Supplementary Fig. S2** Boxplots with median, quartiles (25% and 75%) and outliers of subchondral plate bone volume fraction (BV, a), and trabecular BV (b) between the experimental and control groups. For each presented bar of experiment and control groups, the number of measurements were 14 and 6, respectively. Few locations had varying number of measurements (marked in subfigure a) due to limited accessibility during arthroscopy. Additionally, predictions from the locations with only arthroscopic NIRS measurements (Figure 2b, red dots) are presented (white bars). For each anatomical location (distal, central, and proximal), the leftmost bar presents the location closest to the repair.



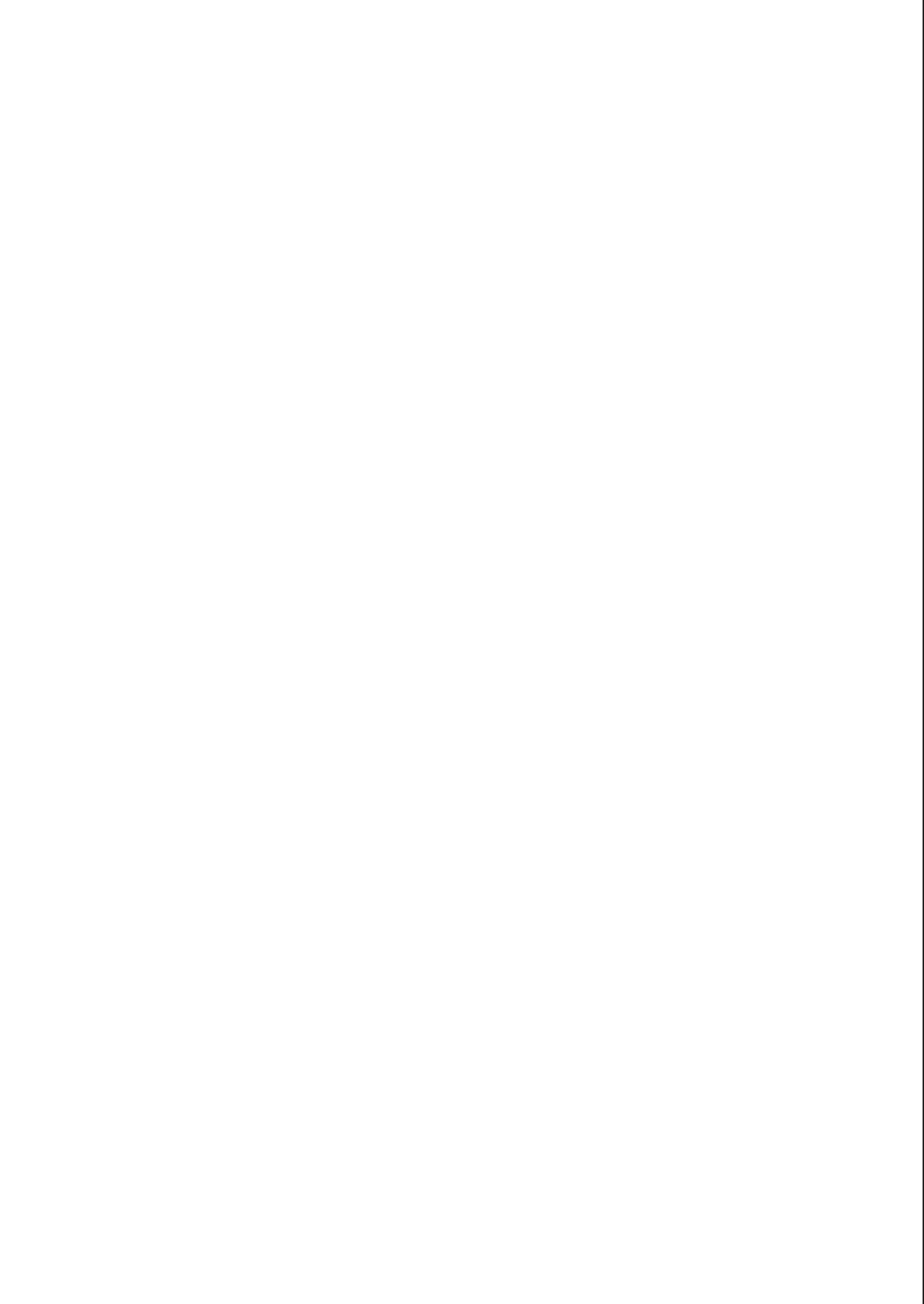
**Supplementary Fig. S3** Boxplots with median, quartiles (25% and 75%) and outliers of subchondral plate thickness (a), and trabecular thickness (b) between the experimental and control groups. For each presented bar of experiment and control groups, the number of measurements were 14 and 6, respectively. Few locations had varying number of measurements (marked in subfigure a) due to limited accessibility during arthroscopy. Additionally, predictions from the locations with only arthroscopic NIRS measurements (Figure 2b, red dots) are presented (white bars). For each anatomical location (distal, central, and proximal), the leftmost bar presents the location closest to the repair.



**Supplementary Fig. S4** Boxplots with median, quartiles (25% and 75%) and outliers of subchondral plate bone mineral density (BMD, **a**), and trabecular BMD (**b**) between the experimental and control groups. For each presented bar of experiment and control groups, the number of measurements were 14 and 6, respectively. Few locations had varying number of measurements (marked in subfigure **a**) due to limited accessibility during arthroscopy. Additionally, predictions from the locations with only arthroscopic NIRS measurements (Figure 2b, red dots) are presented (white bars). For each anatomical location (distal, central, and proximal), the leftmost bar presents the location closest to the repair.



**Supplementary Fig. S5** Boxplots with median, quartiles (25% and 75%) and outliers of cartilage dynamic modulus (**a**), and trabecular structure model index (SMI, **b**) between the experimental and control groups. For each presented bar of experiment and control groups, the number of measurements were 14 and 6, respectively. Few locations had varying number of measurements (marked in subfigure **a**) due to limited accessibility during arthroscopy. Additionally, predictions from the locations with only arthroscopic NIRS measurements (Figure 2b, red dots) are presented (white bars). For each anatomical location (distal, central, and proximal), the leftmost bar presents the location closest to the repair.



# **PART II**

## **The impact of subtle cartilage defects and the role of exercise**







# CHAPTER 7

## Structural, compositional and functional changes of joint tissues in a long-term equine carpal groove model featuring blunt and sharp cartilage damage

---

N.C.R. te Moller<sup>1</sup>

A. Mohammadi<sup>2</sup>

S. Plomp<sup>1</sup>

F.M. Serra Bragança<sup>1</sup>

J.K. Sarin<sup>2,3</sup>

M. Beukers<sup>1</sup>

B. Pouran<sup>4</sup>

J.T.A. Mäkelä<sup>2</sup>

R.K. Korhonen<sup>2</sup>

J. Töyräs<sup>2,3,5</sup>

H. Brommer<sup>1</sup>

P.R. van Weeren<sup>1</sup>

---

<sup>1</sup>Department of Equine Sciences, Faculty of Veterinary Medicine, Utrecht University, <sup>2</sup>Department of applied physics, University of Eastern Finland, <sup>3</sup>Diagnostic imaging Center, Kuopio University Hospital, <sup>4</sup>Department of Orthopaedics, University Medical Center Utrecht, <sup>5</sup>School of Information Technology and Electrical Engineering, The University of Queensland

This chapter is based on data obtained from the equine carpal groove model study that has been performed at the Faculty of Veterinary Medicine, Utrecht University, between 2017 and 2019. The available results of that extensive study were put together in this chapter to provide a comprehensive and coherent overview for the sake of this thesis. This data, and data that currently is still being processed, will be submitted in separate papers for peer-reviewed publication at a later stage.

## ABSTRACT

**Background** Osteoarthritis (OA) affects millions of people and animals worldwide. Better insight is needed into the effects of articular cartilage damage, the interaction between the various joint tissues, and how they influence overall joint health, to help timely recognition of OA and to reveal new treatment targets. We aimed to quantify the longer-term progression of artificially created blunt and sharp cartilage grooves and their effect on other joint tissues in the equine carpal joint by multiple modality monitoring.

**Methods** For 9 adult female Shetland ponies, the cartilage in the radiocarpal and middle carpal joint was grooved (one blunt and one sharp) via arthrotomy. The contra-lateral joint was sham-operated. After 3 weeks of box rest, the ponies were trained for 8 weeks on a treadmill. Following upon groove surgery and during follow-up arthroscopies at 11, 23 and 39 weeks, intra-articular optical coherence tomography and near infrared spectroscopy measurements were performed and synovial biopsies were taken for microscopic and gene expression analysis. Synovial fluid was obtained prior to each surgery and at week 19 and 35 for biomarker measurements. Radiographs of both carpi were taken at baseline and at 38 weeks and consecutive optical motion capture data was collected during the study. At 39 weeks, ponies were euthanized, and osteochondral samples were harvested. Macroscopic and microscopic changes of the articular cartilage were scored according to OARSI guidelines. Cartilage thickness and subchondral bone parameters were calculated from micro-CT images. Biomechanical properties of the cartilage were determined by indentation testing.

**Results** Blunt and sharp grooves led to degenerative changes of the articular cartilage, quantified by higher OARSI scores at microscopy compared with control joints ( $p < 0.0001$ ). Blunt-grooved cartilage scored higher than sharp-grooved cartilage ( $p = 0.007$ ) and showed more loss of collagen type 2 around the defect. Cartilage thickness did not differ between grooved and control joints, but cartilage equilibrium and instantaneous moduli trended lower in grooved joints, being significant for sharp-grooved cartilage ( $p = 0.002$  and  $p = 0.045$ , respectively). Concomitant changes in other articular tissues remained limited to increased radiographic scores in grooved joints at 38 weeks ( $p = 0.007$ ), significantly increased IL-6, CCL2, and ALK5 expression levels compared to baseline in synovium from grooved joints, and an increased CPII/C2C ratio in SF from blunt-grooved joints at week 35 ( $p = 0.03$ ). No differences in the subchondral bone were found. Quantitative gait analysis was consistent with a mild, gradually increasing bilateral lameness.

**Conclusions** Both blunt and sharp articular cartilage grooves in the equine carpal joint, in combination with a period of intensified loading, lead to degenerative changes over a 9-month period. However, the overall effect on joint homeostasis and function in terms of gait quality remained limited. We hypothesize that it is the combination of lesion morphology, together with the loading profile that will determine the speed and characteristics of progression of further degeneration.

## INTRODUCTION

Osteoarthritis (OA) is a joint disorder characterized by progressive articular cartilage degeneration that is accompanied by pathologic changes in other joint tissues including bone remodelling and synovitis, leading to joint pain, swelling and stiffness.<sup>1</sup> Osteoarthritis not only affects millions of people worldwide; it is also a common burden in animals. Particularly in the horse industry, the high incidence of OA is an important concern.<sup>2</sup> Currently, there is no effective therapy available to stop the progression of this disease.

The close similarity between equine and human articular cartilage and the horse being a target species in itself, make equine models very useful for studying early pathobiological events of OA.<sup>3,4</sup> Recently, the articular groove model that was initially used in dogs and later in sheep and rats<sup>5-7</sup>, showed its potential for the investigation of degenerative joint changes in the metacarpophalangeal (MCP) joint of the horse.<sup>8</sup> In this model, the cartilage surface is surgically grooved up to but not through the calcified cartilage layer and subsequently subjected to intensified loading through physical exercise for a certain period. The groove model can be used in various joints. In a pilot study in two Shetland ponies, we showed that after 10 weeks, the model behaved similarly in middle carpal and MCP joints.<sup>9</sup>

The aforementioned studies so far, focussed mostly on structural changes of cartilage and subchondral bone, biochemical analysis of cartilage and, to some extent, synovial fluid biomarkers, all predominantly measured post-mortem.<sup>5-8</sup> Data on biomechanical changes of the cartilage is still limited. Also, longitudinal information on the progress of chondral grooves in the longer-term within individuals is sparse. This kind of data would be highly valuable for the validation of computational models aiming at prediction of the progression of focal defects and development of post-traumatic OA.<sup>10</sup> Furthermore, since OA is considered a whole-joint disease, more emphasis needs to be placed on the interaction between the various joint tissues in order to gain further insight in how structural, compositional, and functional changes influence overall joint health and function. Better insights in disease processes at the earliest possible stage could help timely recognition of (the risk to develop) OA and may reveal new treatment targets.

The aim of this study was to quantify the long-term progression of artificially created cartilage grooves and their effect on other joint tissues in the equine carpal joint, using multiple modalities to monitor changes at a structural, compositional and functional level *in vivo* and *in vitro*. Two variants of the groove model were applied:

grooves created by blunt disruption of the cartilage matrix (“blunt grooves”) and grooves created by sharp incisions of the cartilage layer (“sharp grooves”). We hypothesized that 1) damage to the articular cartilage in combination with intensified loading would always lead to progressive degeneration of the articular cartilage, but that substantial disruption of the matrix (“blunt grooves”) would accelerate this process compared with more subtle damage (“sharp grooves”) and that 2) progressive cartilage degeneration would lead to a disturbed joint homeostasis, which would become detectable by structural and compositional alterations in other joint tissues and functionally as changes in gait pattern.

## MATERIAL AND METHODS

### Animals

Nine adult female Shetland ponies, with a mean ( $\pm$ SD) age of  $6.8 \pm 2.6$  years (range 4-13 years) and a mean ( $\pm$ SD) bodyweight of  $203 \pm 15.3$  kg (range 171-220 kg) were included in this study. Pre-operatively, the ponies did not show lameness and did not suffer from lateral patellar subluxation. The study was authorized by the Utrecht University Animal Experiments Committee and the Central Committee for Animal Experiments (permit AVD108002015307) in compliance with the Dutch Act on Animal Experimentation. Animal care was performed in accordance with Utrecht University guidelines.

### Surgical procedure

Surgery was performed under general anesthesia with isoflurane and continuous rate infusion with detomidine (Domosedan®, 0.01mg/kg/h). Pre-medication consisted of detomidine and butorphanol (Domosedan®, 0.01mg/kg and Dolorex®, 0.02mg/kg bodyweight (BW), iv), meloxicam (Metacam®, 0.6 mg/kg BW, iv) and Ampicilline (Ampi-Dry®, 15 mg/kg BW, iv). Ponies were induced with ketamine and midazolam (Narketan®, 2mg/kg BW and Midazolam®, 0.05 mg/kg BW, iv). Procaine benzylpenicilline (Procapen®, 20mg/kg BW, im) was administered at the end of the procedure.

Grooves were created in one randomly assigned front limb as follows: at the cartilage layer of the radial facet of the third carpal bone and of the dorsoproximal surface of the intermediate carpal bone, three grooves were created via arthrotomy of the middle carpal and radiocarpal joint, respectively. Blunt and sharp grooves were randomly assigned to either of the two joints (fig. 1A). Blunt grooves were made using a hooked arthroscopic probe with a sharpened tip (fig. 1B). Sharp grooves were

made with a surgical blade (Beaver Mini-Blade®, MFID: 376400) that was clamped in a custom-made device (fig. 1C). A new blade was used for each pony and the device was developed in such a way that incisions were of equal depth and could not exceed 400 µm. The contra-lateral joint was sham-operated and designated as the control joint. A single dose of tramadol (Tramagetic®, 5 mg/kg BW, per os) was given approximately 5 hours post-operatively and meloxicam (Metacam®, 0.6 mg/kg BW, per os) was provided once a day for one week. Bandages were changed after 2 days and then every 4 days until 10 days post-surgery. Ponies were kept at stall rest in individual stables for three weeks, with 15 minutes of controlled hand walking per day for the last five days.

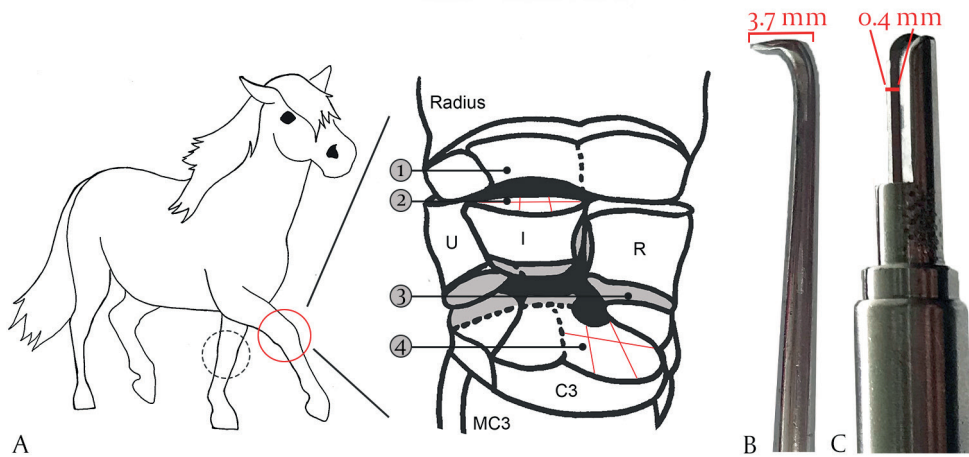


**Fig. 1** The carpal groove model shown for the right carpus (A). U = ulnar carpal bone, I = intermediate carpal bone, R = radial carpal bone, C<sub>3</sub> = third carpal bone, MC<sub>3</sub> = third metacarpal bone. Grooves were created at the dorsoproximal surface of the intermediate carpal bone (2) and at the radial facet of the proximal surface of the third carpal bone (4); 1 = distal surface of the radius (kissing site), 3 = distal surface of the radial carpal bone (kissing site). The left carpus represents the sham-operated control. An arthroscopic probe with a sharpened tip was used to create blunt grooves (B). A surgical mini blade clamped in a custom-made device was used to create sharp grooves (C).

## Exercise program

Starting three weeks prior to surgery, the ponies were accustomed to treadmill exercise (Mustang 200, Kagra AG, Fahrwangen, Switzerland) at walk, trot and canter. Two weeks post-surgery, ponies were hand walked daily and after three weeks, they were moved to an open group shed (approx. 125 m<sup>2</sup>) and subjected to controlled exercise for eight weeks. The training was gradually built up in three weeks (table

1). The final exercise protocol consisted of treadmill training 4 days per week, alternating continuous and interval training, and additionally walking in a horse walker for 30 minutes 7 days per week. After the exercise period, ponies stayed in the open group shed for another 16 weeks before they were allowed to have free exercise in the field until the end of the study.

**Table 1** Training protocol (weeks after groove surgery)

Week	Day	Treadmill (min/gait)							total	Horse walker min/day
		walk	trot	canter	walk	canter	trot	walk		
3	Mo-Fri	10	-	-	-	-	-	-	10	-
4	Mo	3	2	-	2	-	2	5	14	15
	Tue	3	3	-	2	-	3	5	16	
	Thu	3	3	-	2	-	3	5	16	
	Fri	3	4	-	2	-	4	5	18	
5	Mo	3	5	-	2	-	5	5	20	30
	Tue	3	4	1	1	1	2	5	17	
	We	5	4	1	1	1	2	5	19	
	Thu	3	5	-	2	-	2	5	17	
	Fri	5	4	2	-	-	2	5	18	
6-11	Mo	3	5	-	2	-	5	5	20	30
	Tue	5	4	2	-	-	2	5	18	
	Thu	3	5	-	2	-	5	5	20	
	Fri	5	4	2	-	-	2	5	18	

Speed at walk, trot and canter was set at 4.5 km/h, 11 km/h, and 21 km/h, respectively. Walking exercise in the horse walker was performed 7 days/ week.

## In vivo monitoring

Multiple modalities were used during the study to monitor changes in structure and composition of different joint tissues (i.e. optical coherence tomography (OCT), near infrared spectroscopy (NIRS), radiography) as well as changes in joint function in terms of gait quality (optical motion capture (OMC)). Furthermore, serial samples of synovium and synovial fluid were obtained for qPCR, microscopic analysis, and biomechanical analysis of biomarkers levels (fig. 2A).

## Intra-articular measurement with optical modalities

After the grooves were created at the first surgery, the dorsoproximal surface of the intermediate carpal bone and the surface of the radial facet of the third carpal bone in both grooved and control joints were imaged with OCT and subsequently measured with NIRS. (For measurement lines and points, see supplementary figure 1.) Two follow-up arthroscopies were performed at week 11 and week 23 under general anesthesia as described for the groove surgery. The last arthroscopy at 39 weeks was

performed immediately after euthanasia with pentobarbital (Euthasol®, 50m/kg BW, iv) following the same sedation and induction protocol as described for the groove surgery. Intra-articular OCT and NIRS measurements were performed under arthroscopic guidance (using a traditional arthroscope, 4 mm, 30° inclination, Synergy HD3, Arthrex, Naples, FL, USA) in the grooved joint at weeks 11 and 23 and in both grooved and control joints at week 39.

For OCT imaging, the ILUMIEN PCI Optimisation System (Abbott, Chicago, Illinois, USA) was used (wavelength:  $1305 \pm 55$  nm, in plane pixel size of  $10 \times 10 \mu\text{m}^2$ , slice thickness  $100 \mu\text{m}$ , frame rate 100 frames/s) equipped with a Dragonfly DUO or Dragonfly OPTIS Intravascular Imaging Catheter (diameter 0.9 mm). The NIRS system included spectrometers (AvaSpec-ULS2048L, AvaSpec-NIR256-2.5-HSC, Avantes BV, Apeldoorn, The Netherlands), a light source (AvaLight-HAL-(S)-Mini, Avantes BV), and a custom-designed and sterilizable arthroscopic probe ( $d = 3.25$  mm). Visible and NIR spectra ( $\lambda = 0.4\text{-}2.5 \mu\text{m}$ ) were acquired through perpendicular contact between the probe and the cartilage surface. This was followed by preprocessing and exclusion of outlier spectra similarly as presented by Sarin et al.<sup>11</sup> Machine learning was adapted to relate spectral information to cartilage properties (i.e. cartilage thickness and biomechanical properties). The preliminary network architecture comprised an input layer, hidden layers with convolutional and dense neurons, and a linear output layer. The in vivo NIR spectra obtained at week 39 and post-mortem ex vivo NIR spectra, in combination with a reference value for thickness (based on micro-CT imaging as described later in this section) were used to train the network. Pony-specific 4-fold cross-validation (i.e., the calibration and validation group had six and two ponies, respectively) was performed with a single pony as the independent test group. The training was repeated for nine iterations with each pony being the independent test group once. The network with the lowest mean square error in the validation group was retained during each training session. The retained networks were used to predict cartilage thickness from earlier timepoints, where the average of each network's prediction was used as the final result.

## **Radiographic analysis**

Seven radiographs of both carpal joints were taken at two occasions: prior to and at 38 weeks after groove surgery, including the following views: lateromedial, flexed lateromedial, dorsopalmar, dorsomedial-palmarolateral and dorsolateral-palmaromedial oblique and dorsoproximal-dorsodistal oblique at 85 and 55 degree-angles. Radiographs were assessed for subchondral bone lysis, bone proliferation at the joint capsule attachment, osteophyte formation and soft tissue swelling by a board-certified veterinary radiologist (MB). Each abnormality was graded on a scale



of 0-3 for severity (0 = no abnormal findings, 1 = mild changes, 2 = moderate changes, and 3 = severe changes) except for soft tissue swelling, which was scored as being absent (0) or apparent (1).

## Synovial membrane

At each surgery, synovial membrane biopsies were taken for histology and gene expression analysis (n = 144). Samples for histology were fixed in formaldehyde solution 4% (Klinipath 4078.9005) and embedded in paraffin. Five  $\mu\text{m}$  sections were stained with hematoxylin-eosin and blindly graded from 0 to 4 for cellular infiltration, vascularity, intimal hyperplasia, subintimal edema and subintimal fibrosis, according to Osteoarthritis Research Society International (OARSI) histopathological guidelines<sup>12</sup> in randomized order by two observers (NM, SP).

For RNA isolation, the RNeasy Mini kit (QIAGEN, Hilden, Germany) was used according to the manufacturer's guidelines. Any DNA contamination was cleared by DNase digestion. Total RNA yield was determined spectrophotometrically (NanoDrop ND1000; Isogen Life Science). For 11 samples with a yield < 10 ng/ $\mu\text{l}$ , RNA integrity numbers were determined as an extra quality check with a Bioanalyzer system (2100, Agilent). An input of 300 ng total RNA per sample was reverse transcribed into complementary DNA (cDNA) using an iScript cDNA synthesis kit (Biorad) and random primers. SybrGreen quantitative real-time PCR (qPCR) was subsequently performed and measured using a Bio-Rad CFX384 detection system (Bio-Rad Laboratories). A four-fold serial dilution of 10 times diluted and pooled cDNA was used as a standard curve. Primers were designed using computer software (primer BLAST, [www.ncbi.nlm.nih.gov/tools/primer-blast](http://www.ncbi.nlm.nih.gov/tools/primer-blast)) and obtained from Eurogentec (supplementary table 1). Target genes included matrix metalloproteinase-3 (MMP-3), Chemokine (C-C motif) ligand 2 (CCL2), Interleukin-1 receptor (IL1R), Interleukin-6 (IL-6), Transforming growth factor beta-1 (TGF $\beta$ 1), Activin receptor-like kinase-5 and -1 (ALK5 and ALK1) and Plasminogen activator inhibitor-1 (Pai1). Based on expression stability evaluation<sup>13</sup>, Ribosomal protein S19 (RSP19), Ribosomal protein L13 (RPL13), glyceraldehyde-3-phosphate dehydrogenase (GAPDH), tyrosine 3-monooxygenase/tryptophan 5-monooxygenase activation protein zeta (YWHAZ) and succinate dehydrogenase complex flavoprotein subunit A (SDHA) were selected as reference genes (calculations were performed using a custom-made script in R (version 3.5.2). Relative expression was calculated according to the normalized relative quantity (NRQ) method<sup>14</sup> in Excel (version 16.24).

## Synovial fluid

Synovial fluid (SF) was collected in plain tubes prior to each surgery and additionally at weeks -3, 19, and 35. Before arthrocentesis, ponies were sedated with detomidine and butorphanol (Domosedan®, 0.01mg/kg and Dolorex®, 0.02mg/kg bodyweight (BW), iv) and the arthrocentesis area was aseptically prepared. Samples were collected into uncoated 4 ml collection tubes and processed within 30 minutes. Total nucleated cell count (TNC) was determined for each time point (baseline = week 0) and total protein (TP) concentration was measured from week 11 onwards (hand-held refractometer). Predominant cell populations were identified by microscopic evaluation of rapid stained SF smears. The monocytes/neutrophils ratio was classified based on the differentiation of various pathologic joint conditions (>90%/<10%, <75%/>25%, <25%/>75% and <10%/>90%).<sup>15</sup> Control samples from radiocarpal and middle carpal joints were averaged for analysis. The remainder of the sample was centrifuged (at 2520 x g for 5 min) and then the cell-free supernatant was transferred to 2ml Eppendorf tubes and stored at -80°C until further analysis.

A panel of five biomarkers was evaluated in SF collected at baseline (week -3), week 19 and week 35. Concentrations of carboxypeptide of type II collagen (CPII) as a marker of type II collagen synthesis (Ibex, Montreal, Québec, Canada), type II collagen cleavage (C2C) marker (Ibex) and the inflammation and pain-related marker CC-chemokine ligand 2 (CCL2) (KingFisherBiotech, Saint Paul, USA) were measured by use of commercial ELISA kits (supplementary item 1). General MMP activity was measured using a fluorometric assay based on the cleavage of the fluorogenic peptide substrate FS-6.<sup>16</sup> Glycosaminoglycan (GAG) concentrations were measured using a modification of the 1,9-dimethylmethylene blue assay described by Farndale et al.<sup>17</sup> Control samples from radiocarpal and middle carpal joints were pooled. Samples from grooved joints were pooled at baseline only.

## Quantitative gait analysis

For quantitative gait analysis, OMC data was collected two weeks before and at 8, 10, 22, and 38 weeks after groove surgery. Five spherical reflective markers ( $d = 19$  mm) were attached to the skin using double-sided adhesive tape and two to each of the brushing boots the ponies wore on the distal portion of each limb during the measurements. Reflective markers were placed between the eyes on the os frontale (head), on the dorsal spinous process of T6 (withers), on the left and right tuber coxae, and between the two tuber sacralia (pelvis). Ponies were measured at walk and trot on a straight line over a hard surface. Optical motion capture data was recorded by 18 high-speed infrared cameras (Oqus 700+, 200Hz, Qualisys AB, Gothenburg, Sweden). The coordinates of the reflective markers were calculated by motion

capture software Qualisys Track Manager (version 2018). Symmetry parameters MaxDiff and MinDiff (i.e. difference between the two maxima and minima of vertical displacement, respectively) and range of motion (ROM) were calculated for head, withers, and pelvis, as previously described.<sup>18</sup> Filtering and processing of the data was performed according to previously described methods (F. M. Serra Bragança, under review).

## Post-mortem analyses

After euthanasia and the last follow-up arthroscopy at week 39, carpal joints were harvested and stored at -20°C until further analyses (fig. 2B).

## Macroscopic examination

Carpal joints were thawed overnight at 4°C. Middle carpal and radiocarpal joints were opened, and joint surfaces were photographed for macroscopic evaluation. Gross changes of the articular cartilage were scored on a 0-4 scale as described for the induced osteochondral chip fragment-exercise OA model.<sup>12</sup> The actual grooves were excluded from this grading scheme. Photographs were blind-coded and randomly scored twice with one week in between by two observers (NM, HB) and results were averaged. Subsequently, osteochondral samples including the grooved sites and the contact sites (“kissing site”) as well as their contra-lateral controls were harvested using an oscillating saw (multitool PMF 220CE, Bosch, Stuttgart, Germany). Samples from the same sites were harvested from the sham-operated control joint. Samples were frozen at -20°C until micro-CT analysis was performed.

## Micro-CT imaging of osteochondral samples

Micro-CT imaging was acquired using a high-resolution micro-CT scanner (Quantum FX®, Perkin Elmer, USA). The samples were thawed at room temperature prior to the measurements. Imaging was conducted in air, one sample at a time, by placing each sample in a sealed plastic holder containing a wet paper towel to prevent dehydration during scanning. The image acquisition parameters were: X-ray tube voltage = 90 kV, X-ray tube current = 200  $\mu$ A, field of view = 20 mm  $\times$  20 mm, isotropic voxel size = 40  $\mu$ m, and image acquisition time = 120s. Projections were transformed automatically to 3D reconstructed files using in-built software of the micro-CT machine, Quantum FX. After imaging, each sample was stored in a plastic bag and frozen at -20°C. Changes in mean trabecular bone thickness (TBT) and trabecular bone volume fraction (BV/TV) were evaluated using Fiji software (ImageJ, version 2.0.0-rc-69, <https://imagej.net>). Regions of interest were manually selected in sagittally oriented sections. Bone was segmented from the image stack with a local thresholding algorithm (Phansalkar, radius 15).

## Mechanical indentation testing

Samples were thawed at room temperature prior to semi-automated indentation testing. For one sample, 6 measurement locations (3 points each on dorsal and palmar parts of the cartilage surface, between the transverse grooves) were chosen and cartilage thickness at each of these points was precisely determined from the micro-CT images using a custom-made MATLAB code (fig. 2B). In preparation for indentation testing, the bone end was flattened using sandpaper (Mirox P80, Mirka Oy, Uusikaarlepyy, Finland) and then glued (cyanoacrylate) to the bottom of a transparent acrylic chamber, filled with phosphate-buffered saline (PBS). A 1-step stress-relaxation protocol was applied perpendicular to each of the locations at the cartilage surface using Biomomentum Mach-1 v500css (Biomomentum Inc., Laval, Quebec, Canada) with a 70 N multiaxial load-cell and a non-porous spherical tip indenter ( $d = 0.5$  mm, MA034, Biomomentum). The sample surface was located using the surface detection program of the device. Briefly, in this program the stage stops moving when the defined load (0.1 N) is reached and the software automatically calculates load-displacement curves and moves to the position where the load started to increase. Then, a one-step stress-relaxation test followed by 300 s of relaxation was applied with a ramp rate of 100%/s and a step size of 15% of the cartilage thickness.<sup>19-21</sup> The required time to reach equilibrium (300s; relaxation rate at the end of the measurement  $< 0.1$  Pa/min) was determined in pilot testing. The measured equilibrium and instantaneous moduli were corrected using Hayes equation, which considers the measurement geometry<sup>22</sup>. Poisson ratios were set to  $\nu = 0.2$  and  $\nu = 0.5$  for the equilibrium and instantaneous modulus, respectively.<sup>19,23</sup>

## Microscopic examination

After biomechanical analysis, osteochondral samples were cut into 12 mm wide samples; 6 mm from the (virtual) central groove towards the dorsal and the palmar side. These samples were fixated in 10% formalin (Riedel-de Haen 33220) and decalcified in 0.5 M EDTA (prod. 20296.360, VWR, Radnor, USA) at pH 7.0 for 10 weeks. After decalcification, samples were further divided into four parts of 3 mm in width to enable sectioning from three locations per sample (i.e. directly at the horizontal groove and at a distance of 3 mm from the horizontal groove) and embedded in paraffin. Five- $\mu$ m sections were stained with Safranin-O/Fast-green (SOFG), blind coded and graded at a 0-20 scale according to OARSI histopathological guidelines<sup>12</sup> in randomized order by two observers (NM, SP). Collagen type I and II immunohistochemistry was performed on sections from grooved joints using collagen I rabbit monoclonal antibody (ab138492, Abcam) and collagen II mouse monoclonal antibody (II-II6B3, DSHB). Isotype controls with rabbit IgG (X0903, Dako) and mouse IgG (X0931, Dako) respectively, showed no a-specific staining. Technical details are described in supplementary item 2.

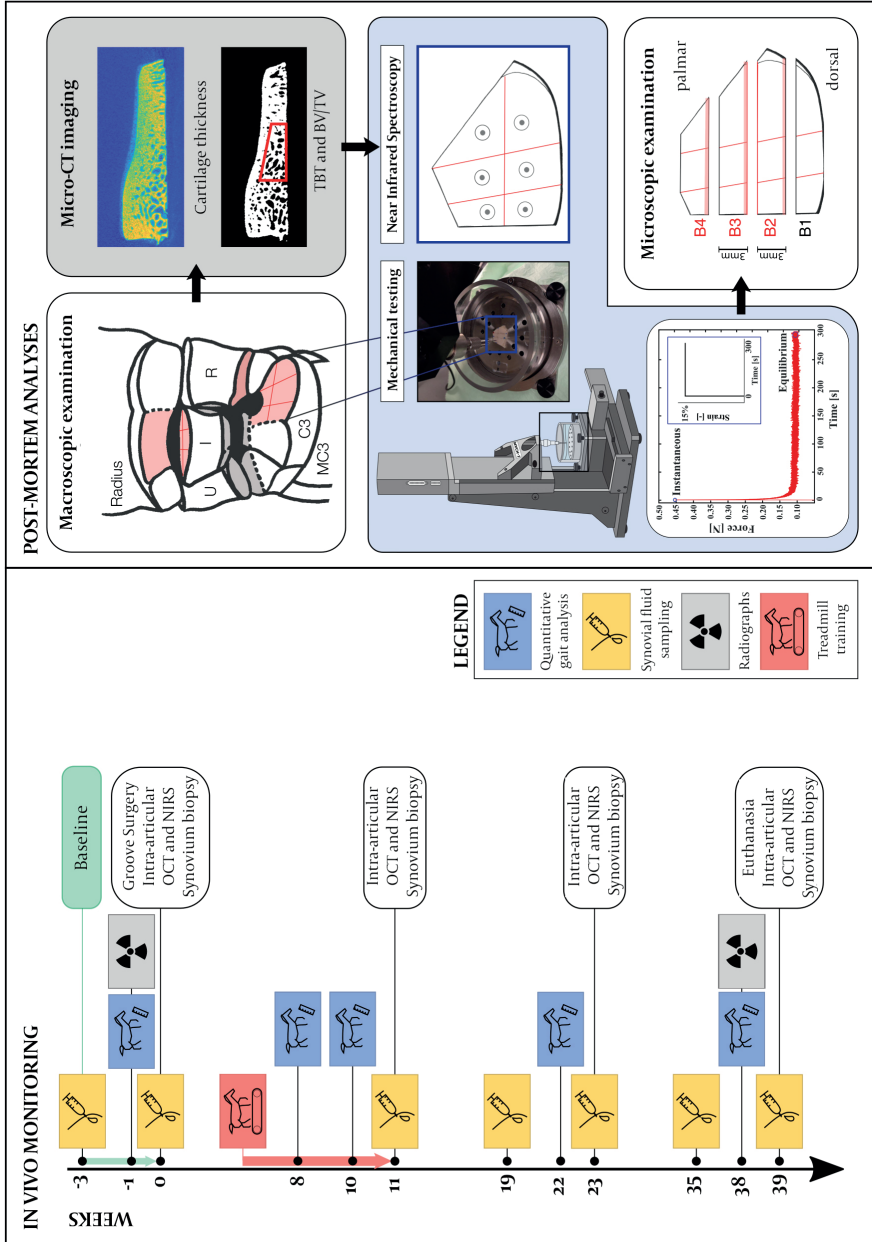


**Fig.2** A) Study design for in vivo monitoring. During baseline period, ponies were accustomed to treadmill exercise. Intra-articular measurements as from week 11 were done through arthroscopy. OCT= optical coherence tomography. NIRS = near infrared spectroscopy. B) Workflow of post-mortem analyses.

## Statistical analysis

For statistical analysis, R software (version 3.5.2) was used. Ordinal data (radiographic and macroscopic scores) were analyzed using Friedman testing with Tukey HSD post-hoc comparison. The nlme package (version 3.1-137) was used for linear mixed effect models on continuous outcomes with pony as random effect. Using these approaches, dependences within animals could be taken into account. Pair-wise comparisons of estimated means with false discovery rate correction were used to test for differences between groups. Continuous data that was not normally distributed was normalized using logarithmic or square root transformations. Model fit was tested using the Akaike's Information Criterion (AIC) and presented model estimates were based on restricted maximum likelihood estimators.  $P < 0.05$  was set as the limit of statistical significance. Macro- and microscopic scores of two observers were averaged for statistical analysis. As a measure of inter-observer agreement, the intraclass Correlation Coefficient (ICC) was calculated (two-way random model for agreement on single measurements). Specifications of data transformation and statistical models are provided in supplementary table 2.

## RESULTS

One pony was withdrawn from treadmill training after five weeks because of recurrent mild lameness (1-2/5) related to mild desmopathy of the interosseous tendon branches and bilateral shoulder OA. Multivariate analysis of SF and synovium markers confirmed that this pony was not an outlier at any of the time points. Therefore, it was only excluded from analysis for the OMC data.

### Intra-articular monitoring

On visual analysis of OCT images, blunt grooves could clearly be recognized at all time points. Sharp grooves were hard to distinguish and mostly only visible at the most superficial layer of the cartilage (supplementary figure 1). Further (quantitative) analysis of OCT data is currently in progress. Regarding NIR spectra, 0.94%, 2.54%, 0.34%, and 2.8% were detected as outliers at baseline, week 11, week 23, and week 39, respectively. Preliminary analysis of NIRS data resulted in mean ( $\pm$  SD) Spearman correlations between the predicted and the reference cartilage thickness of  $0.85 (\pm 0.01)$ ,  $0.50 (\pm 0.05)$ , and  $0.52 \pm (0.13)$  for calibration, validation, and test groups, respectively. The predicted cartilage thickness did not show differences between treatment groups but indicated a significant time-dependent decrease (supplementary fig 2).

## Radiographic analysis

Total radiographic scores were not significantly different between grooved and control joints at 38 weeks but, within the grooved joints, the increase from baseline to 38 weeks was significant ( $p = 0.007$ ). No subchondral bone lysis was observed. Soft tissue swelling had increased in 5/9 cases of the control joints and 7/9 cases of the grooved joints at 38 weeks (table 2; supplementary fig. 3).

**Table 2** Radiographic scores of carpal joints.

	Baseline		38 Weeks	
	Control (n=9)	Grooved (n=9)	Control (n=9)	Grooved (n=9)
Osteophytes (0-3)	0.2 (0-1)	0.1 (0-1)	0.9 (0-2)	0.8 (0-2)
Enthesiophytes (0-3)	0.1 (0-1)	0 (0)	0.3 (0-2)	0.9 (0-2)
Subchondral bone lysis (0-3)	0 (0)	0 (0)	0 (0)	0 (0)
Total score (0-9)	0.3 (0-1)	0.1 (0-1)	1.2 (0-3)	1.7 (0-4)*

Table shows observed means (range). \*\* Indicates a significant difference with baseline.

## Synovial membrane

### Microscopy

A total number of 138/144 of synovium sections could be graded microscopically (4 controls, 1 blunt and 1 sharp were excluded due to insufficient quality of the sample). No significant differences between treatment groups at any time point were found. In all groups, a subtle increasing trend at weeks 11 and 23, followed by a decreasing trend towards week 35 was seen, but this was not significant (suppl. table 3). The ICC (95% CI) of two observers was 0.759 (0.678 - 0.822).

### Quantitative PCR

A mean ( $\pm$ SD) RNA yield of 35.5 ( $\pm$ 26.1) ng/ $\mu$ l was obtained. Seven samples (3 controls, 2 blunt and 2 sharp) were excluded from reverse transcription into cDNA because of poor RNA quality. One control sample was excluded from analysis because Ct values were below the standard curve or out of detection range in 4/5 reference genes and 6/7 target genes. A total number of 136 samples were used for NRQ calculations. Measures of quantitative PCR (qPCR) quality are provided in suppl. table 4.

Gene expression levels in synovium from grooved joints were not significantly different from their contralateral controls. However, blunt- and sharp-grooved joints showed significantly increased expression levels of IL-6, and ALK5 compared with baseline while control joints did not. On the contrary, ALK1 expression showed a gradual downregulation that was significant for grooved joints at week 11 and also

became significant for controls as from week 23. For CCL2, an increasing trend up until week 23 was seen that was significant for blunt- (week 11 and 23) and for sharp-grooved joints (week 23), followed by a significantly lower expression at week 39 in all groups. All groups showed significantly increased MMP3 expression levels as from week 11. Both ILR1 and TGFβ1 showed a similar trend, but the increase became only significant for TGFβ1 at week 39 in blunt-grooved and control joints. Pai1 expression levels were increased in all groups at week 23 only (fig. 3).

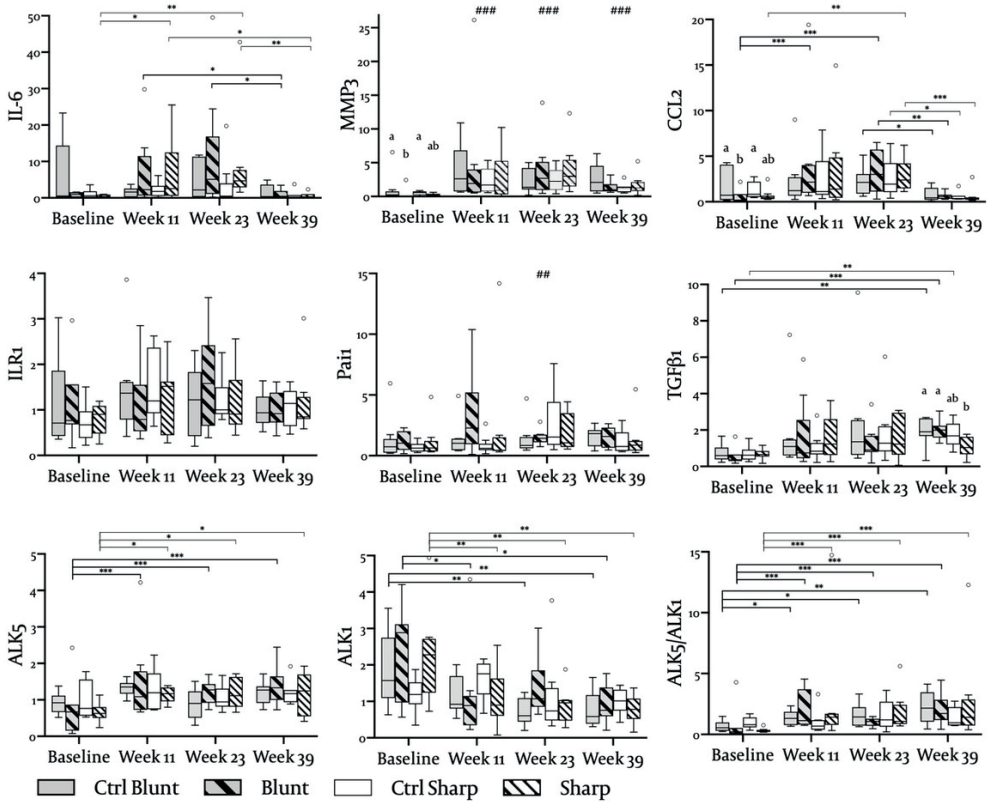


**Fig. 3** Normalized relative quantities of gene expression markers in synovial membrane from blunt and sharp-grooved joints and their contralateral controls. (\*\*\*) Represents significant differences between time points, within treatment groups. (#) Represents significant differences between time points for all treatment groups. \*/# P<0.05; \*\*/## P<0.01; \*\*\*/### P<0.001. Treatment groups that have no corresponding letters are significantly different.



## Synovial fluid

Total nucleated cell count (TNC) could not be measured in 3/216 samples (two blunt grooved and one control) due to a technical error. No differences in TNC or TP concentration were found between grooved and control joints at any time point. Total protein levels significantly decreased as from week 23, but all values were within a clinically normal range (0-3 g/dL). The estimated mean ( $\pm$ SE) TNC significantly increased over time from 0.33 ( $\pm$ 0.09) G/L at baseline to 5.2 ( $\pm$ 1.4) G/L at week 39. A small peak was observed at week 11 (table 3). Microscopic evaluation of rapid stained smears revealed a small shift in monocyte/neutrophil ratio at week 11 (6 samples), week 19 (5 samples), week 23 (1 sample) and week 35 (1 sample). An abundant neutrophil population of > 75% was only seen at week 11 in two samples from the same pony (table 3). An increasing presence of lymphocytes over time explain the overall increasing cell count.

Significant differences in SF biomarker levels between treatment groups were found for CPII (blunt-grooved > sharp-grooved at week 35,  $p = 0.03$ ), C2C (grooved < control at baseline,  $p = 0.002$ ) and for the ratio CPII/C2C (blunt-grooved > sharp-grooved and control at week 35,  $p = 0.008$  and  $p = 0.02$ , respectively.). Additionally, the increase of the CPII/C2C ratio over time was significant in blunt-grooved joints only ( $p = 0.01$ ). For GAG and MMP analysis 1/72 samples and for CCL2 analysis 3/72 samples (blunt) could not be measured due to limited material. For these three markers, no significant differences between groups were found, but significant changes were apparent over time. GAG concentrations in all treatment groups were decreased at week 19 ( $p < 0.0001$ ) and slightly increased at week 35 ( $p = 0.006$ ) compared with baseline. An opposite pattern was observed for MMP activity, which was increased at week 19 ( $p < 0.0001$ ). Although this was followed by a decrease, activity was still higher at week 35 ( $p = 0.03$ ). An increase in CCL2 concentration was found at both week 19 and week 35 ( $p < 0.0001$ ) (fig. 4).

**Table 3** Synovial fluid total protein levels, total nucleated cell counts and differentiation

	Joint	TP (g/dL)	TNC (G/L)	Monocytes / neutrophils %			
				>90/<10	<75/>25	<25/>75	<10/>90
Baseline	Control	NA	0.36 (0.18-0.73)	9	0	0	0
	Blunt	NA	0.36 (0.18-0.73)	9	0	0	0
	Sharp	NA	0.26 (0.13-0.52)	9	0	0	0
Week 11	Control	1.2 (0.8-1.7)	2.69 (1.35-5.36)*	6	2	1	0
	Blunt	1.2 (0.8-1.8)	2.66 (1.32-5.36)*	7	1	0	1
	Sharp	1.2 (0.8-1.8)	1.92 (0.96-3.83)*	8	1	0	0
Week 19	Control	1.5 (1.0-2.2)	1.11 (0.56-2.21)*	7	2	0	0
	Blunt	1.5 (1.0-2.2)	1.10 (0.56-2.19)*	7	2	0	0
	Sharp	1.5 (1.1-2.2)	0.80 (0.40-1.58)*	8	1	0	0
Week 23	Control	0.8 (0.5-1.1)*	2.05 (1.04-4.07)*	8	1	0	0
	Blunt	0.8 (0.5-1.1)*	2.03 (1.02-4.03)*	9	0	0	0
	Sharp	0.8 (0.5-1.1)*	1.46 (0.74-2.90)*	9	0	0	0
Week 35	Ctrl	0.8 (0.5-1.1)*	5.13 (2.59-10.2)*	8	1	0	0
	Blunt	0.8 (0.5-1.1)*	5.08 (2.56-10.1)*	9	0	0	0
	Sharp	0.8 (0.5-1.1)*	3.67 (1.85-7.26)*	9	0	0	0
Week 39	Ctrl	0.6 (0.4-0.8)*	5.85 (2.95-11.6)*	9	0	0	0
	Blunt	0.6 (0.4-0.9)*	5.78 (2.92-11.5)*	9	0	0	0
	Sharp	0.6 (0.4-0.9)*	4.17 (2.11-8.27)*	9	0	0	0

Table shows estimated means ( $\pm 95\%$  CI) for TP and TNC and the number of observations per category for the ratio monocytes / neutrophils. "\*" Indicates significantly different values from baseline.

## Quantitative gait analysis

A gradual increase was found for the absolute difference between the two minima of vertical displacement (MinDiff) of the head. The difference with baseline was significant at all time points and reached a maximum of 6.3 mm at week 22. No significant or clinically relevant changes were found on the other symmetry parameters. The range of motion (ROM) of the head significantly decreased with 6.4 mm at week 8, normalized at week 10 and week 22, followed by a significant increase of 4.0 mm at week 38. For the withers, a significantly decreased ROM was found at week 22 and week 38. (Estimates of all parameters are provided in suppl. table 5).

## Macroscopic and microscopic examination of the cartilage

Macroscopically, blunt grooves looked different to sharp grooves, but both types of grooves were quite homogeneous in appearance over the different individuals. Blunt grooves were clearly visible and showed a crumbling aspect at the edges of the grooves with no visible filling of the defect. In most samples, an imprint was seen at the kissing site. Sharp grooves were hardly visible, and no signs of defect filling were seen here either. The surfaces of both grooved and control joints showed mild

to moderate degenerative changes and no significant differences were found (fig. 5, table 4). The ICC (95% CI) of two observers was 0.443 (-0.089 - 0.771).

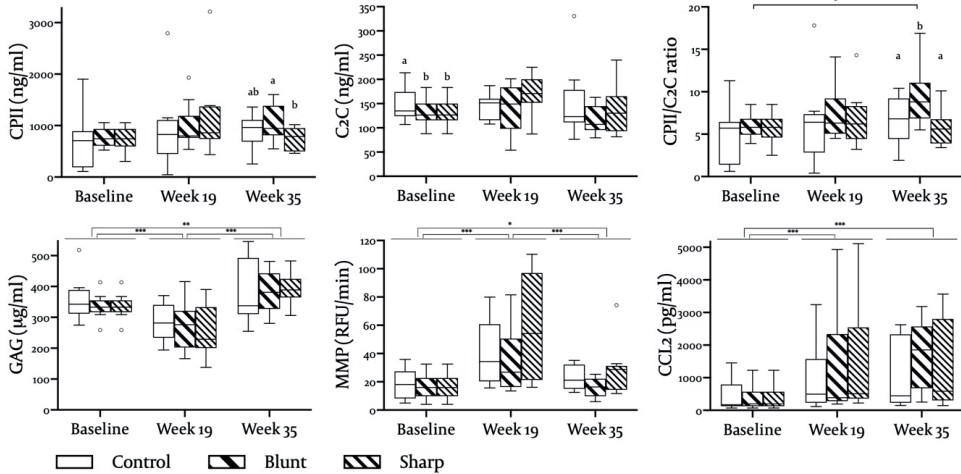


**Fig. 4** Biomarkers in synovial fluid. Medians ( $\pm$  interquartile ranges) of Pro-collagen type II (CII) and Collagen type II cleavage (C2C) concentrations, CII/C2C ratio, glycosaminoglycan (GAG) concentration, matrix metalloproteinase (MMP) activity and chemokine (C-C motif) ligand 2 (CCL2) concentrations in synovial fluid from control joints and blunt- and sharp-grooved joints. \*  $P < 0.05$ ; \*\*  $P < 0.01$ ; \*\*\*  $P < 0.001$ . Treatment groups that have no corresponding letters are significantly different.

Microscopically, both blunt and sharp lesions could be recognized from SOFG stained sections. Blunt lesions typically reached to the calcified cartilage layer and caused detachment of the non-calcified cartilage at the tidemark. Big clusters (up to 19 cells) and loss of SOFG staining characterized the area adjacent to the lesions (fig. 6). Sharp lesions typically reached into the deep zone of the non-calcified cartilage layer and caused relatively mild changes to the adjacent tissue (fig. 6). In ponies 5 and 9, filling of blunt defects with fibrocartilage-like tissue was observed. In pony 9 this was also seen in one sharp defect (fig. 7). Mean OARSI scores were significantly higher in both blunt- and sharp-grooved samples compared with their controls ( $p < 0.0001$ ). This was not the case for the kissing sites. Also, blunt-grooved samples scored significantly higher than sharp grooved samples ( $p = 0.007$ ) (table 4; suppl. table 6). The ICC (95% CI) of two observers was 0.902 (0.874-0.924). Although not surgically damaged, small defects and mild degenerative changes were also found in the control samples. Qualitative evaluation of collagen staining showed collagen type 2 loss in the cartilage directly adjacent to the blunt lesions and, to a lesser extent at the edges of the sharp lesions. Only little collagen type 1 staining was observed in the repair tissue that was found in the 2 blunt-grooved samples.

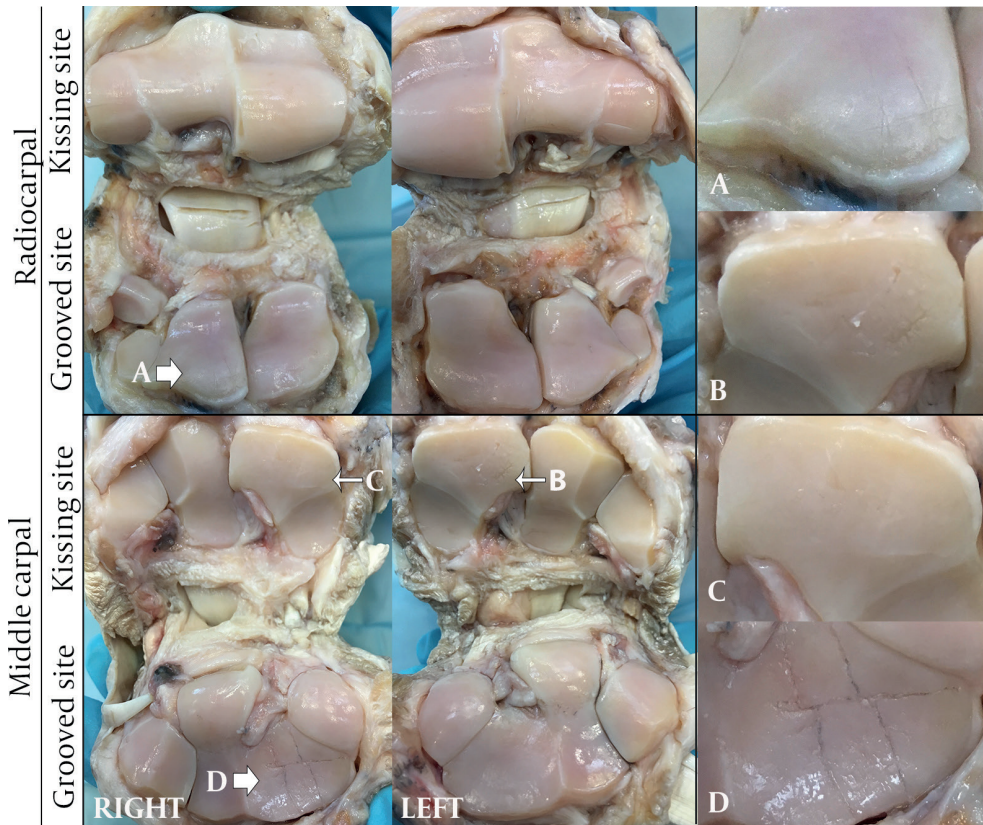


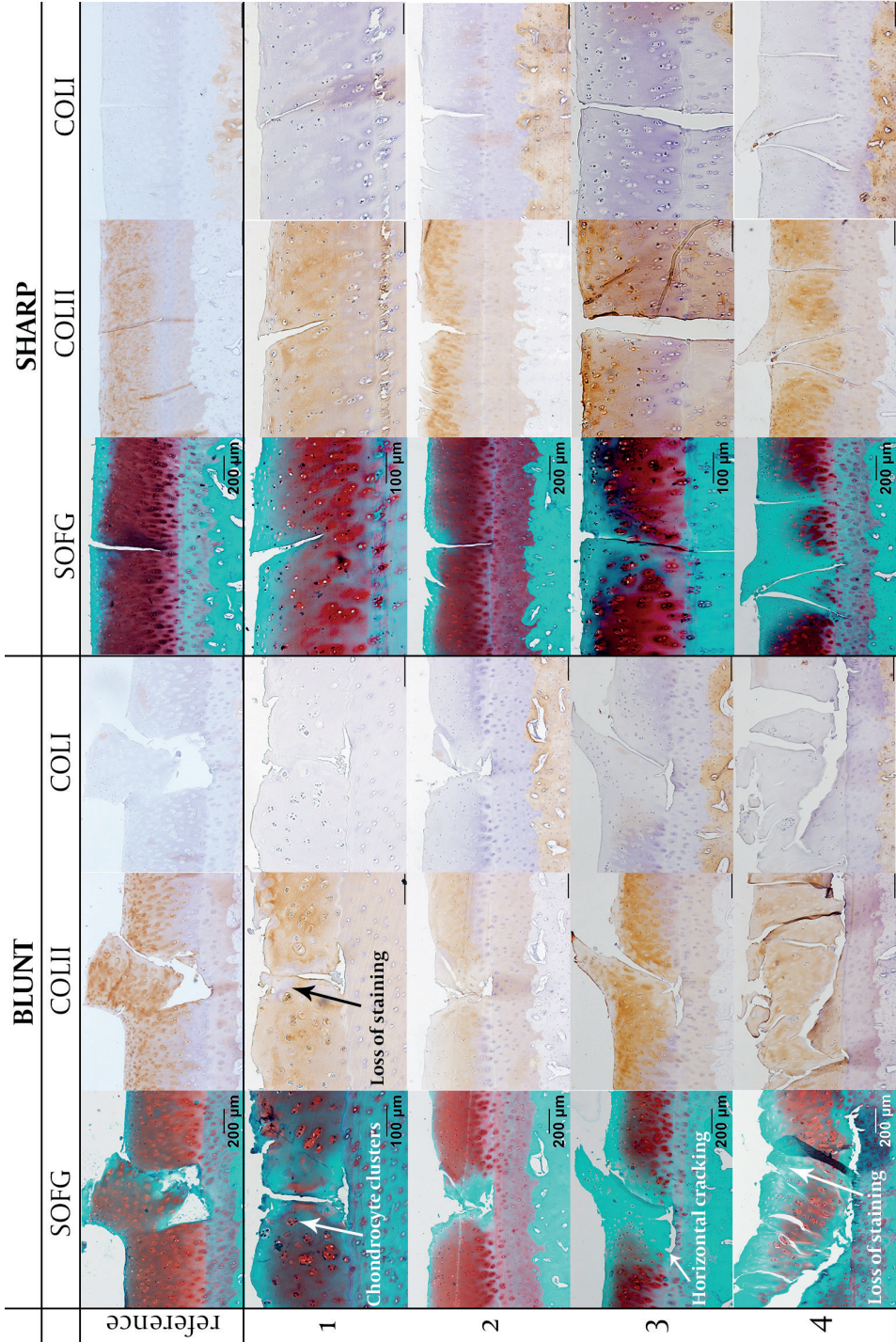
**Fig. 5** Gross appearance of the articular cartilage surface of grooved (right) and sham-operated (left) joints of an individual at 9 months. Sharp grooves (A) and blunt grooves (D) are present in the right joint. The kissing sites in the right middle carpal joint shows a press-pattern of the blunt grooves (C). The kissing site in the left middle carpal control joints shows a grade 3 lesion (B).

### Micro-CT imaging of osteochondral samples

No differences in cartilage thickness, mean trabecular thickness or bone volume fraction were observed between grooved samples and their controls or between blunt- and sharp-grooved samples in the  $\mu$ CT images (table 4, suppl. fig 4).

### Biomechanical measurements

The equilibrium and instantaneous modulus of cartilage in the grooved joints trended lower than in the control joints. This difference was significant for sharp grooved cartilage ( $p = 0.002$  and  $p = 0.045$ , respectively). Blunt-grooved samples were not significantly different from sharp-grooved samples (table 4, fig 7).



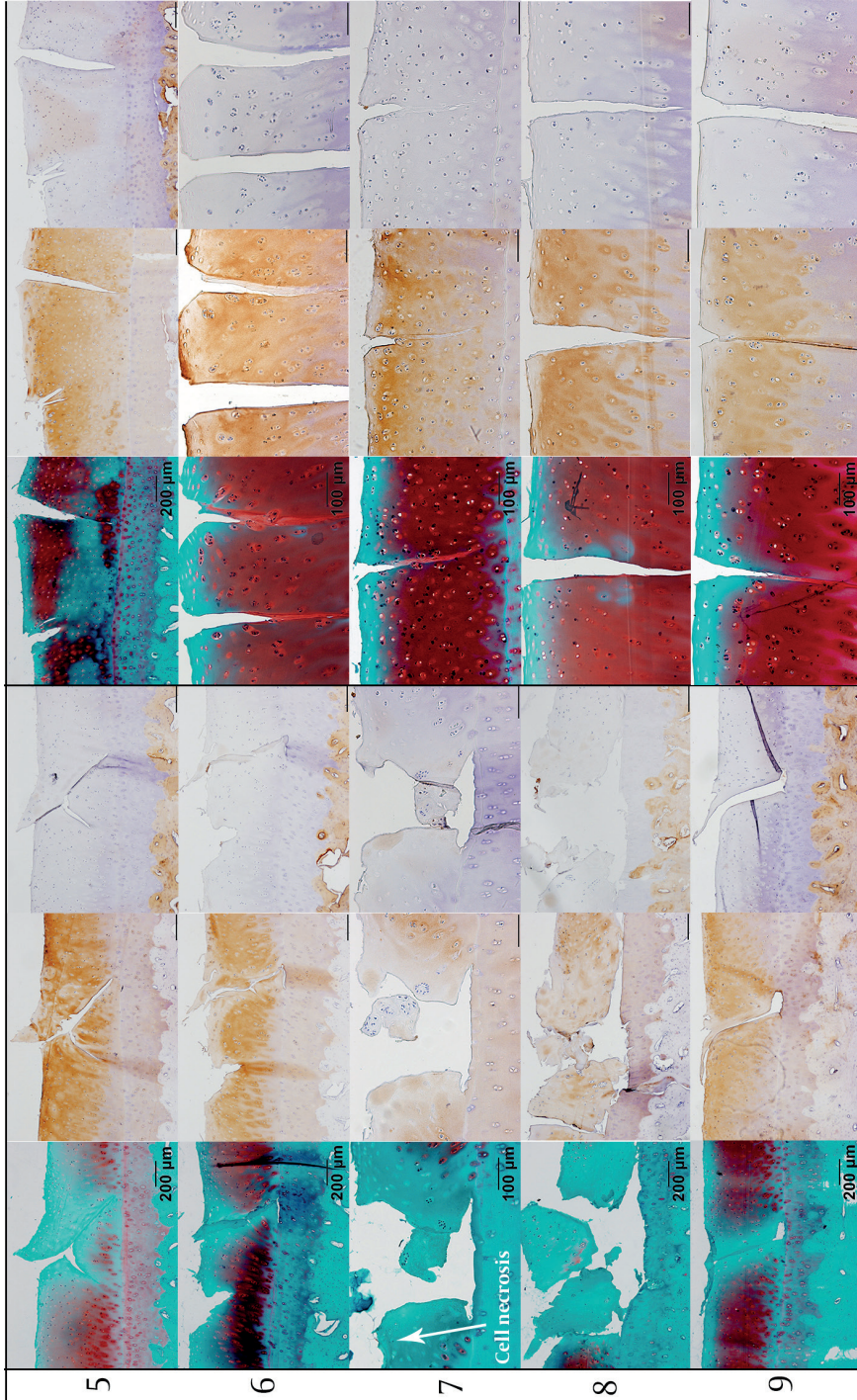


**Fig 6** Light micrographs of articular cartilage surfaces with blunt and sharp grooves of each individual. Reference shows a freshly made blunt and sharp lesion in a cadaver joint. B3 = sagittal section through horizontal groove, B2 and B4 = 3 mm dorsal and palmar of horizontal groove, resp.

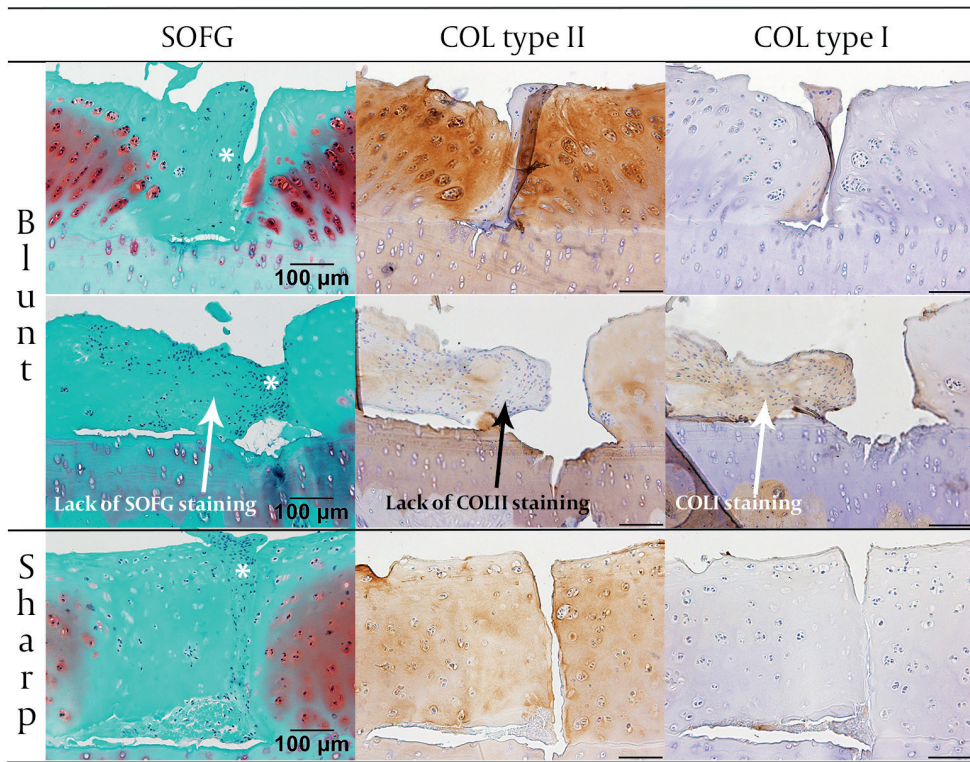


**Fig. 7** Microscopic sections of articular cartilage with fibro-cartilage-like filling of blunt (pony 5 and 9, resp) or sharp (pony 9) grooves. White "\*" Indicates fibro-cartilage-like tissue. Lack of collagen type II staining and positive staining for collagen type I was observed in the blunt grooves. The tissue observed in the SOFG-stained section of the sharp groove, was not found in the collagen type I and II-stained sections.

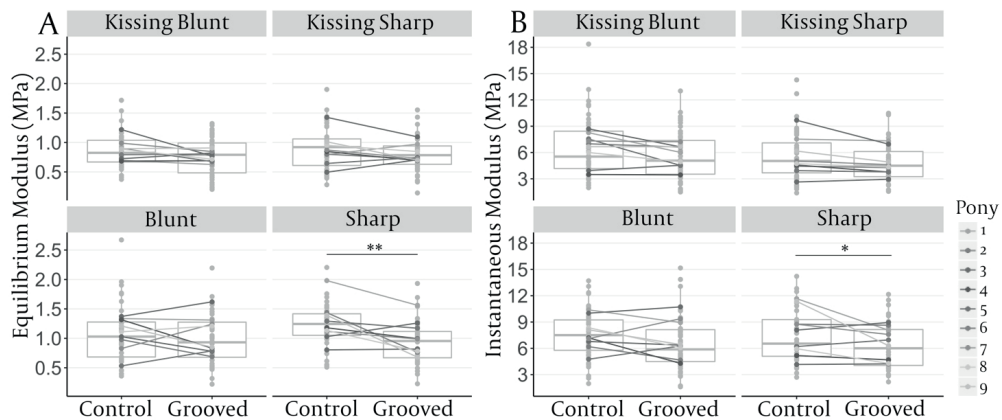


**Fig. 8** Post-mortem cartilage biomechanical properties. Spaghetti plots show cartilage equilibrium modulus (A) and instantaneous modulus (B) averaged over 6 measured locations. Grey boxplots represent medians with interquartile ranges of all measured locations. \*  $P < 0.05$ ; \*\*  $P < 0.01$ .

## DISCUSSION

This study showed that both blunt and sharp cartilage grooves in the equine carpal joint in combination with a period of intensified loading, lead to degenerative changes of the adjacent articular cartilage over a 9-month period. This could be quantified by significantly higher OARSI scores for histology sections from grooved sites compared with their contra-lateral controls. Blunt lesions were inherently bigger and caused more tissue loss than sharp lesions. This resulted in a more extensive lack of proteoglycan and collagen type II staining and more pronounced cluster formation and focal cell loss in the adjacent cartilage and consequently higher OARSI scores. In two ponies, little defect filling with fibro-cartilage-like tissue was found. No differences in cartilage thickness were found, but cartilage stiffness values were lower in grooved joints; however, this was only significant for sharp-grooved cartilage. Concomitant changes in other joint tissues were limited to significantly increased radiographic scores in grooved joints at 38 weeks, significantly increasing IL-6, CCL2 and ALK5 expression levels in synovium from grooved joints, and an increased CPII/C2C ratio in SF from blunt-grooved joints at week 35. No differences in the subchondral trabecular bone parameters were found. Main findings on quantitative gait analysis included a gradually increasing asymmetry of the vertical movement of the head and an initial decrease in ROM of the head that was significantly increased at week 38.



## Natural progression of blunt and sharp cartilage grooves

The observation that both blunt- and sharp-grooved cartilage showed features of degenerative changes confirms that cartilage damage does not heal but always leads to pathological changes within the microenvironment of the lesion, irrespective of the size of the defect. The nature of the blunt grooves in the current study was similar to that described in previous groove model studies: macroscopically visible grooves without signs of healing or fibrin deposition together with visible changes of the opposing articular surface, and increased histological degeneration scores characterized by cell necrosis, chondrocyte clusters around the lesion, moderate loss of staining and horizontal cracking with detachment from the calcified cartilage.<sup>5-8</sup> In our study, fibro-cartilage-like tissue was found in some defects in two individuals. Although this has not been reported for previous groove models, partial defect filling of chondral lesions with fibrous repair tissue has been described in the equine carpus, three months<sup>24</sup> as well as one year<sup>25</sup> after a lesion had been created. The fact that we observed this only in some individuals is interesting and may highlight the variation in individual responses to cartilage damage. Sharp lesions have been studied in the superficial scarification model in rabbits that was described by Meachim and used in the 1960s and 1970s.<sup>26-28</sup> In this model, sharp cuts extending into the deep zone of the articular cartilage of the femoral condyles were induced with a scalpel. Observations after a period of 6 to 34 weeks were similar to ours: chondrocyte clusters adjacent to the incisions, related to loss of matrix staining that extended to the deeper cartilage layer over time, and lesions that remained localized to the traumatized areas in the cartilage and that did not result in overall degenerative joint changes.<sup>26,28</sup>

While macroscopically visible alterations were seen of the kissing sites of, in particular, blunt grooves (imprints), they were not assigned higher OARSI scores than kissing sites in control joints, as described in sheep and rats.<sup>6,7</sup> This could be related to repeated arthrocentesis and repeated joint surgery in the current study that may have caused unintended additional damage to the kissing sites in both control and grooved joints, leveling out the difference in degeneration scores.

## Differences between sharp and blunt grooves and consequences for local biomechanical functioning

Direct comparisons between blunt and sharp trauma have been studied previously in an *in vitro* experiment on immature bovine cartilage explants.<sup>29</sup> Whereas blunt trauma induced with a trephine resulted in a band of cell death adjacent to the lesion edge extending approximately 100  $\mu\text{m}$  into the tissue, viable cells were found immediately adjacent to the edge of sharp lesions made with a scalpel. Also, lack of safranin-O staining at the edge of blunt lesions extended further into the tissue.

Chondrocyte proliferation and up-regulation of new matrix synthesis were found immediately adjacent to the edge of sharp lesions throughout the tissue depth, but behind the region of cell death in blunt lesions.<sup>29</sup> These observations were correlated with the notion that at the initial insult there is less disruption of the matrix and less mechanical stress immediately adjacent to the edge of a defect created with a sharp blade.<sup>29,30</sup> This is in line with the observations in the current study and shows that reaction of the tissue adjacent to the defect varies and is dependent on the characteristics of the lesion.

The reaction of cartilage tissue around a lesion is further influenced by subsequent mechanical loading. It has been shown that cartilage defects cause mechanical changes (e.g. the load bearing capacity and excessive compressive and shear load on the defect rim and the adjacent area) in the surrounding tissue as well as the opposing tissue<sup>31,32</sup> and that these changes become more important with increasing defect size.<sup>33,34</sup> Based on the observations in the current study, we hypothesize that it is not only the size of the defect (with sharp lesions having a geographically much smaller zone of influence than blunt lesions), but the combination with the degree of matrix disruption, and the direction of the defect (perpendicular to or at an angle with the surface) in relation to the degree and direction of loading (i.e. the magnitude of the force and the relative contribution of compressive, shear and tensile components) that will determine the deformation of the tissue and hence the aggravation of the damage over time. Consequently, compressive loading on a sharp lesion in line with the direction of the force can be supposed to have the least effect, while compressive loading at an angle on a blunt lesion (which will also induce shear due to the nature of the lesion) will cause most effect.

Apart from the direct effect on cartilage integrity, mechanical loading also influences cartilage metabolism via mechanotransduction processes, which can induce changes in gene expression and tissue remodelling.<sup>35</sup> The variation in tissue reaction as a result of the nature of the lesion in combination with direct and indirect effects of mechanical loading may explain a perhaps counterintuitive finding in this study, i.e. the tissue in the area between the sharp grooves was significantly less stiff than at the control side while this was not the case for blunt grooves. When looking at the results at an individual level (fig. 7), the biomechanical moduli of the kissing sites and of the tissue adjacent to the sharp lesions mostly stayed constant or tended to decrease. Near the blunt lesions there are several individuals that show a distinct increase in stiffness. There is evidence that articular cartilage damage initially incites an anabolic response in the tissue still capable of that, resulting in a compensatory increase in aggrecan as well as type II collagen synthesis.<sup>36,37</sup> In our study, it is possible

that only the damage provoked by the blunt grooves was sufficient to initiate such an anabolic response and that the minimal damage in the other three groups did not pass that threshold. This theory may be supported by the fact that the CPII/C2C ratio in SF was significantly higher in blunt-grooved joints. Alternatively, or in addition to that, it is likely that an anabolic response in blunt-grooved cartilage occurred behind the described region of cell death, whereas a potential response in sharp-grooved cartilage would probably occur directly adjacent to the lesion, in line with earlier observations by Meachim in the rabbit scarification model<sup>26</sup> and by Redman et al. in bovine explants *in vitro*.<sup>29</sup> Since the biomechanical measurements points were not located directly at the edges of the grooves, but in between them, it might be more likely that such a response in blunt-grooved cartilage rather than sharp-grooved cartilage would affect the biomechanical results in terms of increasing stiffness.

However, these theories should be carefully considered to prevent over-interpretation of the results. The differences between sharp-grooved cartilage and contralateral controls might have been significant, they were relatively small, and 95% confidence intervals were mostly overlapping with blunt-grooved cartilage (table 4). Quantitative evaluation of collagen content and orientation as well as proteoglycan distribution around the grooved areas by means of e.g. fourier transform infrared spectroscopy (collagen content), polarized light microscopy (collagen orientation) and optical density images of SOFG-stained sections (fixed charge density) could be performed to elucidate the proposed hypotheses.

### **Alterations in other articular tissues and gait pattern**

Setting aside the microscopically apparent progress of cartilage degeneration and the significantly increased radiographic scores in grooved joints at week 38, the effect of cartilage defects on other articular tissues was limited. Grooved joints could not be distinguished statistically from their contra-lateral controls based on gene expression levels in the synovium at single time points. Nevertheless, the increase in expression levels of IL-6, CCL2 and ALK5 over time was significant in grooved joints only, suggesting that there might have been an enhancing effect on transcription of these factors induced by cartilage damage. The cytokine IL-6 has previously been associated with equine OA.<sup>38,39</sup> However, when synovium biopsies from diseased and healthy equine joints were compared, positive IL-6 immunostaining was detected in both groups, and no significant difference between OA joints and joints with osteochondral fragments was found.<sup>40</sup> Immunostaining of the synovium for IL-6 or analysis of IL-6 concentrations in SF obtained in the current study may confirm if the observed upregulation in expression levels also resulted in a significant increase in IL-6 production in grooved joints. Consistent with the increased CCL2

expression in synovium, we found increasing levels in SF, although no distinction between samples from grooved and control joints could be made. The chemokine CCL2 is an important attractant of macrophages in OA<sup>41</sup> and has been related to the development of pain rather than to cartilage damage.<sup>42</sup> Investigation of the expression of CCL2 and its receptor (CCR2) in e.g. neurons and dorsal root ganglia may provide interesting insights in the development of pain induced by this model. The TGF $\beta$ 1 receptor ALK5 signals via Smad2/3 phosphorylation in cartilage, which is considered chondroprotective, in contrast to ALK1, which promotes chondrocyte terminal differentiation.<sup>43,44</sup> The significant upregulation of ALK5 in synovium from grooved joints, in combination with a downregulation of ALK1 and the increasing ALK5/ALK1 ratio that was most pronounced in grooved joints, may be interpreted as a chondroprotective response.

The SF CPII/C2C ratio that was found to be significantly higher in blunt-grooved joints than sharp-grooved and control joints at week 35, could be indicative of locally upregulated collagen turnover. Measuring ratios of anabolic versus catabolic markers for specific cartilage matrix components has been advocated as providing more comprehensive information than single biomarkers.<sup>45</sup> Expansion of the current biomarker profile with CS-846, would allow evaluation of the proteoglycan balance instead of GAG concentrations only. In previous equine chondral defect models, no differences in SF biomarker concentrations between the traumatized and sham-operated joints were found,<sup>8,46</sup> while significant differences were present when the defect included the subchondral bone.<sup>47</sup> This indicates that the effect of cartilage damage only is apparently not enough to induce measurable changes in the SF.

Subchondral bone changes have been reported as a result of the cartilage groove model in other species. In sheep, a decrease was found in mean thickness of the trabeculae and cortical bone thickness of the metacarpal bone at 15 weeks, but differences between grooved and control joints mostly vanished after 37 weeks.<sup>6</sup> In a canine knee model, it was the opposing tibial subchondral plate thickness that was reduced compared with the control group at 20 weeks. Bone volume fraction and trabecular thickness were lower but not significantly.<sup>48</sup> In contrast, the tibial subchondral bone in a rat model showed a more sclerotic structure (increased trabecular thickness and bone volume fraction) in grooved joints at 12 weeks compared with controls.<sup>7</sup> In our study, no differences in mean thickness of the trabeculae or bone volume fraction between grooved and control joints were observed at week 39, which is in line with the earlier findings in sheep and dogs.<sup>6,48</sup> Although, blunt grooves almost inevitably extended to the calcified cartilage layer, whereas this was not always the case for sharp grooves, no differences between

blunt- and sharp-grooved joints were found either. It may be that changes have taken place at an earlier phase, following the theory of biphasic bone remodeling.<sup>48</sup> Future analysis of NIRS data obtained during the follow-up surgeries in the current study may elucidate this theory by providing information on bone parameters at the interim time points.<sup>49</sup> Furthermore, subtle changes to the calcified cartilage layer cannot be excluded based on the current methods.

From a clinical point of view, no direct effect of cartilage lesions could be measured in terms of gait quality. Previous groove model studies reported quantitatively measured gait changes only on a relatively short-term after surgery. In the study by Maninchedda et al., the asymmetry related to the grooved limb became already non-significant at 8 and at 10 weeks post-operatively.<sup>8</sup> In dogs, the mild gait changes (measured as ground reaction forces) gradually levelled off and became insignificant at 12 weeks after surgery.<sup>50</sup> We did not find clinically relevant changes in symmetry parameters on a short term. The increased ROM of the head on the longer term (week 38) in combination with gradually increasing absolute MinDiff values of the head (as from week 22) are indicative of a mildly progressive bilateral lameness.<sup>51</sup> It should be realized that changes in gait pattern are more difficult to detect when they are bilateral. Furthermore, only direct kinematic measurements were made. Additional analysis such as the estimation of joint contact forces through musculoskeletal modelling may provide valuable and more specific information.

Taken together, these small effects are well in line with the well-known lack of a relationship between the extent of cartilage lesions and clinical manifestation of OA. Also, it corroborates the huge time lag (of sometimes decades) that may be between initial cartilage damage and the classic clinical presentation of OA that is characterized by painful and less painful periods during years. In fact, these minimal effects are what should have been expected. Lesion progress is slow, but inevitable.

### **Confounding factors that could explain time-related changes in both grooved and control joints**

The observed time-related changes in SF biomarkers and in synovium gene expression levels in both grooved and control joints demand attention for potential confounding factors. Exercise (i.e. mechanical loading) can influence joint homeostasis through various mechanisms.<sup>52</sup> The purpose of the training regimen in the current study was to stimulate the progress of cartilage degeneration via a direct effect of mechanical loading on articular tissue integrity. However, as mentioned before, mechanical loading also influences joint tissue metabolism indirectly by activating signal transduction pathways.<sup>35</sup> Intensive loading has e.g. been shown to

enhance pro-inflammatory effects in synovium<sup>53</sup> and osteoblasts.<sup>54</sup> Also, physiological and excessive mechanical compression could upregulate expression of TGF $\beta$ 1 and activate the Smad2/3 signalling pathway while downregulating the Smad1/5/8 signalling pathway in articular cartilage explants.<sup>55</sup> Furthermore, exercise effects can also be reflected by changes in SF biomarkers.<sup>47,56,57</sup> This tallies well with the overall changes we observed in synovium gene expression and biomarker levels in SF.

Moreover, it is known that the SF composition is affected by (repeated) arthrocentesis.<sup>56,58</sup> In the same line, follow-up surgeries and serial synovial biopsies caused further repetitive trauma to the joint capsule and synovial membrane. An illustrative example is the increased MMP activity in both grooved and sham-operated control joints at week 19, followed by a decrease at week 39. A similar pattern at similar time points was observed in an ovine groove model, but only in the grooved joints.<sup>6</sup> Notably, in that study, controls were not sham-operated. Furthermore, sham-surgery was shown to influence synovium gene expression in a post-traumatic OA model in the rat.<sup>59</sup> Trauma of the joint capsule and the synovial membrane may also explain the slightly increasing trend in synovium scores, and the slow increase in TNCs in all groups that seemed to be mostly due to a growing number of lymphocytes. It might as well explain the radiographic presence of osteophytes and, to a lesser extent, enthesiophytes as well as the soft tissue swelling in control joints at the end of the study and the mild bilateral lameness.

In effused joints and joints with reduced joint capsule compliance due to traumatic synovitis/capsulitis, blood flow might be compromised by modest elevations in intra-articular pressure induced by exercise.<sup>60</sup> This affects SF turnover and composition. In our study, soft tissue swelling in both grooved and control joints was observed, and the repetitive joint procedures likely contributed to diminished quality of the joint capsule. Thus, it may well be that a combination of joint capsule trauma and exercise significantly contributed to the changes that were observed over time in grooved as well as in control joints.

The artificial neural network models based on NIRS data predicted a gradual decrease in cartilage thickness of 19% from baseline to week 39 in both grooved and control joints. This effect might arise (partly) from changes in the calcified cartilage or subchondral bone that contributed to NIRS measurements and as such affected these predictions. However, this preliminary finding does not directly relate to other findings in this study and require further finetuning in terms of data preprocessing, outlier detection, and network design to enhance network performance and hence the reliability of the time-wise predictions. In addition, time-wise predictions of biomechanical properties could provide details related to these findings.

## Implications for the clinical approach of cartilage defects

The inability of articular cartilage to regenerate and repair even the smallest lesions explains why we have thus far not been able to develop successful regenerative medicine strategies. This was also the main argument in a recent proposal by Malda et al. in which the point was made that the classic paradigm in regenerative medicine does not work for articular cartilage and that other avenues should be explored to realize break-throughs in this field.<sup>61</sup> Furthermore, our findings support earlier *in vitro* work that showed that sharp and blunt cartilage trauma induce differential responses in the adjacent tissue. This principle has been hypothesized to be of clinical relevance in terms of creating the optimal lesions edges for successful integration during articular cartilage repair.<sup>62</sup>

Although the potential contribution to early pathobiological events of OA on a longer term cannot be excluded, the direct effect of subtle cartilage damage, blunt or sharp, on the homeostatic balance of the joint is very mild. This may imply that the search for diagnostic molecular biomarkers is rather pointless or, given the minimal impact of such early damage on joint homeostasis, even irrelevant. Taken together, from a clinical viewpoint, it may be more effective and relevant to focus on factors that determine the clinical manifestation of OA (above all pain) than trying to diagnose subtle lesions and finding ways for durable cartilage repair. Damaged cartilage in itself may not be too important as long as it does not disturb the homeostatic balance of the joint and as long as its biomechanical function remains sufficient. On the other hand, it is still lesion size and morphology, together with the loading profile, that determine the progress and hence probably the moment when these lesions do become clinically important. Development of techniques that will reduce lesion progression and permit prolonged functioning with deteriorated cartilage may thus certainly have a great health impact, as those will postpone the moment that arthroplasty (in human medicine), arthrodesis or even euthanasia (in equine medicine) will become necessary as the last option. To enable this, new markers and techniques to detect, quantify and predict subtle changes in the joint are still warranted. The interplay between morphology of the lesion, degree of tissue disruption and mechanical loading, could be further studied by *ex vivo* mechanical testing and computational modelling.<sup>63</sup> Data obtained by *in vivo* studies like ours, is of high value for the validation of such models.

## Strengths, limitations and suggestions for future research

Extensive assessment of various joint tissues as well as monitoring of overall joint function in terms of gait quality provided an integral picture that is necessary to gain better insight in processes following upon cartilage damage. The comprehensive

results from this study on the natural progression of chondral grooves provide a benchmark for (long-term) repair studies that make use of similar chondral defect models. By using multiple advanced modalities, we monitored structural, compositional and functional changes within the same individuals over a relatively long term of 9 months. As such, we could decrease the number of experimental animals and the degree of biological variation between them as each individual could be compared with itself over time, serving as its own control. Although these factors are great strengths, there were limitations too. Sham-operated joints were not entirely free from cartilage lesions (probably partly due to repeated arthrocentesis resulting in needle trauma) and the high cell necrosis that was found at microscopy in all groups may be related to the number of freeze-thaw cycles and post-mortem analyses before osteochondral samples were fixed in formaldehyde. Furthermore, (repeated) surgery and serial synovial fluid and synovium sampling likely induced bilateral inflammatory responses. Together, these factors may have minimized the differences between grooved and control joints.

In the search for leads to improve timely recognition and to find new treatment targets for OA, longer term follow-up (at least 2-3 years) may be needed to bring about measurable effects of cartilage damage on joint homeostasis. However, such studies are practically very demanding, expensive and bear ethical considerations. Quicker progress of degeneration may be achieved with a more extensive groove model or with grooves applied to higher motion joints such as the fetlock that are subjected to more shear forces than the carpal joint. However, the question as to what extent quick and short-term models mimic the natural situation as encountered in the human or equine clinic, and therefore their translational value remains a point of discussion. Higher sensitivity techniques like proteomics and metabolomics could contribute to more extensive profiling of synovial tissues<sup>64-66</sup> and may be able to pick up changes that did not come to light with the current methods. Integration of various 'omics' methods into a multi 'omics' approach could yield even more information<sup>67</sup> and may help to further elucidate the earliest effects of cartilage damage on joint homeostasis.

## **CONCLUSION**

Sharp and blunt grooves, restricted to the non-calcified cartilage layer of the equine carpal joint, both cause degeneration. However, their effect on joint homeostasis is minimal. Microscopic observations and biomechanical data showed that the reaction of the unaffected tissue adjacent to the defect may vary dependent on



the characteristics of the lesion. While the effect of cartilage damage on overall joint health remained limited, this study supported the hypothesis that it is the combination of lesion size and configuration, together with the loading profile that will determine the speed and character of progress of further degeneration and hence the moment when these lesions become clinically important.

## **ACKNOWLEDGEMENTS**

This research was made possible by an NWO Graduate Programme Grant (022.005.018). dr. Isaac Afara, Aleksi Leinonen, dr. Ervin Nippolainen and dr. Rubina Shaikh are acknowledged for their contribution to sample processing for histology and Mithilesh Prakash for his contribution to the NIRS measurements. We would like to thank Emmie Giessen and Angelica Enström for their assistance in training, surgeries and synovial fluid collection and we thank Prof. Ton van Leeuwen for his advice and support in the set-up of OCT measurements.

## REFERENCES

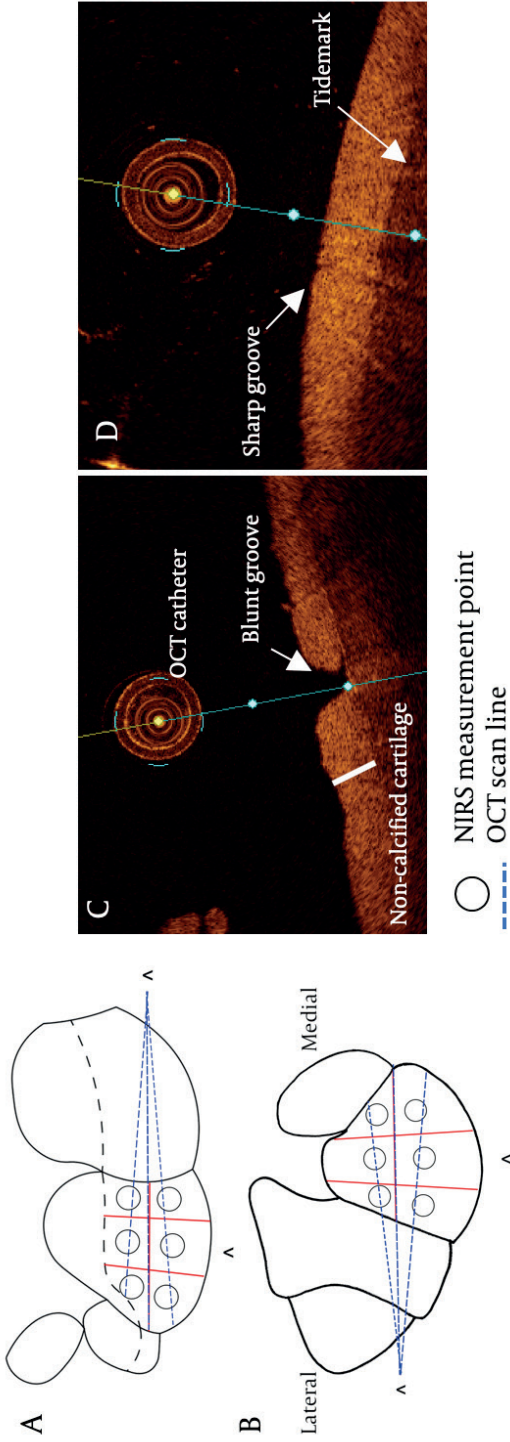
1. Loeser RF, Goldring SR, Scanzello CR, Goldring MB. Osteoarthritis: A disease of the joint as an organ. *Arthritis Rheum*. 2012;64(6):1697-1707.
2. Penell JC, Egenvall A, Bonnett BN, Olson P, Pringle J. Specific causes of morbidity among Swedish horses insured for veterinary care between 1997 and 2000. *Vet Rec*. 2005;157(16):470-477.
3. McIlwraith CW, Fortier L a., Frisbie DD, Nixon a. J. Equine Models of Articular Cartilage Repair. *Cartilage*. 2011;2(4):317-326.
4. Malda J, Benders KE, Klein TJ, et al. Comparative study of depth-dependent characteristics of equine and human osteochondral tissue from the medial and lateral femoral condyles. *Osteoarthritis Cartilage*. 2012;20:1147-1151.
5. Marijnissen ACA, van Roermund PM, Verzijl N, Tekoppele JM, Bijlsma JWJ, Lafeber FPJG. Steady progression of osteoarthritic features in the canine groove model. *Osteoarthr Cartil*. 2002;10(4):282-289.
6. Mastbergen SC, Pollmeier M, Fischer L, Vianen ME, Lafeber FPJG. The groove model of osteoarthritis applied to the ovine fetlock joint. *Osteoarthr Cartil*. 2008;16(8):919-928.
7. de Visser HM, Weinans H, Coeleveld K, van Rijen MHP, Lafeber FPJG, Mastbergen SC. Groove model of tibia-femoral osteoarthritis in the rat. *J Orthop Res*. May 2016.
8. Maninchedda U, Lepage OM, Gangl M, et al. Development of an Equine Groove Model to Induce Metacarpophalangeal Osteoarthritis: A Pilot Study on 6 Horses. *PLoS One*. 2015;10(2):e0115089.
9. te Moller NCR, Brommer H, Plomp S, van Weeren PR. Development of an equine carpal groove model to study early changes in osteoarthritis - a pilot study. *Osteoarthr Cartil*. 2018;26(Supplement 1):S132-S133.
10. Orozco GA, Tanska P, Florea C, Grodzinsky AJ, Korhonen RK. A novel mechanobiological model can predict how physiologically relevant dynamic loading causes proteoglycan loss in mechanically injured articular cartilage. *Sci Rep*. 2018;8(1):15599.
11. Sarin JK, Nykänen O, Tiitu V, et al. Arthroscopic Determination of Cartilage Proteoglycan Content and Collagen Network Structure with Near-Infrared Spectroscopy. *Ann Biomed Eng*. 2019;47(8):1815-1826.
12. McIlwraith CW, Frisbie DD, Kawcak CE, Fuller CJ, Hurtig M, Cruz A. The OARSI histopathology initiative – recommendations for histological assessments of osteoarthritis in the horse. *OAC Histopathol Suppl*. 2010;18, Supple(0):S93-S105.
13. Vandesompele J, De Preter K, Pattyn F, et al. Accurate normalization of real-time quantitative RT-PCR data by geometric averaging of multiple internal control genes. *Genome Biol*. 2002;3(7):RESEARCH0034.
14. Hellemans J, Mortier G, De Paepe A, Speleman F, Vandesompele J. qBase relative quantification framework and software for management and automated analysis of real-time quantitative PCR data. 2007;8(2).
15. Clements D. Arthrocentesis and Synovial Fluid Analysis. In *Pract*. 2006;28:256-262.
16. Neumann U, Kubota H, Frei K, Ganu V, Leppert D. Characterization of Mca-Lys-Pro-Leu-Gly-Leu-Dpa-Ala-Arg-NH<sub>2</sub>, a fluorogenic substrate with increased specificity constants for collagenases and tumor necrosis factor converting enzyme. *Anal Biochem*. 2004;328(2):166-173.
17. Farndale RW, Buttle DJ, Barrett AJ. Improved quantitation and discrimination of sulphated glycosaminoglycans by use of dimethylmethylene blue. *Biochim Biophys Acta*. 1986;883(2):173-177.
18. Rhodin M, Roepstorff L, French A, Keegan KG, Pfau T, Egenvall A. Head and pelvic movement asymmetry during lungeing in horses with symmetrical movement on the straight. *Equine Vet J*. 2016;48(3):315-320.
19. Ebrahimi M, Ojanen S, Mohammadi A, et al. Elastic, Viscoelastic and Fibril-Reinforced Poroelastic Material Properties of Healthy and Osteoarthritic Human Tibial Cartilage. *Ann Biomed Eng*. 2019.

20. Mäkelä JTA, Han SK, Herzog W, Korhonen RK. Very early osteoarthritis changes sensitively fluid flow properties of articular cartilage. *J Biomech.* 2015;48(12):3369-3376.
21. Mäkelä JTA, Rezaeian ZS, Mikkonen S, et al. Site-dependent changes in structure and function of lapine articular cartilage 4 weeks after anterior cruciate ligament transection. *Osteoarthr Cartil.* 2014;22(6):869-878.
22. Hayes WC, Keer LM, Herrmann G, Mockros LF. A mathematical analysis for indentation tests of articular cartilage. *J Biomech.* 1972;5(5):541-551.
23. Kiviranta P, Rieppo J, Korhonen RK, Julkunen P, Töyräs J, Jurvelin JS. Collagen network primarily controls Poisson's ratio of bovine articular cartilage in compression. *J Orthop Res.* 2006;24(4):690-699.
24. French DA, Barber SM, Leach DH, Doige CE. The effect of exercise on the healing of articular cartilage defects in the equine carpus. *Vet Surg.* 1989;18(4):312-321.
25. Salenius E, Rieppo L, Nissi MJ, et al. Critical-sized cartilage defects in the equine carpus. *Connect Tissue Res.* 2019;60(2):95-106.
26. Meachim G. the Effect of Scarification on Articular Cartilage in the Rabbit. *J Bone Joint Surg Br.* 1963;45-B(1):150-161.
27. Forney HJ, Bentley G, Mathews RS. Salicylates and repair in adult articular cartilage: A preliminary report. *Orthop.Oxf.* 1973;6(1):19-31.
28. Simmons DP, Chrisman DO. Salicylate inhibition of cartilage degeneration. *Arthritis Rheum.* 1965;8(5):960-969.
29. Redman SN, Douthwaite GP, Thomson BM, Archer CW. The cellular responses of articular cartilage to sharp and blunt trauma. *Osteoarthr Cartil.* 2004;12(2):106-116.
30. Tew SR, Kwan AP, Hann A, Thomson BM, Archer CW. The reactions of articular cartilage to experimental wounding: role of apoptosis. *Arthritis Rheum.* 2000;43(1):215-225.
31. Gratz KR, Wong BL, Bae WC, Sah RL. The effects of focal articular defects on intra-tissue strains in the surrounding and opposing cartilage. *Biorheology.* 2008;45(3-4):193-207.
32. Komeili A, Chau W, Herzog W. Effects of macro-cracks on the load bearing capacity of articular cartilage. *Biomech Model Mechanobiol.* April 2019.
33. Guettler JH, Demetropoulos CK, Yang KH, Jurist KA. Osteochondral defects in the human knee: influence of defect size on cartilage rim stress and load redistribution to surrounding cartilage. *Am J Sports Med.* 2004;32(6):1451-1458.
34. Peña E, Calvo B, Martínez MA, Doblaré M. Effect of the size and location of osteochondral defects in degenerative arthritis. A finite element simulation. *Comput Biol Med.* 2007;37(3):376-387.
35. Millward-Sadler SJ, Salter DM. Integrin-dependent signal cascades in chondrocyte mechanotransduction. *Ann Biomed Eng.* 2004;32(3):435-446.
36. Heinegård D, Saxne T. The role of the cartilage matrix in osteoarthritis. *Nat Rev Rheumatol.* 2011;7(1):50-56.
37. Goldring MB, Goldring SR. Osteoarthritis. *J Cell Physiol.* 2007;213(3):626-634.
38. da Gracca Macoris D, Bertone A. Intra-articular pressure profiles of the cadaveric equine fetlock joint in motion. *Equine Vet J.* 2001;33(2):184-190.
39. Ley C, Ekman S, Elmén A, Nilsson G, Eloranta M-L. Interleukin-6 and Tumour Necrosis Factor in Synovial Fluid from Horses with Carpal Joint Pathology. *J Vet Med Ser A.* 2007;54(7):346-351.
40. Ley C, Ekman S, Ronéus B, Eloranta M-L. Interleukin-6 and high mobility group protein-1 in synovial membranes and osteochondral fragments in equine osteoarthritis. *Res Vet Sci.* 2009;86(3):490-497.

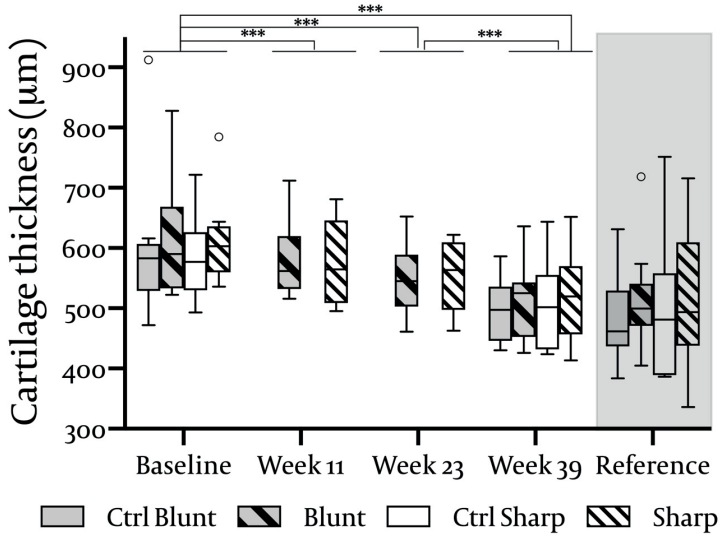
41. Wei Y, Bai L. Recent advances in the understanding of molecular mechanisms of cartilage degeneration, synovitis and subchondral bone changes in osteoarthritis. *Connect Tissue Res.* 2016;57(4):245-261.
42. Miotla Zarebska J, Chanalaris A, Driscoll C, et al. CCL2 and CCR2 regulate pain-related behaviour and early gene expression in post-traumatic murine osteoarthritis but contribute little to chondropathy. *Osteoarthr Cartil.* 2017;25(3):406-412.
43. Finsson KW, Parker WL, ten Dijke P, Thorikay M, Philip A. ALK1 opposes ALK5/Smad3 signaling and expression of extracellular matrix components in human chondrocytes. *J Bone Miner Res.* 2008;23(6):896-906.
44. van der Kraan PM, Blaney Davidson EN, Blom A, van den Berg WB. TGF-beta signaling in chondrocyte terminal differentiation and osteoarthritis: modulation and integration of signaling pathways through receptor-Smads. *Osteoarthr Cartil.* 2009;17(12):1539-1545.
45. de Grauw JC, Donabédian M, van de Lest CHA, et al. Assessment of synovial fluid biomarkers in healthy foals and in foals with tarsocrural osteochondrosis. *Vet J.* 2011;190(3):390-395.
46. Niemelä TM, Tulamo R-M, Carmona JU, López C. Evaluation of the effect of experimentally induced cartilage defect and intra-articular hyaluronan on synovial fluid biomarkers in intercarpal joints of horses. *Acta Vet Scand.* 2019;61(1):24.
47. Frisbie DD, Al-Sobayil F, Billinghamurst RC, Kawcak CE, McIlwraith CW. Changes in synovial fluid and serum biomarkers with exercise and early osteoarthritis in horses. *Osteoarthr Cartil.* 2008;16(10):1196-1204.
48. Intema F, Sniekers YH, Weinans H, et al. Similarities and discrepancies in subchondral bone structure in two differently induced canine models of osteoarthritis. *J Bone Miner Res.* 2010;25(7):1650-1657.
49. Sarin JK, te Moller NCR, Mancini IAD, et al. Arthroscopic near infrared spectroscopy enables simultaneous quantitative evaluation of articular cartilage and subchondral bone in vivo. *Sci Rep.* 2018;8(1):13409.
50. Frost-Christensen LN, Mastbergen SC, Vianen ME, et al. Degeneration, inflammation, regeneration, and pain/disability in dogs following destabilization or articular cartilage grooving of the stifle joint. *Osteoarthr Cartil.* 2008;16(11):1327-1335.
51. Keegan KG, Wilson DA, Smith BK, Wilson DJ. Changes in kinematic variables observed during pressure-induced forelimb lameness in adult horses trotting on a treadmill. *Am J Vet Res.* 2000;61(6):612-619.
52. te Moller NCR, van Weeren PR. How exercise influences equine joint homeostasis. *Vet J.* 2017.
53. Schröder A, Nazet U, Muschter D, Grässel S, Proff P, Kirschneck C. Impact of Mechanical Load on the Expression Profile of Synovial Fibroblasts from Patients with and without Osteoarthritis. *Int J Mol Sci.* 2019;20(3):585.
54. Sanchez C, Gabay O, Salvat C, Henrotin YE, Berenbaum F. Mechanical loading highly increases IL-6 production and decreases OPG expression by osteoblasts. *Osteoarthr Cartil.* 2009;17(4):473-481.
55. Madej W, van Caam A, Blaney Davidson EN, van der Kraan PM, Buma P. Physiological and excessive mechanical compression of articular cartilage activates Smad2/3P signaling. 2014;22(7):1018-1025.
56. van den Boom R, Brama PAJ, Kiers GH, De Groot J, Barneveld A, Weeren PR. The influence of repeated arthrocentesis and exercise on matrix metalloproteinase and tumour necrosis factor activities in normal equine joints. *Equine Vet J.* 2004;36(2):155-159.
57. Skiöldebrand E, Heinegård D, Olofsson B, Rucklidge G, Ronéus N, Ekman S. Altered homeostasis of extracellular matrix proteins in joints of standardbred trotters during a long-term training programme. *J Vet Med.* 2006;53(9):445-449.

58. Lamprecht ED, Williams CA. Biomarkers of antioxidant status, inflammation, and cartilage metabolism are affected by acute intense exercise but not superoxide dismutase supplementation in horses. *Oxid Med Cell Longev*. 2012;2012:Article ID 920932.
59. Salazar-Noratto GE, De Nijs N, Stevens HY, Gibson G, Guldberg RE. Regional gene expression analysis of multiple tissues in an experimental animal model of post-traumatic osteoarthritis. *Osteoarthr Cartil*. 2019;27(2):294-303.
60. James MJ, Cleland LG, Rofe AM, Leslie AL. Intraarticular pressure and the relationship between synovial perfusion and metabolic demand. *J Rheumatol*. 1990;17(4):521-527.
61. Malda J, Groll J, van Weeren PR. Rethinking articular cartilage regeneration based on a 250-year-old statement. *Nat Rev Rheumatol*. 2019;[Epub ahead of print].
62. Archer CW, Redman S, Khan I, Bishop J, Richardson K. Enhancing tissue integration in cartilage repair procedures. *J Anat*. 2006;209(4):481-493.
63. Peloquin JM, Elliott DM. A comparison of stress in cracked fibrous tissue specimens with varied crack location, loading, and orientation using finite element analysis. *J Mech Behav Biomed Mater*. 2016;57:260-268.
64. Anderson JR, Phelan MM, Clegg PD, Peffers MJ, Rubio-Martinez LM. Synovial Fluid Metabolites Differentiate between Septic and Nonseptic Joint Pathologies. *J Proteome Res*. 2018;17(8):2735-2743.
65. Peffers MJ, McDermott B, Clegg PD, Riggs CM. Comprehensive protein profiling of synovial fluid in osteoarthritis following protein equalization. 2015;23(7):1204-1213.
66. Adams SB, Setton LA, Kensicki E, Bolognesi MP, Toth AP, Nettles DL. Global metabolic profiling of human osteoarthritic synovium. *Osteoarthr Cartil*. 2012;20(1):64-67.
67. Peffers MJ, Smagul A, Anderson JR. Proteomic analysis of synovial fluid: current and potential uses to improve clinical outcomes. *Expert Rev Proteomics*. 2019;16(4):287-302.
68. de Grauw JC, Brama PA, Wiemer P, Brommer H, van de Lest CH, van Weeren PR. Cartilage-derived biomarkers and lipid mediators of inflammation in horses with osteochondritis dissecans of the distal intermediate ridge of the tibia. *Am J Vet Res*. 2006;67(7):1156-1162.

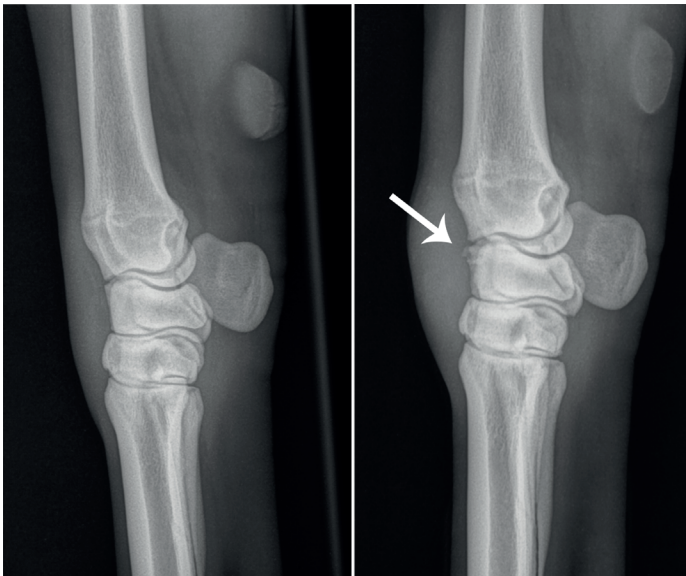
**SUPPLEMENTARY INFORMATION**



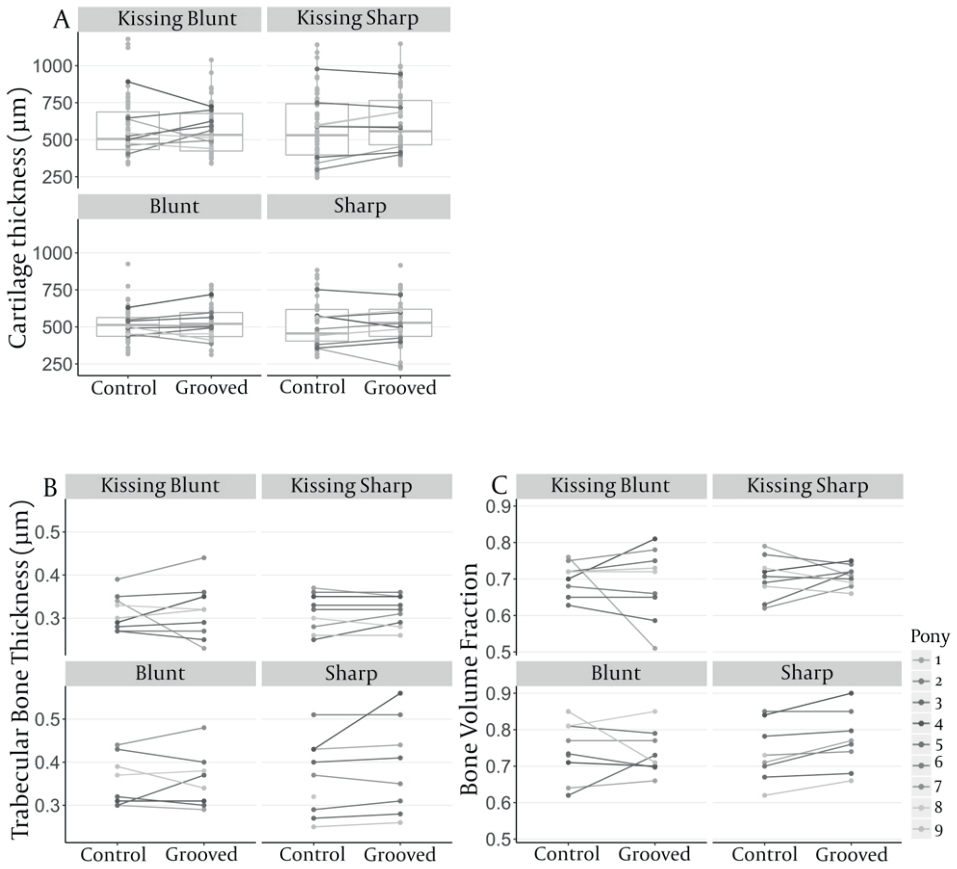
**Supplementary Fig. 1** NIRS measurement points and OCT scan lines at the dorsoproximal surface of the intermediate carpal bone (A) and the radial facet of the third carpal bone (B). ‘^’ symbols indicate place of instrument portals during surgery. Optical Coherence Tomography image of a blunt groove obtained at week 11 (C) and a sharp groove obtained at baseline (D).



**Supplementary Fig. 2** Predicted cartilage thickness values based on in vivo intra-articular NIRS measurements. The boxes in the right panel show the reference thickness measured post-mortem by contrast enhanced micro-CT imaging of osteochondral samples. \*\*\*  $P < 0.001$ .



**Supplementary Fig. 3** Latero-medial radiographic views of the carpal joint of an individual at baseline (left) and 9 months (right). Soft tissue swelling and grade 2 osteophytes (white arrow) are visible at 9 months.



**Supplementary fig. 4** Post-mortem cartilage and bone parameters. A) Spaghetti plots show the average cartilage thickness of 6 measurement points, grey boxplots represent medians with interquartile ranges of all measured locations. Trabecular bone thickness (B) and bone volume fraction (C) were measured in the central area of the sample,  $1/3$  from the sides.



**Supplementary table 1** primer sequences and additional information

Gene symbol	Primer sequence (5' - 3')	Amplification length (bp)	Annealing T (°C)	Gene bank accession number
<b>Reference genes</b>				
RPL13	Fw GCGGAAGAAGCTCAAATTGG Rv GCCTGAAGTCTCTCCT	112	63	XM_005608504.3
RPS19	Fw CACGATGCCTGGAGTACTG Rv GGAGCAAGCTCTTTATGTTTGG	144	63	XM_001501566.5
GAPDH	Fw ATCTGACCTGCCGCTGGAG Rv CGATGCCTGCTTACCACCTTC	68	66	NM_001163856
YWHAZ	Fw CAAGCGGAGAGCAAAGTC Rv AGACCCAATCTGATAGGATGT	179	61	XM_001492988.6
SDHA	Fw GAGGAATGGTCTGGAATAC Rv GCCTCTGCTCCATAAATCG	91	59	XM_023625909.1
<b>Target genes</b>				
MMP3	Fw AAATAGCAGAAGACTTCCAGG Rv TCAAAGTGAAGATCCACTG	96	65	NM_001082495
ILR-1	Fw TGGTACAGGGATTCTTGC Rv GAGTTAGAGGTGGACCCT	112	58	XM_014730874
IL-6	Fw GACGGATGCTCCAATCTG Rv GTACTCCAGGTATATCTGAAACTC	89	62	NM_001082496
TGFβ1	Fw CTAAGGCTCAAGTTAAGCGTG Rv GTTACTGAGGTAGCGCCA	80	67	XM_005596086
ALK1	Fw CCTTTGGTCTGGTCTGTG Rv CGAAGCTGGGATCATTGGG	107	63	XM_005636802.1
ALK5	Fw TGATATTGCTCCAAACCACAG Rv CTATTTCCAGAACACTAAGCC	139	59	XM_023629744.1
Pai1	Fw GCCCTACCAACATTCTG Rv GGTCCACTTCACTCTCCA	111	65	XM_001492517.5
CCL2	Fw AGCCAGATGCAATTATTCTCC Rv GACGGTCTTGAAGATCACAG	133	59	NM_001003297.1

**Supplementary table 2** specifications of data transformation and statistical models.

Ordinal data – Friedman + Tukey HSD					
Parameter	Transformation	Block indicator	Group indicator		
Radiography	None	Pony	Treatment <sub>1</sub> Week		
Macroscopy cartilage	None	Pony	Treatment <sub>2</sub> . Surface		
Continuous data – linear mixed model					
Parameter	Transformation	Random effect	Fixed effects	Interactions	varIdent
Predicted cartilage thickness NIRS	Log	Pony	Treatment <sub>2</sub> Week	No	No
SM microscopy	None	Pony	Treatment <sub>2</sub> Week	No	No
SM qPCR target genes	Log	Pony	Treatment <sub>2</sub> Week	IL6, MMP <sub>3</sub> , TGFb <sub>1</sub> , ALK <sub>1</sub> , ALK <sub>5</sub> , CCL <sub>2</sub>	MMP <sub>3</sub> , ILR-1, TGFb <sub>1</sub>
SF biomarkers	Log: TNC, TP, C <sub>2</sub> C, CCL <sub>2</sub> , MMP Sqrt: C <sub>PII</sub> , C <sub>PII</sub> /C <sub>2</sub> C	Pony	Treatment <sub>2</sub> Week	C <sub>2</sub> C, C <sub>PII</sub> , C <sub>PII</sub> /C <sub>2</sub> C	C <sub>2</sub> C, C <sub>PII</sub> , C <sub>PII</sub> /C <sub>2</sub> C, CCL <sub>2</sub>
OMC MaxDiff, MinDiff (absolute values)	None	Pony	Week	No	Yes
OMC ROM	Log	Pony	Week Stride speed	Yes	Yes
Cartilage microscopy	None	Pony	Treatment <sub>1</sub> Groove type Surface Location	Yes	No
Cartilage thickness micro-CT	Log	Pony	Treatment <sub>1</sub> Groove type Surface Location	No	No
TBT, BV/TV micro-CT	Sqrt: TBT	Pony	Treatment <sub>1</sub> Groove type Surface	No	TBT
EqMod, InstMod	Sqrt	Pony	Treatment <sub>1</sub> Groove type Surface Location	Treatment <sub>1</sub> Groove type Surface	No

Week was used as a categorical value. Treatment<sub>1</sub> = control / grooved. Treatment<sub>2</sub> = control blunt / blunt-grooved / control sharp / sharp-grooved. Surface = grooved / kissing. Groove type = blunt / sharp. Location = dorsal / palmar of horizontal groove line.

**Supplementary table 3** Microscopic scores synovial membrane

Time point	Treatment	Cellular infiltration	Vascularity	Intimal hyperplasia	Subintimal edema	Subintimal fibrosis	Total
		0-4	0-4	0-4	0-4	0-4	0-20
Baseline	Control blunt	0.2 (±0.4)	0.8 (±0.4)	1.1 (±0.9)	1.0 (±1.0)	0.6 (±0.6)	3.7 (±1.3)
	Blunt	0.3 (±0.3)	1.5 (±0.9)	1.1 (±0.6)	1.2 (±0.7)	0.8 (±0.8)	4.8 (±2.4)
	Control sharp	0.0 (±0.0)	0.6 (±0.4)	1.1 (±0.4)	1.4 (±1.3)	0.9 (±0.9)	4.0 (±2.4)
	Sharp	0.6 (±0.6)	1.3 (±0.8)	1.6 (±0.8)	1.3 (±0.7)	0.8 (±0.5)	5.7 (±2.3)
Week 11	Control blunt	0.7 (±0.9)	1.4 (±0.8)	1.2 (±0.7)	1.0 (±1.0)	0.8 (±0.7)	5.2 (±2.8)
	Blunt	1.1 (±0.8)	1.7 (±0.8)	1.4 (±0.7)	1.2 (±0.9)	1.3 (±0.8)	6.7 (±2.2)
	Control sharp	0.9 (±0.8)	1.3 (±0.8)	1.5 (±0.8)	0.6 (±0.7)	0.7 (±0.7)	5.1 (±2.1)
	Sharp	0.7 (±0.8)	2.1 (±1.2)	0.9 (±0.5)	0.8 (±1.1)	0.7 (±0.7)	5.2 (±3.2)
Week 23	Control blunt	1.1 (±0.7)	1.6 (±0.7)	1.2 (±0.4)	0.6 (±0.9)	0.8 (±1.0)	5.2 (±2.7)
	Blunt	0.6 (±0.9)	1.7 (±1.3)	1.2 (±0.5)	0.8 (±0.6)	1.2 (±0.7)	5.4 (±2.5)
	Control sharp	0.8 (±0.8)	1.5 (±0.9)	1.3 (±0.8)	0.9 (±1.0)	0.8 (±0.8)	5.4 (±3.0)
	Sharp	0.9 (±0.7)	1.7 (±1.5)	1.3 (±0.8)	1.1 (±1.3)	1.2 (±1.1)	6.3 (±3.8)
Week 39	Control blunt	0.5 (±0.4)	1.3 (±1.0)	0.8 (±0.8)	1.2 (±0.7)	0.9 (±0.8)	4.8 (±2.2)
	Blunt	0.7 (±0.6)	1.3 (±0.9)	0.8 (±0.5)	1.3 (±1.0)	0.6 (±0.7)	4.7 (±2.2)
	Control sharp	0.6 (±0.4)	1.9 (±0.9)	1.4 (±0.4)	0.9 (±0.8)	0.6 (±0.4)	5.4 (±2.0)
	Sharp	0.3 (±0.4)	1.5 (±0.6)	1.2 (±0.5)	0.8 (±0.6)	0.6 (±0.5)	4.3 (±1.0)

Table shows observed means (±SD).

**Supplementary table 4** measures of qPCR quality

Gene marker	Mean (range) Ct value	Negative control Ct value	qPCR Efficiency value (%)	GeNorm M <sup>3</sup>
<b>Reference genes</b>				
RPL13	21.3 (18.4-30.1)	NA	107	0.41
RPS19	20.0 (16.9-27.9)	NA	107	0.41
SDHA	26.4 (22.9-33.4)	NA	109	0.58
GAPDH	22.4 (19.2-30.7)	NA	112	0.64
YWHAZ	27.0 (22.5-34.9)	NA	97.9	0.73
<b>Target genes</b>				
MMP3	26.0 (20.3-34.6)	NA	125	
CCL2	30.0 (24.6-37.1)	NA	95.1	
ILR-1	29.0 (24.4-39.2)	NA	101	
IL-6	31.1 (24.1-36.9)	NA	106	
TGFβ1	26.8 (22.1-34.8)	NA	133	
ALK1	29.0 (26.0-35.1)	NA	109	
ALK5	28.1 (24.1-35.0)	NA	103	
Pair	28.1 (22.7-33.9)	NA	100	

**Supplementary table 5** Quantitative gait analysis parameters

Time point	Baseline	Week 8	Week 10	Week 22	Week 38
MinDiff head	8.43 (6.23-10.6)	10.4 (7.99-12.9)*	10.7 (8.40-13.1)*	14.8 (12.2-17.3)*	13.4 (11.1-15.6)*
MinDiff withers	3.24 (2.35-4.14)	4.09 (3.12-5.05)*	3.22 (2.34-4.10)	4.46 (3.54-5.38)*	4.38 (3.52-5.24)*
MinDiff pelvis	3.62 (2.95-4.30)	3.75 (3.08-4.42)	3.28 (2.61-3.95)	3.96 (3.32-4.59)	3.97 (3.39-4.56)
MaxDiff head	10.2 (7.38-13.1)	10.5 (7.54-13.4)	10.1 (7.25-13.0)	12.0 (9.03-14.9)	11.1 (8.32-13.8)
MaxDiff withers	3.86 (3.12-4.61)	4.05 (3.29-4.81)	3.43 (2.72-4.13)	3.73 (2.95-4.52)	3.14 (2.46-3.82)*
MaxDiff pelvis	4.28 (3.39-5.16)	4.99 (4.03-5.96)	4.67 (3.80-5.53)	3.45 (2.67-4.23)*	3.11 (2.36-3.86)*
ROM head	44.0 (37.8-51.2)	37.6 (32.5-43.6)*	42.0 (36.6-48.3)	43.9 (38.5-50.2)	48.0 (42.1-54.5)*
ROM withers	39.7 (35.8-44.1)	39.8 (36.0-44.0)	40.9 (37.2-45.1)	36.7 (33.3-40.5)*	32.0 (29.0-35.2)*
ROM pelvis	46.5 (42.0-51.5)	45.8 (41.4-50.5)	48.8 (44.3-53.7)*	43.0 (39.0-47.4)*	40.1 (36.4-44.1)*

MinDiff = absolute difference between the two minima of vertical displacement, MaxDiff = absolute difference between the two maxima of vertical displacement, ROM = range of motion. Table shows estimated means ( $\pm 95\%$  CI). \*\* Indicates significant difference compared with baseline.

**Supplementary table 6** Results of OARSI microscopic scoring of articular cartilage

	Chondrocyte necrosis	Cluster formation	Fibrillation / fissuring	Focal cell loss	SOFG stain uptake	Total
Kissing site	Control blunt	3.1 (0.9)	1.4 (0.6)	2.0 (0.7)	1.7 (0.5)	10.1 (2.4)
	Blunt	3.2 (0.8)	2.0 (0.6)	1.6 (0.8)	1.8 (0.6)	10.5 (2.3)
	Control Sharp	3.1 (0.6)	1.3 (0.9)	1.5 (0.8)	1.3 (0.4)	8.8 (1.9)
	Sharp	2.9 (0.9)	1.3 (0.7)	1.5 (0.9)	1.8 (0.4)	9.3 (1.9)
Grooved site	Control blunt	3.5 (0.5)	1.6 (0.5)	1.8 (0.9)	1.8 (0.7)	10.2 (2.5)
	Blunt	3.9 (0.1)	3.8 (0.3)	3.9 (0.2)	2.8 (0.5)	16.9 (0.8)*#
	Control Sharp	3.6 (0.4)	1.8 (0.4)	2.5 (0.8)	1.7 (0.7)	11.2 (1.6)
	Sharp	3.9 (0.1)	3.1 (0.6)	3.4 (0.5)	2.4 (0.7)	14.9 (1.3)*

For SOFG staining, each parameter was evaluated on a 0-4 scale and observed means ( $\pm$ SD) are shown. \*\* Indicates significant difference compared to contra-lateral control. # Indicates significant difference compared to the other groove type.

### Supplementary item 1 Enzyme linked immunosorbent assays

Synovial fluid concentrations of carboxypropeptide of type II collagen (CPII) as a marker of type II collagen synthesis and type II collagen cleavage (C2C) marker were measured by a commercial enzyme linked immunosorbent assay (ELISA) kit (Ibex, Montreal, Québec, Canada). The CPII assay was performed on SF that was diluted 10-fold and subsequently digested with 0.1mg/ml hyaluronidase (H2126, Sigma-Aldrich, Saint Louis, USA) in a 7:1 ratio for 5 min at 37°C. For C2C analysis, undigested SF was diluted 2-fold. Both of these assays were previously validated in the investigators' lab for use in the horse.<sup>68</sup> Concentrations of the inflammation and pain-related marker CC-chemokine ligand 2 (CCL2) were measured using an ELISA developed for use in the horse (KingFisherBiotech, Saint Paul, USA). For this analysis, undigested and 2-fold diluted SF was used.

### Supplementary item 2 Collagen type I and II immunohistochemistry

For collagen type II immunohistochemistry (IHC), the sections were deparaffinized with xylene (two times 5 min) and graded ethanol (2 times 100%, 96% and 70%). Thereafter, they were blocked for 10 min with 0.3 % H<sub>2</sub>O<sub>2</sub> (Dako, Glostrup, Denmark) and washed two times for 5 min with PBS + 0.1 % Tween (PBSTo.1 %). Antigen retrieval was performed with 1 mg/ mL pronase (11459643001, Roche Diagnostics, Almere, the Netherlands) and 10 mg/mL hyaluronidase (H3506, Sigma-Aldrich, Saint Louis, USA) in PBS for 30 25min at 37 °C. After washing with PBSTo.1 %, the sections were blocked with 5 % BSA in PBS for 30 min at 37 °C. Thereafter, they were incubated for 1hour at room temperature with collagen type II mouse monoclonal antibody (II-II6B3, DSHB, Iowa City, IA) 1:1500 diluted in 5 % BSA in PBS. In control staining, the first antibody was substituted with isotype mouse IgG<sub>1</sub> (X0931, Dako). Then the sections were washed with PBSTo.1 % before the secondary antibody (Brightvision poly HRP-Anti-Mouse, KDPVM110, Immunologic, Amsterdam, the Netherlands) was applied for 30 min at room temperature. After washing with PBS, the sections were incubated with the liquid DAB substrate chromogen system (K3468, Dako) for 10 min and counterstained with Mayers hematoxylin (Merck) for 10 sec. Thereafter, they were washed with tap water for 10 min and dehydrated with graded ethanol (2 times 70 %, 96 % and 100 %) and xylene (two times 5 min) and mounted. For collagen type I IHC, the same procedures were followed using collagen I rabbit monoclonal antibody (ab138492, Abcam, Cambridge, UK) 1:400. Normal rabbit IgG (X0903, Dako) 1:10000 was used in control staining and anti-Rabbit (Brightvision poly HRP-Anti-Rabbit, KDPVR110, Immunologic, Amsterdam, the Netherlands) was used as secondary antibody.



# CHAPTER 8

## How exercise influences equine joint homeostasis

*The Veterinary Journal* 222, 60-67 (2017)

*Invited review*

---

N.C.R. te Moller

P.R. van Weeren

## **ABSTRACT**

The maintenance of joint homeostasis is integral to joint health. Knowledge of the influence of exercise on joint homeostasis is not only relevant for determining sustainable levels of equine athletic training, but also for the study of early development of osteoarthritis or cartilage repair in animal models. This review provides an overview of findings derived from in vivo studies and postmortem analyses investigating exercise effects on various joint tissue components in the horse, supplemented where appropriate with data from small animal models. The concept of joint homeostasis and possible methods to quantify this are also discussed, with special attention to the potential benefits and pitfalls of biomarker analysis in synovial fluid. The main conclusion is that biomechanical loading in the form of deliberate exercise has a major influence on the delicate homeostatic balance within the tissues constituting the diarthrodial joint and on their interactions, which is crucial for proper and durable joint function. The amount and intensity of exercise can have a lasting effect on tissue characteristics in juvenile animals, but affects joint homeostasis in mature animals and can affect the delicate balance between physiologic adaptation and development of pathology. Biomarkers in synovial fluid can be helpful in assessing joint homeostasis, but their use and interpretation require caution and are often far from straightforward.



## INTRODUCTION

Although the ability of living beings to maintain stability of their internal milieu were proposed by Claude Bernard in the 19<sup>th</sup> century,<sup>1</sup> Walter B. Cannon was the first who named this concept 'homeostasis'.<sup>2</sup> Internal disturbances caused by changes in the environment, affecting the system indirectly or directly, are kept within narrow limits by automatic adjustments to preserve normal tissue function and development. The concept applies to the body in general, but also to its constituent elements.<sup>3</sup> In a functional, healthy joint, a dynamic equilibrium between cellular processes within and between articular tissues is maintained. Disturbances in joint homeostasis that cannot be kept within physiological limits cause an imbalance between catabolic and anabolic processes and can lead to the onset and progression of joint disorders such as osteoarthritis (OA).<sup>4-6</sup>

The horse has always been kept primarily for its athletic performances, both in historical roles in warfare, transport and agriculture, and nowadays in its role as a sport and leisure animal. This emphasis on physical exercise means that high demands are placed upon the equine musculoskeletal system. In particular, the appendicular joints are subject to substantial compressive and shear forces and consequently, joint damage leading to impaired mobility and lameness is an important concern in the horse industry.<sup>7,8</sup> It is clear from the published literature that exercise, both in terms of intensity and duration, plays an important role in joint development and function.<sup>9-11</sup>

At the two extremes, both joint immobilisation and the sudden application of substantial mechanical force can lead to degenerative changes of the articular cartilage.<sup>12,13</sup> Although physical exercise is the most recommended non-pharmacological intervention for human OA patients,<sup>14</sup> its efficacy depends on various factors and it might not always be beneficial.<sup>15,16</sup> In the horse, regular canter exercise has been reported to be generally beneficial for joint health, whereas prolonged high-speed training could be a risk factor for metacarpo- and metatarsophalangeal joint injury.<sup>17</sup> This indicates that exercise influences joint homeostasis and can up- or downregulate anabolic or catabolic processes. There appears to be a window in which exercise has beneficial effects on the joint, while outside this window, joint homeostasis is disturbed to such a degree that compensatory mechanisms cannot cope.<sup>18</sup>

Appreciation of the effects of exercise in physiological situations is not only relevant for establishing sustainable levels of athletic training in the (young) performance horse. It is also necessary to understand the influence of exercise on the onset and progression of joint pathology, as well as its influence on the capabilities of articular tissues to heal or regenerate.<sup>19,20</sup> In addition, injured tissues and healthy tissues might respond differently to mechanical loading.<sup>21</sup> These are important considerations when studying early OA development or effects of (tissue-engineered) cartilage repair strategies in experimental animal models. This review concentrates on findings derived from *in vivo* studies and postmortem analyses investigating the influence of exercise on various joint components of the healthy equine joint, supplemented where appropriate with data from small animal models. Special attention is given to synovial fluid (SF) biomarker levels as surrogate outcome measures.

### **Defining and assessing 'joint homeostasis'**

The diarthrodial joint is a complex organ consisting of several key components, including the subchondral bone, the articular cartilage, the synovial membrane lining the inner layer of the fibrous joint capsule and, in some joints, intra-articular structures such as ligaments and menisci. These elements closely interact directly and/or indirectly via the SF that fills up the joint cavity.<sup>22</sup> The SF is an ultrafiltrate of plasma to which various components are added by articular tissues. Apart from its function as an important communication medium between the various tissues, the SF serves as a joint lubricant and it helps redistributing forces during loading and unloading. Furthermore, it fulfils an important role in the nourishment of the articular cartilage layer which is avascular in nature and thus depends mainly on SF for its nutrition and removal of waste products.<sup>23</sup>

Joint homeostasis can be defined as the dynamic balance of catabolic and anabolic processes within and between all these joint components, which is required to maintain tissue integrity and biomechanical functionality through physiological cellular processes.<sup>4</sup> Given the close interaction, the concomitant cross-talk and reciprocal feedback mechanisms between the various joint components, joint homeostasis should be considered a variable or dynamic equilibrium rather than a static state.<sup>4</sup> Breaking down 'joint homeostasis' into numerous homeostatic processes and assuming that derangement in any of these might cause a disruption of homeostatic balance in general not only avoids over-simplification of a highly complex biological system, but also allows the assessment of single joint components or specific aspects of the joint tissue status; combining this information at a later stage can then help to obtain a comprehensive picture of joint homeostasis and its derangement.<sup>4,22</sup>

Joint components can be isolated and studied *in vitro*. This can give important insights in molecular events responsible for beneficial or detrimental effects of specific interventions at the tissue level.<sup>6</sup> However, *in vitro* studies might not reflect the complexity of the situation *in vivo*, since the interactions of each component with its natural environment, the large range of stress spectra in biomechanical loading, and individual differences, play important roles. For the clinical evaluation of joint health, diagnostic imaging and physical examination are useful parameters that can provide information about tissue structure and function. However, they reflect the structural or functional consequences of disturbed homeostasis rather than providing real-time information on the molecular processes inside the joint. Since SF undergoes continuous turnover and is in direct contact with all relevant joint tissues except the subchondral bone, its composition provides approximately real-time information on joint homeostasis.<sup>24</sup> Furthermore, SF is the only joint component that can be obtained relatively easily from a live animal without causing significant tissue destruction. Therefore, molecular biomarkers in synovial fluid have been studied extensively in relation to joint diseases.<sup>25</sup> where early recognition of disruption of homeostatic processes can have high diagnostic and prognostic value.<sup>5</sup>

## Mechanisms of exercise effects

‘Exercise’ is a rather broad term, usually referring to regular physical activity (or physical/mechanical loading) that is performed to improve fitness and strength. The mechanisms by which exercise can influence joint homeostasis are complicated and closely related. For the purpose of this review, we distinguish between three main mechanisms: 1) the direct effect of mechanical impact on articular tissue integrity, 2) the indirect influence on joint tissue metabolism, and 3) the influence of exercise on joint circulation (fig. 1).

### *Direct mechanical effects of exercise on articular tissue integrity*

Maintenance of the integrity of articular tissues in general and the articular cartilage extracellular matrix in particular is imperative to preserve the properties required to meet the functional demands placed upon the joint. Structural damage to the articular cartilage could in itself affect the force distribution in the joint,<sup>26</sup> meaning that the limit of beneficial exercise might shift in the pathologic joint. The sudden application of substantial mechanical force, also referred to as ‘impact’, is a common cause of articular cartilage injury and often leads to post-traumatic OA.<sup>27</sup> Repeated joint loading results in an increase in subchondral bone thickness and density,<sup>28-30</sup> subsequently leading to increased shear stresses at the base of the articular cartilage. This can cause deep horizontal splits which can progress to the articular surface,

disrupting the integrity of the cartilage layer.<sup>31</sup> In retired Thoroughbred racehorses of different ages, progressive subchondral micro-cracking was observed in the metacarpophalangeal joint in younger animals, escalating to severe subchondral bone collapse and concomitant lesion formation in the cartilage layer with increasing age and thus cumulative athletic workload.<sup>32</sup>

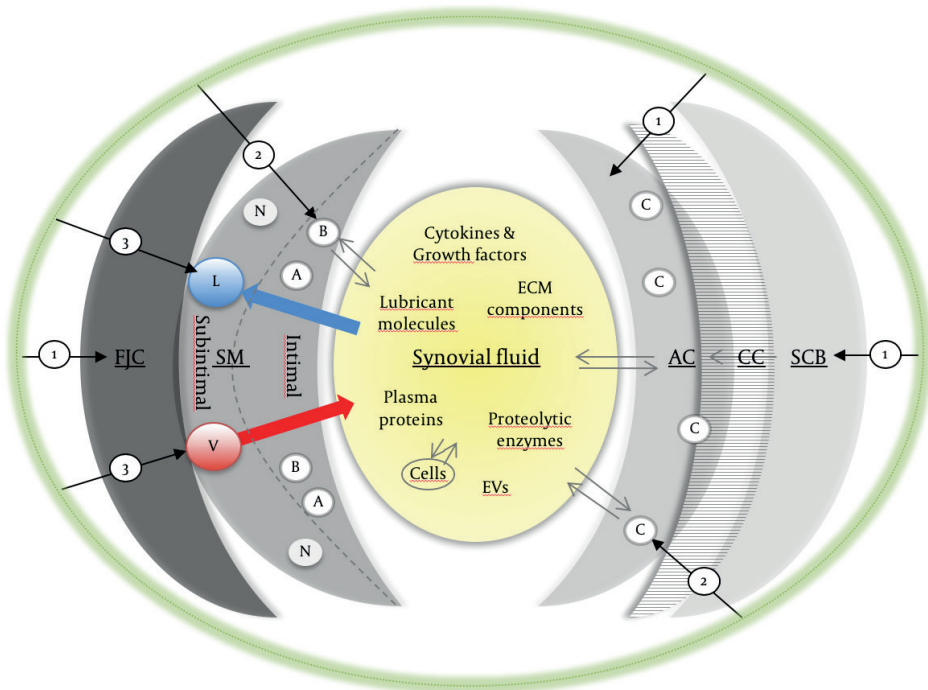


**Fig. 1** Schematic representation of the mechanisms of exercise effects on joint homeostasis. SCB, subchondral bone; CC, calcified cartilage; AC, articular cartilage; SM, synovial membrane; FJC, fibrous joint capsule; L, lymph vessel; V, blood vessel; N, nerve fibre; A, type A/macrophage-like synoviocytes; B, type B/fibroblast-like synoviocytes; C, chondrocytes; EVs, extracellular vesicles. The green circle represents exercise that influences various joint components via 1) direct mechanical effects on SCB, AC, and FJC, 2) synoviocytes and chondrocyte metabolism, and 3) joint circulation. Grey open arrows represent interaction between different joint components.

Disruption of the integrity of articular tissues does not necessarily refer only to the existence of cracks or tears in cartilage or bone, as the accumulation of repair ('scar') tissue due to overuse could affect the balance between catabolic and anabolic processes.<sup>33</sup> Inflammation of soft tissues (synovitis/capsulitis) due to trauma induced by (repeated) athletic activities can also contribute to degradative processes by the

release of inflammatory mediators and cytokines into the SF.<sup>34</sup> The very limited repair capacity of the articular cartilage<sup>35</sup> makes it particularly susceptible to initiation of a vicious cycle, in which micro-damage and subsequent inflammatory responses from the synovial membrane result in depression of chondrocyte synthetic activities and release of numerous catabolic mediators, causing further disturbance of joint homeostasis and articular cartilage breakdown (fig. 2).<sup>4</sup>

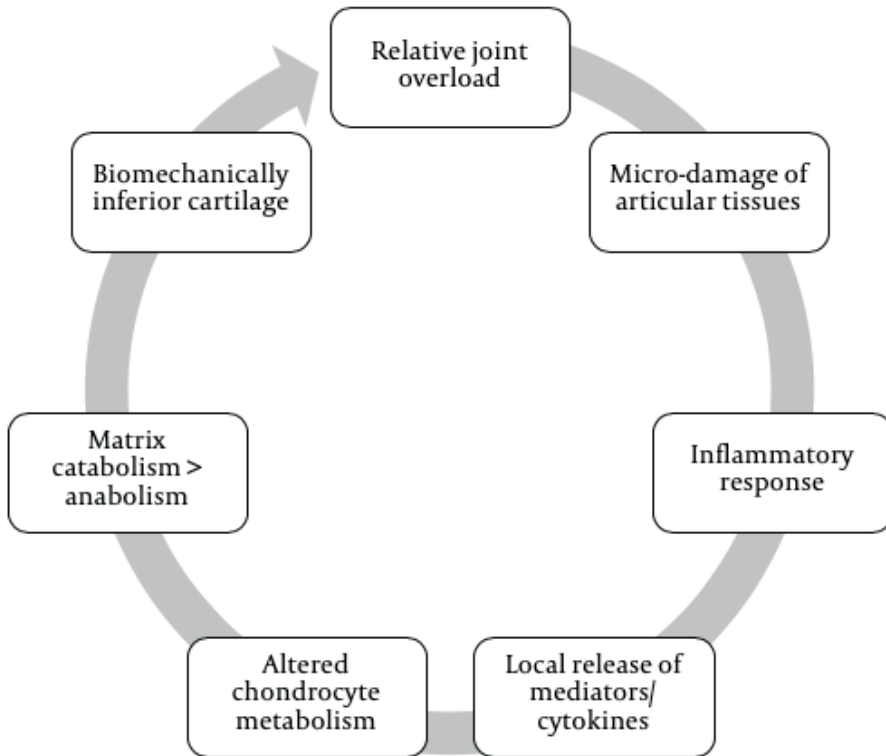


**Fig. 2** Vicious cycle of articular cartilage breakdown (adapted from de Grauw, 2011<sup>4</sup>)

### *Influence of exercise on articular tissue metabolism*

Mechanical loading modulates articular tissue metabolism by activating signal transduction pathways that translate mechanical stimulation into biochemical signals, altering cellular processes and leading to matrix remodelling.<sup>21</sup> This 'adaptive response' can be detected in each of the joint components and has been studied extensively in equine articular cartilage. The juvenile equine joint in particular is an excellent example of how exercise influences tissue turnover, leading to changes in cartilage matrix composition.

*Exercise-induced changes in juvenile articular cartilage matrix composition*

Whereas mature cartilage is known to be a highly immutable tissue with minimal repair capacity due to the extremely long turnover time of extracellular matrix (ECM) components and in particular of the collagen network,<sup>35</sup> the situation in juvenile animals is inherently different, as they are going through a process of active growth and development. The joint of a newborn foal displays a homogeneous distribution of proteoglycan and collagen content, including posttranslational modifications of collagen such as cross-links, across the articular cartilage. Over time, these tissue components reach mature levels and important structural changes occur.<sup>9,36</sup> Over the past decades, several large-scale *ex vivo* studies in juvenile horses (from neonates to 18 months old) have provided important insights into the crucial role of exercise in articular cartilage maturation.<sup>9,37-39</sup>

Briefly, these studies led to the conclusion that withholding any form of exercise during the first 5 months of life results in the lack of formation of articular cartilage topographic heterogeneity, which could have serious consequences for future tissue resistance to injury.<sup>9</sup> However, an increased workload appeared to speed up the normal process of maturation of ECM components. By 18 months of age, articular cartilage from foals kept on pasture and subjected to additional trot and canter exercise showed a biochemical composition closer to that of mature animals when compared to pasture-kept foals without additional exercise.<sup>39</sup> Advanced maturation of the ECM can be beneficial in horses that have to perform athletically at a very early age, because of the reinforcement of the cartilage ECM through increased matrix crosslinking. However, there might also be disadvantages. Although the advancement of the maturation process can be reversible in the case of glycosaminoglycans (GAGs), this is unlikely to be the case for collagen and collagen related structures. Therefore, it could be argued that foals subjected to additional training might reach a stage at which the collagen network no longer enables further cartilage remodelling. This could lead to a reduced capacity for repair, which is inherently disadvantageous.<sup>39</sup> This suggests that moderate exercise protocols can induce substantial changes in the biochemical composition of the articular cartilage if implemented at an early age. Therefore, the gap between the beneficial or detrimental effects of exercise on articular cartilage metabolism might be relatively narrow in young animals.

**Exercise-induced changes in articular cartilage matrix composition in young adults**  
In 2-year-old horses, no overall effect on collagen content of the middle carpal articular cartilage has been observed after 19 weeks of high-intensity treadmill exercise compared with daily walking exercise. However, exercise was shown to decrease collagen content at sites predisposed to clinical lesions.<sup>40</sup> In another study

in 2-year-olds, it was concluded that strenuous exercise (i.e. race training) provoked significant alterations in the characteristics of the collagen network of the articular cartilage of the fetlock joint compared with a pasture-kept control group of the same age. These changes were suggestive of micro-damage and loosening of the collagen network.<sup>41</sup>

For the most abundant non-collagenous protein present in articular cartilage, cartilage oligomeric matrix protein (COMP), exercise effects have been found at both intermittently loaded high weight-bearing (i.e. dorsal) joint areas and at more constantly loaded lower weight-bearing (i.e. palmar) areas of the cartilage in the middle carpal joint. In 2-year-old horses trained on a treadmill, COMP content was lower than in daily-walked control horses and it was mostly lower at dorsal sites than at palmar sites. In the control horses, this pattern was not observed.<sup>42</sup> In a study of 3-year-olds, COMP content was lower in animals that had been trained for 1.5 years and had raced regularly than in pasture-kept control horses. However, in contrast to the findings in 2-year-old treadmill trained horses, the pasture-kept controls had higher COMP content in dorsal areas than in palmar areas. These findings suggest that adequate dynamic loading promotes COMP synthesis, while excessive loading could have the opposite effect.<sup>43</sup>

For proteoglycans, anabolic effects of exercise have been reported. In 2-year-old treadmill exercised horses, GAG content was higher at heavily loaded sites of cartilage in the middle carpal joint than in cartilage from horses that underwent daily walking exercise.<sup>40</sup> In contrast, no significant difference in endogenous proteoglycan content was found after 6 weeks of exercise consistent with early race training compared with box-rested control horses.<sup>44</sup> However, in cartilage explants from the exercise group, the amount of newly synthesised proteoglycan was increased.<sup>44</sup> Enhanced proteoglycan synthesis and reduced proteoglycan breakdown has also been observed in equine cartilage explants cultured in SF obtained after moderate exercise compared with cultures in pre-exercise SF.<sup>20</sup> This supported the hypothesis that the effects of intensified loading on articular cartilage metabolism were not only a direct result of the transduction of mechanical stress on chondrocytes into biochemical signals, but that they might also be mediated by substances released into the synovial fluid, emphasising the complex interactions between the various articular components. Molecular markers in SF that could reflect changes in tissue metabolism are discussed separately in the next section.

It is worthwhile to briefly mention the consequences of the opposite of exercise, namely joint immobilisation, on articular cartilage metabolism. These have been studied extensively in adult dogs.<sup>12</sup> Immobilisation of the stifle joint led to significant decreases in cartilage GAG content and synthesis. No changes in collagen content were found, but immobilisation reduced the amount of collagen cross-linkage.<sup>45</sup> To a certain extent, these changes were reversible during remobilisation, with remarkably better results when small movements during immobilisation were allowed.<sup>45,46</sup>

### *Exercise induced changes in the metabolism of other articular tissues*

Although under physiologic conditions, the subchondral bone is not in direct contact with the synovial cavity, it has an intimate physical association with the articular cartilage layer. Therefore, alterations of either tissue will modulate the properties and function of the other, through biochemical and molecular crosstalk across their interface.<sup>47,48</sup> Crosstalk between bone and cartilage plays an important role in joint homeostasis and has been described extensively in relation to the pathogenesis of osteoarthritis.<sup>48</sup> For the mature equine carpal, metacarpophalangeal and tarsal joints, subchondral bone has been shown to undergo functional adaptation, influenced by exercise and by the specific site within the joint. Reported effects include regional changes in thickness and density, which tend to increase under the influence of loading.<sup>28-30,49</sup> Studies in foals have shown that, similar to articular cartilage, loading appears to play a key role in the development of site-related differences in the biochemical composition of subchondral bone.<sup>50</sup> In foals withheld from exercise, bone calcium content and hydroxylsilypyridinoline and lysylpyridinoline crosslinks in subchondral bone of the proximal first phalanx were reduced compared with foals subjected to daily sprint training or foals kept at pasture 24 h per day. The fact that these differences were observed at the dorsal site, which sustained intermittent peak loading during exercise, and not at a more constantly loaded site, supports the role of biomechanical loading in subchondral bone metabolism, as dictated by Wolff's law.<sup>51,52</sup>

Limited information is available on in vivo effects of physical loading on synovial membrane integrity and its metabolic activities, especially in the horse. In juvenile horses, effects of superimposed exercise on the synovial membrane have been examined histologically.<sup>53</sup> Although detrimental effects such as cellular infiltration, hyperplasia, oedema, fibrosis or hyperemia were not reported in that study, these particular changes as well as markedly elevated expression of pro-inflammatory interleukin (IL)-15 expression have been observed in stifle joint synovial membrane of rabbits subjected to repetitive impulse loading or high-intensity treadmill training.<sup>54-56</sup> In rats, a long distance running protocol for 45 days led to an increased synovial expression of matrix metalloproteinases (MMP)-1, -9 and -13 compared



to cage-restrained animals.<sup>57</sup> These findings suggest potential detrimental pro-inflammatory effects of supramaximal exercise on the synovial membrane.

### *Influence of exercise on joint circulation*

Blood flow plays a major role in the efficiency of fluid exchange between synovial capillaries and the joint cavity and thus in the maintenance of joint homeostasis. It is influenced by motion (i.e. exercise), either directly or indirectly via alterations in the intra-articular pressure (IAP). Changes in joint angle cause a pulsatile capillary flow, and articular soft tissues, particularly the synovial membrane, have been shown to receive an increased blood flow in response to short-term treadmill exercise in the canine stifle and radiocarpal joint.<sup>58</sup> An alternating IAP in different joint compartments stimulates fluid exchange to the interstitium and lymph flow from the interstitium. These mechanisms promote the clearance and turnover of SF, maintaining the normally negative IAP (fig. 3).<sup>59-61</sup>

Relative overload of the joint can lead to a disruption of this physiological mechanism through joint effusion, which could occur in response to high intensity exercise,<sup>62,63</sup> or through reduced joint capsule compliance (fibrosis) due to traumatic synovitis/capsulitis. The net result is a pathological increase in IAP and eventually destruction of the capillary and neuronal network (fig. 3).<sup>64</sup> This can have consequences for nociceptive and proprioceptive function of the joint, and loss of a normally innervated vascular bed could disturb circulation in the articular tissues. Moreover, increased IAP can cause great reduction of synovial membrane blood flow<sup>61</sup> and in effused joints, blood flow might be further compromised by modest elevations in IAP induced by exercise.<sup>60,65</sup> Decreased blood flow negatively affects both SF turnover and SF composition, as it leads to decreased filtration and consequently decreased SF production, as well as impaired oxygen delivery, resulting in local lactic acidosis.<sup>61</sup>

### **Synovial fluid biomarkers**

As SF is a composite result of joint circulation and metabolic activity of the articular cartilage and synovial membrane, all effects of exercise on joint homeostasis described above change the molecular composition of the SF, and this might be reflected by changes in its biomarker profile. A biomarker can be defined as a 'characteristic that is objectively measured and evaluated as an indicator of normal biologic processes, pathogenic processes, or pharmacologic responses to a therapeutic intervention'.<sup>66</sup> A practical approach classifies biomarkers in SF into direct and indirect markers.<sup>67</sup> Direct markers include cleavage fragments and synthesis (by-)products of articular tissue components that directly reflect anabolic and catabolic processes, for example markers related to collagen or aggrecan metabolism, lubricant molecules or COMP.<sup>68</sup>

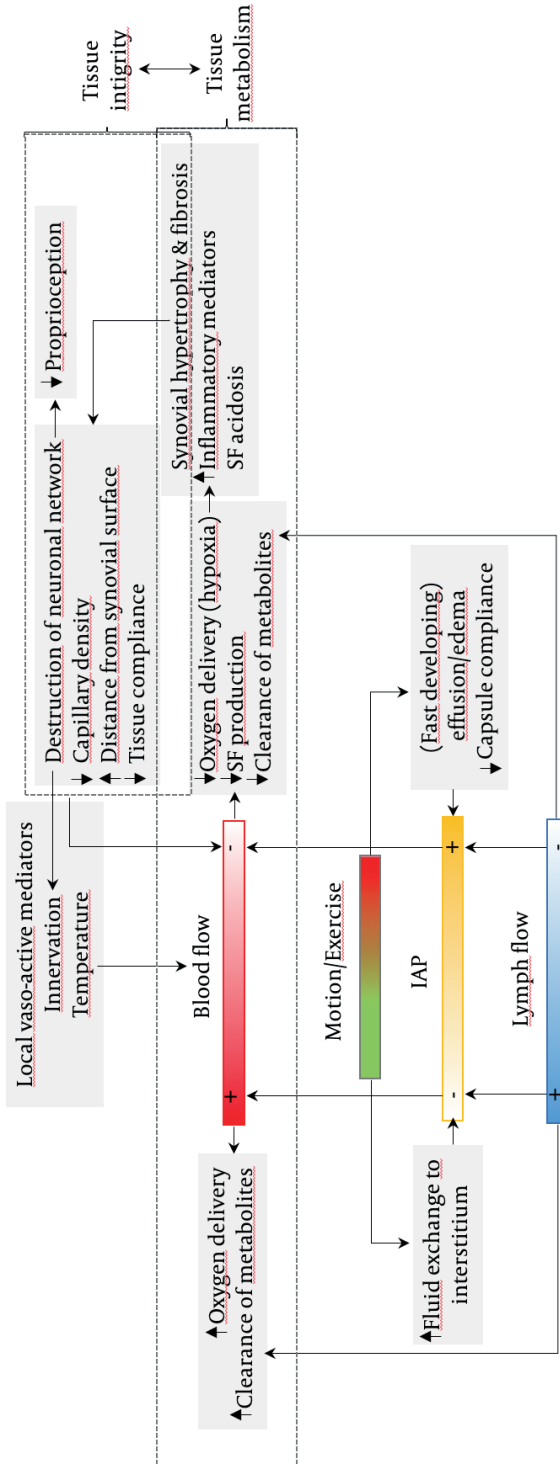


**Fig. 3** Schematic representation of the effect of exercise on circulation in articular tissues and mechanisms involved with their relation to tissue integrity and tissue metabolism.

Indirect biomarkers are molecules that affect tissue metabolism, but are not generated during tissue synthesis or breakdown, e.g. enzymes, inflammatory mediators, cytokines and growth factors. Direct and indirect molecular biomarkers have been studied in relation to exercise (Supplementary table 1). To enable critical interpretation of biomarker data, it is important to identify methodological issues and variables that can help explain the disparities between the effects observed in different studies.

### *Methodological concerns and confounding factors when studying exercise effects on SF biomarker profiles*

The importance of intensity and duration of exercise emerges from several studies, as biomarker changes seem to occur mostly under conditions of high intensity and long-term training. In horses, this was reflected by an increase in levels of C1,2C, COL CEQ, CPII, GAG, CS846 and PGE<sub>2</sub>.<sup>63</sup> In dogs and rabbits, a similar effect was found for levels of COMP, MMP-1 and -3 and TIMP-1.<sup>69,70</sup> However, the contribution of exercise intensity and duration is not always clear. For example, in two studies, a mild to moderate intensity protocol was used for the training period, after which a last exercise bout with a higher intensity was performed prior to a single SF collection procedure within 30 min or 1 h after exercise.<sup>20,71</sup> This approach makes it impossible to discriminate between the direct contribution of a single, high intensity exercise challenge and the effects of long-term, moderate-level training. Thus, any exercise regimen should be well defined and unambiguous.

Apart from the intensity and duration of exercise, several other factors could confound the relationship between SF biomarkers and exercise. Importantly, disparate effects have been observed for different joints, as evidenced by the exercise-induced increase in chondroitin sulphate in the tibiotarsal but not the radiocarpal joint.<sup>72</sup> Secondly, exercise history might influence effects of exercise on biomarker changes. For example, in polo ponies, a significant increase in hyaluronic acid concentration during the season was demonstrated in young ponies (3 to 4 years old) starting their careers, but not in older ponies (10 to 16 years old) with a career spanning 5 years or longer.<sup>73</sup> There might have been an age-related adaptation effect, as the younger ponies showed an initial increase followed by a more or less steady state, whereas in the older ponies, a non-significant initial rise followed by a decline back to baseline was observed. Similarly, a canine study showed an overall rise in COMP levels within a period of 10 weeks of exercise, consisting of an increase from week 2, a peak at week 4, and a decline after week 6 that continued until the end of the study.<sup>69</sup> These observations stress the importance of frequent sampling, especially when aiming to evaluate biomarker dynamics over a longer period.

The moment of sampling after completing an exercise session is also of great importance. Increases in  $\text{PGE}_2$  and  $\text{TNF}\alpha$  were measured at 3 and 6 h ( $\text{PGE}_2$ ) and at 2 h ( $\text{TNF}\alpha$ ) after exercise, and these biomarkers presented a return to baseline levels within 6 to 24 h ( $\text{PGE}_2$ ) and within 12 h ( $\text{TNF}\alpha$ ), suggesting recovery of joint homeostasis.<sup>73,74</sup> Therefore, the interval between the end of an exercise session and SF collection should be specified and standardised during the study period. In this context, the influence of repeated arthrocentesis also needs to be taken into consideration, as SF levels of  $\text{PGE}_2$ , CS, NO and MMP activity can be affected for 2 to 60 h following the previous joint aspiration.<sup>72-76</sup> The time frame varies with each marker, as one study demonstrated that GAG levels were not affected at 12 h after arthrocentesis, but after another 60 h, there was a significant increase; this effect disappeared 7 days later.<sup>74</sup>

Pathologic conditions such as the development of OA, which manifest clinically as lameness and which might or might not be exercise-induced, are important factors that can influence the SF biomarker profile and are additional to the effect of exercise. Decreased COMP concentrations correlating with an increase in total days of training were seen in lame horses but not in sound horses in one study.<sup>77</sup> In another study, an observed significant increase in CS concentration in young polo ponies was mainly due to three animals that developed OA within 24 months after the end of the study.<sup>73</sup>

Another confounding factor in SF biomarker analysis is joint effusion resulting from high intensity exercise or from exercise-induced pathology. Due to dilution effects, apparently decreased biomarker levels can occur, despite increased absolute synthesis. Reporting marker ratios (e.g.  $\text{MMP}/\text{TIMP}$ ,  $\text{CPII}/\text{C2C}$ ,  $\text{CS-846}/\text{GAG}$ ) rather than absolute concentrations of single markers might circumvent bias due to dilution effects,<sup>69,78</sup> but this approach assumes equal clearance rates of each marker from the joint space. In reality, individual markers present wide variations in SF clearance rates.<sup>79</sup>

As a last precaution to interpretation of SF biomarker data, it should be noted that when conducting biomarker research in equine SF, it is imperative to use analytic techniques that have been validated for use in this sample matrix and this species. It goes without saying that failure to do so may lead to severe misinterpretations of results.

## CONCLUSIONS

Exercise is a prerequisite for the maintenance of joint homeostasis and plays a crucial role in the physiologic maturation process of the juvenile joint. Moreover, exercise has a major influence on the delicate homeostatic balance within the articular tissues and on their interplay, which is crucial for proper and durable joint function. However, there appears to be a fine line between the beneficial and detrimental effects of exercise on joint homeostasis, and the amount and intensity of exercise potentially has a lasting effect on tissue characteristics in juvenile animals, and affects joint homeostasis in mature animals. Physical overload disrupts the integrity of joint structures, resulting in inflammatory responses, hence affecting joint homeostasis. Such disturbances of joint homeostasis have negative effects on chondrocyte vitality and responses, and can eventually lead to irreparable damage to articular cartilage. However, the appropriate amount of exercise could stimulate the restitution of joint homeostasis and recovery of joint function, by stimulating proteoglycan synthesis and by promoting circulation within the various joint components. Biomarkers in SF can provide real-time information on the effects of exercise on joint homeostasis in *in vivo* situations, but the complexity of joint physiology and many other confounding factors, including the type of exercise, exercise history, timing of sampling and sampling intervals, joint type and concomitant pathology, complicate the interpretation of results and comparisons between studies.

## ACKNOWLEDGEMENTS

Dr. Janny de Grauw is acknowledged for thoroughly proofreading the manuscript and her expert advice. Financial support from The Netherlands Organisation for Scientific Research (NWO) and the Dutch Arthritis Foundation (Grant LLP-22) is acknowledged.

## REFERENCES

1. Bernard C. Deuxième Leçon: Les trois formes de la vie. In: Dastre A, ed. *Leçons Sur Les Phénomènes de La Vie Communs Aux Animaux et Aux Végétaux*. Paris: J.-B. Baillière; 1878:65-124.
2. Cannon WB. Physiological regulation of normal states: Some tentative postulates concerning biological homeostatics. *Jubil Vol Charles Richet*. 1926:91-93.
3. Cannon WB. Organization for physiological homeostasis. *Physiol Rev*. 1929;9(3).
4. de Grauw JC. Molecular monitoring of equine joint homeostasis. *Vet Q*. 2011;31(2):77-86.
5. Chu CR, Andriacchi TP. Dance between biology, mechanics, and structure: A systems-based approach to developing osteoarthritis prevention strategies. *J Orthop Res*. 2015;33(7):939-947.
6. Goldring MB, Marcu KB. Cartilage homeostasis in health and rheumatic diseases. *Arthritis Res Ther*. 2009;11(3):224.
7. Penell JC, Egenvall A, Bonnett BN, Olson P, Pringle J. Specific causes of morbidity among Swedish horses insured for veterinary care between 1997 and 2000. *Vet Rec*. 2005;157(16):470-477.
8. Dyson PK, Jackson BF, Pfeiffer DU, Price JS. Days lost from training by two- and three-year-old Thoroughbred horses: a survey of seven UK training yards. *Equine Vet J*. 2008;40(7):650-657.
9. Brama PAJ, TeKoppele JM, Bank RA, Barneveld A, van Weeren PR. Development of biochemical heterogeneity of articular cartilage: influences of age and exercise. *Equine Vet J*. 2002;34(3):265-269.
10. Steel CM, Hopper BJ, Richardson JL, Alexander GR, Robertson ID. Clinical findings, diagnosis, prevalence and predisposing factors for lameness localised to the middle carpal joint in young Standardbred racehorses. *Equine Vet J*. 2006;38(2):152-157.
11. Vigre H, Chriél M, Hesselholt M, Falk-Rønne J, Kjær Ersbøll A. Risk factors for the hazard of lameness in Danish Standardbred trotters. *Prev Vet Med*. 2002;56(2):105-117.
12. Vanwanseele B, Lucchinetti E, Stüssi E. The effects of immobilization on the characteristics of articular cartilage: current concepts and future directions. *Osteoarthr Cartil*. 2002;10(5):408-419.
13. Anderson DD, Chubinskaya S, Guilak F, et al. Post-traumatic osteoarthritis: improved understanding and opportunities for early intervention. *J Orthop Res*. 2011;29(6):802-809.
14. McAlindon TE, Bannuru RR, Sullivan MC, et al. OARSI guidelines for the non-surgical management of knee osteoarthritis. *Osteoarthr Cartil*. 2014;22(3):363-388.
15. Regnaud J-P, Lefevre-Colau M-M, Trinquart L, et al. High-intensity versus low-intensity physical activity or exercise in people with hip or knee osteoarthritis. Regnaud J-P, ed. *Cochrane Database Syst Rev*. 2015;10:CD010203.
16. Liu SH, Driban JB, Eaton CB, McAlindon TE, Harrold LR, Lapane KL. Objectively Measured Physical Activity and Symptoms Change in Knee Osteoarthritis. *Am J Med*. 2016;129(5):497-505.
17. Reed SR, Jackson BF, Wood JLN, Price JS, Verheyen KLP. Exercise affects joint injury risk in young Thoroughbreds in training. *Vet J*. 2013;196(3):339-344.
18. Hallett MB, Andrish JT. Effects of exercise on articular cartilage. *Sports Med Arthrosc*. 1994;2(1):29-37.
19. Saris DBF, Dhert WJA, Verboort AJ. Joint homeostasis: the discrepancy between old and fresh defects in cartilage repair. *J Bone Jt Surg*. 2003;85(7):1067-1076.
20. Van den Hoogen BM, van de Lest CH, van Weeren PR, et al. Loading-induced changes in synovial fluid affect cartilage metabolism. *Br J Rheumatol*. 1998;37(6):671-676.
21. Khan KM, Scott A. Mechanotherapy: how physical therapists' prescription of exercise promotes tissue repair. *Br J Sports Med*. 2009;43(4):247-252.
22. Hui AY, McCarty WJ, Masuda K, Firestein GS, Sah RL. A systems biology approach to synovial joint lubrication in health, injury, and disease. *Syst Biol Med*. 2012;4(1):15-37.

23. Levick JR. Microvascular architecture and exchange in synovial joints. *Microcirculation*. 1995;2(3):217-233.
24. van den Boom R. Synovial fluid as a mirror of equine joint (patho) physiology. 2004.
25. Lotz M, Martel-Pelletier J, Christiansen C, et al. Republished: Value of biomarkers in osteoarthritis: current status and perspectives. *Postgrad Med J*. 2014;90(1061):171-178.
26. Schett G, Tohidast-Akrad M, Steiner G, Smolen J. The stressed synovium. *Arthritis Res*. 2001;3(2):80-86.
27. Buckwalter JA, Felson DT. Post-traumatic arthritis: Definitions and burden of disease. In: Olson SA, Guilak F, eds. *Post-Traumatic Arthritis: Pathogenesis, Diagnosis and Management*. Springer, New York, USA; 2015:7-15.
28. Firth EC, Delahunt J, Wichtel JW, Birch HL, Goodship AE. Galloping exercise induces regional changes in bone density within the third and radial carpal bones of Thoroughbred horses. *Equine Vet J*. 1999;31(2):111-115.
29. Murray RC, Branch MV, Dyson SJ, Parkin TDH, Goodship AE. How does exercise intensity and type affect equine distal tarsal subchondral bone thickness? *J Appl Physiol*. 2007;102(6):2194-2200.
30. Kawcak CE, McIlwraith CW, Norrdin RW, Park RD, Steyn PS. Clinical effects of exercise on subchondral bone of carpal and metacarpophalangeal joints in horses. *Am J Vet Res*. 2000;61(10):1252-1258.
31. Radin EL, Rose RM. Role of subchondral bone in the initiation and progression of cartilage damage. *Clin Orthop Relat Res*. 1986;(213):34-40.
32. Turley SM, Thambyah A, Riggs CM, Firth EC, Broom ND. Microstructural changes in cartilage and bone related to repetitive overloading in an equine athlete model. *J Anat*. 2014;224(6):647-658.
33. Hart DA, Scott A. Getting the dose right when prescribing exercise for connective tissue conditions: the Yin and the Yang of tissue homeostasis. *Br J Sports Med*. 2012;46(10):696-698.
34. McIlwraith CW, Frisbie DD, Kawcak CE. The horse as a model of naturally occurring osteoarthritis. *Bone Jt Res*. 2012;1(11):297-309.
35. Heinemeier KM, Schjerling P, Heinemeier J, et al. Radiocarbon dating reveals minimal collagen turnover in both healthy and osteoarthritic human cartilage. *Sci Transl Med*. 2016;8(346):346ra90.
36. Little CB, Ghosh P, Rose R. The effect of strenuous versus moderate exercise on the metabolism of proteoglycans in articular cartilage from different weight-bearing regions of the equine third carpal bone. *Osteoarthr Cartil*. 1997;5(3):161-172.
37. Barneveld A, van Weeren PR. Conclusions regarding the influence of exercise on the development of the equine musculoskeletal system with special reference to osteochondrosis. *Equine Vet J Suppl*. 1999;(31):112-119.
38. Rogers CW, Firth EC, McIlwraith CW, et al. Evaluation of a new strategy to modulate skeletal development in Thoroughbred performance horses by imposing track-based exercise during growth. *Equine Vet J*. 2008;40(2):111-118.
39. van Weeren PR, Firth EC, Brommer H, et al. Early exercise advances the maturation of glycosaminoglycans and collagen in the extracellular matrix of articular cartilage in the horse. *Equine Vet J*. 2008;40(2):128-135.
40. Murray RC, Birch HL, Lakhani K, Goodship AE. Biochemical composition of equine carpal articular cartilage is influenced by short-term exercise in a site-specific manner. *Osteoarthr Cartil*. 2001;9(7):625-632.
41. Brama PA, Tekoppele JM, Bank RA, Barneveld A, Firth EC, van Weeren PR. The influence of strenuous exercise on collagen characteristics of articular cartilage in Thoroughbreds age 2 years. *Equine Vet J*. 2000;32(6):551-554.

42. Murray RC, Smith RK, Henson FMD, Goodship A. The Distribution of Cartilage Oligomeric Matrix Protein (COMP) in Equine Carpal Articular Cartilage and its Variation with Exercise and Cartilage Deterioration. *Vet J.* 2001;162(2):121-128.
43. Skiöldebrand E, Ekman S, Heinegård D, Hultenby K. Ultrastructural immunolocalization of cartilage oligomeric matrix protein (COMP) in the articular cartilage on the equine third carpal bone in trained and untrained horses. *Res Vet Sci.* 2010;88(2):251-257.
44. Palmer JL, Bertone AL, Malesud CJ, Carter BG, Papay RS, Mansour J. Site-specific proteoglycan characteristics of third carpal articular cartilage in exercised and nonexercised horses. *Am J Vet Res.* 1995;56(12):1570-1576.
45. Haapala J, Arokoski JPA, Hyttinen MM, et al. Remobilization does not fully restore immobilization induced articular cartilage atrophy. *Clin Orthop Relat Res.* 1999;362:218-229.
46. Behrens F, Kraft EL, Oegema TR. Biochemical changes in articular cartilage after joint immobilization by casting or external fixation. *J Orthop Res.* 1989;7(3):335-343.
47. Pan J, Zhou X, Li W, Novotny JE, Doty SB, Wang L. In situ measurement of transport between subchondral bone and articular cartilage. *J Orthop Res.* 2009;27(10):1347-1352.
48. Findlay DM, Kuliwaba JS. Bone-cartilage crosstalk: a conversation for understanding osteoarthritis. *Bone Res.* 2016;4:16028.
49. Murray RC, Vedi S, Birch HL, Lakhani KH, Goodship AE. Subchondral bone thickness, hardness and remodelling are influenced by short-term exercise in a site-specific manner. *J Orthop Res.* 2001;19(6):1035-1042.
50. Brama PA, Bank RA, Tekoppele JM, Van Weeren PR. Training affects the collagen framework of subchondral bone in foals. *Vet J.* 2001;162(1):24-32.
51. Brama PAJ, Tekoppele JM, Bank RA, Barneveld A, van Weeren PR. Biochemical development of subchondral bone from birth until age eleven months and the influence of physical activity. *Equine Vet J.* 2002;34(2):143-149.
52. Wolff J. Ueber die innere Architectur der Knochen und ihre Bedeutung für die Frage vom Knochenwachsthum. *Virchows Arch für Pathol Anat und Physiol.* 1870;50:389-450.
53. Kawcak CE, McIlwraith CW, Firth EC. Effects of early exercise on metacarpophalangeal joints in horses. *Am J Vet Res.* 2010;71(4):405-411.
54. Wang YH, Li XD, Zhu WB, Sun GF. Effect of high-intensity exercise on interleukin-15 expression in rabbit synovia. *Genet Mol Res.* 2015;14(4):13852-13859.
55. Walker ER, Boyd RD, Wu DD, Lukoschek M, Burr DB, Radin EL. Morphologic and morphometric changes in synovial membrane associated with mechanically induced osteoarthrosis. *Arthritis Rheum.* 1991;34(5):515-524.
56. Lukoschek M, Boyd RD, Schaffler MB, Burr DB, Radin EL. Comparison of joint degeneration models: Surgical instability and repetitive impulsive loading. *Acta Orthop.* 1986;57(4):349-353.
57. Shangguan YX, Wei XC, Li K, Wei JP. Expression of matrix metalloproteinases in the synovium of rat knee joint during long-distance running. *Chinese J Tissue Eng Res.* 2013;17(33):5909-5916.
58. Simkin PA, Huang A, Benedict RS. Effects of exercise on blood flow to canine articular tissues. *J Orthop Res.* 1990;8(2):297-303.
59. Bertone AL, Hardy J, Simmons EJ, Muir WW. Vascular and transsynovial forces of the isolated stationary equine joint. *Am J Vet Res.* 1998;59(4):495-503.
60. da Gracca Macoris D, Bertone A. Intra-articular pressure profiles of the cadaveric equine fetlock joint in motion. *Equine Vet J.* 2001;33(2):184-190.



61. Hardy J, Bertone AL, Muir WW. Joint pressure influences synovial tissue blood flow as determined by colored microspheres. *J Appl Physiol.* 1996;80(4):1225-1232.
62. Persson L. On the synovia in horses. A clinical and experimental study. *Acta Vet Scand.* 1971;suppl 35:3-77.
63. Frisbie DD, Al-Sobayil F, Billingham RC, Kawcak CE, McIlwraith CW. Changes in synovial fluid and serum biomarkers with exercise and early osteoarthritis in horses. *Osteoarthr Cartil.* 2008;16(10):1196-1204.
64. Eitner A, Pester J, Nietzsche S, Hofmann GO, Schaible H-G. The innervation of synovium of human osteoarthritic joints in comparison with normal rat and sheep synovium. *Osteoarthr Cartil.* 2013;21(9):1383-1391.
65. James MJ, Cleland LG, Rofe AM, Leslie AL. Intraarticular pressure and the relationship between synovial perfusion and metabolic demand. *J Rheumatol.* 1990;17(4):521-527.
66. Biomarkers Definitions Working Group. Biomarkers and surrogate endpoints: Preferred definitions and conceptual framework. *Clin Pharmacol Ther.* 2001;69(3):89-95.
67. Sipe JD. Acute-phase proteins in osteoarthritis. *Semin Arthritis Rheum.* 1995;25(2):75-86.
68. Saxne T, Heinegård D. Cartilage oligomeric matrix protein: a novel marker of cartilage turnover detectable in synovial fluid and blood. *Br J Rheumatol.* 1992;31(9):583-591.
69. Qi C, Changlin H. Effects of moving training on histology and biomarkers levels of articular cartilage. *J Surg Res.* 2006;135(2):352-363.
70. Qi C, Changlin H, Zefeng H. Matrix metalloproteinases and inhibitor in knee synovial fluid as cartilage biomarkers in rabbits: the effect of high-intensity jumping exercise. *J Surg Res.* 2007;140(1):149-157.
71. Brown MP, Trumble TN, Plaas AHK, et al. Exercise and injury increase chondroitin sulfate chain length and decrease hyaluronan chain length in synovial fluid. *Osteoarthr Cartil.* 2007;15(11):1318-1325.
72. Lamprecht ED, Williams CA. Biomarkers of antioxidant status, inflammation, and cartilage metabolism are affected by acute intense exercise but not superoxide dismutase supplementation in horses. *Oxid Med Cell Longev.* 2012;2012:Article ID 920932.
73. Baccarin RYA, Rasera L, Machado TSL, Michelacci YM. Relevance of synovial fluid chondroitin sulphate as a biomarker to monitor polo pony joints. *Can J Vet Res.* 2014;78(1):50-60.
74. van den Boom R, van de Lest CHA, Bull S, Brama PA., van Weeren PR, Barneveld A. Influence of repeated arthrocentesis and exercise on synovial fluid concentrations of nitric oxide, prostaglandin E<sub>2</sub> and glycosaminoglycans in healthy equine joints. *Equine Vet J.* 2005;37:250-256.
75. Brama PAJ, van den Boom R, De Groot J, Kiers GH, van Weeren PR. Collagenase-1 (MMP-1) activity in equine synovial fluid: influence of age, joint pathology, exercise and repeated arthrocentesis. *Equine Vet J.* 2004;36(1):34-40.
76. van den Boom R, Brama PAJ, Kiers GH, De Groot J, Barneveld A, Weeren PR. The influence of repeated arthrocentesis and exercise on matrix metalloproteinase and tumour necrosis factor activities in normal equine joints. *Equine Vet J.* 2004;36(2):155-159.
77. Skiöldbrand E, Heinegård D, Olofsson B, Rucklidge G, Ronéus N, Ekman S. Altered homeostasis of extracellular matrix proteins in joints of standardbred trotters during a long-term training programme. *J Vet Med.* 2006;53(9):445-449.
78. de Grauw JC, Donabédian M, van de Lest CHA, et al. Assessment of synovial fluid biomarkers in healthy foals and in foals with tarsocrural osteochondrosis. *Vet J.* 2011;190(3):390-395.
79. Simkin PA. Synovial perfusion and synovial fluid solutes. *Ann Rheum Dis.* 1995;54(5):424-428.

## SUPPLEMENTARY INFORMATION

Supplementary table 1: Synovial fluid molecular biomarkers that have been studied in relation to exercise in in vivo studies.

Marker	Reference	Subject (Age)	Joint	Intensity of training (Type of training)	Duration of training	Measurement time points	Interval Ex-SFCOL	Significant effect (Time point)
<b>Compositional molecules</b>								
COL1I	Skiöldbrand et al., 2006 <sup>1</sup>	Horse (1.5-3.5 years)	Carpus	N/A (trotter race training)	24 months	Months: 0, 3, 6, 9, 12, 18-24	N/A	Gradual increase
COL1I	Frisbie et al., 2008 <sup>8</sup>	Horse (2 years)	Carpus	High (simulated race training)	3 months	Day: 0, 7, 14, 21, 28, 35, 42, 56, 70, 84, 91	N/A	Increase (as of day 42)
C12C	Frisbie et al., 2008 <sup>8</sup>	Idem	Idem	Idem	Idem	Idem	Idem	Gradual increase (as of day 21)
COL1CEQ	Frisbie et al., 2008 <sup>8</sup>	Idem	Idem	Idem	Idem	Idem	Idem	Gradual increase (as of day 28)
CTX-II	Cleary et al., 2010 <sup>3</sup>	Horse (1-2 years)	Carpus, MCP	High (race training)	5-6 months	Months: 0, 5-6	N/A	No
CPII	Frisbie et al., 2008 <sup>8</sup>	Horse (2 years)	Carpus	High (simulated race training)	3 months	Day: 0, 7, 14, 21, 28, 35, 42, 56, 70, 84, 91	N/A	Increase (as of day 7)
ACAN	Skiöldbrand et al., 2006 <sup>1</sup>	Horse (1.5-3.5 years)	Carpus	N/A (trotter race training)	24 months	Months: 0, 3, 6, 9, 12, 18-24	N/A	No
GAG	Frisbie et al., 2008 <sup>8</sup>	Horse (2 years)	Carpus	High (simulated race training)	3 months	Day: 0, 7, 14, 21, 28, 35, 42, 56, 70, 84, 91	N/A	Gradual increase (as of day 14)
	van den Boom et al., 2005 <sup>4</sup>	Horse (5-17 years)	Carpus, MCP, tarsus	Moderate (treadmill exercise)	14 days	Day: 0, 14	2 h	No
CS	Lamprecht and Williams, 2012 <sup>2</sup>	Horse (8±1 years)	Carpus, tarsus	High (repeated sprint exercise)	Once	H: -24, 0.5	0.5 h	Increase <sup>a</sup>
	Brown et al., 2007 <sup>6</sup>	Horse (3-6 years)	Carpus	Moderate/ High (treadmill exercise)	9 months/ once	Months: 0, 9	<1 h	No
	Baccarin et al., 2014 <sup>7</sup>	Horse (9-12 years)	MCP	N/A (polo match)	Once	H: -24, 3, 6, 24	3, 6, 24 h	No
	Baccarin et al., 2014 <sup>7</sup>	Horse (3-4 & 10-16 years)	MCP	N/A (polo training)	320 days	Day: 0, 40, 80, 240, 320	24 h	No <sup>b</sup>

CS846	Frisbie et al., 2008 <sup>7</sup>	Horse (2 years)	Carpus	High (simulated race training)	3 months	Day: 0, 7, 14, 21, 28, 35, 42, 56, 70, 84, 91	N/A	Increase (as of day 14)
COMP	Qj and Changlin, 2006 <sup>8</sup>	Dog (adult)	Knee	High (treadmill exercise)	10 weeks	Week: 0, 2, 4, 6, 8, 10	12 h	Increase
	Skiöldbrand et al., 2006 <sup>1</sup>	Horse (1.5-3.5 years)	Carpus	N/A (trotter race training)	24 months	Months: 0, 3, 6, 9, 12, 18-24	N/A	No <sup>c</sup>
OC	Frisbie et al., 2008 <sup>7</sup>	Horse (2 years)	Carpus	High (simulated race training)	3 months	Day: 0, 7, 14, 21, 28, 35, 42, 56, 70, 84, 91	N/A	Gradual increase (as of day 56)
<b>Lubricant molecules</b>								
HA	Baccarin et al., 2014 <sup>7</sup>	Horse (3-4/10-16 years)	MCP	N/A (polo training)	320 days	Day: 0, 40, 80, 240, 320	24 h	Increase <sup>d</sup> (as of day 40)
	Ingram et al., 2009 <sup>9</sup>	Rabbit (N/A)	Knee	N/A (passive cyclic movement)	5 h	H: 5	0 h	Increase
	Baccarin et al., 2014 <sup>7</sup>	Horse (9-12 years)	MCP	N/A (polo match)	Once	H: -24, 3, 6, 24	3, 6, 24 h	No
	Brown et al., 2007 <sup>6</sup>	Horse (3-6 years)	Carpus	Moderate/high (treadmill exercise)	9 months/ once	Months: 0, 9	<1 h	No <sup>c</sup>
	Van den Hoogen et al., 1998 <sup>10</sup>	Horse (2 years)	Carpus	Mild/moderate (treadmill exercise)	8 days/ once	Day: 0, 8	0.5 h	No
PRG4	Musumeci et al., 2015 <sup>11</sup>	Rat (12-24 months)	Knee	Moderate-high (treadmill interval training)	2 months	Week: 8	24 h	Increase
<b>Degradative enzymes and inhibitors</b>								
MMP	van den Boom et al., 2004 <sup>2</sup>	Horse (5-17 years)	Carpus, MCP, tarsus	Moderate (treadmill exercise)	14 days	Day: 0, 14	2 h	No
	Van den Hoogen et al., 1998 <sup>10</sup>	Horse (2 years)	Carpus	Mild/Moderate (treadmill exercise)	8 days/ once	Day: 0, 8	0.5 h	No
MMP-1	Qj et al., 2007 <sup>3</sup>	Rabbit (10-12 months)	Knee	High (jumping exercise)	4-8 wk	Week: 4, 8	N/A	Increase (at wk 8)
	Qj and Changlin, 2006 <sup>8</sup>	Dog (adult)	Knee	High (treadmill exercise)	10 wk	Week: 0, 2, 4, 6, 8, 10	12 h	Increase
	Brama et al., 2004 <sup>14</sup>	Horse (5-17 years)	MCP	Moderate (treadmill exercise)	14 days	Day: 0, 14	2 h	No



MMP-3	Qi et al., 2007 <sup>33</sup>	Rabbit (10-12 months)	Knee	High (jumping exercise)	4-8 wk	Week: 4, 8	N/A	Gradual increase (as of wk 4)
	Qi and Changlin, 2006 <sup>8</sup>	Dog (adult)	Knee	High (treadmill exercise)	10 wk	Week: 0, 2, 4, 6, 8, 10	12 h	Increase
TIMP-1	Qi et al., 2007 <sup>33</sup>	Rabbit (10-12 months)	Knee	High (jumping exercise)	4-8 wk	Week: 4, 8	N/A	Gradual increase (as of wk 4)
	Qi and Changlin, 2006 <sup>8</sup>	Dog (adult)	Knee	High (treadmill exercise)	10 wk	Week: 0, 2, 4, 6, 8, 10	12 h	Increase
MMP-3/ TIMP-1	Qi et al., 2007 <sup>33</sup>	Rabbit (10-12 months)	Knee	High (jumping exercise)	4-8 wk	Week: 4, 8	N/A	Gradual increase (as of wk 4)
	Qi and Changlin, 2006 <sup>8</sup>	Dog (adult)	Knee	High (treadmill exercise)	10 wk	Week: 0, 2, 4, 6, 8, 10	12 h	Increase
<b>Inflammatory mediators</b>								
PGE <sub>2</sub>	Baccarin et al., 2014 <sup>7</sup>	Horse (9-12 years)	MCP	N/A (polo match)	Once	H: 24, 3, 6, 24	3, 6, 24 h	Increase (at 3 h and 6 h)
	Frisbie et al., 2008 <sup>8</sup>	Horse (2 years)	Carpus	High (simulated race training)	3 months	Day: 0, 7, 14, 21, 28, 35, 42, 56, 70, 84, 91	N/A	Increase (as of day 14)
	van den Boom et al., 2005 <sup>4</sup>	Horse (5-17 years)	Carpus, MCP, tarsus	Moderate (treadmill exercise)	14 days	0, 14	2 h	Increase
	Baccarin et al., 2014 <sup>7</sup>	Horse (3-4 and 10-16 years)	MCP	N/A (polo training)	320 days	Day: 0, 40, 80, 240, 320	24 h	No
	Lamprecht and Williams, 2012 <sup>5</sup>	Horse (8±1 years)	Carpus, tarsus	High (repeated sprint exercise)	Once	H: 24, 0.5	0.5 h	No
<b>Cytokines and growth factors</b>								
TNF- $\alpha$	van den Boom et al., 2004 <sup>2</sup>	Horse (5-17 years)	Carpus, MCP, tarsus	Moderate (treadmill exercise)	14 days	Day: 0, 14	2 h	Increase
IL-15	Wang et al., 2015 <sup>5</sup>	Rabbit (N/A)	Knee	High (treadmill exercise)	4 wk	Week: 4	N/A	Increase
NO	van den Boom et al., 2005 <sup>4</sup>	Horse (5-17 years)	Carpus, MCP, tarsus	Moderate (treadmill exercise)	14 days	Day: 0, 14	2 h	No

Nitrite	Lamprecht et al., 2009 <sup>66</sup>	Horse (8.5±1.7 years)	Carpus, tarsus	High (treadmill exercise)	Once	Hi: 24; 0.5; 2; 24	0.5, 2, 24 h	No
LOX	Vernon et al., 2010 <sup>67</sup>	Lamb (5 months)	MCP	N/A	8 wk	Week: 6-8	N/A	No
IGF-1/II	van den Hoogen et al., 1998 <sup>68</sup>	Horse (2 years)	Carpus	Mild/Moderate (treadmill exercise)	8 days/ once	Day: 0, 8	0.5 h	No

COLII, Collagen type II; COLI, Collagen type I; C1, 2C, Collagen I and II cleavage neopeptide; COL CEQ, Collagen II neopeptide; CTX-II, Collagen II Carboxy-terminal telopeptide; CPII, Collagen II pro-peptide; ACAN, Aggrecan; GAG, Glycosaminoglycan; CS, Chondroitin sulphate; CS846, Chondroitin sulphate epitope 846; COMP, Cartilage oligomeric matrix protein; OC, Osteocalcin; HA, Hyaluronic acid; PRG4, Proteoglycan 4 (Lubricin). MMP, Matrix metalloproteinase; MMP-1, Matrix metalloproteinase 1; MMP-3, Matrix metalloproteinase 3; TIMP-1, Tissue inhibitor of metalloproteinase; PGE<sub>2</sub>, Prostaglandin E<sub>2</sub>; TNF- $\alpha$ , Tumor necrosis factor  $\alpha$ ; NO, Nitric oxide; IL-15, interleukine 15; LOX, lipoxigenase; IGF-1/II, Insulin-like growth factor 1 and 2; Interval Ex-SFCol, interval between exercise and collection of synovial fluid; N/A, not applicable or not available. Significant effect defined as  $P < 0.05$  in the publication. Training intensity, as specified in the publication.

<sup>a</sup>Only for the tarsal joint; <sup>b</sup>At day 240, a significant increase was seen only in polo prospects. This finding was mainly due to three animals that developed OA within 24 months after termination of the study; <sup>c</sup>Decreased in correlation with an increase in total days of training in lame but not sound horses; <sup>d</sup>No significant effect in the 10-16 year-old group; <sup>e</sup>SF HA profile changed significantly.

## Supplementary references

1. Skiöldebrand E, Heinegård D, Olofsson B, Rucklidge G, Ronéus N, Ekman S. Altered homeostasis of extracellular matrix proteins in joints of standardbred trotters during a long-term training programme. *J Vet Med.* 2006;53(9):445-449.
2. Frisbie DD, Al-Sobayil F, Billinghamurst RC, Kawcak CE, McIlwraith CW. Changes in synovial fluid and serum biomarkers with exercise and early osteoarthritis in horses. *Osteoarthr Cartil.* 2008;16(10):1196-1204.
3. Cleary OB, Trumble TN, Merritt KA, Brown MP. Effect of exercise and osteochondral injury on synovial fluid and serum concentrations of carboxy-terminal telopeptide fragments of type II collagen in racehorses. *Am J Vet Res.* 2010;71(1):33-40.
4. van den Boom R, van de Lest CHA, Bull S, Brama PA., van Weeren PR, Barneveld A. Influence of repeated arthrocentesis and exercise on synovial fluid concentrations of nitric oxide, prostaglandin E<sub>2</sub> and glycosaminoglycans in healthy equine joints. *Equine Vet J.* 2005;37:250-256.
5. Lamprecht ED, Williams CA. Biomarkers of antioxidant status, inflammation, and cartilage metabolism are affected by acute intense exercise but not superoxide dismutase supplementation in horses. *Oxid Med Cell Longev.* 2012;2012:Article ID 920932.
6. Brown MP, Trumble TN, Plaas AHK, et al. Exercise and injury increase chondroitin sulfate chain length and decrease hyaluronan chain length in synovial fluid. *Osteoarthr Cartil.* 2007;15(11):1318-1325.
7. Baccarin RYA, Rasera L, Machado TSL, Michelacci YM. Relevance of synovial fluid chondroitin sulphate as a biomarker to monitor polo pony joints. *Can J Vet Res.* 2014;78(1):50-60.
8. Qi C, Changlin H. Effects of moving training on histology and biomarkers levels of articular cartilage. *J Surg Res.* 2006;135(2):352-363. doi:10.1016/j.jss.2006.03.011
9. Ingram KR, Wann AKT, Wingate RM, Coleman PJ, McHale N, Levick JR. Signal pathways regulating hyaluronan secretion into static and cycled synovial joints of rabbits. *J Physiol.* 2009;587(Pt 17):4361-4376.
10. Van den Hoogen BM, van de Lest CH, van Weeren PR, et al. Loading-induced changes in synovial fluid affect cartilage metabolism. *Br J Rheumatol.* 1998;37(6):671-676.
11. Musumeci G, Castrogiovanni P, Trovato FM, et al. Physical activity ameliorates cartilage degeneration in a rat model of aging: a study on lubricin expression. *Scand J Med Sci Sport.* 2015;25(2):e222-230.
12. van den Boom R, Brama PAJ, Kiers GH, De Groot J, Barneveld A, Weeren PR. The influence of repeated arthrocentesis and exercise on matrix metalloproteinase and tumour necrosis factor activities in normal equine joints. *Equine Vet J.* 2004;36(2):155-159. doi:10.2746/0425164044868602
13. Qi C, Changlin H, Zefeng H. Matrix metalloproteinases and inhibitor in knee synovial fluid as cartilage biomarkers in rabbits: the effect of high-intensity jumping exercise. *J Surg Res.* 2007;140(1):149-157.
14. Brama PAJ, van den Boom R, De Groot J, Kiers GH, van Weeren PR. Collagenase-1 (MMP-1) activity in equine synovial fluid: influence of age, joint pathology, exercise and repeated arthrocentesis. *Equine Vet J.* 2004;36(1):34-40. <http://www.ncbi.nlm.nih.gov/pubmed/14756369>. Accessed November 2, 2015.
15. Wang YH, Li XD, Zhu WB, Sun GF. Effect of high-intensity exercise on interleukin-15 expression in rabbit synovia. *Genet Mol Res.* 2015;14(4):13852-13859.
16. Lamprecht ED, Bagnell CA, Williams CA. Inflammatory responses to three modes of intense exercise in Standardbred mares – a pilot study. *Comp Exerc Physiol.* 2009;5(3-4):115-125.
17. Vernon KL, Riggs L, Coverdale J, Bodine AB, Gibbons J. The Effects of Forced Exercise on Collagen Type II Fragments, Lysyl Oxidase Concentrations, and Total Protein Concentrations in Sera and Synovial Fluid of Lambs. *J Equine Vet Sci.* 2010;30(5):266-274.







# CHAPTER 9

## Summarizing discussion



Well-functioning synovial joints are of vital importance for smooth and pain-free movement. Disturbances in the homeostatic balance between and within articular components can lead to the onset and progression of joint disorders such as osteoarthritis (OA). The high incidence of OA is a concern in human as well as equine health care and there is no effective therapy available. Due to the long time it may take to develop OA, it is difficult to test the exact relationship between potential risk factors and the events leading to OA on the longer term. Particularly focal cartilage defects, commonly observed during arthroscopic examination both in horses and humans, are subject of discussion on if, when and how they should be treated. Currently, the clinical appreciation of such lesions is mainly based on subjective interpretation of arthroscopic evaluations, a situation that hampers reliable prognostication and evidence-based choices for (novel) therapies.<sup>1,2</sup> For both clinical and research purposes, the possibility to assess characteristics of cartilage defects and the condition of the surrounding cartilage in a more accurate and objective manner would be of great value.

To this end, the intra-articular use of several imaging and non-imaging modalities, including ultrasound (US), optical coherence tomography (OCT), and near infrared spectroscopy (NIRS) have been proposed in the last few decades.<sup>3-6</sup> The first aim of this thesis was to investigate the potential of these advanced modalities to improve arthroscopic evaluation of subtle changes in cartilage structure, composition and mechanical properties in the horse (part I). Furthermore, a better and more quantitative insight in the relation between lesion development, joint homeostasis and functionality is needed, since OA is not only a disease of the cartilage but of the whole joint. This led to our second aim, that was to monitor the progression of artificial cartilage defects and their impact on the joint as a whole in an equine carpal groove model. We did this by multiple modality monitoring of changes at a structural, compositional and functional level *in vivo* and *ex vivo* (part II). Since biomechanical loading of the joint is related to both progressive degeneration of articular cartilage and, on the other hand, to maintenance of joint health, a review on the relationship between exercise and joint homeostasis was included.

## PART I – REFLECTING ON ARTICULAR CARTILAGE

### Visual characterization of cartilage lesions with intra-articular OCT

Optical coherence tomography has been widely investigated for possible applications in various medical fields and is clinically used in cardiovascular surgery and ophthalmology.<sup>7</sup> In **chapter 2** we determined whether OCT is an effective tool for advanced clinical assessment of lesions in equine articular cartilage during arthroscopic examinations. By producing high-resolution cross-sectional images, OCT arthroscopy provided detailed information on the superficial as well as the deeper zones of the cartilage layers in the metacarpophalangeal joint. A full spectrum of articular cartilage characteristics could be visualized, including cavitation, fibrillation of the cartilage surface, superficial and deep horizontal cleft formation, erosion, and anomalies below the cartilage surface. The full thickness images enabled determination of the cartilage thickness and the extension of cartilage lesions along the International Cartilage Repair Society (ICRS) guidelines.

Besides the improvement in lesion characterization that was achieved with OCT arthroscopy, we showed (**chapter 3**) that levels of intra- and interobserver agreement of OCT-based ICRS scoring were better than those reported for ICRS scoring based on conventional arthroscopy.<sup>8</sup> These results were similar to those reported previously.<sup>9</sup> However, the visual assessment still remained subjective and therefore, a software package for semi-automated ICRS scoring of articular cartilage lesions in OCT images was introduced. By using this software, interobserver and mean intra-observer agreement could be improved compared with visual ICRS scoring, but semi-automated ICRS scoring also had some limitations. To quantify thresholds for ICRS grades, the optical roughness index (as a measure of surface fibrillation) and relative lesion depth (as a percentage of cartilage thickness) were calculated. However, the software was unable to detect thin, closed cracks extending into the cartilage layer, leading to an underestimation of ICRS grades. Furthermore, it was noted that the scoring system itself has limitations too. The classification of lesions in only four grades may be relatively straightforward but it can lead to inaccuracies due to intra-grade differences; meaning that absolute differences in lesion depth may be less between two successive grades than within the same grade or vice versa. This could lead to over- or underestimations of lesion development in the course of an evaluation period.

## Quantitative evaluation of cartilage properties based on OCT and US imaging

To improve the visual evaluation-based diagnosis of chondral defects and early signs of cartilage degeneration, methods to obtain more quantitative information through processing of OCT data were investigated in chapters 4 and 5. Quantitative OCT parameters introduced in literature<sup>4,10,11</sup> for the evaluation of articular cartilage include surface reflection and roughness parameters, and homogeneity, attenuation and backscattering indices. The possibility to accurately measure cartilage thickness based on OCT images was previously shown in rabbit and goat cartilage.<sup>12,13</sup> In **chapter 4**, we confirmed that OCT images derived from the system used in our studies (ILUMIEN PCI Optimisation System, Abbott, Chicago, Illinois, USA) can be used to accurately measure thickness of articular cartilage (particularly the non-calcified layer) in the equine metacarpophalangeal joint up to 1.8 mm. By combining OCT thickness and US time-of-flight measurements, we determined speed of sound (SOS) in cartilage with chondral defects of various degrees of severity. The speed of US is lower in osteoarthritic cartilage than in healthy cartilage.<sup>14</sup> Consequently, reduced SOS in articular cartilage could serve as a quantitative indicator of early and local cartilage degeneration. However, in our study no statistically significant dependence was found between SOS and the structural (i.e. collagen fibril orientation and parallelism index), compositional (i.e. collagen and proteoglycan contents) or mechanical properties (i.e. fibril network modulus, non-fibrillar matrix modulus and permeability) of the cartilage. Although the concept of simultaneous OCT and US imaging for SOS measurements in cartilage samples appeared feasible, measurement inaccuracies and the lack of statistically significant dependences between SOS and cartilage properties make the combination unsuitability for clinical use.

Optical coherence tomography imaging is based on the measurement of light that is backscattered and reflected from the different layers of the tissue that is investigated. The intensity of this signal depends on the light attenuation in the tissue and the amount of light scattering that is directed to the detector. Changes in the composition and structure of cartilage, could thus lead to changes in attenuation and back-scattering properties. In **chapter 5**, we showed that full thickness attenuation and backscattering parameters determined from the OCT signal were not linearly correlated with structural or compositional changes in articular cartilage. Similarly, Nebelung et al. stated that signal attenuation was not capable of differentiating between various cartilage degeneration stages.<sup>11</sup> Instead, we developed multivariate partial least square regression (PLSR) models to estimate cartilage properties based on depth-dependent (i.e. superficial zone, middle zone, deep zone) as well as the full thickness OCT attenuation and backscattering parameters. These models

showed high correlations between the measured and predicted microscopic scores, permeability, and full thickness optical density as well as optical density at different depths. A good correlation was found between predicted and measured collagen orientation in cartilage.

### **Optical coherence tomography: benefits and limitations**

Taken together, the advantages of OCT imaging include high-resolution real-time visualization of small morphological changes within articular cartilage. The catheters used in our studies fit through normal arthroscopic portals and, given their small size (diameter = 0.9 mm), even reached areas that are not accessible with conventional arthroscopy (chapter 2). Optical coherence tomography was found to enable accurate measurements of cartilage thickness and lesion depth. In addition, multivariate analysis of depth-wise OCT attenuation and backscattering parameters provided information on cartilage compositional, structural and mechanical properties. Further refinement of OCT-based evaluation of articular cartilage could be achieved with e.g. three-dimensional surface profiling.<sup>15,16</sup>

In the studies described in chapters 2-5, we used metacarpophalangeal joints of adult horses. The articular cartilage layer of this joint typically had a thickness of around 1 mm at the proximal surface of the first phalanx and 0.8 mm at the distal surface of the third metacarpal bone. In most human joints and also in some other equine joints such as the femoropatellar and femorotibial joints, the thickness of the articular cartilage layer exceeds the maximum imaging depth of OCT (1.5–2 mm). This limits visualization of thicker cartilage to the more superficial layers, making proper classification of cartilage lesions more challenging. Simultaneous use of arthroscopic OCT and US could be a solution for this short coming.<sup>4</sup> Ultrasound has a higher penetration depth and therefore also enables subchondral bone evaluation while OCT benefits from superior resolution enabling automatic evaluation of lesion severity. In a recent study, multiple modalities (arthroscopic US, OCT and indentation) were used simultaneously for ICRS-scoring of chondral defects.<sup>17</sup> None of the techniques were found to be clearly superior but compared with lesion severity that was scored based on light microscopic images (as the gold standard), US showed a lower reliability than OCT and conventional arthroscopy. Arthroscopic indentation could provide quantitative real-time information on the biomechanical quality of the cartilage, but measurements performed with the device (Artscan 200®) that was used in the study by Sarin et al. appeared to be time-consuming and prone to errors due to non-perpendicular alignment of the indenter with the articular surface.

## Quantitative monitoring of cartilage and bone with arthroscopic NIRS

Another optical technique that has shown its potential for quick and quantitative evaluation of articular tissues is NIRS.<sup>6,18</sup> Near infrared spectra have been shown to correlate with compositional and functional properties of cartilage as well as with cartilage thickness and severity of cartilage defects.<sup>19–21</sup> In **chapter 6**, a novel arthroscopic NIRS probe was introduced for the determination of articular cartilage and subchondral bone properties *in vivo*. In contrast to OCT, NIRS does not produce images. Instead, the scattered and reflected light from the tissue that is investigated, is collected and transmitted to a spectrometer that finally displays the signal as an absorbance spectrum. We investigated the potential of arthroscopic NIRS to simultaneously monitor progressive degeneration of cartilage and subchondral bone *in vivo*. Recently, artificial neural networks (ANN) combined with variable-selection methods were introduced for analysis of cartilage spectral data.<sup>22</sup> This technique showed potential for evaluation of tissue properties and enhanced prediction performance compared to PLSR techniques. Therefore, ANN were used for prediction of tissue properties of articular cartilage based on both *in vivo* NIRS arthroscopy in Shetland ponies that were undergoing experimental cartilage repair procedures and *ex vivo* NIRS measurements of the same articular tissues that were harvested after euthanasia at the end of the cartilage repair study. The model performance was optimized by a variable selection technique that determined the most relevant wavelengths for each cartilage and bone parameter.

Significant degenerative changes were observed in cartilage biomechanical properties adjacent to the defect, in subchondral plate bone volume fraction (BV), and in bone mineral density (BMD), when compared with healthy control joints. From *in vitro* spectral data, ANN enabled reliable estimation of the following parameters: articular cartilage biomechanical properties, subchondral bone plate thickness and BMD, and subchondral trabecular bone thickness, BV, BMD, and structure model index. Although the performance of arthroscopic predictions (i.e. *in vivo* measurements) was inferior to the predictions based on *in vitro* measurements, discrimination between healthy and post-traumatic tissue was still possible. This makes NIRS a promising technique for *in vivo* assessment of both articular cartilage and subchondral bone properties. To further improve the prediction performance, ANN sub-models could be developed based on the characterization of lesion severity and subsequent categorization.<sup>22</sup> Because NIRS cannot measure the absence of tissue (e.g. lesion size or depth), a combination of NIRS with a high-resolution imaging technique like OCT would be preferable.

Current limitations of the technique include the difficulty of maintaining perfect contact of the NIRS probe with the, often curved, cartilage surface during in vivo arthroscopy. Also, the conventional arthroscope light source was found to interfere in the visible spectral region, limiting the spectral range that could be used for the NIR region (0.75–1.90  $\mu\text{m}$ ). These issues might have contributed to the less reliable predictions based on spectra collected during in vivo arthroscopies and need further optimization. This emphasizes the importance of the step from ex vivo to in vivo testing and stressed the need for optimization of new diagnostic techniques prior to clinical implementation. In the carpal groove model described in chapter 7 (part II), both OCT and NIRS were used as in vivo monitoring tools.

## PART II – DOOMED OR DIE-HARD?

### The impact of subtle cartilage defects in the carpal joint

Longitudinal data on the progress of chondral lesions and their effect on joint homeostasis is limited. In **chapter 7** we evaluated the long-term progression of artificially created blunt and sharp grooves and their effect on other joint components in the equine carpal joint. Multiple modalities (including OCT, NIRS, radiography and optical motion capture) were used to monitor changes at a structural, compositional and functional level in vivo. Post-mortem analyses of tissues harvested at 39 weeks after the initial surgery included macroscopic and microscopic evaluation,  $\mu\text{CT}$ -based analysis of cartilage thickness and subchondral bone parameters, and mechanical indentation testing of cartilage stiffness. Both blunt and sharp cartilage trauma in combination with a period of intensified loading (i.e. horse walker and treadmill training), were found to cause degenerative changes to the adjacent area over the 9-month follow-up period. Only in two ponies, minor defect filling with fibro-cartilage-like tissue was observed in some histology sections. This confirmed what we have known for centuries: articular cartilage does not regenerate.<sup>23</sup> We showed that even the smallest lesions are not repaired. Instead, cartilage damage always leads to pathological changes within the microenvironment of the lesion. Microscopic observations and biomechanical data showed that the reaction of the tissue adjacent to the defect may vary dependent on the characteristics of the lesion. We hypothesized that it is the combination of the size, the degree of matrix disruption, and the direction of the defect (perpendicular to or at an angle with the surface) in relation to the degree and direction of loading that will determine the deformation of the tissue and hence the aggravation of the damage over time.

The effect of cartilage grooves on joint homeostasis as reflected by gene expression levels in the synovium and by a panel of biomarkers in the synovial fluid was minimal. Synovium from grooved joints revealed significantly increasing expression levels of IL-6, CCL2 and ALK5 and an increased CPII/C2C ratio was measured in synovial fluid from blunt-grooved joints at week 35. Other changes that were found in the course of the study were predominantly bilateral. Quantitative gait analysis indicated a mildly progressive bilateral lameness. Radiographic scores at week 38 were only significantly increased in grooved joints but, the contra-lateral control joints at that point also showed radiographic presence of osteophytes, enthesiophytes, and soft tissue swelling. Furthermore, a slightly increasing trend in synovium scores, and a gradual increase in total nucleated cell counts were found in both grooved and control joints. We related these findings to the repetitive trauma of the joint capsule and synovial membrane, induced by arthrocentesis, surgeries, and serial synovial biopsies of both grooved and control joints. This was considered one of the limitations of the study as it may have minimized the differences between grooved and control joints: subtle differences due to cartilage damage, may have been overshadowed by inflammatory responses. On the other hand, it underlines the importance of sham-operation effects and prevented certain changes from being undeservedly attributed to cartilage damage.

We proposed the use of higher sensitivity techniques, such as 'omics' methods, to compile more extensive profiles of synovial tissues. These techniques may be able to pick up changes that did not come to light with the methods that were currently used. However, it might well be that 9 months were not enough for chondral grooves to induce measurable changes in joint homeostasis, which would be in line with the well-known time lag (of sometimes decades) that often exists between initial cartilage damage and the manifestation of clinical OA. The minimal effects that were found may imply that chondral defects are not too important as long as they do not disturb the homeostatic balance of the joint and as long as the biomechanical function of the cartilage remains sufficient. As such, it may seem more relevant to focus research efforts on factors that determine the clinical manifestation of OA, with pain being the leading actor. On the other hand, cartilage damage is irreversible and always to a certain extent progressive, depending on e.g. size and morphology of the lesion in combination with the loading profile. Lesion progress might be slow, but it is inevitable. This means that, at some point, defects will become clinically important. Therefore, techniques that can reduce this progression and permit prolonged functioning with deteriorated cartilage may certainly have a great health impact if they can postpone the moment when arthroplasty (in human medicine) or arthrodesis or even euthanasia (in equine medicine) is the only option.



## **The inextricable interrelation between exercise and joint (t)issues**

In **chapter 8**, we concluded that exercise (i.e. biomechanical loading) has a major influence on the delicate homeostatic balance within and between the various joint components. When contemplating the time-related changes that were observed in the course of the carpal groove model (chapter 7), the role of the training period should thus be noted. In chapter 8, three mechanisms by which exercise can influence joint homeostasis were distinguished. These mechanisms could help in reflecting on the role of exercise in the carpal groove model.

First of all, exercise has a direct effect on articular tissue integrity. The purpose of the training regimen in the groove model study was not to be detrimental in itself, but to exacerbate the progress of cartilage degeneration in grooved joints via this mechanism.

Secondly, exercise can modulate the metabolism in articular tissues by activating signal transduction pathways that translate mechanical stimulation into biochemical signals. This mechanism has been shown to be of particular importance in juvenile articular cartilage.<sup>24</sup> Although the response in mature cartilage is limited, adaptation in terms of cartilage oligomeric matrix protein<sup>25</sup> and proteoglycan synthesis<sup>26</sup> have been reported in young adults too. Furthermore, subchondral bone in mature equine joints tended to increase in thickness and density under the influence of loading.<sup>27</sup> We suggested that the combination of direct and indirect effects of loading could explain the variation in tissue responses between blunt and sharp-grooved cartilage (chapter 7). With respect to the adaptive response of the subchondral bone to exercise, increasing subchondral bone thickness and density may have influenced the NIRS measurements and as such affected the predictions of cartilage thickness over time. However, further in-depth analysis of the data obtained during the follow-up surgeries is required to confirm this theory.

Following up on this, the question whether the exercise program could have actually stimulated a reparative response rather than exaggerated the induced trauma is warranted. However, based on previous studies that evaluated the potential beneficial effect of exercise on repair of (osteo)chondral defects in the equine carpal joint, it is not likely that the latter was the case.<sup>28,29</sup> Vice versa, the presence of joint pathology might change the effects of exercise. Cartilage defects can alter the stress distribution in the joint<sup>30,31</sup> and, even as synovial proliferation, they can affect the magnitude of shear forces.<sup>32</sup> Furthermore, it has been shown that cellular responses of chondrocytes derived from osteoarthritic cartilage are different from those of cells from normal cartilage.<sup>33</sup> This suggests that the effect of exercise on

joint homeostasis may have been slightly different in grooved joints compared with sham-operated control joints. If, and to what extent the exercise has contributed to the small differences that were found between grooved and sham-operated joints is hard to say at this stage and would require further investigation.

The third mechanism that plays a major role in the maintenance of joint homeostasis is that of joint circulation. In effused joints and joints with reduced joint capsule compliance due to traumatic synovitis/capsulitis, blood flow might be compromised by modest elevations in intra-articular pressure induced by exercise.<sup>34</sup> Repetitive joint procedures as performed in chapter 7, likely contribute to soft tissue swelling and may result in increased stiffness of the joint capsule due to fibrosis in the chronic stage. This, in combination with exercise may thus have significantly contributed to the changes that were observed over time in both grooved and control joints.

Taken together, the 8-week training period made the interpretation of our results more complicated. The question may be if this was actually necessary. Particularly when considering that for the canine groove model, intensified loading was found not to be required for the development of osteoarthritic changes.<sup>35</sup> However, the same study also showed that intensified loading did slightly exacerbate cartilage degeneration (based on histology) over a 20 week-period. Furthermore, we assumed that the addition of a training regimen would contribute to a better representation of the real-life situation, where training is continued despite the presence of (unnoticed) cartilage defects as long as they remain clinically silent.

## GENERAL CONCLUSIONS

The studies included in this thesis aimed at the improvement of arthroscopic diagnosis of subtle focal cartilage defects, and at the evaluation of the impact of such defects on joint homeostasis and function in the horse. Based on our studies it can be concluded that, irrespective of the size of the defect, cartilage damage does not heal but always leads to some degree of degeneration within the surrounding tissue. The response of the tissue adjacent to the defect was shown to be dependent on the lesion morphology and varied slightly between individuals. The impact of focal cartilage defects on overall joint health was limited. However, cartilage damage is irreversible and progression inevitable; meaning that cartilage damage will ultimately become manifest clinically. Therefore, quantification of cartilage defects is still important in order to predict their long-term progress and to be able to develop tailored, evidence-based repair strategies. To this end, the arthroscopy-guided use of OCT and NIRS was shown to be of high potential in equine metacarpophalangeal, carpal, and stifle joints. High-resolution imaging of cartilage lesions and prediction of the surrounding cartilage properties based on a combination of intra-articular OCT and NIRS can accurately assess the severity of damage and the degree of tissue degeneration extending from an injury during arthroscopy. Especially at early phases of degeneration, this could help in determining the need for any intervention and, if so, what treatment would carry the best prognosis. Because this information can be obtained during conventional arthroscopic procedures, its value is not limited to diagnostic goals, but makes it also appropriate for guidance of surgical interventions, in vivo monitoring, and evaluation after cartilage repair procedures. Although this thesis focused on the horse as the target patient, these techniques are similarly applicable to the human joint. Furthermore, the resemblance between the articular cartilage as well as the etiological background of OA, makes the comprehensive data on structural, compositional and functional changes in the various joint components in response to cartilage damage in this work not only of interest for equine but also for human medicine. Apart from its translational value, this data could be highly valuable for the validation of comprehensive in vitro models aiming at representing the complex joint (patho)physiology, as well as for computational models aiming at prediction of the progression of focal defects under biomechanical loading, and subsequent development of post-traumatic OA. Both approaches will contribute to further reduction and replacement of animal experiments and eventually to the breakthroughs that are needed for life-long preservation of well-functioning joints in horses and humans.

## REFERENCES

1. Spahn G, Klinger HM, Baums M, Pinkepank U, Hofmann GO. Reliability in arthroscopic grading of cartilage lesions: results of a prospective blinded study for evaluation of inter-observer reliability. *Arch Orthop Trauma Surg.* 2011;131(3):377-381.
2. Siston RA, Geier D, Bishop JY, et al. The high variability in sizing knee cartilage defects. *J Bone Joint Surg Am.* 2013;95(1):70-75.
3. Kaleva E, Virén T, Saarakkala S, et al. Arthroscopic Ultrasound Assessment of Articular Cartilage in the Human Knee Joint. *Cartilage.* 2011;2(3):246-253.
4. Virén T, Huang YP, Saarakkala S, et al. Comparison of ultrasound and optical coherence tomography techniques for evaluation of integrity of spontaneously repaired horse cartilage. *J Med Eng Technol.* 2012;36(3):185-192.
5. Chu CR, Lin D, Geisler JL, Chu CT, Fu FH, Pan Y. Arthroscopic microscopy of articular cartilage using optical coherence tomography. *Am J Sports Med.* 2004;32(3):699-709.
6. Spahn G, Plettenberg H, Kahl E, Klinger HM, Muckley T, Hofmann GO. Near-infrared (NIR) spectroscopy. A new method for arthroscopic evaluation of low grade degenerated cartilage lesions. Results of a pilot study. *BMC Musculoskelet Disord.* 2007;8:47.
7. Fercher AF. Optical coherence tomography - development, principles, applications. *Z Med Phys.* 2010;20(4):251-276.
8. Spahn G, Klinger HM, Baums M, Pinkepank U, Hofmann GO. Reliability in arthroscopic grading of cartilage lesions: results of a prospective blinded study for evaluation of inter-observer reliability. *Arch Orthop Trauma Surg.* 2011;131(3):377-381.
9. Niemelä T, Virén T, Liukkonen J, et al. Application of optical coherence tomography enhances reproducibility of arthroscopic evaluation of equine joints. *Acta Vet Scand.* 2014;56(3):1-8.
10. Saarakkala S, Wang SZ, Huang YP, Zheng YP. Quantification of the optical surface reflection and surface roughness of articular cartilage using optical coherence tomography. *Phys Med Biol.* 2009;54(22):6837-6852.
11. Nebelung S, Marx U, Brill N, et al. Morphometric grading of osteoarthritis by optical coherence tomography - An ex vivo study. *J Orthop Res.* 2014;32(10):1381-1388.
12. Rogowska J, Bryant CM, Brezinski ME. Cartilage thickness measurements from optical coherence tomography. *J Opt Soc Am Opt Image Sci Vis.* 2003;20(2):357-367.
13. Cernohorsky P, Kok AC, Bruin DM de, et al. Comparison of optical coherence tomography and histopathology in quantitative assessment of goat talus articular cartilage. *Acta Orthop.* 2015;86(2):257-263.
14. Myers SL, Dines K, Brandt DA, Brandt KD, Albrecht ME. Experimental assessment by high frequency ultrasound of articular cartilage thickness and osteoarthritic changes. *J Rheumatol.* 1995;22(1):109-116.
15. Nebelung S, Brill N, Marx U, et al. Three-dimensional imaging and analysis of human cartilage degeneration using Optical Coherence Tomography. *J Orthop Res.* 2015;33(5):651-659.
16. Brill N, Riedel J, Schmitt R, et al. 3D Human cartilage surface characterization by optical coherence tomography. *Phys Med Biol.* 2015;60(19):7747-7762.
17. Sarin JK, Brommer H, Argüelles D, et al. Multimodality scoring of chondral injuries in the equine fetlock joint ex vivo. *Osteoarthr Cartil.* 2017;25(5):790-798.
18. Afara IO, Prasadam I, Crawford R, Xiao Y, Oloyede A. Near infrared (NIR) absorption spectra correlates with subchondral bone micro-CT parameters in osteoarthritic rat models. *Bone.* 2013;53(2):350-357.

19. Afara IO, Hauta-Kasari M, Jurvelin JS, Oloyede A, Töyräs J. Optical absorption spectra of human articular cartilage correlate with biomechanical properties, histological score and biochemical composition. *Physiol Meas.* 2015;36(9):1913-1928.
20. Spahn G, Plettenberg H, Nagel H, et al. Evaluation of cartilage defects with near-infrared spectroscopy (NIR): an ex vivo study. *Med Eng Phys.* 2008;30(3):285-292.
21. Sarin JK, Amissah M, Brommer H, Argüelles D, Töyräs J, Afara IO. Near Infrared Spectroscopic Mapping of Functional Properties of Equine Articular Cartilage. *Ann Biomed Eng.* 2016;44(11):3335-3345.
22. Sarin JK, Rieppo L, Brommer H, Afara IO, Saarakkala S, Töyräs J. Combination of optical coherence tomography and near infrared spectroscopy enhances determination of articular cartilage composition and structure. *Sci Rep.* 2017;7(1):10586.
23. Hunter W. On the structure and diseases of articulation cartilage. *Philos Trans R Soc L.* 1743;9(267):514-521.
24. Barneveld A, van Weeren PR. Conclusions regarding the influence of exercise on the development of the equine musculoskeletal system with special reference to osteochondrosis. *Equine Vet J Suppl.* 1999;(31):112-119.
25. Skiölddebrand E, Ekman S, Heinegård D, Hultenby K. Ultrastructural immunolocalization of cartilage oligomeric matrix protein (COMP) in the articular cartilage on the equine third carpal bone in trained and untrained horses. *Res Vet Sci.* 2010;88(2):251-257.
26. Murray RC, Birch HL, Lakhani K, Goodship AE. Biochemical composition of equine carpal articular cartilage is influenced by short-term exercise in a site-specific manner. *Osteoarthr Cartil.* 2001;9(7):625-632.
27. Firth EC, Delahunt J, Wichtel JW, Birch HL, Goodship AE. Galloping exercise induces regional changes in bone density within the third and radial carpal bones of Thoroughbred horses. *Equine Vet J.* 1999;31(2):111-115.
28. Barr AR, Wotton SF, Dow SM, Waterman AE, Goodship AE, Duance VC. Effect of central or marginal location and post-operative exercise on the healing of osteochondral defects in the equine carpus. *Equine Vet J.* 1994;26(1):33-39.
29. French DA, Barber SM, Leach DH, Doige CE. The effect of exercise on the healing of articular cartilage defects in the equine carpus. *Vet Surg.* 1989;18(4):312-321.
30. Gratz KR, Wong BL, Bae WC, Sah RL. The effects of focal articular defects on intra-tissue strains in the surrounding and opposing cartilage. *Biorheology.* 2008;45(3-4):193-207.
31. Komeili A, Chau W, Herzog W. Effects of macro-cracks on the load bearing capacity of articular cartilage. *Biomech Model Mechanobiol.* April 2019.
32. Schett G, Tohidast-Akrad M, Steiner G, Smolen J. The stressed synovium. *Arthritis Res.* 2001;3(2):80-86.
33. Millward-Sadler SJ, Salter DM. Integrin-dependent signal cascades in chondrocyte mechanotransduction. *Ann Biomed Eng.* 2004;32(3):435-446.
34. James MJ, Cleland LG, Rofe AM, Leslie AL. Intraarticular pressure and the relationship between synovial perfusion and metabolic demand. *J Rheumatol.* 1990;17(4):521-527.
35. Vos P, Interma F, van El B, et al. Does loading influence the severity of cartilage degeneration in the canine Groove-model of OA? *J Orthop Res.* 2009;27(10):1332-1338.



# ADDENDUM

Nederlandse samenvatting (Summary in Dutch)

Dankwoord (Acknowledgements)

List of publications

Curriculum Vitae

---

## NEDERLANDSE SAMENVATTING (SUMMARY IN DUTCH)

Synoviale gewrichten faciliteren de beweging van het ene bot ten opzichte van een ander en zijn daarmee de spil van het bewegingsapparaat bij alle vertebraten. Het paard wordt al sinds jaar en dag gehouden vanwege zijn atletische kwaliteiten en kracht. Vroeger voor oorlog, transport en landbouw. Tegenwoordig voor hobby en sport. De nadruk ligt dus op de fysieke belastbaarheid en daarom worden hoge eisen gesteld aan het bewegingsapparaat van het paard. Om met die belasting om te kunnen gaan, zijn goed functionerende gewrichten van vitaal belang en in de praktijk niet zelden zelfs een kwestie van leven of dood.

Het synoviale gewricht is een ingewikkeld orgaan dat bestaat uit verschillende onderdelen, waaronder het gewrichtskraakbeen, het gewrichtskapsel (met aan de binnenzijde het synoviaalmembraan), de synoviale vloeistof en het subchondrale bot (fig. 1). In een gezond gewricht wordt een dynamisch evenwicht in stand gehouden tussen cellulaire processen binnen al deze componenten en tussen de componenten onderling; de gewrichtshomeostase. Echter, een verstoring van die gewrichtshomeostase kan leiden tot gewrichtsziekten zoals artrose.

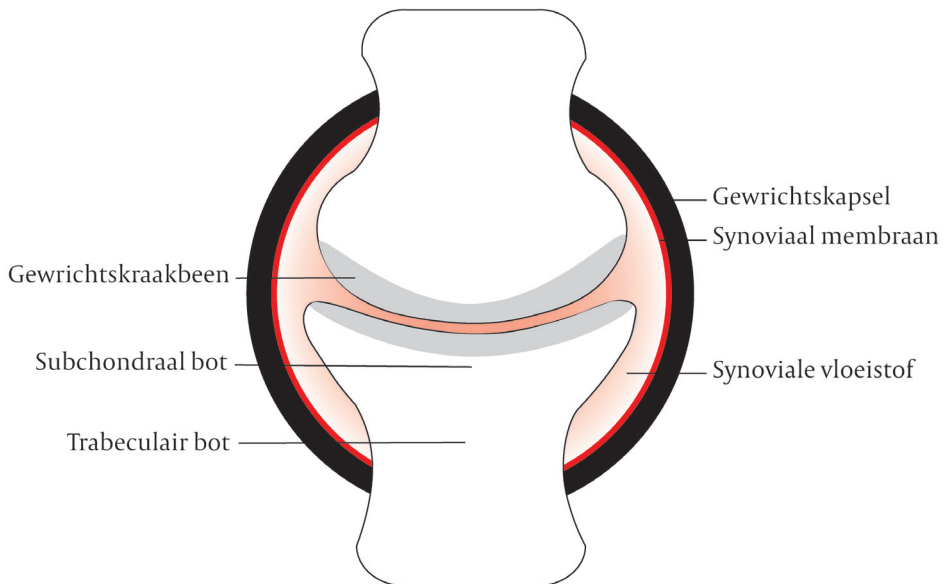


Fig. 1 Schematische representatie van een synoviaal gewricht



Artrose wordt gekenmerkt door de progressieve afbraak van het gewrichtskraakbeen, vergezeld door pathologische veranderingen in andere gewrichtsweefsels zoals remodellering van bot, synovitis en veranderingen in de samenstelling en het volume van de gewrichtsvloeistof. Dit leidt uiteindelijk tot pijnlijke, gezwollen en stijve gewrichten. Artrose is een groot probleem in zowel de humane als de paardengezondheidszorg en naast dat de exacte oorzaak nog grotendeels onduidelijk is, is er tot op heden ook geen effectieve therapie beschikbaar.

Doordat artrose zich vaak langzaam ontwikkelt, is het moeilijk om de precieze relatie te onderzoeken tussen potentiële risicofactoren en de processen die op de langere termijn tot artrose leiden. Met name lokale kraakbeendefecten, die vaak worden gevonden tijdens arthroscopisch onderzoek bij zowel paarden als mensen, zijn onderwerp van de discussie of ze moeten worden behandeld en zo ja, wanneer en hoe? De huidige klinische beoordeling van deze letsels is met name gebaseerd op de subjectieve interpretatie van het arthroscopische onderzoek; een situatie die betrouwbare prognoses en wetenschappelijke onderbouwde therapiekeuzes beperkt. Voor zowel klinische doeleinden als onderzoeksdoeleinden zou het dus van grote toegevoegde waarde zijn om de eigenschappen van kraakbeendefecten en de conditie van het omliggende kraakbeen accurater en objectiever in te kunnen schatten.

Om dat te bereiken, zijn in de afgelopen decennia verschillende intra-articulaire beeldvormende en niet-beeldvormende technieken geïntroduceerd, waaronder ultrageluid (echografie), optische coherentie tomografie (OCT) en nabij-infrarood spectroscopie (NIRS). Het eerste doel van dit proefschrift was te onderzoeken of deze geavanceerde technieken potentie hebben voor het verbeteren van de arthroscopische evaluatie van subtiele veranderingen in de structuur, samenstelling en biomechanische eigenschappen van het kraakbeen (**deel I**).

Omdat artrose een ziekte is die niet alleen het kraakbeen, maar het hele gewricht betreft, is er tevens een beter en meer kwantitatief inzicht nodig in de relatie tussen de ontwikkeling van kraakbeenletsel, gewrichtshomeostase en functionaliteit. Daarom was het tweede doel: het monitoren van de progressie van kraakbeendefecten en hun impact op het gewricht in zijn geheel, binnen het zogenaamde 'groefmodel'. Dit is een experimenteel model waarin groefjes in het gewrichtskraakbeen aangebracht worden en waarvan vervolgens de verdere ontwikkeling bestudeerd wordt, al dan niet onder invloed van een vorm van interventie zoals medicatie of chirurgie. Het groefmodel wordt in het gewrichtsonderzoek veelvuldig toegepast bij de hond en de rat. In dit proefschrift is het model bij het paard toegepast in het carpale gewricht (de

“voorknie” in paardentermen) en wordt verder aangeduid als het ‘carpale groefmodel’ (**deel II**). Hierbij zijn veranderingen in de verschillende gewrichtscomponenten zowel in vivo als ex vivo gemonitord op het niveau van structuur, samenstelling en functie met behulp van verschillende modaliteiten.

Omdat biomechanische belasting van het gewricht van belang is voor het behoud van een gezond gewricht, maar aan de andere kant ook gerelateerd is aan progressieve afbraak van gewrichtskraakbeen, bespreekt het laatste hoofdstuk de relatie tussen fysieke training en gewrichtshomeostase bij het paard.

## **DEEL I – REFLECTEREN OP GEWRICHTSKRAAKBEEN**

### **Kwantitatieve karakterisering van kraakbeenletsels op basis van intra-articulaire OCT-beelden**

In **hoofdstuk 2** hebben we bepaald of OCT een effectieve methode is voor het verbeteren van de diagnostiek van letsels in paardenkraakbeen tijdens arthroscopisch onderzoek. Door het genereren van dwarsdoorsnede-beelden met een hoge resolutie, konden met OCT-artroscopie verschillende soorten letsels getypeerd worden. Ook abnormaliteiten onder het oppervlak die met conventionele artroscopie niet zichtbaar waren, werden nu herkend. De beelden maakten het tevens mogelijk om de dikte van het kraakbeen te bepalen, en om de diepte van letsels te scoren volgens het systeem van de International Cartilage Repair Society (ICRS).

Naast dat letsels beter werden gekarakteriseerd, hebben we ook aangetoond dat ICRS-scores tussen en binnen waarnemers beter overeenkomen wanneer gescoord wordt op basis van OCT-beelden in plaats van conventionele artroscopie beelden (**hoofdstuk 3**). Echter, deze visuele beoordeling blijft subjectief. Daarom introduceerden we een softwarepakket waarmee kraakbeenletsels in OCT-beelden op semi-geautomatiseerde wijze gescoord kunnen worden volgens het ICRS-scoresysteem.

### **Kwantitatieve evaluatie van kraakbeeneigenschappen op basis van OCT en echografische beeldvorming**

Om de puur visuele diagnostiek van kraakbeendefecten en vroege kraakbeendegeneratie te verbeteren, onderzochten we in **hoofdstuk 4 en 5** methoden om meer kwantitatieve informatie te verkrijgen door het nader analyseren van OCT-data en door OCT te combineren met echografie. In eerder onderzoek is aangetoond dat de snelheid van ultrageluid in artrotisch kraakbeen lager is dan in gezond kraakbeen.

Daarom kan een afgenomen geluidssnelheid in gewrichtskraakbeen dienen als een kwantitatieve indicator van vroege en lokale kraakbeendegeneratie. Door de dikte, gemeten met OCT, te combineren met de tijd die een geluidsgolf nodig heeft om door het kraakbeen te reizen, konden we de geluidssnelheid in kraakbeen met defecten van verschillende gradaties meten. Hoewel het concept van gelijktijdige OCT en echografie voor het meten van geluidssnelheid in kraakbeen mogelijk bleek, maakten onnauwkeurigheden en het gebrek aan een statistisch significante afhankelijkheid tussen geluidssnelheid en kraakbeeneigenschappen, deze combinatie ongeschikt voor klinisch gebruik (**hoofdstuk 4**).

OCT-beeldvorming is gebaseerd op het meten van licht dat wordt verstrooid en gereflecteerd door de verschillende lagen van het weefsel. De intensiteit van het signaal hangt dus af van de verzwakking van het licht in het weefsel en de hoeveelheid verstrooid licht dat terugkomt op de detector. Hierdoor kunnen veranderingen in de samenstelling en structuur van kraakbeen leiden tot een ander OCT-signaal. In **hoofdstuk 5** hebben we laten zien dat, met behulp van speciale multivariabele regressie-modellen, kraakbeeneigenschappen inderdaad kunnen worden ingeschat op basis van verzwakkings- en verstrooiingsparameters gemeten in zowel de volledige kraakbeenlaag als in verschillende sublagen.

## **Kwantitatieve monitoring van kraakbeen en bot met arthroscopische NIRS**

Een andere optische techniek met potentie voor snelle en kwantitatieve evaluatie van gewrichtsweefsels, is NIRS. In **hoofdstuk 6** werd een nieuwe arthroscopische NIRS-sonde geïntroduceerd. In tegenstelling tot OCT, produceert NIRS geen beelden maar absorptiespectra. We onderzochten of arthroscopische NIRS de potentie heeft om tegelijkertijd zowel progressieve kraakbeendegeneratie, als het subchondrale bot in vivo te monitoren. Hiervoor werden NIRS-metingen gedaan bij Shetlandpony's die een experimentele kraakbeentherapie ondergingen (in vivo), en waarbij vervolgens hetzelfde kraakbeen en bot, afgenomen na euthanasie aan het einde van dat onderzoek, gemeten werd (ex vivo).

Artificiële Neurale Netwerken (ANNs) maakten het mogelijk om, op basis van in vitro gegenereerde spectra, een betrouwbare schatting te doen van verschillende kraakbeen- en botparameters. Hoewel de voorspellingen op basis van arthroscopische metingen in vivo minder goed waren dan de voorspellingen gebaseerd op de in vitro metingen, konden ze nog steeds onderscheid maken tussen gezonde en post-traumatische weefsels. Dit maakt NIRS een veelbelovende techniek voor in vivo onderzoek van zowel gewrichtskraakbeen als subchondraal bot. Omdat NIRS niet

de afwezigheid van weefsel kan meten (bijvoorbeeld letselgrootte of -diepte), zou een combinatie van NIRS met een beeldvormende techniek met hoge resolutie, zoals OCT, wenselijk zijn. In het carpale groefmodel, beschreven in hoofdstuk 7 (deel II), werden zowel OCT als NIRS gebruikt voor in vivo monitoring.

## DEEL II – GEDOEMD OF DIEHARD?

### De impact van subtiele kraakbeendefecten op het carpaalgewricht

Longitudinale gegevens met betrekking tot de progressie van kraakbeenletsels en hun effect op de gewrichtshomeostase zijn maar uiterst beperkt beschikbaar in de literatuur. In **hoofdstuk 7** evalueerden we de langetermijnprogressie van kunstmatige ‘stompe’ en ‘scherpe’ groeven in het kraakbeen en hun effect op andere gewrichtscomponenten in het carpaalgewricht van het paard. In dit model werden, in een gestandaardiseerd patroon, via een arrotomie groeven gecreëerd in het kraakbeen van het radiocarpale en het intercarpale gewricht. De controlegewrichten aan de contralaterale zijde werden wel geopend, maar hier werd het kraakbeen intact gelaten. Verschillende modaliteiten (waaronder OCT, NIRS, röntgen, kwantitatieve bewegingsanalyse en qPCR) werden gebruikt om gedurende 9 maanden veranderingen te monitoren op het niveau van structuur, samenstelling en functie. Na 9 maanden werden de pony's geëuthanaseerd zodat alle verschillende gewrichtsweefsels konden worden afgenomen voor verder onderzoek. Post-mortem analyses van het weefsel betroffen: macroscopische en microscopische evaluatie, analyse van kraakbeendikte en botparameters op basis van micro-CT, en biomechanische testen van het kraakbeen.

Zowel stomp als scherp kraakbeentrauma, in combinatie met een periode van verhoogde belasting (d.w.z. stapmolen en loopbandtraining gedurende 8 weken), bleken degeneratieve veranderingen te veroorzaken in het omliggende kraakbeen. Slechts bij twee pony's werd in enkele histologische secties een kleine opvulling van het defect met fibreus kraakbeen gevonden. Dit bevestigde wat we eigenlijk al eeuwen weten: gewrichtskraakbeen regeneert niet. We toonden aan dat zelfs de kleinste letsels niet worden gerepareerd, maar dat kraakbeenschade altijd leidt tot pathologische veranderingen in de micro-omgeving rondom het letsel. Microscopische observaties en biomechanische data lieten zien dat de reactie van het omgevende kraakbeenweefsel op het defect, afhankelijk kan zijn van de eigenschappen van dat defect. Onze hypothese is dat het de grootte, mate van matrixdisruptie en de richting van het defect (loodrecht op, of in een hoek ten opzichte van het oppervlak), in combinatie met de mate en richting van de belasting

is, die de deformatie van het weefsel en dus de verergering van de schade over de tijd bepaalt.

Het effect van de gecreëerde kraakbeenschade op de gewrichtshomeostase was minimaal. Het synoviaalmembraan van gewrichten met kraakbeengroeven, liet een significante toename zien in de genexpressieniveaus van de ontstekingsmarkers IL-6 en CCL2 en in de TGF $\beta$ 1-receptor ALK5. In de gewrichtsvloeistof van gewrichten met stompe groeven werd een toegenomen CPII/C2C ratio gemeten op week 35, suggestief voor een verhoogde turn-over van collageen type II. Andere veranderingen die in de loop van de tijd werden gevonden, waren met name bilateraal. Kwantitatieve bewegingsanalyse wees op een milde, progressieve, bilaterale kreupelheid. Röntgenscores namen weliswaar alleen significant toe in gewrichten met groeven, maar op week 38 lieten ook de contralaterale controlegewrichten vorming van botwoekeringen (osteofyten en enthesiofyten), en tevens zwelling van de weke delen zien. Verder was er beiderzijds een licht toenemende trend in histologische scores van het synoviaalmembraan (duidend op de aanwezigheid van een pathologisch proces) en een graduele toename in het aantal witte bloedcellen in de synoviale vloeistof. Deze bevindingen zijn mogelijk te relateren aan herhaald trauma van het gewrichtskapsel en het synoviaalmembraan door gewrichtspuncties, chirurgie en het herhaaldelijk nemen van biopten van het synoviaalmembraan bij zowel de gewrichten met groeven als de controlegewrichten.

Meer gevoelige technieken, zoals 'omics'-methoden, zouden gebruikt kunnen worden om een uitgebreider profiel van gewrichtsweefsels samen te stellen. Met deze technieken zou het mogelijk kunnen zijn om veranderingen te detecteren die met de huidige gebruikte methoden niet aan het licht kwamen. Echter, mogelijk was 9 maanden ook niet genoeg voor de gemaakte (relatief minimale) kraakbeenletsels om meetbare veranderingen in de gewrichtshomeostase te induceren. Dit zou in overeenstemming zijn met het bekende lange tijdsinterval, van soms wel decennia, dat vaak tussen initiële kraakbeenschade en de klinische manifestatie van artrose ligt. De minimale effecten die werden gevonden, impliceren mogelijk dat kraakbeendefecten klinisch gezien niet al te belangrijk zijn, zolang ze de balans in het gewricht niet verstoren en zolang de biomechanische functie van het kraakbeen voldoende blijft. Aan de andere kant; kraakbeenschade is irreversibel en altijd in bepaalde mate progressief, afhankelijk van o.a. de grootte en morfologie van het letsel, in combinatie met de belasting van het gewricht. De progressie mag dan langzaam zijn, maar is wel onvermijdelijk. Dit betekent dat kraakbeendefecten op een bepaald moment altijd klinisch van belang zullen worden. Behandelingen die deze progressie kunnen vertragen en een duurzamere functie van aangedaan kraakbeen

mogelijk kunnen maken, zullen daarom zeker een groot effect op de gezondheid kunnen hebben. Bijvoorbeeld wanneer ze daarmee het moment kunnen uitstellen waarop vervanging door een kunstgewricht (humane geneeskunde) of het laten verstijven van het gewricht (artrodesis), of zelfs euthanasie (paardeneeskunde) de laatste optie is.

## **Het tweesnijdende zwaard van het effect van beweging op (beschadigde) gewrichten**

In **hoofdstuk 8** concludeerden we dat training (d.w.z. de daaruit voortvloeiende biomechanische belasting) een belangrijke invloed heeft op de gewrichtshomeostase. Wanneer we de veranderingen die gedurende het carpale groefmodel optraden (hoofdstuk 7) in beschouwing nemen, moet de rol van de trainingsperiode dus in overweging worden genomen. In hoofdstuk 8 onderscheiden we drie mechanismen waardoor belasting een invloed kan hebben op de gewrichtshomeostase. Deze mechanismen kunnen helpen bij het reflecteren op de rol van belasting in het carpale groefmodel.

Ten eerste heeft belasting een direct effect op de integriteit van de gewrichtsweefsels. Het doel van het trainingsregime in het groefmodel was niet om op zichzelf schadelijk te zijn, maar om de progressie van kraakbeendegeneratie in gewrichten met groeven te versnellen. Ten tweede kan belasting het metabolisme in gewrichtsweefsels beïnvloeden door signaaltransductiepaden te activeren die mechanische stimulatie omzetten in biochemische signalen. De aanwezigheid van schade kan dit positieve effect van belasting weer (in negatieve zin) beïnvloeden doordat in het beschadigde weefsel de productie van ontstekingsmediatoren gestimuleerd kan worden door belasting. Of, en in welke mate, training heeft bijgedragen aan de kleine verschillen die werden gevonden tussen gewrichten met kraakbeengroeven en controlegewrichten is in dit stadium moeilijk te zeggen en behoeft verder onderzoek. Ten derde speelt de circulatie een belangrijke rol bij het behoud van de gewrichtshomeostase. In gewrichten met effusie en een verminderde compliantie van het kapsel door traumatische synovitis of capsulitis, kan belasting de doorbloeding in gevaar brengen door kleine toenames van de intra-articulaire druk. Herhaaldelijke traumatische procedures in het gewricht zoals in **hoofdstuk 7**, kunnen resulteren in een toegenomen stijfheid van het gewrichtskapsel door fibrosering in het chronische stadium. Dit, in combinatie met training, zou dus een significante bijdrage kunnen hebben geleverd aan de veranderingen die met de tijd werden waargenomen in zowel de gewrichten met kraakbeengroeven als in de controlegewrichten.

## ALGEMENE CONCLUSIES

De onderzoeken beschreven in dit proefschrift hadden als doel om de artroskopische diagnostiek van subtiele, focale kraakbeendefecten te verbeteren en om de impact van zulke defecten op de homeostase en de functie van het paardengewricht te evalueren. Op basis van onze studies, kan worden geconcludeerd dat, onafhankelijk van de grootte van het defect, kraakbeenschade niet herstelt maar altijd tot een bepaalde mate van degeneratie in het omliggende weefsel leidt. We lieten zien dat de reactie van het weefsel rondom het defect afhankelijk lijkt te zijn van de morfologie van het letsel en dat deze reactie enigszins verschilde tussen individuen. De impact van focale kraakbeendefecten op de algehele gezondheid van het gewricht bleek beperkt. Echter, kraakbeenschade is onomkeerbaar en progressie onvermijdelijk. Dit betekent dat kraakbeenschade zich uiteindelijk klinisch zal manifesteren. Daarom is het kwantificeren van kraakbeendefecten nog steeds belangrijk om hun langetermijnprogressie te kunnen voorspellen en om de ontwikkeling van op maat gemaakte en wetenschappelijk onderbouwde therapieën mogelijk te maken.

We lieten zien dat artroscoopisch begeleide OCT en NIRS in het kootgewricht, de carpus en de knie van het paard, veel potentie hebben voor deze kwantificering. Op basis van een combinatie van intra-articulaire OCT en NIRS kan tijdens artroskopie nauwkeurig en kwantitatief de ernst van de weefseldegeneratie en de mate van uitbreiding vanuit een defect worden beoordeeld. Tevens kunnen de eigenschappen van het omliggende kraakbeen met behulp van deze technieken worden voorspeld. Met name in vroege stadia van degeneratie kan dit helpen om te bepalen of interventie nodig is en zo ja, welke behandeling de beste prognose heeft.

Omdat deze informatie verkregen kan worden tijdens conventionele artroskopische procedures, is de waarde ervan niet beperkt tot diagnostische doeleinden, maar is het ook geschikt voor het begeleiden van chirurgische interventies, monitoring en de evaluatie van kraakbeenherstelprocedures. Hoewel de focus in dit proefschrift op het paard als de patiënt ligt, zijn deze technieken op vergelijkbare wijze toe te passen in humane gewrichten. Verder maken de gelijkenis tussen zowel het gewrichtskraakbeen als de etiologische achtergrond van artrose, de uitgebreide dataset in dit werk niet alleen interessant voor de paarden- maar ook voor de humane geneeskunde. Afgezien van de translationele waarde, kunnen deze gegevens ook zeer bruikbaar zijn voor de validatie van zowel uitgebreide in vitro modellen, met als doel de complexe (patho)fysiologie van het gewricht te representeren, als computermodellen, die de progressie van focale defecten onder invloed van biomechanische belasting en de

daaropvolgende ontwikkeling van posttraumatische artrose kunnen voorspellen. Deze beide benaderingen zullen bijdragen aan verdere vermindering en vervanging van dierexperimenten en uiteindelijk aan de doorbraken die nodig zijn voor het levenslange behoud van goed functionerende gewrichten voor zowel paarden als mensen.

## Begrippenlijst:

In vivo	In het levende organisme. Hier; in het levende dier.
Ex vivo	Buiten het levende organisme. Hier; in het gewricht of gewrichtsweefsel afgenomen van het dier na overlijden.
IL-6	Interleukine-6; een eiwit dat betrokken is bij ontstekingsreacties in het lichaam.
CCL2	Chemokine (C-C motif) ligand; een eiwit dat betrokken is bij ontstekingsreacties in het lichaam.
TGFβ1	Transformerende groeifactor beta-1; een eiwit dat betrokken is bij vele processen in het lichaam waaronder weefselregeneratie, celdifferentiatie, embryonale ontwikkeling en de regulering van het immuunsysteem.
ALK5	Activin receptor-like kinase; een belangrijke receptor voor de binding van TGFβ1.
Stompe kraakbeengroeven	Groeven in het kraakbeen, gemaakt met een aangescherpte punt van een artroscopie-sonde. Deze groeven zijn duidelijk zichtbaar, hebben onregelmatige randen en worden gekenmerkt door enige mate van weefselverlies.
Scherpe kraakbeengroeven	Groeven in het kraakbeen gemaakt met een klein chirurgisch scalpel. Deze groeven zijn zeer subtiel, moeilijk zichtbaar en hebben scherp belijnde randen.



## DANKWOORD (ACKNOWLEDGEMENTS)

*“Een grote verdienste is het, te weten wanneer men klaar is.”*

*Thomas Carlyle*

En opeens is het klaar. Opluchting, trots en heel veel dankbaarheid. Dankbaarheid voor de kansen die ik heb gekregen, voor wat ik allemaal geleerd heb en vooral, voor alle bijzondere, inspirerende, behulpzame en lieve mensen die ik om me heen heb gehad, heb gekregen en nog steeds heb. Dit proefschrift is een co-productie in de breedste zin van het woord en ik wil graag eenieder die daar, groot of klein, zichtbaar of achter de schermen, aan heeft bijgedragen, bedanken.

Mijn eerste promotor en mentor: René, we vergeten beiden nooit meer het, inmiddels bijna legendarische, moment dat je me voorstelde om mijn HP-project voort te zetten in de vorm van een promotieonderzoek. Het was het begin van een samenwerking die zich door de jaren heen uitbreidde van m.n. adviseren en het reviseren van mijn wetenschappelijke schrijfsels, naar het samen uitdenken van een vierjarig onderzoeksproject, tot gesprekken over velerlei filosofische thema's, geitenmanagement en speciaalbiertjes. Ik ben een groot bewonderaar van je brede kennis, je multilingualiteit, je schrijftalent en de bescheidenheid waarmee je dat alles inzet. Ik ben je dankbaar voor je vertrouwen en interesse, je altijd snelle en constructieve feedback en voor nog meer clichés, maar nog het meest voor het begrijpen en steunen van mijn zoektocht naar de juiste dosis creatief tegenwicht in de wereld van de wetenschap.

My second promotor and Finnish guide: Juha, to me you are a shining example of a scientist in heart and soul. From the very moment I entered your lab, you taught me to be critical and concise, but also when to stop working and go horse riding. I admire your curiosity, perseverance, and efficiency. I am most grateful for the warm welcome you and Anu gave me every time I visited Kuopio, for introducing me into new experiences (I won't forget my first scuba diving lesson or the formula-1 track where I risked my life for the perfect picture), for teaching me some proper Finnish, and for updating me on the adventures of Timppa. I am looking forward to seeing you soon in Brisbane, Utrecht or Kuopio!

Door jouw recente benoeming tot hoogleraar, ben ik gezegend met maar liefst drie promotoren: Harold, bijna 8 jaar na dato kunnen we wel stellen dat jouw e-mail met de voorzichtige vraag of ik het zag zitten om midden in de winter twee maanden in Finland door te brengen voor biomechanische metingen aan kraakbeen, nogal verstrekkende gevolgen heeft gehad. Een groot deel van dit boek is het indirecte resultaat van die ene uitnodiging. Ik ben je dankbaar voor het vertrouwen dat je me destijds al gegeven hebt en voor alle steun, tips en adviezen waarvoor ik altijd bij je terecht kon. Je gaf me altijd het gevoel dat het allemaal wel zou lukken, ook wanneer het even tegen zat.

No final thesis or a defense without a committee. To all members, thank you for your time and effort.

Lieve Saskia, zonder jou was ik nog wel een paar jaar bezig geweest. Jij was (en bent) mijn wandelende lab-gids, liefvallige en altijd bereidwillige assistent, sparring-partner (of het nou gaat om de optimale label-methode of het best passende scoring-systeem), kritische vragensteller (“heb je aan een negatieve controle gedacht?”), favoriete koffie-maatje, redder in nood (“Sas, ik ben vergeten in welk kluisje ik mijn spullen heb gestopt”)... eigenlijk ben je gewoon mijn idool op de werkvloer. Ik voelde me gezegend en soms zelfs een beetje verwend met jou in het team. Dankjewel dat je altijd voor me klaar staat, je maakt een wereld van verschil.

Lieve Janny, het was moeilijk (om niet te zeggen onmogelijk) om níet te worden aangestoken door jouw enthousiasme over een HP-onderzoeksproject over kraakbeen. In feite ben jij hoofdschuldige van waar ik de afgelopen 8 jaar aan gewerkt heb... en daar ben ik je heel dankbaar voor. Niet alleen heb je me mijn ontgroeningstijd in de wetenschap doorgeholpen, ook na mijn HP-jaar was je geïnteresseerd en bereid om mee te denken. Aan jou hoef ik altijd maar half uit te leggen wat m'n probleem of idee is, en je snapt niet alleen waar het over gaat, maar weet ook altijd wel een handvat aan te reiken waardoor ik weer verder kan. Ik hoop dat we ook in de toekomst samen aan (nieuwe) projectjes kunnen blijven werken.

My dear colleagues in Finland. I would be most afraid of forgetting someone when trying to mention all of you, but to each of you I want to express my sincere gratitude. You made Kuopio feel like a second home and I am always looking forward to coming over (even during the darkest periods of the year).

Pia, thank you for being my bestie since my very first visit, for making the (sometimes late) hours in the lab more fun, for taking me out for a coffee or outdoor activity, for answering all my questions about OCT, and for being my paranymph, I feel honoured. Jaakko, thank you very much for sharing your talent and helping me out so many times; from getting the semi-automated scoring on track, taking over the OCT measurements when I was out of circulation during one of the surgery weeks, to making Matlab do in a split second what would cost me and my excel file an entire week. By the way, I don't know anyone who replies emails as efficiently as you do. Ali, you chose tough weeks to come over to Utrecht for performing the micro-CT part of the groove study: long hours and strict deadlines. Pretty stressful weeks, but it was a total pleasure to work with you and to discover our shared love for music. (I am still watching the videos of Jacob Collier's concert, from time to time.) I am looking forward to continuing our collaboration and to the results of our ongoing projects!

Alle lieve, leuke en kundige collega's van de Faculteit Diergeneeskunde: al tijdens m'n studie voelde ik me enorm thuis en het voelt als een voorrecht daar, met jullie, te mogen werken.

Filipe, ik ken geen grotere nerd die zo gezellig en behulpzaam is als jij. Ik heb grote bewondering voor wat je allemaal doet en gedaan hebt gekregen de afgelopen jaren. Het is altijd leuk om met je te sparren over onderzoeksprojectjes, R-hacks, kreupelheidscases of mixed models. Naast je PhD afronden, ben je tegenwoordig ook druk in de kliniek, maar niet vergeten om af en toe lekkere koffie en een kleine peptalk bij ons te komen halen hè! Veel succes met de laatste loodjes! Ineke, ik vind het superknap hoe snel je bent 'ingeburgerd'! Wat fijn om jou als nieuw kantoormaatje te hebben. Niet alleen omdat je er altijd voor zorgt dat er koffie in biologisch afbreekbare cupjes is, maar vooral ook omdat je het werk een stuk gezelliger maakt en altijd bereid bent te helpen (of het nu om een PCA-plot of het naaien van een proteoglycaan-danskostuum gaat), dankjewel daarvoor. Maria, my big sister. I admire what you do and how you do it. Thank you for listening, for your advice, for sharing your view of the world and the nice pizza-evenings. All other colleagues from the Centaur group, Nicoline, Chris, Irina, Laura, Lotte, Kelly, Paweena, thank you for your intellectual input and your support.

Marianna, dankjewel voor je oprechte interesse, voor je advies en voor het plaatsnemen in mijn commissie. Michelle, wat doe je toch veel en knappe dingen; ik raak altijd geïnspireerd van je ideeën. Enne, ons hyaluronzuurprojectje krijgt nog wel een vervolg.

Hanneke, Tijn en Mathijs, bedankt voor jullie interesse in mij en mijn onderzoek. Het was fijn te kunnen delen in zowel onderzoeksideeën als -perikelen. Ik heb veel bewondering voor hoe jullie dat combineren met het werk in de kliniek. Ellen, dankjewel voor het meedenken en je tips en tricks t.a.v. de trainingsprotocollen. Alle kliniekassistenten en dierverzorgers, en in het bijzonder Bert, Peter, Jan, Henk en Henk, dankjulliewel voor al jullie hulp rondom en tijdens de trainingen en operaties van de pony's. Jan, dankzij jou is het gelukt de dansvideo in één dag op te nemen. Je was de meest geweldige assistent. Jan en Gerben, bedankt dat jullie me telkens weer de oscillerende zaag toevertrouwen. Dierenartsen van de Heelkunde, bedankt voor het verzamelen van synovia voor allerlei testjes en experimenten. Marloes en Suzanne, dank voor het helpen regelen van allerlei dingetjes en de gezellige praatjes. Carroll, zonder jou was ik failliet gegaan, dankjewel dat je er altijd voor zorgde dat m'n declaraties op de juiste plek terecht kwamen.

Yteke, Aukje, Janneke en Dax, bedankt dat ik een tijdje onderdeel mocht zijn van jullie team bij de Ambulante, waardoor ik naast mijn onderzoek ook wat klinische ervaring heb kunnen opdoen.

Kaatje, lieve Buuf, dankjewel voor je energie en gezelligheid, voor de cappuccino's die je altijd op het juiste moment maakte, voor het aanhoren van mijn gezeur en voor het meedenken. Hopelijk worden we ooit weer burens en dan beginnen we samen die koffiebar!

Rosan, zonder jou was "Joints Jumping for Joy" niet zo'n succes geworden! Dank voor al je tips, hulp en ideeën.

Rowan, Thera, Donata, Emmie en Angelica, het was een voorrecht om jullie een beetje wegwijs te mogen maken in het wetenschappelijk onderzoek. Niet alleen maakten jullie de weken in het Derona een stuk gezelliger, jullie hebben me ook een boel werk uit handen genomen en dankzij jullie ontbrak het de pony's nooit aan hun verdiende liefde, aandacht en wortels. Natalia, thank you for being part of our team last year and for bringing the work on in vitro culturing of chondrocytes a step further.

Het perfecte bruggetje van het Departement Paard naar Regenerative Medicine Utrecht: Jos, hoewel we niet zoveel direct samenwerken, heb jij een sleutelrol gespeeld op twee momenten die heel bepalend zijn geweest voor het verloop van mijn promotietraject. De eerste was je telefoontje met het voorstel om een aanvraag te doen voor het NWO-fellowship, dat me de kans heeft gegeven om mijn eigen aanvraag te schrijven voor het project waar ik de afgelopen vier jaar aan heb kunnen werken. De tweede was de tip om eens naar de video's van de 'Dance your Ph.D. contest' van Science magazine te kijken. Ruim twee jaar en een Public Engagement Seed Fund later, staat "Joints Jumping for Joy" online en is de live-versie succesvol uitgevoerd op het Weekend van de Wetenschap. Het waren wellicht kleine ideeën, maar door ze met me te delen, konden ze uitgroeien tot bijzondere projecten waar ik heel trots op ben. Dankjewel voor je betrokkenheid.

Ook wil ik graag alle andere collega's van RMU en/of UMC bedanken. Flor, Mylène and Susanna, it's been great to brainstorm and work on several side projects together. I hope we can continue our collaboration in the future. Margo, Margot, and all other Minions of the Pipets, thanks for the supportive work meetings and the nice conversations about life in general and as a PhD in particular. Miguel, thank you for your help, motivational words at the right moments and for refining my front crawl technique. Iris, fellowship-partner-in-crime. Je zei het al eens heel treffend: we hebben vaak 'similar thoughts'. Het is altijd fijn om die met je te delen; dankjewel voor de goede en leuke gesprekken, je bent een topper! Sander, bedankt voor de fijne samenwerking en je immer geduldige uitleg over MRI. To all people that I did not mention personally, thank you for sharing your ideas, cookies, Pizza Nights and the great retreat experiences in Normandy!

Ze zullen het lezen noch horen, maar toch wil ik graag mijn dank uitspreken naar alle pony's zonder wie een groot deel van de verworven resultaten en inzichten niet verkregen zouden zijn... Dorinde, Dirk, Frida, Flicka, Gracia, Elsje, Eline, Tessa, Geke, Foncita, Camora, Valfera en Elivia, waren stuk voor stuk geweldig en, toegegeven, ze hebben mijn ietwat bevooroordeelde beeld over Shetlandpony's drastisch bijgesteld (in positieve zin).

Ook wil ik graag mijn lieve intervisiegroepje bedanken voor de goede gesprekken en de gezelligheid op doordeweekse avondjes of (als we voor dubbele punten gingen) zondagmiddagen. Aimy, Anna, Annick, Charlotte, Els, Lotte, Marilou en Mariska, ik vind het bijzonder en bijzonder leuk dat we elkaar, ondanks de afstanden, met regelmaat blijven zien en vind het heerlijk om dan jullie mooie, bizarre of hilarische verhalen uit de praktijk te horen.

Lieve Manon, van zandtaartjes bouwen op de peuterspeelzaal, leren lezen in groep drie, de eerste wiskundeles op de middelbare school, tot ons allereerste wetenschappelijke onderzoek naar 'de duikreflex', samen met Karlijn, in 6vwo. Ik overdrijf niet als ik zeg dat jij aan de basis staat van mijn ontwikkeling als wetenschapper. Dat onze levens er de afgelopen 10 jaar wat anders uit zijn gaan zien, verandert daar niks aan. Ik ben nog altijd even trots op je en had me geen betere paranimf kunnen wensen. Dankjewel dat je er nog steeds voor me bent.

Lieve Karlijn, ook jij hebt, een tijdje na ons eerste wetenschappelijke project, je weg in het onderzoek gevonden. De afgelopen jaren konden we veel ervaringen van het leven als promovenda met elkaar delen. Of je nou in Amsterdam zit, of ergens in de VS voor allerlei ingewikkelde analyses, de live-chat is onze beste vriend! Ik wens je veel succes met de laatste loodjes!

Lieve Anrien, als je samen in een box hebt gelegen, oneindig veel logeerpartijtjes hebt gehouden, de eerste en de laatste dag op de middelbare school hebt gedeeld, vakantie-avonturen hebt beleefd, en zo kan ik nog wel even doorgaan; scheidt dat een band voor het leven. Dankjewel dat je er altijd voor me bent wanneer het nodig is.

Lieve neefjes en nichtjes, ooms en tantes, van Amsterdam, via Utrecht, Nijmegen, Kerikeri, tot onze 'roots' in het Achterhoekse Lichtenvoorde; dankjulliewel voor jullie interesse, warmte, nuchterheid en humor tijdens feestjes en partijtjes, spontane dinertjes of onze jaarlijkse fietstocht (jullie weten me altijd weer die net iets te slecht voorbereide 120 km door te krijgen en/of op te lappen met een goede barbecue). Lieve oma, met je actieve en sociale leefstijl ben je een voorbeeld voor velen, onder wie ikzelf. Ik ben dankbaar dat jij er nog altijd bij kunt zijn.

Lieve Guilty Pleasures: Arlinda, Eline, Elise, Eva, Karin en Sanne. Tijdens het schrijven van dit dankwoord zijn we net begonnen aan wat misschien (voorlopig) wel onze laatste productie samen is. Gouden tops en zilveren leggings, repetities en optredens, lief en leed, weekendjes weg, heel veel mooie liedjes en catchy dansspasjes... wat hebben we veel gedeeld in de afgelopen vier jaar. Liefste Manon, oneindig veel dank voor het bij elkaar brengen en houden van de aller-leukste, -lekkerste, -uitbundigste, -getalenteerdste, en -gezelligste zanggroep van Utrecht en omstreken. Whatever happens, jullie blijven mijn échte guilty pleasures.

Lieve L.O.F.-dancers, tijdens elke training en elke voorstelling met jullie kon ik mijn werk even helemaal vergeten. Ik had nooit kunnen dromen een eigen dansproject te kunnen maken met zo'n lieve en getalenteerde groep mensen. Liefste Charlotte,

dankzij jou kan ik een beetje de balletdanseres zijn die ik als klein meisje wilde worden. Dankjewel voor de prachtige dingen die je maakt, je oneindige optimisme en al je hulp het afgelopen jaar.

Allerliefste Lotus: Anna, Eef en Suus, jullie zijn mijn rots in de branding (ook als ik denk dat ik letterlijk zal verdrinken). Met jullie is alles gezelliger, grappiger en gekker en door jullie is alles beter te relativieren, te begrijpen (zelfs voor het hoogst onbegrijpelijke is een verklaring) en vol te houden... Ik kijk er enorm naar uit weer meer tijd met jullie door te kunnen brengen en kan niet wachten op onze volgende ontdekking!

Lieve Noor en Bram, dat kleine beslissingen grote gevolgen kunnen hebben, is iets waar we af en toe licht verwonderd bij stilstaan. Dankjulliewel voor alle gezelligheid, het luisterende oor, de recent wat dungezaaide maar altijd goede pannenkoeken- of port-avondjes, de droge humor, het delen van het Donald Duck abonnement en voor alles dat bij Schijn en Wezen hoort. Het is niet alleen een klein paleisje, het is ook een thuis, waar het altijd fijn is.

Lieve Timo, we zijn in veel dingen verschillend, maar we kunnen alles delen. Die combinatie maakt misschien wel dat er niemand is die me zo goed een spiegel kan voorhouden als jij. Ik ben heel trots op wat je doet en hoe je dat doet. Dat we samen de video voor het publieksproject konden maken, was voor mij een van de hoogtepunten van het afgelopen jaar en ik hoop dat we in de toekomst nog eens vaker samen projectjes kunnen doen. Lieve papa en mama, dat het zonder jullie niet gelukt was, is op z'n minst in praktische zin een open deur, maar ik beseft dat het minder vanzelfsprekend is dat de deur altijd open staat en ik met al mijn verhalen (of het nou te volgen is, of niet), buien (uitgelaten, of moe en chagrijnig) en vraagstukken welkom ben. Dankjulliewel dat jullie me altijd steunen bij de uitdagingen die op m'n pad komen. Ik houd van jullie.

## LIST OF PUBLICATIONS

### Peer reviewed publications

**Moller, N.C.R. Te**, Brommer, H., Liukkonen, J., Virén, T., Timonen, M., Puhakka, P.H., Jurvelin, J.S., Weeren, P.R. and Töyräs, J. (2013) Arthroscopic optical coherence tomography provides detailed information on articular cartilage lesions in horses. *Vet. J.* 197, 589–595. doi:10.1016/j.tvjl.2013.05.031

Niemelä, T., Virén, T., Liukkonen, J., Argüelles, D., **Moller, N.C.R. te**, Puhakka, P.H., Jurvelin, J.S., Tulamo, R.-M. and Töyräs, J. (2014) Application of optical coherence tomography enhances reproducibility of arthroscopic evaluation of equine joints. *Acta Vet. Scand.* 56, 1–8. doi:10.1186/1751-0147-56-3

Visser, J., Levett, P. a., **Moller, N.C.R. te**, Besems, J., Boere, K.W.M., Rijen, M.H.P. van, Grauw, J.C. de, Dhert, W.J. a., Weeren, P.R. van and Malda, J. (2015) Crosslinkable Hydrogels Derived from Cartilage, Meniscus, and Tendon Tissue. *Tissue Eng. Part A* 21, 1195–1206. doi:10.1089/ten.tea.2014.0362

Puhakka, P.H., **Moller, N.C.R. te**, Afara, I.O., Mäkelä, J.T.A., Tiitu, V., Korhonen, R.K., Brommer, H., Virén, T., Jurvelin, J.S. and Töyräs, J. (2015) Estimation of articular cartilage properties using multivariate analysis of optical coherence tomography signal. *Osteoarthr. Cartil.* 23, 2206–13. doi:10.1016/j.joca.2015.05.034

Puhakka, P.H., **Moller, N.C.R. te**, Tanska, P., Saarakkala, S., Tiitu, V., Korhonen, R.K., Brommer, H., Virén, T., Jurvelin, J.S. and Töyräs, J. (2016) Optical coherence tomography enables accurate measurement of equine cartilage thickness for determination of speed of sound. *Acta Orthop.* 87, 418–424. doi:10.1080/17453674.2016.1180578

**Moller, N.C.R. te** and Weeren, P.R. van (2017) How exercise influences equine joint homeostasis. *Vet. J.* 222, 60–67. doi:10.1016/j.tvjl.2017.03.004

**Moller, N.C.R. te**, Pitkänen, M., Sarin, J.K., Väänänen, S., Liukkonen, J., Afara, I.O., Puhakka, P.H., Brommer, H., Niemelä, T., Tulamo, R.-M., Argüelles Capilla, D. and Töyräs, J. (2017) Semi-automated International Cartilage Repair Society scoring of equine articular cartilage lesions in optical coherence tomography images. *Equine Vet. J.* 49, 552–555. doi:10.1111/evj.12637



Sarin, J.K., **Moller, N.C.R. te**, Mancini, I.A.D., Brommer, H., Visser, J., Malda, J., Weeren, P.R. van, Afara, I.O. and Töyräs, J. (2018) Arthroscopic near infrared spectroscopy enables simultaneous quantitative evaluation of articular cartilage and subchondral bone in vivo. *Sci. Rep.* 8, 13409. doi:10.1038/s41598-018-31670-5

Nykänen, O., Sarin, J.K., Ketola, J.H., Leskinen, H., **Moller, N.C.R. Te**, Tiitu, V., Mancini, I.A.D., Visser, J., Brommer, H., Weeren, P.R. van, Malda, J., Töyräs, J. and Nissi, M.J. (2019) T2\* and quantitative susceptibility mapping in an equine model of post-traumatic osteoarthritis: assessment of mechanical and structural properties of articular cartilage. *Osteoarthr. Cartil.* Epub ahead. Accessed August 16, 2019. doi:10.1016/j.joca.2019.06.009



ORCID

### Other publications

Moller, Nikae te. (2019) Is diergeneeskunde wetenschap? Wetenschappelijke kennis in een praktische context. *Tijdschrift voor Diergeneeskunde*. Jaargang 144, Aflevering 9.



Podcast version (Dutch)

## **Public Engagement Seed Fund Project**

With her project “Joints Jumping for Joy”, supported by the UU Public Engagement Seed Fund, Nikae te Moller explains the beautiful dynamics of the joint and the complexity of osteoarthritis by dancing it. She does this together with L.O.F. DanceCrew Utrecht.

*“With this project, I want to share my research with the general public in a creative and accessible way and call for attention to research on osteoarthritis. Also, I would like to inspire other scientists to share their work in a creative way by showing that science and art can reinforce each other.”*

This project resulted in an online video and a live presentation that was performed at Weekend van de Wetenschap (the national Weekend of Science) in October 2019 in Utrecht.



Online video (English)

## CURRICULUM VITAE



Nikae te Moller was born on the 28<sup>th</sup> of September 1990 in Winterswijk, the Netherlands. She grew up in Lichtenvoorde and passed her secondary school exam in 2008 at R.K.S.G. Marianum in Groenlo. From 2008 to 2015 she studied Veterinary Medicine at Utrecht University's Faculty of Veterinary Medicine (FVM).

In the last year of the bachelor program, Nikae was admitted to the Honours Program of the FVM; from 2011 to 2012 she worked on the assessment of subtle changes in equine articular cartilage under the supervision of dr. Janny de Grauw, prof. dr. Harold Brommer, and prof. dr. René van Weeren. She performed part of her project, on OCT analysis, under the supervision of prof. dr. Juha Töyräs (Department of Applied Physics, University of Eastern Finland, Kuopio) in Finland. From 2012 to 2015 she continued her project as a student researcher, alongside her master program in Equine Health. In 2015, she was awarded a PhD fellowship by NWO (The Dutch Research Council). This enabled her to extend her research in a full-time position as a PhD candidate at the Department of Equine Sciences in Utrecht. Her focus was on intra-articular imaging of the articular cartilage and investigating biomarkers for early stages of articular cartilage damage, as well as the influence of cartilage damage and exercise on the equine joint.

The work described in this thesis was presented by Nikae at several national and international conferences. During her PhD, she followed several courses on statistics (Biostatistics, Mixed models, Statistics for metabolomics (Liverpool, UK)), as well as courses within the Regenerative Medicine program of the Graduate School of Life Sciences. Her broader scientific interest was served by courses on Analytic storytelling and Science philosophy (Utrecht University). She supervised 6 Master students during their research internship, and she was a board member of the Veterinary PhD council (2016 to 2017). From 2016 to 2017 she also worked as a certified equine practitioner in the on-call rota of the Equine Ambulatory Clinic of the FVM. Since 2012, she visited the group of prof. dr. Juha Töyräs in Kuopio multiple times for collaborative projects on optical evaluation of articular cartilage, which resulted in multiple peer reviewed publications. In 2018 she was granted a UU Public Engagement Seed Fund which she used to gain outreach, expressing her research to the general public through dance, together with L.O.F. DanceCrew Utrecht where she dances herself.

Currently, she continues her research at the FVM in Utrecht. Besides her work, Nikae is passionate about dance and music, and she likes outdoor sports and visiting the theatre.